TAMPEREEN TEKNILLINEN YLIOPISTO
TAMPERE UNIVERSITY OF TECHNOLOGY

Tharaka Rama Krishna Chowdary Doddapaneni

Process Integration Approaches to Improve the Techno-Economic Feasibility of Torrefaction Process

Julkaisu 1539 • Publication 1539

Tampere 2018

Tampereen teknillinen yliopisto. Julkaisu 1539
Tampere University of Technology. Publication 1539

Tharaka Rama Krishna Chowdary Doddapaneni

Process Integration Approaches to Improve the Techno-Economic Feasibility of Torrefaction Process

Thesis for the degree of Doctor of Science in Technology to be presented with due permission for public examination and criticism in Festia Building, Auditorium Pieni Sali 1, at Tampere University of Technology, on the 6th of April 2018, at 12 noon.

Tampereen teknillinen yliopisto - Tampere University of Technology
Tampere 2018

Doctoral candidate: Tharaka Rama Krishna Chowdary Doddapaneni
Laboratory of Chemistry and Bioengineering
Faculty of Natural Sciences
Tampere University of Technology
Finland

Supervisor: Professor Jukka Konttinen
Laboratory of Chemistry and Bioengineering
Faculty of Natural Sciences
Tampere University of Technology
Finland

Pre-examiners: Associate Professor Manuel Garcia-Perez
Biological Systems Engineering
Washington State University
USA

Professor Anastasia A. Zabaniotou
School of Chemical Engineering
Aristotle University of Thessaloniki
Greece

Opponent: Professor Eva Thorin
Department of Energy, Building and Environment
Mälardalen University
Sweden

ISBN 978-952-15-4119-3 (printed)
ISBN 978-952-15-4125-4 (PDF)
ISSN 1459-2045

Abstract

Over the past few years, the torrefaction process has evolved into a promising pre-treatment process to improve the properties of biomass to a level at which it is competitive with coal. However, in order to make torrefied biomass pellets an economically viable alternative to coal and wood pellets, the techno-economic feasibility of the torrefaction process needs to be improved. Thus, new process configurations are required to produce torrefied biomass pellets and other high value products from the torrefaction process. This thesis presents new process configurations, which have been evaluated with laboratory experiments, process simulations and mathematical modeling.

Two different biomass samples i.e. eucalyptus clone and pinewood were used in torrefaction experiments. Initially, the effect that torrefaction pretreatment has on the kinetics, reaction mechanisms and heat flow during biomass pyrolysis was studied using TGA and DSC analysis. The results showed that the pyrolysis reaction mechanism varied significantly with torrefaction treatment. The heat flow data from DSC showed that torrefied biomass pyrolysis requires more energy than dried biomass in order to initiate the pyrolysis reactions.

In the second stage, the anaerobic digestion of torrefaction condensate for the efficient utilization of torrefaction volatiles was studied through batch anaerobic digestion assays. Torrefaction condensate produced at 225, 275 and 300 °C was used at various substrate to inoculum ratio i.e. 0.1, 0.2 and 0.5. The methane yield was in the range of 430 - 492 mL/g volatile solids (VS) and 430 - 460 mL/g VS under mesophilic and thermophilic conditions, respectively. With the higher loading, i.e. > 0.2 $VS_{substrate}$:$VS_{inoculum}$, the production of methane was inhibited because of the inhibitory compounds in the torrefaction condensate, such as furfural and guaiacol.

Large quantities of binders are required to make the pelletization process effective and to improve the quality of the pellets. An innovative process configuration is hereby proposed for detoxifying the torrefaction condensate and to reduce the binders' requirement. The removal of a major inhibitory compound, i.e. furfural, through adsorption using torrefied biomass as an adsorbent was also studied. The adsorption of furfural from the torrefaction condensate at 250 g/L dosage was around 54%. Finally, the influence of the detoxification of the torrefaction condensate on the AD process was studied through batch assays.

Finally, the experimental results were used to simulate industrial scale operations to evaluate the feasibility of integrating the torrefaction process with anaerobic digestion. In addition, different process integration approaches were studied to identify possible heat energy recovery options in the torrefaction process, on its own, and also when integrated with AD. The standalone torrefaction process was compared with three different process configurations, which varied according to the intended application for the produced biogas. The mass balance showed that bio-methane can be produced at 369 m^3/h, at 10 t/h of torrefied biomass pellets production capacity. A sensitivity analysis showed that the cost of the feedstock has a significant effect on the economics of the overall process. The economic analysis showed that the price of torrefied biomass pellets could be significantly reduced if the torrefaction process is integrated with AD.

Preface

This thesis work was carried out at the Department of Chemistry of the University of Jyväskylä (2013 - 2014) and at the Laboratory of Chemistry and Bioengineering of Tampere University of Technology (2015 - 2018). The financial support received from Academy of Finland, and Faculty of Natural Sciences at Tampere University of Technology is gratefully acknowledged. The last part of this thesis work was carried out with the funding from Ella and Georg Ehrnrooth foundation. The encouragement grant received from Gasum foundation is also appreciated.

I would like to thank my supervisor Prof. Jukka Konttinen for his guidance during these years. The freedom, support and encouragement he gave to build this research topic independently is greatly appreciated. I would like to express my special thanks to Prof. Jukka Rintala for his valuable suggestions and comments at various stage of this thesis work. I would also like to thank Prof. Raimo Alen for his valuable suggestions during the early stage of my PhD work at University of Jyväskylä. My sincere thanks to Dr. Ramasamy Praveenkumar for his continuous guidance in the experimental work and on research writing. His suggestions are not only limited this thesis work, and are also helpful to build my research carrier after this thesis work. I am grateful to Dr. Rohan Jain for his extensive guidance on adsorption experiments. His guidance and suggestions are highly appreciated and they are helpful to further advance my scientific knowledge. I would like to thank Dr. Jason Kramb for his suggestions in the different aspects of this thesis work. I owe a special thanks to Dr. Henrik Tolvanen for his support with the laboratory work during the early stage of this thesis work at Tampere University of Technology. I wish to thank Dr. Terttu Hukka for her support with the TGA and DSC equipment. I would like to thank Dr. Marja R.T Palmroth for assisting with the GC-MS and Dr. Leo Hyvärinen for assisting with the SEM images. I also would like to thank Dr. Henrik Romar for his assistance with the BET surface measurement. In addition, I would like to thank laboratory engineers Jarmo Ruusila and Juha Savolainen for their support with the torrefaction reactor setup. Moreover, the support from the administrative staff of the Faculty of Natural Sciences and the Laboratory of Chemistry and Bioengineering is also deeply appreciated.

Finally, I want to thank my family and friends for their support and encouragement during these years.

Tampere, February 2018

Tharaka Rama Krishna Chowdary Doddapaneni

Contents

Abstract i

Preface iii

List of symbols and abbreviations vi

List of publications ix

Author's contribution xi

1 Introduction 1

2 Background 3

2.1 Towards biomass-based economy 3

2.2 Biomass and its properties 4

2.3 Wood pellets and related statistics 5

2.4 Issues with biomass with respect to bioenergy 6

2.5 Torrefaction 6

2.6 The Influence of torrefaction treatment on biomass structure 9

2.8 Applications of torrefied biomass 10

2.9 Market and economic aspects of torrefied pellets 12

2.10 Challenges with torrefaction 13

2.11 Process integration approaches for torrefaction 14

2.12 Anaerobic digestion 14

3 Objectives 18

4 Materials and methods 20

4.1 Process configurations studied under this thesis work 20

4.2 Experimental methods 23

4.3 Analytical methods 27

4.4 Process simulation (paper IV) 28

4.5 Economic analysis 32

4.6 Pyrolysis kinetic modeling 34

4.7 Adsorption kinetics 38

5 Results and discussion 39

5.1 Torrefaction product distribution 39

5.2 Characterization of torrefaction products 39

5.3 Influence of torrefaction treatment on biomass pyrolysis (paper I) 42

5.4 Integrating torrefaction with AD (paper II) 51

5.5 Integrating torrefaction with adsorption and AD (paper III) 55

5.6 Operational and economic feasibility of integrating torrefaction with AD (paper IV) 61

5.7 A view on the process integration approaches to torrefaction 69

6 Conclusion 70

7 Future prospects 72

Bibliography 73

List of symbols and abbreviations

Abbreviations

AD	Anaerobic digestion
BET	Brunauer–Emmett–Teller
BJH	Baret-Yoymer-Halenda
CEPCI	Chemical engineering plant cost index
CHP	Combined heat and power
CIE	Capital investment on equipment
COD	Chemical oxygen demand
CRF	Capital recovery factor
DB	Dried biomass
DEC	Dried Eucalyptus clone
DSC	Differential scanning calorimetry
DTG	Differential thermogravimetric
EPA	Environmental protection agency
FCI	Total fixed capital invest
FWO	Flynn-Wall-Ozawa
GC-MS	Gas chromatography mass spectrometer
HAA	hydroxy-acetaldehyde
HPWS	High-pressure water scrubbing
HTC	Hydrothermal carbonization
IRR	Internal rate on return
IT	Income tax
KAS	Kissinger-Akahira-Sunose
KCE	Kinetic compensation effect
LCF	Lignocellulosic feedstock
LHV	Lower heating value

NPV	Net present value
PC	Production cost
PSA	Pressure swing adsorption
REN21's	Renewable energy policy network for the 21st century
ROI	Return on investment
SEM	Scanning electron microscopy
SSF	Sugar and starchy feedstock
TB	Torrefied biomass
TCI	Total capital investment
TFG	Triglycerides feedstock
TG	Thermogravimetric
TGA	Thermogravimetric analysis
TOC	Total organic carbon
TR	Total revenue
TV	Torrefaction volatiles
UNFCC	*United Nations Framework Convention on Climate Change*
USAB	Up flow anaerobic sludge blanket
VOC	Volatile organic compounds
VS	Volatile solid content
5-HMF	5-Hydroxymethylfurfural

Symbols

α	Extent of reaction	-----
$ß_{LS}$	External mass transfer coefficient	m/min
k_s	Second order rate constant	g/mg min
k_f	First order rate constant 1/min	-----
k	Global apparent rate constant	1/min
q	Equilibrium adsorption capacity	mg/g
k_{id}	Intra-particle rate constant	mg/g min $^{0.5}$
k_d	k-factor of the digester material	W/m^2 ^{0}C

k_b	Bangham's rate constant	-----
V_m	Volume of the methane produced	mL
$\eta_{elc.}$	Electrical efficiency	%
A	Pre-exponential factor	1/min
R	Universal gas constant	J/K. mol
Cp	Specific heat capacity	kJ/kg K
E_a	Activation energy	kJ/mol
Q	Heat energy	kJ/sec
D_e	Diffusional coefficient	m^2/min

List of publications

I. Doddapaneni TRKC, Konttinen J, Hukka TI, Moilanen A. Influence of torrefaction pretreatment on the pyrolysis of Eucalyptus clone: A study on kinetics, reaction mechanism and heat flow. Industrial Crops and Products 2016; 92:244–254.

II. Doddapaneni TRKC, Praveenkumar R, Tolvanen H, Palmroth MRT, Konttinen J, Rintala J. Anaerobic batch conversion of pine wood torrefaction condensate. Bioresource Technology 2017; 225:299–307.

III. Doddapaneni TRKC, Jain R, Praveenkumar R, Rintala J, Romar H, Konttinen J. Adsorption of furfural from torrefaction condensate using torrefied biomass. Chemical Engineering Journal 2018; 334:558–568.

IV. Doddapaneni TRKC, Praveenkumar R, Tolvanen H, Rintala J, Konttinen J. Techno-economic evaluation of integrating torrefaction with anaerobic digestion. Applied Energy 2018; 213:272–284.

Author's contribution

I. The author planned and conducted the experiments, analyzed the experimental data, wrote the kinetic modeling program and wrote the manuscript. The manuscript was finalized in consultation with all co-authors.

II. The author planned and executed the experimental setup together with Dr. Ramasamy Praveenkumar, interpreted the data and wrote the first manuscript draft. The manuscript was finalized in consultation with all co-authors.

III. The author planned the experimental setup together with Dr. Rohan Jain, conducted the experiments, analyzed the results and wrote the manuscript. Dr. Henrik Romar carried out the BET analysis. The manuscript was finalized by discussing with all co-authors.

IV. The author developed process simulation models, carried out the economic analysis, analyzed the results and wrote the manuscript. The coauthors contributed through discussions and commenting the manuscript draft.

1 Introduction

Ever since the industrial revolution, the CO_2 level in the atmosphere has increased by 45%. This has resulted in global warming as evidenced by melting ice, changes in sea level, changes in rainfall patterns and floods [1]. Government policies and international treaties aimed at dealing with these issues have stimulated the scientific community into initiating new research activities in order to reduce the level of CO_2 in the atmosphere. The Paris Agreement is one such global-level action plan aimed at mitigating global warming and climate change [1,2]. The ultimate goal of the Paris agreement is to reduce greenhouse gas emissions to a level at which the global average temperature will remain less than 2 ^{0}C above its pre-industrial level [1]. The goals of the Paris agreement can only be achieved by building a low carbon society. However, our current global economic system still relies mainly on fossil fuels, which are the main source for greenhouse gas CO_2.

The EU has also set targets for reducing our production of CO_2. The goal is that 20% of primary energy consumption should come from renewable energy resources by 2020, rising to 27% by 2030 [3]. According to IEA statistics, coal power plants were accountable for 45% of the total CO_2 emissions released globally in 2014 [4]. Reducing or replacing the use of coal to produce electrical energy is one possible approach to achieve the above energy and environmental goals.

Biomass has already been recognized as a feasible alternative to coal. Biomass is more attractive than fossil fuels because it has the ability to fix atmospheric CO_2 [5]. However, the benefits of this reduction in the CO_2 level will only be seen in the long term [6]. There are still many issues with biomass, such as its high moisture content, its low energy density, its fibrous, hydrophilic nature, and the ash and inorganic materials that it contains [3,7]. Because of these issues, biomass needs to be pre-treated before it can be used for its end application. One of these pretreatment methods involves torrefaction [3,7,8].

The torrefaction process can improve the fuel characteristics of biomass to a level at which it is a competitive alternative to coal. Thus, interest in the torrefaction process has increased rapidly in recent years, both in the scientific and industrial communities [3,7,9]. Although there is an increasing demand for torrefied biomass, the torrefaction process itself has not yet been fully optimized in either technical or economic terms [7]. The economics of producing torrefied biomass pellets is not yet fully competitive with the economics of producing conventional wood pellets and coal. Thus, further technological development is required in order to maintain the competitiveness of torrefied biomass pellets in a clean, solid-fuels market.

The overall feasibility of the torrefaction process needs further study in order to reduce the production costs of torrefied pellets. At the moment, the

torrefaction process has mainly been regarded as a way to improve the properties of biomass in order to make it an alternative solid-fuel equivalent to coal. However, by integrating the torrefaction process more closely with the other thermochemical and biochemical processes, it would be possible to produce multiple products, all of which would make the torrefaction process more economically feasible. For example, torrefaction volatiles can be condensed and the resulting condensate can be further processed to produce high value products such as bio-methane, wax esters and other bio-chemicals. At the same time, the heat energy produced by torrefaction can also be utilized.

Thus, in this thesis different approaches to process integration have been developed in order to improve the feasibility of the torrefaction process both technically and economically. The feasibility of various process configurations was studied through laboratory scale experiments and process simulations to the level required for commercial operation. Firstly, the influence of torrefaction treatment on the pyrolysis of woody biomass was studied using thermogravimetric analysis (TGA) and differential scanning calorimetry (DSC). As pyrolysis is a preliminary step in biomass combustion and gasification, it is vital to thoroughly understand the decomposition mechanism of torrefied biomass during pyrolysis. Such an understanding is needed to better utilize torrefied biomass in other thermochemical processes. Laboratory experiments were carried out on the anaerobic digestion of torrefaction condensate in order to investigate the feasibility of integrating the torrefaction process with anaerobic digestion. As a general rule, microbial processes are sensitive to certain inhibitory compounds present in the substrate and this rule applies to torrefaction condensate, which contains several such inhibitory compounds. Another issue is that torrefied biomass requires large quantities of binders during pelletization. Therefore, an innovative adsorption-based process has been developed for the detoxification of torrefaction condensate, thus reducing the need for large quantities of binders during the pelletization stage of producing torrefied biomass pellets. Finally, the data generated through laboratory scale experiments was used to simulate a commercial scale torrefaction process integrated with anaerobic digestion, in order to evaluate its techno-economic feasibility. This included an analysis of possible heat energy recovery options.

2 Background

This chapter presents a literature review of the different topics covered in this thesis. At present, torrefaction is mainly used in order to improve the biomass' properties, so the review covers the bioenergy aspects of biomass. Then, different aspects of the torrefaction process are presented in order to identify any knowledge gaps. Being an integral part of this research, the principles and processes of anaerobic digestion are also presented.

2.1 Towards biomass-based economy

Biomass, in the form of firewood and charcoal, is mankind's oldest energy source, and until the commercial production of coal and oil took off in the 19th century, biomass, in its raw form, was our main source of heat and energy [10]. Even today, untreated biomass is still a primary energy source in many rural areas of Asia and Africa [11]. Although most developed economies have moved away from burning wood for basic energy needs such as cooking, these economies still utilize processed biomass, both as fuel, and also in a number of different fields such as the chemical and plastic industries.

One of the advantages of biomass is that, besides being a source of renewable energy, it can also be used to produce a variety of other products. Nevertheless, the combustion of biomass to produce heat and electrical energy is still its most commonly considered application. The total amount of energy produced from biomass in 2015 was approximately 60 EJ [12], which represents 10% of global primary energy consumption [13]. According to [12], the use of biomass for energy applications has increased at a rate of 2% per year since 2010. The heat energy production from biomass can be divided into two categories: 1) its use as a primary fuel (wood) for heating and cooking; and 2) as a source of heat energy for urban power stations in order to provide centralized 'district heating' as is common in Scandinavia, for instance. The majority of biomass used as a primary fuel (wood) comes from Asia, South America and Africa [14]. According to REN21's (renewable energy policy network for the 21st century) [12] global status report, the use of charcoal for cooking has been increasing at a rate of around 3% a year since 2010, and in 2015 the total global consumption of wood for this purpose was 55 million tons.

More modern heat energy applications from biomass are found in many industrial processes and in heating for both residential and commercial buildings. For example, 43% of the total heat energy required in the paper and pulp industry is generated from process residues such as bark and black liquor [12]. The use of wood for heat energy production is increasing in the Baltic and Eastern European countries because of their large forest resources and their widely distributed district-heating networks [12].

2.2 Biomass and its properties

The definition of the term biomass varies from country to country. In some countries, organic matter derived from plants is only considered to be biomass if it includes organic municipal waste and animal waste. In other countries, the term biomass is restricted to the fuels arising from agricultural and forestry sources [10,15]. The *United Nations Framework Convention on Climate Change* (UNFCC), defined biomass as non-fossilized organic matter that is biodegradable and originates from plants, animals and microorganism [10].

The EU's renewable energy directive (2009/28/EC) defines biomass as the biodegradable fractions in the products, waste and residues originating from agriculture and allied industries such as fisheries and aquaculture. The biodegradable parts of municipal and industrial waste are also regarded as biomass [10].

Various approaches to categorizing biomass can be found in the literature, but in essence they fall into the following types [10,13].

Based on source: Agriculture, forestry, aquaculture and waste

Based on chemistry:

1. Triglycerides feedstock (TGF): Vegetable oils, animal fats, waste cooking oil and micro-algal oils.
2. Sugar and starchy feedstock (SSF): Sugar beet, sweet sorghum, sugar cane, wheat, corn, barley and maize.
3. Lignocellulosic feedstock (LCF): Wood, straw and grass.

2.2.1 Composition

Although the characteristics of biomass vary significantly according to the above classifications (section 2.2), lignocellulosic biomass (LCF) is the most common type of biomass used in bioenergy applications. Therefore, the characteristics of biomass presented in this chapter only apply to lignocellulosic biomass, unless otherwise specified.

Photosynthesis in plants results in the production of sugars, which are stored in the form of organic polymers: cellulose, hemicellulose and starch [16]. Biomass also contains small quantities of other materials such as lipids, resins, waxes and ash. The composition of these compounds varies significantly depending on the types of species of the source material, its growth condition, the stage of the growth and the part of the plant that it comes from, e.g. stem wood, bark or roots [17]. In terms of dry solids, lignocellulosic biomass contains cellulose, hemicellulose and lignin in the range of 40 - 45%, 25 – 35% and 20 – 30% respectively. Cellulose is a linear polymer of glucose molecules linked by glucosidic linkage. Hemicellulose is a polysaccharide that in general contains more than one type of monosaccharide unit, e.g. hexose and pentose. Depending on the type of biomass, hemicellulose

consists of xylan and /or galactomannans. Lignin has a complex amorphous structure that consists of phenylpropane units [17,18]. Lignin gives mechanical strength to the plant cell wall through its covalent linkage to hemicellulose [19].

In addition to organic polymers, biomass also contains ash. Biomass ash consists largely of calcium, potassium and magnesium, but it has small quantities of many other compounds such as manganese, sulphur, phosphorus, Al, Zn, Fe, Pb, Cu, Ti, Ni, Co, V, Ag and Mo. However, the composition of the ash varies with the biomass type, for example woody biomass contains much less ash (4%) than rice straw (20%) [10].

Based on the elemental composition of the different biomass types presented in [10], it can be concluded that the carbon, oxygen and hydrogen content in biomass varies from 40-55%, 35-45% and 4-6.5% respectively. Biomass usually contains more oxygen than coal because of the carbohydrates present in its structure [19]. Biomass also contains nitrogen, sulphur and chlorine, but at less than 1 wt.% dry matter, which is lower than coal, and is thus an advantage for ecologically friendly biomass systems. Sulphur and chlorine are responsible for corrosion, and the formation of atmospheric pollutants such as SO_2 and dioxins. On the other hand, biomass has a higher silica content than coal, and this can cause the formation of slag and even glass in biomass combustion systems.

2.2.2 Heating value

As a rule, the heating value of biomass is lower than coal, presumably because of its higher oxygen content. In general, the heating value for woody biomass on a dry basis is in the range of 15-19 MJ/kg [10]. However, it should be noted that this value depends on the moisture content. For example, the heating value of woody biomass with 50 % moisture is only around 10 MJ/kg [20].

2.2.3 Moisture content

Moisture content is one of the most important parameters in biomass energy systems. The moisture content of biomass can range from as little as 3% to up to 60% [10]. Thus, the moisture content of the biomass can significantly influence the logistical and economic feasibility of bioenergy systems. Therefore, wet biomass is often dried to reduce its moisture content to <10% prior to its being used in thermal conversion processes.

2.3 Wood pellets and related statistics

Wood pellets are a form of renewable energy carrier, which can be used instead of coal in order to reduce greenhouse gas emissions. Globally, the demand for wood pellets has been increasing constantly. For example, the total global production of wood pellets increased from 6 – 7 Mt (million ton) in 2006 to more than 26 Mt in 2015 [21]. This demand mainly comes from their use as fuel in stoves and

boilers in domestic heating systems, but also in part from electrical energy production [21].

Today, the major exporters of wood pellets are Germany, Sweden, Latvia, the USA, Canada and Russia, while Japan and Korea are major importers [12]. According to [12], the USA exported more than 4.5 million metric tons of wood pellets in 2015, 84% of which went to the United Kingdom. Canada is also a major producer of wood pellets, exporting 1.6 million tons in 2015, 23% of which went to the UK and 30% to Japan [12].

Wood pellets are used in different ways. For example, in Italy, Germany, and Austria they mainly used for residential heating, while in Sweden, Denmark and Finland they are also used for centralized district heating. They are used for large-scale power production in Belgium, Netherlands and the UK [12], and according to [21], in the future wood pellets might be used as a source for producing bio-based materials and chemicals.

2.4 Issues with biomass with respect to bioenergy

Biomass offers the flexibility to produce different products through different processing routes. Despite its many advantages, biomass as an energy source has its drawbacks. The major issues include heterogeneity, high moisture content, low bulk density, low heating value, poor grindability, low energy density, fibrous and hydrophilic nature, ash, other inorganic elements and tars [3,7,19]. Because of these issues, the processes and/or systems for the thermal conversion of biomass face considerable difficulties. The pretreatment of biomass is often required, and these processes can be mechanical, chemical and/or thermal. The method chosen depends on the biomass conversion process, i.e. thermal or biochemical. Torrefaction is one of several biomass pretreatment methods proposed in the literature [3,7,22].

2.5 Torrefaction

Torrefaction is a thermal pretreatment process which improves the biomass properties to a level at which it is competitive with coal [3,7]. In general, torrefaction is carried out in a temperature range of 200 to 300 ^{0}C at slow heating rates (< 50 /min) and at a residence time of 30 to 60 min [19]. Usually, the torrefaction process is carried out in an inert environment. Data from the literature clearly shows that torrefied biomass has better fuel characteristics than ordinary biomass. The major advantages of the torrefaction treatment with respect to specific biomass characteristics are listed below in Table 2.1.

The thermal decomposition of biomass components such as cellulose, hemicellulose and lignin occur at 220 – 315 ^{0}C, 315 – 400 ^{0}C and 160 – 900 ^{0}C respectively. In practice, the torrefaction process is usually divided into light (200 – 235 ^{0}C), mild (235 – 275 ^{0}C) and severe (275 – 300 ^{0}C) [23]. Hemicellulose starts to

decompose during light torrefaction, and as the temperature further increases, most of the hemicellulose and some of the cellulose and lignin degrade [24].

Table 2.1. The major advantages biomass torrefaction treatment considering biomass properties

Biomass characteristics	Advantage of torrefaction treatment
Reduced moisture content	Higher heating value Reduced transportation costs Increases the overall efficiency
Increased fixed carbon i.e. reduced O/C and H/C ratio	Increases heating value Increases energy density
Grindability	Decreases the grinding energy requirement
Increased energy density	Reduces the transportation costs Reduces the feeding capacity
Reduced hydrophobicity	Adsorbs low moisture during storage Reduces investment on the storage facilities

An overview of the conventional torrefaction process is presented below in Fig. 2.1. Briefly put, the wooden logs are first processed into wood chips, which usually have a moisture content of 40 – 50 wt.%. The wood chips are then dried in order to reduce the moisture content to a level of 10 wt.%. Then the dried biomass is torrefied at the required intensity. The torrefied biomass is then cooled to a surface temperature of below 50 ^{0}C, and is then ground into a fine powder, from which the pellets are produced. Here, it should be noted that preconditioning of torrefied biomass is required to produce high quality pellets and to reduce energy requirement during pelletization.

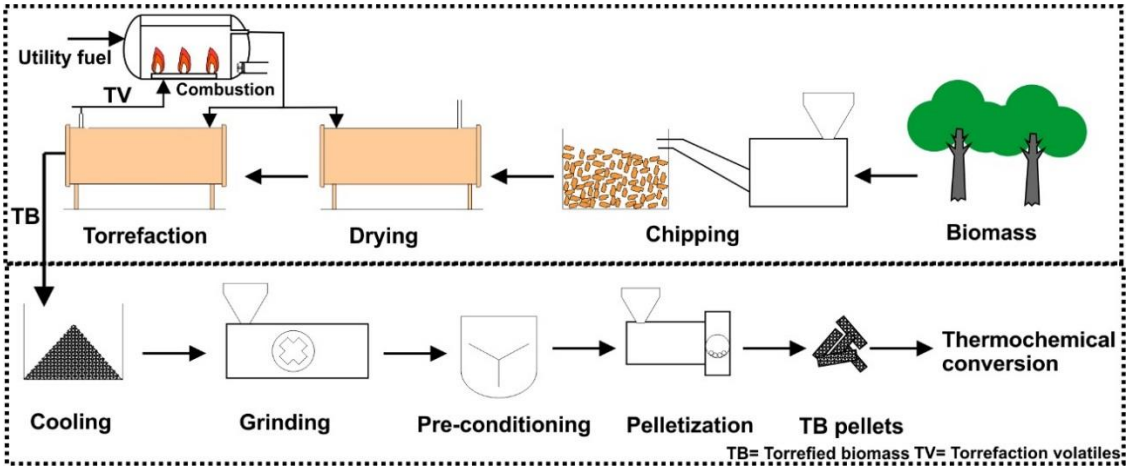

Fig. 2.1. Process flow of torrefied biomass pellets production.

The torrefaction process produces torrefied biomass and torrefaction volatiles. The energy yield of these products depends on the severity of the torrefaction process, the residence time and the properties of the raw biomass. The torrefied biomass energy yield varies from 90% to 40% in the temperature range of 200 to 300 ^{0}C [25]. For example, Chen et al. [25] reported that for bamboo torrefaction, as the temperature increased from 250 to 300 ^{0}C, the solid yield fell from 86% to 52% at a residence time of 30 min. In another study, Lu et al. [26] reported a solid yield of 58% for eucalyptus torrefaction at 300 ^{0}C and 60 min residence time.

The heating value of the torrefied biomass is higher than the original biomass because of its reduced moisture, oxygen and hydrogen content. In general, the HHV of torrefied biomass varies in the range of 14 to 23 MJ/kg for different types of biomass produced in the torrefaction operating temperature range of 220 to 300 ^{0}C [25]. Table 2.2 gives a comparative analysis of torrefied biomass pellets with wood chips and coal.

Table 2.2. Comparative analysis of different properties of wood chips, wood pellets, torrefied wood pellets and coal (adopted from [27])

	Wood chips/ saw dust	Wood pellets	Torrefied wood chips	Torrefied pellets	Coal
Moisture Content (wt.%)	20-50	7-10	1-5	1-5	10-15
Calorific value (MJ/kg)	15-16	15-16	20-24	20-24	23-28
Volatiles (wt.%)	70-75	70-75	50-60	50-60	15-30
Bulk density (kg/m3)	100-200	550-750	450-850	450-850	800-850
Volumetric density (GJ/m^3)	2-3	8-11	4-5	15-18	18-24
Hydroscopic properties	Hydrophilic		Hydrophobic	Hydrophobic	Hydrophobic
Biological degradation	Yes	Yes	No	No	No
Handling properties	Difficult	Easy	Difficult	Easy	Easy
Product consistency	Heterogeneous	Good	High	High	High
Transport cost	High	Average	Low	Low	Low

Torrefaction volatiles contains both condensable and un-condensable compounds. In general, the yield varies from 20% to 45% depending on the operating parameters of the torrefaction process [25]. The condensable fraction mainly contains water, acetic acid, furfural, methanol, lactic acid, formic acid and phenolic compounds such as vanillin, conifer aldehyde, and guaiacol [28,29]. The non-condensable fraction contains mainly CO_2, CO and other compounds (CH_4 and H_2) in traceable amounts [30]. The heating value of torrefaction volatiles varies from 2 to 10 MJ/kg [31,32].

2.6 The Influence of torrefaction treatment on biomass structure

Previous studies have shown that torrefaction treatment reduces the H/C and O/C ratio in the biomass with increased torrefaction temperature and residence time[33,34]. This suggests that deoxygenation could be the primary reaction during torrefaction [33]. Hemicellulose has the least thermal stability in comparison with other biomass components such as cellulose and lignin [35]. Thus, at the early stage of the torrefaction < 250 °C, it is mainly the hemicellulose which degrades [35]. According to [36], at lower temperatures, the hemicellulose degradation results in the formation of char and volatiles. The volatiles released at this stage mainly contain water, acetic acid, methanol, formic acid and furfural [36,37]. At this stage, the O-acetyl branches in the hemicellulose maybe dissociated. This indicates that the small molecules produced at the early stage of the torrefaction process, i.e. water and acetic acids occur because of dehydration and deacetylation, respectively [34]. At the same time, the formation of CO and CO_2 could be because of decarbonylation and decarboxylation, respectively [34].

Other studies [36,38] which have utilized NMR and FTIR analysis have reported a decrease in the carboxylic groups in hemicellulose due to decarboxylation. According to [35], in addition to O-acetyl branches, the other linkages such as glycosidic bonds and aryl ether linkages can be degraded easily at lower temperatures. Zheng et al. [33] observed an increase in the crystalline content when the torrefaction temperature increased from 250 – 275 °C, although this was then significantly reduced when the temperature increased further to 300 °C. This increased crystallinity could be because of the degradation of the hemicellulose and an amorphous region of cellulose [33]. Through 2D-PICS analysis, [34] indicated that during torrefaction the alkane groups may be transformed into alkene groups through dehydration.

The ether linkages are less thermally stable than the aryl C-C linkages. Thus, torrefaction treatment could result in the depolymerization of lignin through the cleavage of β-O-4 linkages[34]. In another study it was reported that, during torrefaction treatment (200 – 300 °C), the syringyl units present in lignin could be transformed into guaiacol units through demethoxylation [34,39]. Yet another study, Zheng et al. [33] observed that, the aromatic carbon content in the torrefied biomass increased from 11.48% at 250 °C to 30.8% at 300 °C and, at the same time, the carbohydrate carbon content decreased from 80% at 250 °C to 42% at 300 °C.

In general, pulverizing the biomass requires more energy because of the biomass's long fibers. The dehydration and depolymerization reactions of cellulose that occur during torrefaction reduces the length of these fibres, meaning that less energy is required to grind torrefied biomass [40].

2.7 Torrefaction reaction and kinetic schemes

The details of the reaction kinetics are important for identifying the most feasible operating conditions when designing a torrefaction reactor [19].

Several reaction schemes for biomass torrefaction have been presented in the literature. Some of these reaction schemes have developed by building on the previous knowledge of biomass pyrolysis. According to Bates et al. [41] these reaction models can be grouped into two categories: 1) by considering the reaction schemes of the biomass components (cellulose, hemicellulose and lignin) individually; and 2) by considering the biomass as a single solid which reacts to produce char and volatiles. In one study [42] the different reaction models, such as single step, successive reaction, two competitive reactions and two parallel reactions have been investigated (see Fig. 2.2). The same author observed similar thermal decomposition behavior for different biomasses, such as beech, willow and spruce with two different parallel reaction mechanisms. In another study, [41] used a two-step reaction mechanism (Fig. 2.2) in which the torrefaction products are lumped into five pseudo-components. Anca-couce et al. [43] proposed a detailed reaction scheme to predict the composition of the torrefaction volatiles. In contrast to previously discussed models [41,42], in this study, the different reaction schemes for biomass components were considered. Through a comparative analysis with the torrefaction of biomass on a laboratory-scale packed bed reactor the authors [43] concluded that this model predicts the composition of the torrefaction volatiles more accurately. According to [19], the two-step reaction model proposed by Di blasi – Lanzetta [44] for xylan thermal decomposition in the temperature range of 200 – 340 °C was able to accurately predict the mass loss kinetics of the torrefaction process.

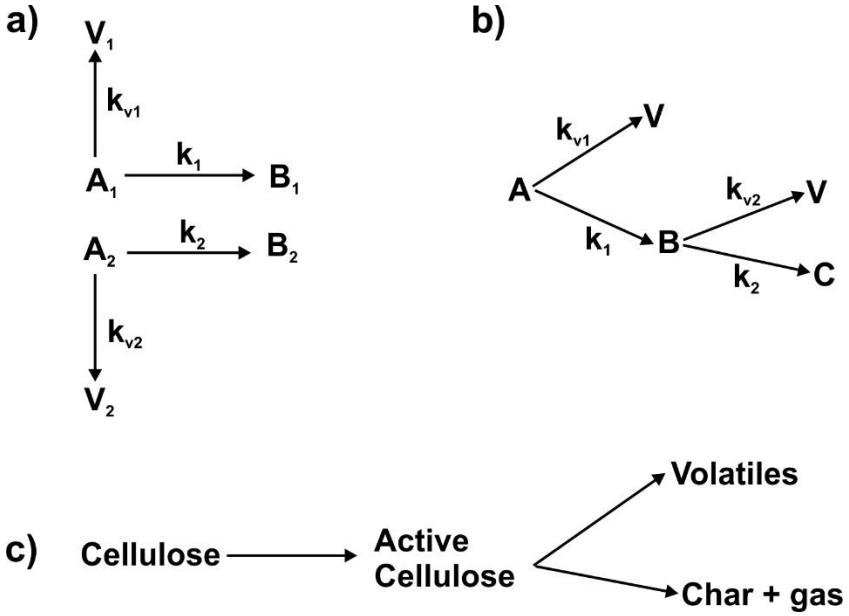

Fig. 2.2 Different reaction schemes of biomass torrefaction process a) two parallel reactions [42] b) two step reaction mechanism [41] c) Broido-shafizadeh reaction for cellulose degradation scheme [45]

2.8 Applications of torrefied biomass

At present, the potential heating-energy applications of torrefied biomass are confined to co-firing with coal and/or replacing the coal in combustion-

based power plants. However, several research studies have also reported on using torrefied biomass in pyrolysis and gasification processes. Another potential application of torrefied biomass is, for instance, using it in place of coke in the steel industry.

Replacing the raw biomass with torrefied biomass in thermochemical conversion processes could also reduce the energy requirement for grinding the biomass, as reported in previous section (2.6)

2.8.1 Torrefied biomass combustion

Lasek et al. [46] studied emissions such as SO_2, NO_x, and HCL in the flue gas released during the combustion of torrefied biomass. They reported that the torrefied willow combustion resulted in lower SO_2 and HCL and Higher NO_x emissions than Polish hard coal combustion. The reason for this could be the reduced sulphur and increased fuel nitrogen in the torrefied biomass.

The higher the oxygen content present in the biomass, the higher the thermal reactivity. This can result in unsteady burning during combustion. Torrefaction treatment reduces the oxygen content and thereby enables steady-state combustion [47]. However, the nitrogen content increases in proportion with the raw biomass, which leads to increased NO_x emissions. When it comes to the ash and ash-forming elements, torrefaction may reduce the sulphur and chlorine but it has no influence on the amounts of silicon, calcium and potassium. These compounds are usually responsible for combustion-related issues such as corrosion, fouling and agglomeration in the biomass combustion boilers. Thus, the influence of torrefaction on these issues is relatively low [48]. In another study on the single particle combustion of torrefied schima hardwood of a diameter of 3 - 5 mm, it was shown that torrefaction reduced the devolatilization time of the fuel, but increased the char burnout time [49].

2.8.2 Pyrolysis of torrefied biomass

Pyrolysis is a thermochemical process, which is carried out in a temperature range of 400 to 700 ^{0}C and in the absence of oxygen [50]. During pyrolysis, the biomass can be converted into multiple products such as solid char, volatiles and pyrolysis oil. However, the operational feasibility of the pyrolysis process and the properties of its products depend on the physiochemical properties of the input material.

Torrefaction has a significant influence on the composition of pyrolysis oil. Because the hemicellulose degrades during torrefaction, the resulting pyrolysis oil from torrefied biomass contains lower concentrations of organic acids and furans. Worasuwannarak et al. [51] reported that the tar yield from the pyrolysis of torrefied woody biomass (*Leucaena leucocephala)* fell in line with the biomass' residence time in the torrefaction treatment process. Other studies [51,52] have shown that torrefaction has a significant influence on the formation of volatiles during biomass

pyrolysis. For example, during the pyrolysis of raw Leucaena biomass, water started to form at 120 ^{0}C, while for torrefied biomass pyrolysis this only occurs above 200 ^{0}C. The same authors [52] also reported that the amount of CO_2 produced from torrefied biomass pyrolysis is significantly lower than it is from raw biomass pyrolysis. In another study [53], it was reported that the oxygen-to-carbon ratio in the pyrolysis oil produced from torrefied biomass was significantly reduced when the torrefaction was increased. The same authors [53] also reported that the concentration of lignin oligomers and anhydrosugars in the pyrolysis oil increased when the torrefaction temperature increased in comparison with pyrolysis oil produced from raw biomass. According to [53], pyrolysis of torrefied biomass could be a promising approach to producing phenolic-based chemicals.

2.8.3 Gasification of torrefied biomass

Previous studies [54–56] on the gasification of torrefied biomass have shown that torrefaction treatment has a significant influence on the properties of the syngas produced during gasification. For example, the LHV of syngas produced from raw wood was 3 MJ/Nm^3 , while for torrefied wood it was 5.8 MJ/Nm^3 [54]. According to [55,56] torrefaction treatment also reduced the tar and enhanced the H_2, CO and CH_4 yield in syngas. Char reactivity is one of the most important parameters in the gasification process. One study [57] observed higher char reactivity when torrefied woody biomass and agricultural waste were gasified in a CO_2 environment. The reason for this increased char reactivity could be the higher concentration of alkali and alkaline earth metals. However, [58] observed reduced char reactivity for terrified biomass during steam gasification.

2.9 Market and economic aspects of torrefied pellets

The demand for torrefied pellets mainly comes from the power sector, where they are often co-fired with coal. The major markets are in Europe, North America and Asia (China, Japan and Korea) [27]. According to [21], the demand for torrefied pellets is likely to increase once the standard ISO-17225-8 is issued by the International Standards Organization (ISO). According to the most optimistic forecasts [59], the demand for torrefied biomass is expected to reach 70 million tons per year by 2020. On the other hand, more conservative forecasts [60] put the demand at 8 -10 million tons by 2030.

Although torrefied pellets are not yet competitive with wood pellets and coal in terms of price, studies have shown that the production cost of the pellets varies significantly depending on the cost of the feedstock and the capital investment. For example, [3] reported that the cost of producing torrefied pellets fell from 43 €/MWh to 29 €/MWh when the cost of the feedstock fell from 18-25 €/MWh to 15 €/MWh. These prices were for plants with production capacities of 72,800 and 500,000 t/year. The production cost of torrefied pellets also depends on process integration. For example, it has been reported [61] that production cost fell from 45

€/MWh to 35 €/MWh when the torrefaction process was integrated into a new saw mill.

With current production methods, the market price for torrefied pellets may not be competitive with white pellets and coal. However, torrefied pellets have other advantages. For example, the capital investment required to convert a power plant so that it can co-fire wood pellets with coal is significantly higher than it is for torrefied pellets. One study [3] showed that white wood pellets require 83% higher investment than torrefied pellets to achieve 30% co-firing with coal. According to other researchers [27,62] torrefied wood pellets can also benefit from emissions allowances (or) carbon credits at a level of up to 50 €/t. This could bring the production costs down to 27 €/MWh. Indeed, many previous studies [3,27] have clearly shown that the economic feasibility of the torrefied pellets will depend on a number of factors, such as feedstock costs, process integration and renewable energy policies.

2.10 Challenges with torrefaction

One of the main challenges in developing the torrefaction process is how to handle the torrefaction volatiles and how to utilize the energy produced by the process[63]. At present, the torrefaction volatiles are combusted to meet the energy demand of the torrefaction process along with other utility fuels such as LPG, biomass and natural gas [22,29,63]. The energy content of the torrefaction volatiles depends on the severity of the torrefaction process. Because of the high water and CO_2 content, the heating value of the torrefaction volatiles is correspondingly low. In addition, because of the presence of organic acids such as acetic acid and formic acid, the torrefaction volatiles might be corrosive. [63]. According to [29], these issues indicate that combusting torrefaction volatiles for heat energy production has little effect on the overall efficiency of the torrefaction process.

The densification of torrefied biomass is also a challenge. Torrefied biomass has a relatively low bulk density so it must be densified before it can be transported in bulk. Research data [64] has shown that it takes more energy to produce pellets from torrefied biomass than from raw biomass. The energy requirements to pelletize raw biomass and torrefied biomass are in the range of 757 kJ/kg and 1164 kJ/kg respectively [64]. Another issue is that the pellets from torrefied biomass have lower mechanical properties than conventional wood pellets. The weaker bonding mechanism and increased friction during the pelletization of torrefied biomass is because the hydroxyl groups have been removed in the form of volatiles [65]. Previous studies have shown that water and/or other binding materials must be added to produce better quality torrefied pellets. For example, Peng et al. [66] reported that pretreating the torrefied biomass with water to raise its moisture content to 10 % improved the hardness and density of the pellets. Research has also been carried out with other binding materials, for example wheat flour [64], lignin, starch, calcium hydroxide and sodium hydroxide [67]. Reza et al. [68] studied the possibilities for increasing the durability of torrefied biomass pellets by mixing the char produced from hydrothermal carbonization (HTC) with torrefied

biomass. They reported that such pellets are 33% more durable than the conventional pellets produced from torrefied biomass. The problem is that the external sourcing of these binders may significantly increase the production costs, which would be challenging if the torrefied biomass pellets are to be produced in large, commercially viable quantities [62].

2.11 Process integration approaches for torrefaction

According to [63], the torrefaction process still needs to prove its techno-economic feasibility, and [22] reported that heat integration and waste heat utilization of the torrefaction process has not yet been optimized. It is clear that there is a lot of potential in integrating torrefaction with the other biomass conversion processes. Nevertheless, although a variety of products could be harvested in this way, there have been relatively few studies on process integration approaches to torrefaction in the literature. Winjobi et al. [69] studied the feasibility of integrating torrefaction with fast pyrolysis through a two-stage approach to produce pyrolysis oil. They reported that integrating torrefaction with fast pyrolysis by increasing the torrefaction treatment temperature has the potential to significantly reduce the emission of greenhouse gases. The effect of heat integration and torrefaction temperature on the performance of a CHP unit integrated with the torrefaction process was studied by [70], who concluded that the trigeneration efficiency of the integrated process is higher than it is for the non-integrated case. In another study [71], the same research group performed operational and economic analyses of integrating torrefaction with a CHP. They reported that one feasible option is to use live steam to meet the heat energy demand of the torrefaction process, while low grade steam from a back pressure turbine could be used to meet the drying energy requirement.

Clausen et al. [72] studied the integration of torrefaction with gasification in two different approaches, i.e. integrated and external torrefaction. The results showed that integrated torrefaction has a higher biomass to syngas conversion efficiency (86%) than external torrefaction (63%) at a torrefaction temperature of 300 ^{0}C. Fagernas et al. [28] reported that the additional revenue from the sale of torrefaction condensate could help to reduce the price of the torrefied biomass. Liaw et al. [29] studied the biomethane potential of torrefaction condensate and reported that the biogas yield varied between 32 – 106 mL/g of condensate for different biomass.

2.12 Anaerobic digestion

AD is a biochemical process in which a group of microorganisms convert organic matter into biogas and digestate without the need for oxygen. This biogas mainly consists of CH_4 (50 - 75%) and CO_2 (20 – 40%) [73]. The digestate usually contains nutrients such as NPK and can be used as a fertilizer in agriculture.

A simplified pathway for AD is shown in Fig. 2.3. This comprises four main stages, as described below.

Hydrolysis: This is the first stage in the AD process during which complex organic materials such as proteins, lipids, and carbohydrates are hydrolyzed into soluble products such as amino acids, sugars, glycerol, and long chain fatty acids by extra cellular enzymes released by the microorganisms [74,75].

Acidogenesis: In this stage, the monomers of simple soluble compounds such as amino acids, sugars and long chain fatty acids produced during hydrolysis are further converted into organic acids, alcohols, hydrogen and carbon dioxide. The most common organic acids are acetic, propionic and butyric, among others [74,75].

Acetogenesis: The short chain fatty acids produced during acidogenesis (propionic, butyric and valeric) are further converted into acetate, carbon dioxide and hydrogen. According to [74], it is difficult to make a clear distinction between the acidogenesis and acetogensis reactions in the AD process [74,75].

Methanogenesis: This is the final stage in the AD process, in which a group of methanogenic archaea produce methane along two pathways 1) acetic acid to methane and carbon dioxide 2) using hydrogen as a donor to reduce the CO_2 content. Two-thirds (66%) of the methane is produced in the first pathway and one-third is produced through 2 [74,75].

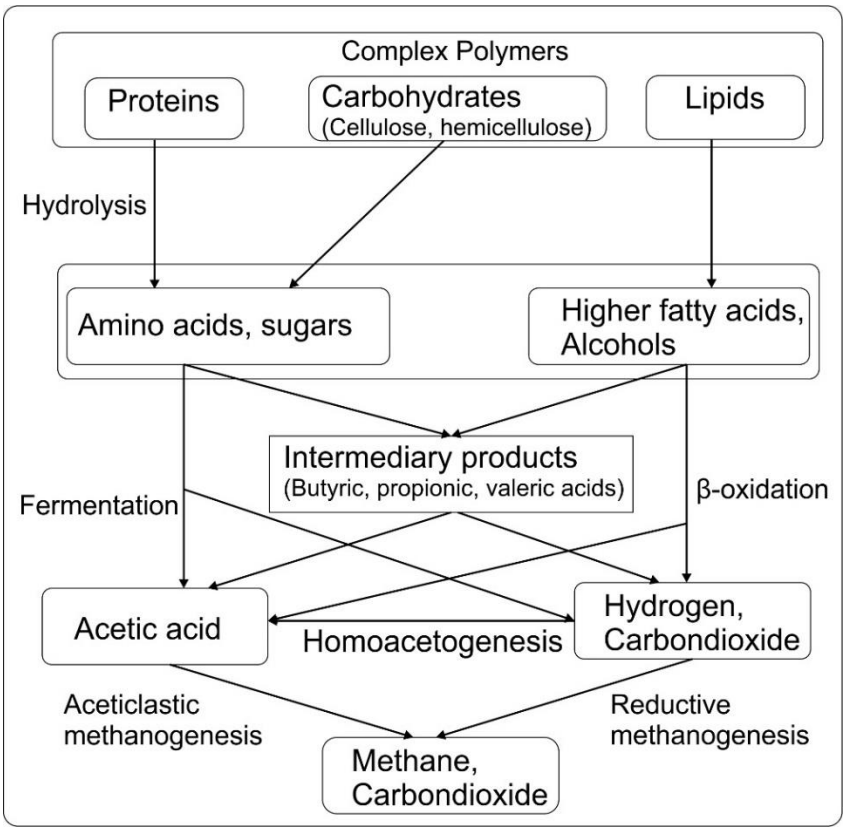

Fig. 2.3. Simplified pathway of anaerobic digestion process (adopted from [74])

2.12.1 AD of biomass derived oils

The literature reports that a number of different substrates have been tested in the AD process, and some of them have been successfully utilized on an industrial scale. Some examples of substrates that are widely used in the AD process are organic fractions of municipal solid waste, maize, cow dung, and food processing wastes [73]. More recently, researchers have begun to concentrate on the AD of biomass-derived liquid fractions such as pyrolysis oil, torrefaction condensate, and the liquid fraction from hydrothermal liquefaction processes. Hübner et al. [76] studied the integration of pyrolysis with AD where the aqueous liquors from the digestate pyrolysis were reused in the AD process to produce methane. Their experimental results showed that the pyrolysis temperature (at which the aqueous liquors were produced) has a significant effect on COD conversion and TOC degradation. Another study [77] which linked pyrolysis with AD reported that adding pyrolysis char into the AD process reduces the inhibitory effects of the pyrolysis oil on the microorganisms. Liaw et al. [29] reported that the biomethane potential of torrefaction condensate produced at 310 ^{0}C varied significantly with the biomass type. For example, the methane yield from the torrefaction condensate of sorghum biomass was 32 mL/g while the corresponding figure for pea hay was 106 mL/g.

2.12.2 Inhibition of biomass derived oils

Biomass-derived liquids such as pyrolysis oil and torrefaction condensate mainly consist of organic acids, furans, phenolic and other sugar-derived compounds [5,28]. The major furans are furfural and 5-Hydroxymethylfurfural (5-HMF), while the major phenolic compounds are phenol, coniferyl aldehyde, vanillin and cresol. The concentrations of these compounds depend on the operating temperature of the selected process. According to [78], concentrations of furfural and 5-HMF than 2000 and 1000 mg/L respectively are highly inhibitory to the AD process. In the phenolic groups, a concentration of guaiacol higher than 0.01 wt.% can also inhibit the AD process [29]. Biomass-derived oils also contain other inhibitory compounds such as hydroxy-acetaldehyde and formaldehyde.

2.12.3 The removal of inhibitory compounds

Several methods have been proposed in the literature for the effective detoxification of biomass-derived oils (i.e. pyrolysis oil). These include solvent extraction, over-liming, evaporation and adsorption using activated carbon [79,80]. Lian et al. [81] studied the removal of acetol and hydroxyacetaldehyde through evaporation and the removal of phenolic compounds using activated carbon from pyrolysis oil. Zhao et al. [80] studied the detoxification of fast pyrolysis oil derived from softwood using alkali treatment. In addition to pyrolysis, several studies have been reported on the detoxification of biomass hydrolysates produced through acid treatment. Weil et al. [82] reported on the removal of the furfural generated during the thermal pretreatment of corn using polymeric adsorbents i.e. XAD-4 and XAD-

7. Lee et al. [83] studied the detoxification of woody hydrolysates using activated carbon prior to ethanol production. They reported that T. saccharolyticum strain MO1442 was able to produce a theoretical 100 % ethanol yield from detoxified hydrolysate. In another study, Soleimani, et al. [84] looked into the removal of microbial inhibitors like phenol, furfural and acetic acid using powdered activated carbon and reported that the detoxification increased the xylitol yield by 10 %. Björklund et al. [85] studied the feasibility of detoxifying lignocellulose hydrolysates using lignin. They concluded that, depending on the lignin dosage, this treatment improved ethanol production and the removal of inhibitory compounds. Cavka and Jönsson [86] used sodium borohydride for the detoxification of spruce wood hydrolysate and reported that ethanol yield was tripled. Chan and Duff [79] studied the detoxification of pyrolysis oil using different organic solvents like tri-n-octylamine, tributyl phosphate, oleyl alcohol and oleic acid. Of all these detoxification methods, adsorption using activated carbon seems to be the most promising, and cost-effective, method for industrial scale operations.

3 Objectives

The objective of this thesis is to explore possible integration approaches to improve the techno-economic feasibility of the torrefaction process. To be specific, the effect and/or influence of integrating the torrefaction process with other thermochemical and biochemical processes with respect to the technical and economic feasibility of the torrefaction process will be studied. In order to achieve this overall goal, the task has been divided into the following six specific objectives.

- To identify the influence torrefaction pretreatment has on the parameters of the lignocellulosic biomass pyrolysis process, such as the reaction kinetics, the reaction mechanisms and heat flow.

- To integrate the torrefaction process with anaerobic digestion in order to utilize the torrefaction condensate effectively by producing biogas.

- To integrate torrefaction with adsorption to reduce the demand for external binders and improving the quality of the torrefied biomass pellets.

- To integrate torrefaction with adsorption to reduce the microbial inhibition of torrefaction condensate and thereby improve the feasibility of processing the torrefaction condensate with AD.

- To study the technical and economic feasibility of integrating the torrefaction process with anaerobic digestion.

- To identify the possible heat-energy recovery options in the torrefaction process.

Ultimately, the aim of this thesis work is to develop innovative and techno-economically feasible bio-refinery approaches to torrefaction in order to produce a range of valuable products with a special emphasis on improving the techno-economic feasibility of torrefaction process.

Figure 3.1 shows the scope of this thesis needed to achieve the above objectives.

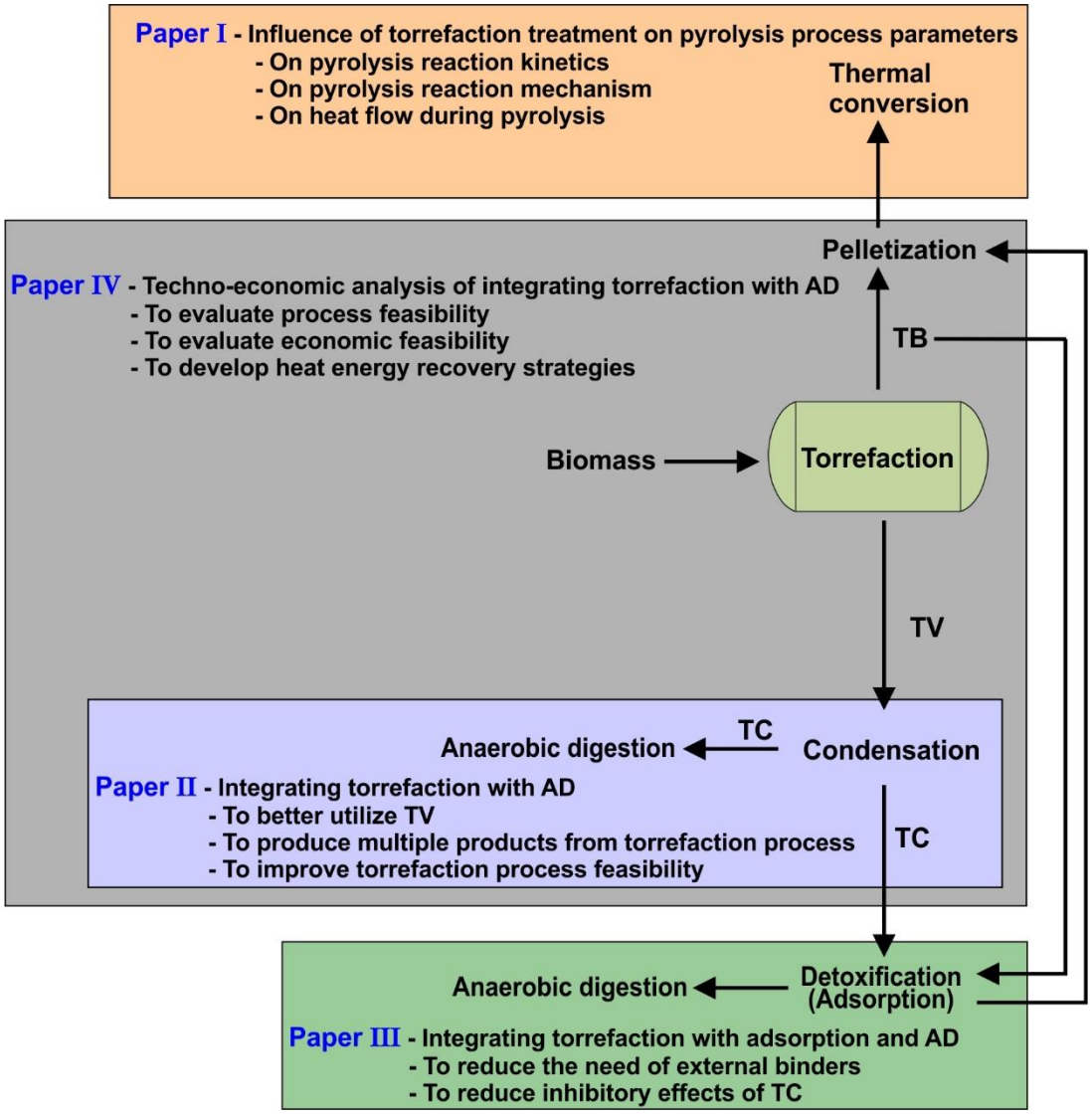

Fig. 3.1 An overview of the scope of this thesis work and the objectives of the original research papers. TB=torrefied biomass, TC=torrefaction condensate, TV=torrefaction volatiles, AD=anaerobic digestion.

4 Materials and methods

This chapter presents the experimental, analytical and modeling methods used in this thesis work.

4.1 Process configurations studied under this thesis work

This section describes three approaches to process integration studied in this thesis work. These are:

1) Integrating torrefaction with pyrolysis

2) Integrating torrefaction with AD

3) Integrating torrefaction with adsorption and AD

4.1.1 Integrating torrefaction with pyrolysis (paper I)

As discussed in section 2.8.2, torrefaction treatment has a significant influence on the properties of the pyrolysis oil, such as reduced O/C ratio, increased lignin oligomers and anhydrosugars, and reduced light oxygenates i.e. acids and aldehydes [52]. Thus, integrating torrefaction with pyrolysis should be interesting. First, it is important to understand the decomposition characteristics of the torrefied biomass in order to better design and optimize the pyrolysis process. The most important of these characteristics are the reaction kinetics, the reaction mechanism and the heat flow data. In this thesis, the influence of the torrefaction treatment on the pyrolysis process parameters of kinetics, reaction mechanism and heat flow was studied using TGA and DSC devices (paper I) and mathematical modeling. Fig 4.1 shows the overall process flow of the experimental procedure, which was carried out in order to investigate the influence torrefaction treatment, has on pyrolysis.

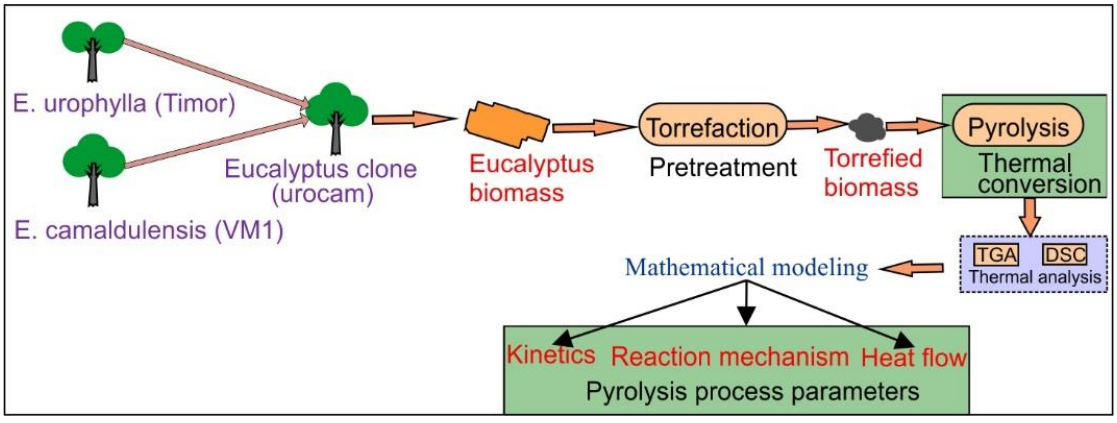

Fig. 4.1. Process flow of experimental procedure carried out in order to investigate the influence of torrefaction treatment on pyrolysis

4.1.2 Integrating torrefaction with anaerobic digestion (paper II)

At present, torrefaction volatiles are combusted along with wood chips and/or with other utility fuels such as natural gas or LPG to produce the heat energy needed in drying and torrefaction units. As discussed in section 2.10, torrefaction volatiles have different problematic characteristics, such as low heating value and high corrosivity. Therefore, combusting these volatiles may not be a feasible option. On the other hand, torrefaction volatiles can be condensed and the resulting condensate can be utilized more effectively in other processes.

AD is a well-known and established industrial process whereby a group of microorganisms converts the organic fraction into biogas (mainly containing CH_4 and CO_2). Acetic acid and other volatile acids are intermediate products in the anaerobic digestion process (Fig 2.3). The torrefaction condensate mainly consists of water (50 to 85%) and acetic acid (5 to 15%) depending on the severity of the torrefaction process. Thus, torrefaction condensate could be utilized as a feedstock for the anaerobic digestion process [29]. Fig. 4.2 shows the process flow of integrating torrefaction with AD. For this study, the AD of torrefaction condensate was studied with batch and cyclic batch experiments, the results of which are presented in paper II. The produced biogas could be used either in a biogas engine or as a vehicle fuel. The techno-economic feasibility of integrating torrefaction with AD was carried out for different end applications of produced biogas. The results were presented in paper IV.

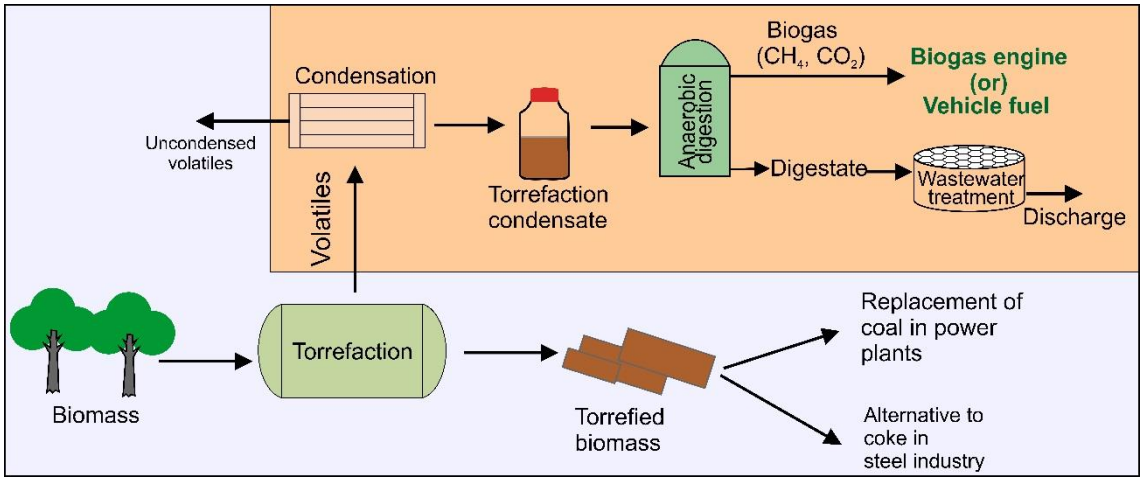

Fig. 4.2 Process flow of integrating the torrefaction with AD

4.1.3 Integrating torrefaction with adsorption and AD (paper III)

The experimental results reported in paper II showed that torrefaction condensate is a feasible feedstock for the AD process. However, under higher substrate loading it inhibited the production of methane. The major inhibitory compounds are furfural, 5-HMF and Guaiacol, all of which must be removed and/or reduced to improve the viability of the process. As discussed in section 2.12.3, several methods have been proposed in the literature for the detoxification of biomass-

derived oils, such as solvent extraction, over-liming, evaporation, and adsorption using activated carbon. Of these, adsorption is the most widely used because of its cost effectiveness and easy operation.

With large volumes, the torrefaction process requires binders during the pelletization process in order to reduce the energy requirement and to improve the quality of the pellets. The different types of binders that have been studied are discussed in section 2.10. Another way to improve the quality of the pellets, as reported by [87], is to mix the torrefaction condensate with torrefied biomass.

In this study, a new process configuration was developed to address the two above-mentioned issues: (1) detoxification of the torrefaction condensate, and (2) reducing the energy requirement for the pelletization of the torrefied biomass. Fig. 4.3 shows the process flow for an integrated approach to adsorption, AD and pelletization. The basic idea is to use part of the produced torrefied biomass as an adsorbent for the removal of inhibitory compounds from torrefaction condensate. Later, the same torrefied biomass will be mixed with the rest of the torrefied biomass before pelletization. During the adsorption process, the torrefied biomass adsorbs furans, phenolic compounds and water from the torrefaction condensate. Thus, it acts as a binding material and thereby reduces the energy requirement in the densification process. The proposed process can also improve the quality and durability of the torrefaction pellets.

During adsorption, the inhibitory compounds from the furan and phenolic groups in the torrefaction condensate can be reduced or removed. In this case, a major compound in the resulting torrefaction condensate will be an aqueous fraction rich in organic acids i.e. for example acetic acid. Thus, after detoxification the torrefaction condensate may be effectively used as an ideal feedstock for the AD process. The ultimate aim of this process was to improve the properties of the torrefied biomass pellets and to detoxify the torrefaction condensate without adding any external chemicals or materials.

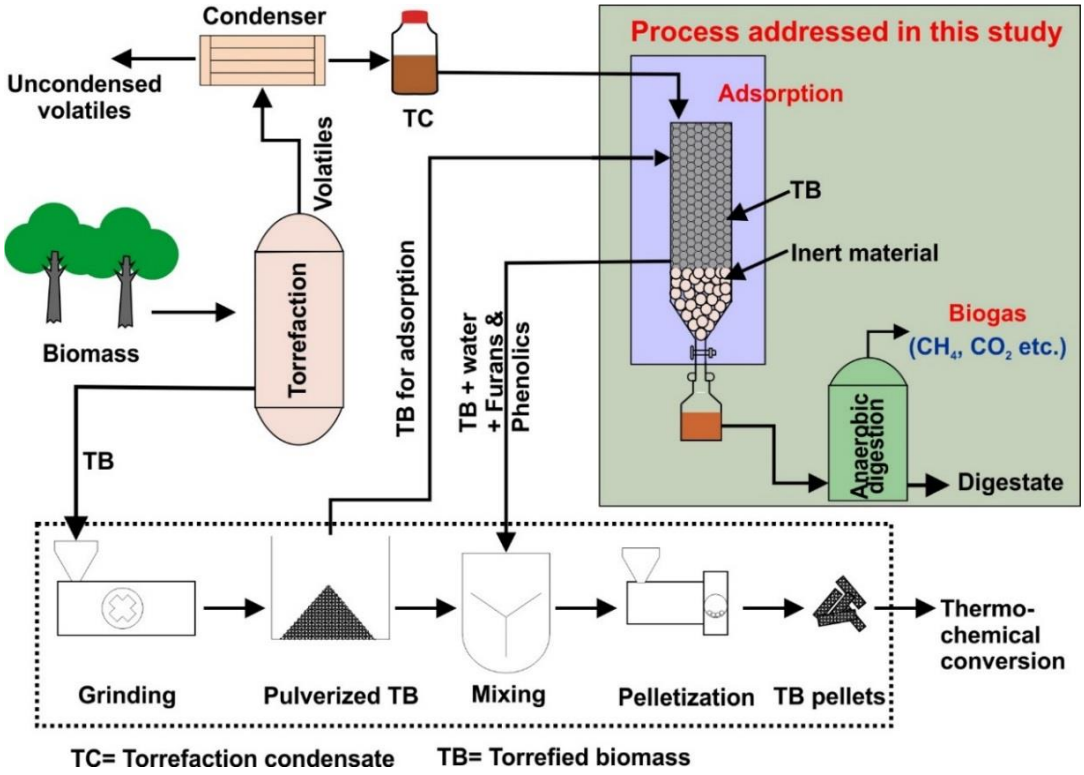

Fig. 4.3 Process flow of integrating torrefied biomass pelletization with adsorption and AD (paper III)

4.2 Experimental methods

4.2.1 Raw materials

The biomasses used in this thesis work was Eucalyptus clone E. urophylla (Timor) x E. camaldulensis (VM1) and Finnish pinewood. Their details were presented in Table 4.1.

Table 4.1 Details of the biomass used in this study.

Name	Supplied by	Description	Used in
Eucalyptus clone of E. urophylla (Timor) x E. camaldulensis (VM1). The trade name of this clone was "urocam"	Department of Forest Engineering, Federal University of Vicosa, Minas Gerais, Brazil	Debarked stem wood.	Paper I
Finnish Pinewood	Kuljetusliike Viikari Oy, Narva, Finland	Debarked Stem wood chips	Paper II and Paper III

A proximate analysis of the biomass selected for this thesis is presented in Table 4.2. A detailed compositional analysis of the eucalyptus clone can be found in [88,89]

Table 4.2 Proximate analysis (wt.%) of Eucalyptus clone ('urocam') and Finnish pine wood.

Biomass sample	Fixed Carbon	Volatiles	Ash	Reference
Eucalyptus clone	12.1	87.6	0.27	Adopted from [88]
Finnish Pinewood	13.4	82.5	4	Evaluated using TGA (Mettler Toledo TGA850 and following the methodology presented in [90].

4.2.2 Sample preparation

Initially, the biomass samples were dried in an air driven furnace at 105 ^{0}C for 24 h. The dried biomass samples were ground using a Retsch ZM 200 centrifugal mill. The grounded biomass was sieved to a particle size of 100 to 125 μm for the TGA and DSC experiments (paper I) in order to avoid the effects of internal heat transfer. A particle size of less than 100 μm was used in the adsorption experiments (paper III).

4.2.3 Torrefaction treatment

The torrefaction process was carried out with three different approaches. For the TGA studies, the torrefied biomass was produced in a Mettler Toledo TGA850. For each run, the furnace temperature was raised from 50 ^{0}C to 105 ^{0}C at 20 ^{0}C/min and kept at that temperature for 30 min to ensure complete drying. Then the reactor temperature was raised at 50 ^{0}C/min from 105 ^{0}C to one of the three selected torrefaction temperatures, i.e. 250 ^{0}C, 275 ^{0}C and 300 ^{0}C and kept at that temperature for 1 h. There was a nitrogen flow of 80 mL/min which created an inert environment and removed the released volatile gases. A sample size of about 7.5 mg in a 70 μL alumina oxide crucible was used.

For the DSC experiments, the torrefied biomass was produced in a tube furnace located in the university's (TUT) materials science department. The drying procedure was the same as with the TGA furnace. The torrefaction procedure would have been the same, but owing to the limitations of the equipment, the temperature of the biomass was raised at 20 ^{0}C/min instead of 50 ^{0}C/min. In each run, a sample size of 10 mg in a ceramic crucible was used for each run.

The torrefaction reactor system presented in Fig. 4.4 was used to produce torrefied biomass and torrefaction condensate for the experiments on

integrating torrefaction with AD (paper II and paper III). The main reactor and other components such as the volatiles, flow pipes and air-circulating coil were made of stainless steel. A detailed description of the reactor system was presented in paper II and in [91] . Briefly, 1 kg of previously oven-dried biomass was loaded into the reactor for each run. The temperature of the reactor was raised from room temperature to the torrefaction temperature at around 5 ^{0}C/min and kept at that temperature for 1 h. Initially, a nitrogen flow of 20 L/min was used to maintain the inert environment. Later, during the isothermal period N_2 flow was reduced to 5 L/min.

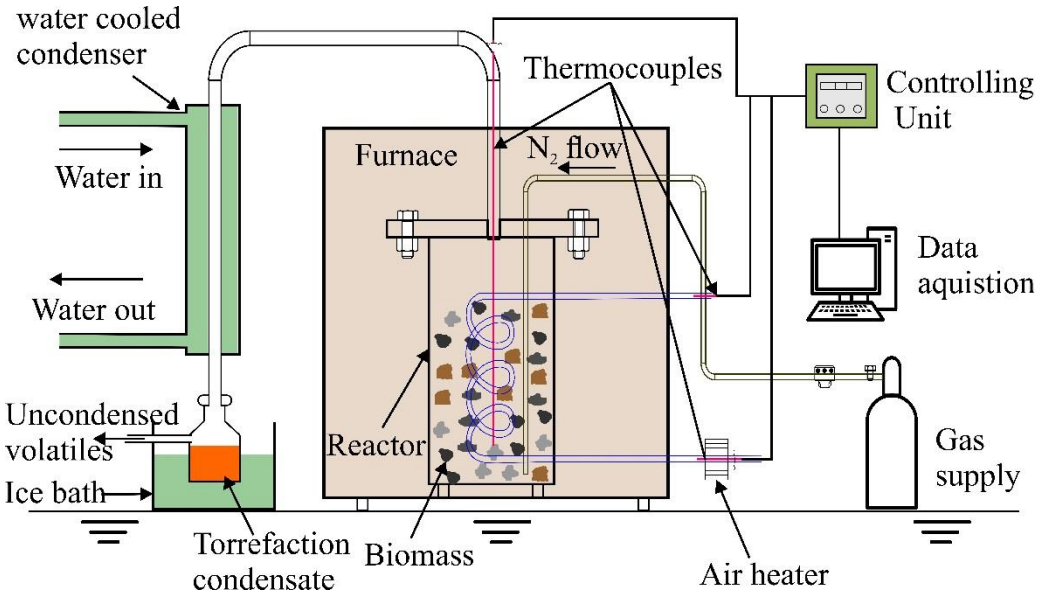

Fig. 4.4 The torrefaction reactor system used to produce torrefied biomass and torrefaction condensate (paper II)

The volatile gases were condensed using a water-circulated condenser that is connected with a glass bottle submerged in an ice-water bath. It should be noted that, because of the large sample volume and thickness of the wood chips, the sample temperature at some places in the reactor might deviate from the thermocouple reading. The torrefied biomass is stored in a closed container while the torrefaction condensate was stored at 4 ^{0}C to avoid further aging reactions.

4.2.4 TGA experiments

The pyrolysis of both the original and torrefied biomass was carried out in a Mettler Toledo TGA850. Initially, the samples were dried according to the procedure explained in section 4.2.3. Later, the TGA furnace temperature was raised from 105 ^{0}C to 700 ^{0}C at one of the selected heating rates, i.e. 5, 8, 12, 20 ^{0}C/min. Finally, the samples were kept at 700 ^{0}C for 40 min to ensure that pyrolysis was complete. The nitrogen flow was 80 mL/min. A sample of about 7.5 mg in a 70 µL alumina oxide crucible was used.

4.2.5 DSC experiments

The Mettler Toledo DSC821e was employed to carry out the DSC experiments. Samples (both dried and torrefied biomass) of 3.5 to 4 mg were loaded into 40 µl aluminum crucibles, and later sealed with a pierced lid. An empty crucible of the same size, i.e. 40 µl, was used as a reference material. A nitrogen flow of 50 cm^3/min was used to create the inert environment. The drying zone was same as for the TGA experiments (section 4.2.3). Because of the limitations of the equipment, the pyrolysis temperature was set at 500 ^{0}C. The temperature was raised from 105 ^{0}C to 500 ^{0}C at a heating rate of 20 ^{0}C/min.

4.2.6 AD batch assays of torrefaction condensate

Two different types of inoculums were used in this thesis work. These are pre-collected inoculums that were stored at 4 ^{0}C. The inoculum used in paper II was sludge from mesophilic (35 ^{0}C) and thermophilic (55 ^{0}C) anaerobic digesters from our laboratory. These digesters were operated at the respective temperature with pulp-paper industry sludge as a substrate. Before using the inoculum in the AD batch assays, they were incubated at the appropriate temperature for 48 h in order to allow them to adapt them to the mesophilic and thermophilic conditions.

In paper III, the inoculum used was granular sludge collected from the mesophilic up flow anaerobic sludge blanket (USAB) reactor that treats wastewater from an integrated plant, which produces Beta-amylase and ethanol (Jokioinen, Finland).

The bio-methane potential of torrefaction condensate was studied through batch experiments using 120 mL serum bottles at mesophilic and thermophilic conditions. The operating volume was 60 mL. The torrefaction condensate produced at 225 ^{0}C, 275 ^{0}C and 300 ^{0}C was used as a substrate (paper II). The substrate to inoculum ratios, i.e. $VS_{substrate}$:$VS_{inoculum}$ of 0.1, 0.2 and 0.5 were tested. A bottle with water and inoculum only was used as a blank to find out the methane yield from the inoculum. All the experiments were carried out in duplicate and the methane yield presented as mean. In case of paper III, the AD batch assays were carried out with original and detoxified torrefaction condensate produced at 300 ^{0}C.

4.2.7 Cyclic batch AD experiments

Cyclic batch experiment were carried out to better understand the type of inhibition that torrefaction condensate exerts on the inoculum. For the cyclic batch experiments, the initial setup was same as for the batch assays as explained in section 4.2.6. However, at selected intervals, the bottles with no gas production were diluted to approximately match the COD of 0.1 $VS_{substrate}$:$VS_{inoculum}$ loading. For dilution, the liquid phase from the batch assays was removed and then the same volume of water and the required amount of substrate were added. The cyclic batch experiments were carried out at 0.1, 0.2 and 0.5 $VS_{substrate}$:$VS_{inoculum}$ using torrefaction

condensate produced at 300 ^{0}C. Two intermittent points, i.e. after 30 days and 50 days were selected and the total operating time was 72 days.

4.2.8 Adsorption

The adsorption of furfural using torrefied biomass was studied at varied torrefied biomass dosages, i.e. 25, 50, 100 and 150 g/L. The batch adsorption experiments were carried out in a volume of 20 mL at room temperature (≈20 ^{0}C) and with continuous mixing at 150 rpm. An initial furfural concentration of 6000 mg/L at its initial pH 3.6 was selected. The isotherm studies were carried out by varying the initial concentration from 300 to 6000 mg/L at 50 g/L dosage. The selected residence time was 1, 2, 4, 6, 8, and 12 h. The effect of the pH was tested by varying it between 2 to 9 with an initial concentration of 6000 mg/L and torrefied biomass dosage of 100 g/L.

Batch adsorption studies of torrefaction condensate were carried out at torrefied biomass dosages of 25, 50, 100, 200 and 250 g/L of torrefied biomass. A sample volume of 10 mL was selected. The torrefaction condensate was used at its original pH. After adsorption, the solid liquid separation was achieved by centrifugation at 5018 Xg for 5 min. Supernatants were filtered using 0.45 μm (Chromafill® - PET 45/25) prior to gas chromatography mass spectrometer (GC-MS) analysis. All the experiments were carried out in duplicate.

4.3 Analytical methods

4.3.1 Characterization of torrefied biomass

The surface characteristics of the torrefied biomass were studied using scanning electron microscopy (SEM) and Brunauer–Emmett–Teller (BET) analysis. The SEM images of torrefied biomass were captured using JSM –T10 (Jeol, USA). The specific surface area (SSA) and pore size distributions were studied using a Micrometrics ASAP 2020 (Norcross, USA) by physical adsorption of N_2 following the methodology reported in [92]. Briefly, prior to adsorption with nitrogen, the contaminant gases were removed by evacuating the samples at 10 μm Hg at a temperature of 150 ^{0}C. The surface area and pore distribution were evaluated according to the BET and Baret-Yoymer-Halenda (BJH) models respectively.

4.3.2 Characterization of torrefaction condensate (paper II)

The chemical composition of the torrefaction condensate such as organic acids, aldehydes, methanol and Acetol were quantified at Nab labs Oy, Oulu, Finland (paper II). For that, the organic fraction extracted from the condensate with water was used to analyze the organic analytes. The Karl Fischer titration was used to estimate the water content. High-pressure liquid chromatography (HPLC), according to EPA 8315A was used to analyze the organic acids, acetaldehyde, formaldehyde, furfural and 5-HMF. Gas chromatography and headspace gas

chromatography with a mass spectrometer was used to analyze the methanol, Acetol and 2-hydroxyacetaldehyde.

The total solid (TS) and volatile solid (VS) content of the torrefaction condensate was studied using the APHA 2540 method. The chemical oxygen demand (COD) was analyzed according to APHA 5220D. The pH was measured using a TPS WP-81 pH meter.

4.3.3 Biogas analysis

The methane content in the biogas was measured using gas chromatography equipped with a flame ionization detector (Perkin Elmer, Clarus 500, USA). The standard gas composition of 50% CH_4 and 50% CO_2 was used to evaluate the methane concentration in the biogas through comparative analysis. The detector, oven and injector temperatures were 225 ^{0}C, 100 ^{0}C, and 230 ^{0}C respectively. The methane yield was presented as a cumulative methane yield and also as a specific methane yield per VS of torrefaction condensate added (mL CH4/g VS).

4.3.4 Analyzing torrefaction condensate for adsorption studies (paper III)

The analysis of standard furfural solution and torrefaction condensate before and after adsorption was carried out using (GC; Agilent series 6890) equipped with a mass spectrometry (MS) detector (Agilent 5975B). A capillary column HP-5MS (30 m, 0.25 mm ID, 0.25 μm film thickness; Agilent) was used. For the standard furfural solution, initially the GC-column was held for 2 min at 50 ^{0}C, and then temperature was raised to 250 ^{0}C at 5 ^{0}C/min. Later, the oven was heated to a final temperature of 280 ^{0}C at 10 ^{0}C /min and held for 10 min at that temperature. However, for the torrefaction condensate analysis the oven temperature was raised from 50 ^{0}C to 180 ^{0}C at a heating rate of 2 ^{0}C/min and then to a final temperature of 280 ^{0}C at 10 ^{0}C/min and then held there for 10 min. The sample injection volume was 0.2 μL with a split ratio of 1:20. Helium gas was used as a carrier gas with a flow rate of 1 mL/min. The injection port and MS temperature was maintained at 250 ^{0}C.

4.4 Process simulation (paper IV)

The experimental results from paper II were used to simulate industrial scale operations of 10 t/h of torrefied biomass pellets production integrated with AD.

4.4.1 Process description

The different process configurations considered in this thesis for the technical and economic evaluations were presented in Fig. 4.5. The major difference between the standalone torrefaction process (case 1) and the integrated approaches lays with the application of torrefaction volatiles. For the standalone torrefaction process, combustion of torrefaction volatiles along with wood chips to provide heat

energy for the drying and torrefaction units was considered. For integrated approaches (cases 2 and 3), the condensation of volatiles to produce torrefaction condensate and later producing biogas through AD of torrefaction condensate was considered. In these cases, combustion of un-condensed volatiles along with wood chips was considered to meet the required heat energy demand.

Again, the difference between case 2 and case 3 was with the end application of the biogas. In case 2, using biogas in a gas engine to produce electrical energy and heat energy was considered and in case 3 upgrading the biogas using high-pressure water scrubbing (HPWS) and pressure swing adsorption (PSA) to use it as a vehicle fuel was considered. The possible heat energy recovery options were also considered for both standalone and integrated approaches.

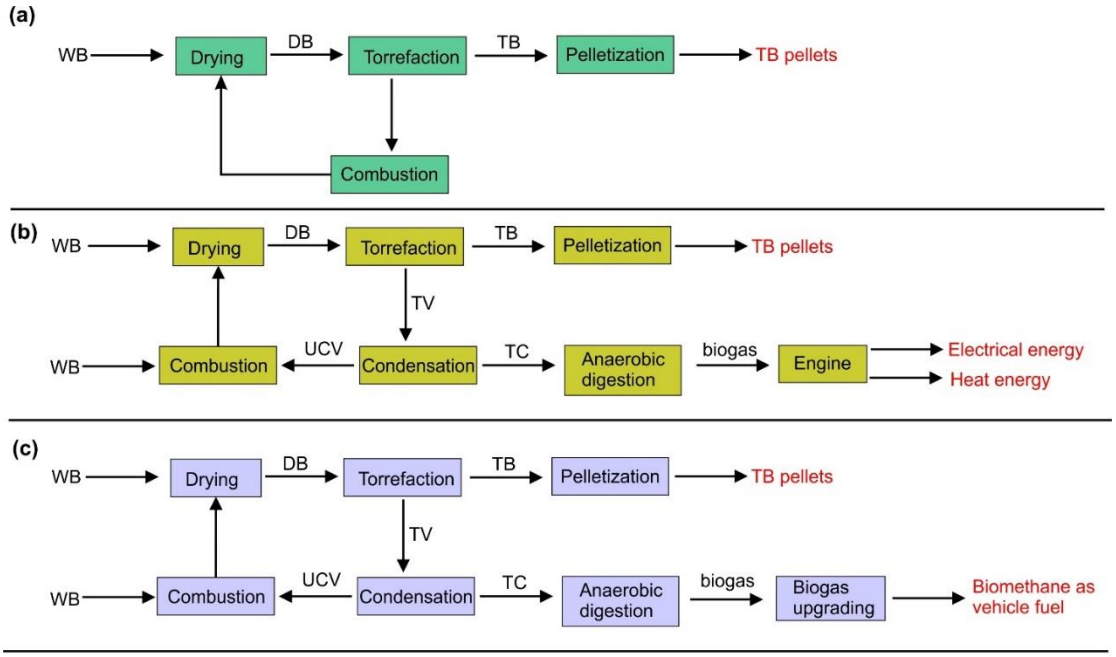

WB = Wet biomass, DB = Dried biomass, TB = Torrefied biomass TC = Torrefaction condensate, TV = Torrefaction volatiles, UCV = uncondensed volatiles, HPWS = High pressure water scrubbing, PSA = Pressure swing adsorption

Fig. 4.5. Different process configurations considered in this thesis for technical and economic evaluation. a) Case 1 (standalone torrefaction) (b) Case 2 (Torrefaction – AD_Engine), (c) Case 3 (Torrefaction –AD_Biomethane) (paper IV).

4.4.2 Process parameters

The operating characteristics of the drying and torrefaction processes are presented in Table 4.3. The wood chips with a moisture content and heating value of 40% and 10 MJ/kg respectively were considered as raw material for torrefaction process. Reducing the moisture content from 40 to 10 % during drying was considered. The total heat energy required at drying unit was calculated considering latent heat of evaporation of water and the sensible heat requirement of wood chips at dryer operating conditions.

Table 4.3 Properties and operating characteristics (paper IV)

Feedstock properties	Raw wood chips	After drying	After torrefaction
Moisture content (%)	40	10	0
Lower heating value (LHV) (MJ/kg)	10	16.5	22
Operating characteristics			
Dryer operating temperature (^{0}C)	150		
Torrefaction temperature (^{0}C)	300		
AD operating temperature (^{0}C)	35		
Engine exhaust gases temperature (^{0}C)	480		

The operating temperature of the torrefaction was selected as 300 ^{0}C. The yield of torrefied biomass, uncondensed torrefaction volatiles and torrefaction condensate was selected as 0.55, 0.2 and 0.25 kg/kg of dry wood chips respectively (based on paper II). The energy balance at torrefaction reactor was evaluated based on the equation (1). The loss of heat energy (radiative) was considered as 3% on the LHV of the dried biomass.

$$m_{DB} \times [LHV_{DB} + (Cp_{DB} \times T_{DB})] + Q_{in} = m_{TB} \times [LHV_{TB} + (Cp_{TB} \times T_{TB})] + m_{TV} \times [LHV_{TV} + (Cp_{TV} \times T_{TV})] + Q_{loss} \quad (1)$$

Where, m, LHV, C_p and T are the mass, lower heating value (kJ/kg), specific heat capacity (kJ/kg.K) and temperature and *DB*, *TB* and *TV* are the dried biomass, torrefied biomass and torrefaction volatiles respectively. Q_{in} is the heat energy input to the torrefaction reactor and Q_{loss} is the heat energy loss from the torrefaction reactor.

As reported in previous studies the heating value of the torrefied biomass varies from 19 – 24 MJ/kg depending on the torrefaction operating condition [20]. However, in this study a heating value of 22 MJ/kg of torrefied biomass was selected. The heating value of the torrefaction volatiles was calculated using the equation (2). It was assumed that the uncondensed gases mainly contain CO_2 and CO. The yield of CO_2 and CO was calculated based on the correlation presented by [93] i.e. the CO_2 and CO ratio is equal to 2.5.

$$LHV = \sum_{i=1}^{n} m_i . LHV_i \quad (2)$$

Where, 'i' denotes the major compounds present in the torrefaction volatiles.

4.4.4 Process flow for pellets production

The operational procedure for producing torrefied pellets from torrefied biomass reported by Kumar et al. [27] was followed in this study. Initially torrefied biomass is cooled to 50 ^{0}C and then ground. Preconditioning of torrefied biomass with 15% moisture was considered as a binding agent. The material loss at different stages during pelletization was negligible.

4.4.5 Anaerobic digestion

The operating parameters for the AD are presented in Table 4.4. The digester volume was calculated following the methodology presented by [94] and a design factor of 1.25 was selected to allow the calculation errors and safety. The Heat energy required at digester was calculated using equation (3) and (4) [95].

$$Q_{AD} = [m_{TC} \times Cp \times (T_2 - T_1)] + Q_{AD-loss} \quad (3)$$

$$Q_{AD-loss} = k_d \times A_D \times \Delta T_D \quad (4)$$

Where Q_{AD}, is the heat energy demand for AD, m_{TC} is the mass of the torrefaction condensate, Cp is the specific heat capacity of the torrefaction condensate, T_2 is the AD operating temperature, and T_1 is the torrefaction condensate inlet temperature. The Cp of the torrefaction condensate was selected as 2.8 kJ/kg-K [96]. Where, $Q_{AD-loss}$ is the heat loss at digester. k_d is the k-factor of the digester material, A_D is the surface area of the digester, and ΔT_D is the average temperature difference between the heating medium and the substrate (torrefaction condensate).

Table 4.4 Operating parameters selected for the process scale-up of anaerobic digestion

AD operating parameter	Selected value
Temperature (^{0}C)	35 ^{0}C
Organic loading rate	3 kg VS/m^3
Inlet temperature of the torrefaction condensate	20 ^{0}C
k-factor of the digester material k_d	0.5 W/m^2 ^{0}C
Outside wall temperature	-10 ^{0}C
Digester height to diameter ratio	0.5

The amount of electrical energy produced was calculated using equation 5 [97]. The energy potential of bio-methane was considered as 10 kWh of electricity.

$$E_{elc.} = V_m \, x \, 10 \, x \, \eta_{elc.} \quad (5)$$

Where, V_m is the volume of the methane produced, $\eta_{elc.}$ is the electrical efficiency of the biogas engine (considered to be 45% in this study) [98].

In case of biogas upgrading, the methane yield of 96% for both HPWS and PSA was considered. Currently no published data is available on the properties of the digestate that is produced during the AD of torrefaction condensate. However, the previous studies [96,99] and [100], have established that the release of nitrogen, phosphorous and potassium to the gas phase during the thermal treatment of biomass at 300 ^{0}C is limited. This implies that, the possibilities for the application of digestate, as a fertilizer is limited. Thus, in this study the digestate was considered as wastewater that needed to be treated.

4.4.6 Energy recovery

In this thesis work, the heat energy recovery possibilities with in the torrefaction process were also presented with an aim of improving the overall thermal efficiency and generating additional revenue to improve the economic feasibility of the process. Three different possibilities were considered for heat energy recovery such as from: 1) biogas engine (flue gases, water jacket, and lube oil), 2) dryer exhaust gases and 3) torrefaction products cooling. However, the combination of these heat energy recovery options are different for different cases studied. The combination of heat energy recovery options for different cases were as presented in Table 4.5.

Table 4.5 The combination of heat energy recovery options for different cases.

Heat energy recovery from	Case 1	Case 2	Case 3
Dryer exhaust gases	✓	✓	✓
Torrefied biomass cooling	✓	✓	✓
Torrefaction volatiles cooling	×	✓	✓
Biogas engine	×	✓	×

It was considered that the engine's exhaust gases temperature was reduced from 485 ^{0}C to a stack temperature of 135 ^{0}C. Previously [101], different process configurations for heat energy recovery from biomass dryer exhaust gases have been reported. However, in this study the recovered heat energy from dryer exhaust gases was considered for district heating and air preheating. It was assumed that combustion air is preheated from 10 ^{0}C to 50 ^{0}C. It was considered that torrefaction products are cooled to 50 ^{0}C in two stages. Initially from 300 ^{0}C to 95 ^{0}C and later from 95 ^{0}C to 50 ^{0}C. The high-grade heat energy recovered from torrefaction product cooling (when cooled from 300 ^{0}C to 95 ^{0}C) was considered for district heating. The heat energy requirement at AD could be meet by using the low-grade heat energy from torrefaction volatiles cooling (when cooled from 95 ^{0}C to 50 ^{0}C). The district heating water operating temperatures were selected as 60 ^{0}C and 90 ^{0}C for the inlet and outlets respectively. A process modeling software Aspen hysys® was used to simulate the heat energy recovery.

4.5 Economic analysis

4.5.1 Capital costs

The cost of the main items of equipment were taken from the literature [27,62]. However, these values were converted specifically for this thesis to account for the plant operating capacity and the required equipment size using equation (6).

$$C = C_0 \times (\frac{A}{A_0})^n \quad (6)$$

Where C and A are the cost and capacity of the present equipment and C_0 and A_0 are the cost and capacity of the basic equipment respectively; n represents the scaling factor in this study, which was 0.6.

Later, the equipment cost were converted to current costs with the chemical engineering plant cost index (CEPCI) data of June 2017 and using equation (7).

$$Cost_{year\ X} = Cost_{Year\ Y} \times \frac{CEPCI_Y}{CEPCI_X} \quad (7)$$

According to [102], the cost of the AD digester varies from 300 to 500 USD/m^3, so in this study a value of 400 USD/m^3 was used. The fixed capital investment on equipment (CIE) was calculated by adding up all the major equipment costs. Other capital costs taken into account include startup expenses (10% of CIE), engineering and supervision (12% of CIE) and contingency (10% of CIE). The total fixed capital investment (FCI) was the sum of the CIE and the other capital expenses.

4.5.2 Production costs

Utilities and other specific costs presented in Table 4.6 were used to evaluate production costs. It was assumed that the plant operates for 7920 hours per year (330 days, 24 h a day) with three 8 h shifts per day. The correlations presented in [103] were used to evaluate the operating costs, such as factory overheads and administration and the marketing and distribution costs. The cost of depreciation of assets was calculated using the straight-line method for a period of 10 years [103].

Table 4.6 Cost parameters considered for the calculation of production costs.

Utility	Cost (€)	Reference
Wet wood chips (forest) (€/MWh)	17.5	[104]
Electrical energy purchasing price (€/MWh)	100	[20]
Steam as binding agent (€/t)	22	[103]
Wages (€/hour)	14	
Expenses on the supervising staff	15 % of operating labor expenses	[103]
Maintenance and repair cost	4% of FCI	[103]
Wastewater treatment costs	1.2 €/m^3	[105]

4.5.3 Profitability and sensitivity analysis

The selling price information presented in Table 4.7 was used to evaluate the economic performance of the process configurations presented in Fig. 4.5 using NPV and IRR. The NPV was calculated using equation (8). The IRR (%) value was calculated by solving iteratively from equation (8), for such i value the NPV becomes zero.

$$NPV = \left(\frac{(1+i)^n - 1}{i \times (1+i)^n} \times net\ cash\ flow\right) - TCI \quad (8)$$

Table 4.7 Cost parameters considered for the calculation of production costs.

Utility	Cost (€)	Reference
Electrical energy selling price (€/MWh)	83.5	[106]
District heat selling price (€/MWh)	60	[20]
Bio-methane selling price (€/m3)	1.18	[107]

The minimum selling price of the torrefied biomass pellets is vital for evaluating the economic feasibility of torrefaction integrated with AD. For that, the minimum selling price of the torrefied pellets was calculated using the following equations (9 to 11).

$$TR = PC + ROI + IT \quad (9)$$

$$ROI = CRF \times TCI \quad (10)$$

$$IT = Taxation\ rate \times (TR - PC - D) \quad (11)$$

Where TR is the total revenue (€), PC is the total production cost (€), ROI is the return on investment (€), IT is the income tax (€), CRF is the capital recovery factor calculated using equation (12) TCI is the total capital investment and D is the depreciation amount (€).

$$CRF = \frac{i \times (1+i)^n}{(1+i)^n - 1} \quad (12)$$

A Sensitivity analysis was carried out by varying the input parameters such as TCI, working capital, cost of wood chips, selling price of the products (Table 4.7) in the range of ± 25% from the base values.

4.6 Pyrolysis kinetic modeling

The devolatilization of lignocellulosic biomass can be represented with a single-step endothermic reaction as presented in equation (R1) [108].

$$\text{Solid Biomass} \xrightarrow{k} \text{Char + Volatiles} \quad (R1)$$

Where k is the global apparent rate constant and can be represented by the Arrhenius equation as,

$$k(T) = A\ exp\left(\frac{-E_a}{RT}\right) \quad (13)$$

Where 'T' is the absolute temperature (K), 'R' is the universal gas constant (J/K. mol), 'A' is the frequency factor or pre-exponential factor (min-[1]), and 'E_a' is the activation energy.

According to [109], the reaction rate equation for a solid-state decomposition reaction depends on several factors such as the rate of nuclei formation, the geometry of the solid particles and diffusion phenomena. There have been several mathematical models (presented in Table 4.8), which represent these factors for solid-state reactions kinetics.

The basic rate equation under isothermal conditions can be expressed as equation (14).

$$\frac{d\alpha}{dt} = k(T) \cdot f(\alpha) \qquad (14)$$

Where $\frac{d\alpha}{dt}$ is the reaction rate, $k(T)$ is the rate constant and $f(\alpha)$ is a conversion function which represents the reaction mechanism. α is the extent of reaction (-) and it can be defined as the amount of material decomposed in mass fraction as,

$$\alpha = \frac{m_o - m_t}{m_o - m_f} \qquad (15)$$

where, m_0 is the initial mass of the sample, m_t is the mass of the material present at time 't' and m_f is the final residual mass of the material.

Table 4.8 Differential $f(\alpha)$ and integral form $g(\alpha)$ of commonly employed solid state reaction models [109]

Model	$f(\alpha) = \frac{1}{k}(\frac{d\alpha}{dt})$	$g(\alpha) = kt$
Reaction order models		
First order (F1)	$1-\alpha$	$-\ln(1-\alpha)$
Second order (F2)	$(1-\alpha)^2$	$(1-\alpha)^{-1}-1$
Third order (F3)	$(1-\alpha)^3$	$0.5[(1-\alpha)^{-1}-1]$
Diffusion models		
1-D diffusion (D1)	$\frac{1}{2}\alpha$	α^2
2-D diffusion (D2)	$[-\ln(1-\alpha)]^{-1}$	$[(1-\alpha)\ln(1-\alpha)]+\alpha$
3-D diffusion (D3)	$3(1-\alpha)^{\frac{2}{3}}/2(1-(1-\alpha)^{\frac{1}{3}})$	$[1-(1-\alpha)^{\frac{1}{3}})]^2$
Geometrical contraction models		
Contracting area (R2)	$2(1-\alpha)^{1/2}$	$1-(1-\alpha)^{1/2}$
Contracting volume (R3)	$3(1-\alpha)^{2/3}$	$1-(1-\alpha)^{1/3}$

Combining equations (13) and (14), equation (14) becomes

$$\frac{d\alpha}{dt} = A\exp\left(-\frac{E_a}{RT}\right)\cdot f(\alpha) \qquad (16)$$

The integral from of the rate equation can be represented using equation (17).

$$g(\alpha) = kt \quad (17)$$

In case of non-isothermal conditions, the rate equation (16) can be expressed through equation (18).

$$\frac{d\alpha}{dT} = \left(\frac{A}{\beta}\right) \cdot \exp\left(-\frac{E_a}{RT}\right) \cdot f(\alpha) \quad (18)$$

where β is the linear heating rate $\left(\frac{dT}{dt}\right)$.

In general the terms 'E_a', 'A ' and $'f(\alpha)'$ in equation (18) are called as kinetic triplets. Several mathematical models have been developed to evaluate these parameters. These models are basically divided into model-fitting and model-free methods. The Model-free methods are also designated as iso-conversional methods. These kinetic models can also be classified as differential and integral methods based on the approach used in their development [109].

Integrating equation (18) with the limits of $0\ to\ \alpha$ and $T_0\ to\ T$ gives equation (19)

$$g(\alpha) = \frac{A}{\beta} \int_0^T e^{-\frac{E_a}{RT}} dT \quad (19)$$

The temperature integral in equation (19) i.e. $\int_0^T e^{-\frac{E_a}{RT}} dT$ does not have any analytical solution and it must be evaluated through approximation.

4.6.1 Kinetic models

The kinetic models presented in Table 4.9 were used to evaluate the kinetic parameters of pyrolysis. The Coats-Redfern model-fitting method and commonly-used model free methods such as Friedman, Flynn-Wall-Ozawa (FWO) and Kissinger-Akahira-Sunose (KAS) were used.

Table 4.9 Kinetic models used to evaluate the kinetic parameters of pyrolysis

Model	Equation	Plot	Reference
Coats-Redfern	$\ln\left(\frac{g(\alpha)}{T^2}\right) = \ln\left[\frac{AR}{\beta E}\left(1 - \frac{2RT}{E_a}\right)\right] - \frac{E_a}{RT}$	$\ln\left(\frac{g(\alpha)}{T^2}\right)$ versus $\frac{1}{\mathrm{T}}$	[109]
Friedman	$\ln\left[\beta\left(\frac{d\alpha}{dT}\right)\right]_\alpha = \ln[A\, f(\alpha)] - \frac{E_a}{RT_\alpha}$	$\ln\left[\left(\frac{\mathrm{d}\alpha}{\mathrm{dt}}\right)\right]_\alpha$ versus $\frac{1}{T_\alpha}$	[109]
Flynn-Wall-Ozawa (FWO)	$(\log\beta)_\alpha = \log\left(\frac{AE_a}{R\, g(\alpha)}\right) - 2.315 - 0.4567\ \frac{E_a}{RT_\alpha}$	$(\log\beta)_\alpha$versus $\frac{1}{T_\alpha}$	[109]
Kissinger-Akahira-Sunose (KAS)	$\ln\left(\frac{\beta}{T_\alpha^2}\right) = \frac{-E_a}{R}\left(\frac{1}{T_\alpha}\right) - \ln\left[\left(\frac{E_a}{AR}\right)\int_0^\alpha \frac{d\alpha}{f(\alpha)}\right]$	$\ln\left(\frac{\beta}{T_\alpha^2}\right)$ versus $\frac{1}{T_\alpha}$	[108]

4.6.2 Evaluating pre-exponential factor (A) and reaction mechanism

The activation energy values for the model-free methods are calculated without having any knowledge of the reaction models, i.e. $f(\alpha)$. Thus, it is not recommended to evaluate the pre-exponential factor (A) directly from model-free methods. However, there were several approaches developed in the literature for evaluating the pre-exponential factor and the reaction mechanisms. More detailed information on some of those methods can be found in [110,111]. This thesis used two different approaches, i.e. master plots and the kinetic compensation effect (KCE) to evaluate 'A' and the pyrolysis reaction mechanism.

4.6.3 Integral master plots

In the master plots method the experimental master plots for different reaction models are drawn based on the kinetic data calculated from TGA experiments. These curves are compared with theoretical master curves of different reaction models to identify the reaction mechanism. For this reduced master plots with a reference point at α=0.5 are used, as shown in equation (20) [110,111].

$$\frac{g(\propto)}{g(0.5)} = \frac{p(x)}{p(x)_{0.5}} \tag{20}$$

where $p\ (x)$ is the temperature integral at α=0.5.

Equation (20) can be derived upon applying the Coats-Redfern approximation to the equation (19).

$$\frac{g(\propto)}{g(0.5)} = \frac{exp(-E_a/RT)T^2}{exp(-E_a/RT_{0.5})T_{0.5}{}^2} \tag{21}$$

The reduced theoretical curves for different reaction models at a varied α value can be calculated from the left hand side of the equation (21). At the same time, the experimental reduced curves can also be produced with calculated E_a values using the right side of the equation (21) [111].

4.6.4 Kinetic compensation effect (KCE)

KCE can be described through equation (22), which represents the co-relation between kinetic parameters such as activation energy 'E_a' and 'A' [110,112].

$$\ln A_i = a + bE_i \tag{22}$$

From the equation (22), it can be observed that if there is a change in the E_a value then there will be a compensatory change in the 'A' values. The linear plot between ln (A) versus E_a represents the existence of KCE. For that, the kinetic parameters calculated from model-fitting methods can be used and in this thesis, the Coats-Redfern method was used. Initially the constants 'a' and 'b' are evaluated from the plot of ln (A) versus E_a. Later, the 'A' can be calculated from equation (22) using E_a values from the model-free methods (in this study the Friedman model was used). Once $E_\propto$ and $A_\propto$ are known, then the conversion function $f(\alpha)$ can be evaluated at

the respective α values using equation (16). Finally, the procedure followed for integral master plots (section 4.6.3) can be used to identify the reaction mechanism, i.e. comparing the theoretical $f(\alpha)$ curves with the experimental $f(\alpha)$ curves. In this study, a total of eight reaction models presented in Table 4.8 were used.

4.7 Adsorption kinetics

The kinetics of the furfural adsorption on torrefied biomass was studied using pseudo first order and second order kinetic models following the equations presented in Table 4.10.

Table 4.10 Models used to evaluate the kinetics of furfural adsorption on torrefied biomass

Kinetic model	Equation	Plot	Reference
pseudo first-order	$\log(q_e - q_t) = \log q_e - \frac{k_f}{2.303} t$	log (q_e-q_t) versus t	[113]
pseudo second-order	$\frac{t}{q_t} = \frac{1}{k_s q^2{}_e} + \frac{1}{q_e} t$	q_t/t versus t	[113]

According to [114] the adsorption process proceeds with four different steps 1) bulk solution transport i.e. external mass transfer 2) external diffusion i.e. boundary layer diffusion, 3) intra-particle diffusion and 4) adsorption. However, the rate of the overall adsorption process could be controlled either by one step and/or a combination of steps [115]. In this study, the rate-limiting step was identified using the kinetic models presented in Table 4.11.

Table 4.11 Kinetic models used to identify the rate-limiting step during furfural adsorption on torrefied biomass.

Kinetic model	Equation	Plot	Reference
Mass-transfer	$\frac{d(\frac{C_t}{C_0})}{dt} = -\beta_L S$	C_t/C_o versus t	[116]
Intra-particle diffusion	$q_t = k_{id}\, t^{1/2} + C$	q_t versus $t^{1/2}$	[115]
Boyd's diffusion model	$ln\left[\frac{1}{(1 - F^2\,(t))}\right] = \frac{\pi^2 D_e t}{r^2}$	$ln\left[\frac{1}{(1-F^2\,(t))}\right]$ versus t	[115]
Bangham's model	$log\ log\left[\frac{C_o}{C_0 - q_t\, m}\right] = \log\left(\frac{k_b\, m}{2.303\, V}\right) + \alpha \log(t)$	$log\ log\left[\frac{C_o}{C_0 - q_t\, m}\right]$ versus $\log(t)$	[115]

5 Results and discussion

This chapter summarizes the main results of the research carried out for this thesis. When needed, the original publications are referred to with Roman numerals, i.e. I, II, III, IV.

5.1 Torrefaction product distribution

After one hour of torrefaction at 225, 275 and 300 ^{0}C respectively, the torrefied biomass yield was 82, 75 and 55 wt.%, while the condensate yield was 7, 18 and 25 wt.% respectively. The uncondensed volatiles yield was calculated by a difference (100% - [solid yield (%) + condensate (%)]). The uncondensed gases yield was 11, 7, 20 wt.% for 225, 275 and 300 °C respectively. The product yield reported in this study is in accordance with that of other studies on the torrefaction of woody biomass. For example, [117] reported a torrefied biomass yield of 77% for hardwood chips torrefied at 250 ^{0}C for 45 min. Fagernas et al. [28] reported a yield of 29 wt.% of torrefaction condensate when spruce biomass was torrefied at 300 ^{0}C for 1 h residence time. In another study [118] reported a yield of 16.14 wt.% of torrefaction condensate for pine wood torrefaction at 300 ^{0}C for 40 min.

5.2 Characterization of torrefaction products

5.2.1 Characterization of torrefied biomass

The SEM images and BET surface area of pine wood biomass torrefied at 225, 275 and 300 ^{0}C was presented in Fig. 5.1 and Table 5.1 respectively. The BET analysis shows that biomass torrefied at 225 ^{0}C has no specific surface area (SSA) and pore diameter. However, further increasing the temperature to 275 ^{0}C and 300 ^{0}C resulted in a SSA of 1.47 m^2/g and 1.10 m^2/g respectively. The reason for no SSA at 225 ^{0}C could be the partial degradation of hemicellulose and the release of H_2O and CO_2 [119]. However, the further degradation of hemicellulose, cellulose and lignin happens when torrefaction temperature is further increased and this leads to the formation of micro pores [68,119]. The existing pores are enlarged when torrefaction temperature further increased to 300 ^{0}C and this could be the reason for the reduced SSA at 300 ^{0}C of torrefaction temperature.

In this study, N_2 adsorption was considered to evaluate the surface area of the torrefied biomass. According to [120], biomass samples treated at low temperatures may shrink during N_2 adsorption, which can lead to experimental errors in the surface area measurement. Therefore, CO_2 adsorption could be a better approach to measuring the surface area of torrefied biomass. For example, [121] observed a surface area of 1.53 m^2/g for rice straw torrefied at 300 °C in the case of N_2 adsorption, while at the same torrefaction temperature, a surface area of 39.71 m^2/g was observed in the case of CO_2 adsorption.

Table 5.1 BET surface analysis of torrefied biomass produced at different torrefaction temperatures (paper III).

Torrefaction temperature (^{0}C)	Specific surface area (m^2/g)	Pore Volume (cm^3/g)	Mean pore diameter (nm)
225	Nd	No pores	_
275	1.47	0.0065	17.8
300	1.10	0.0043	15.7

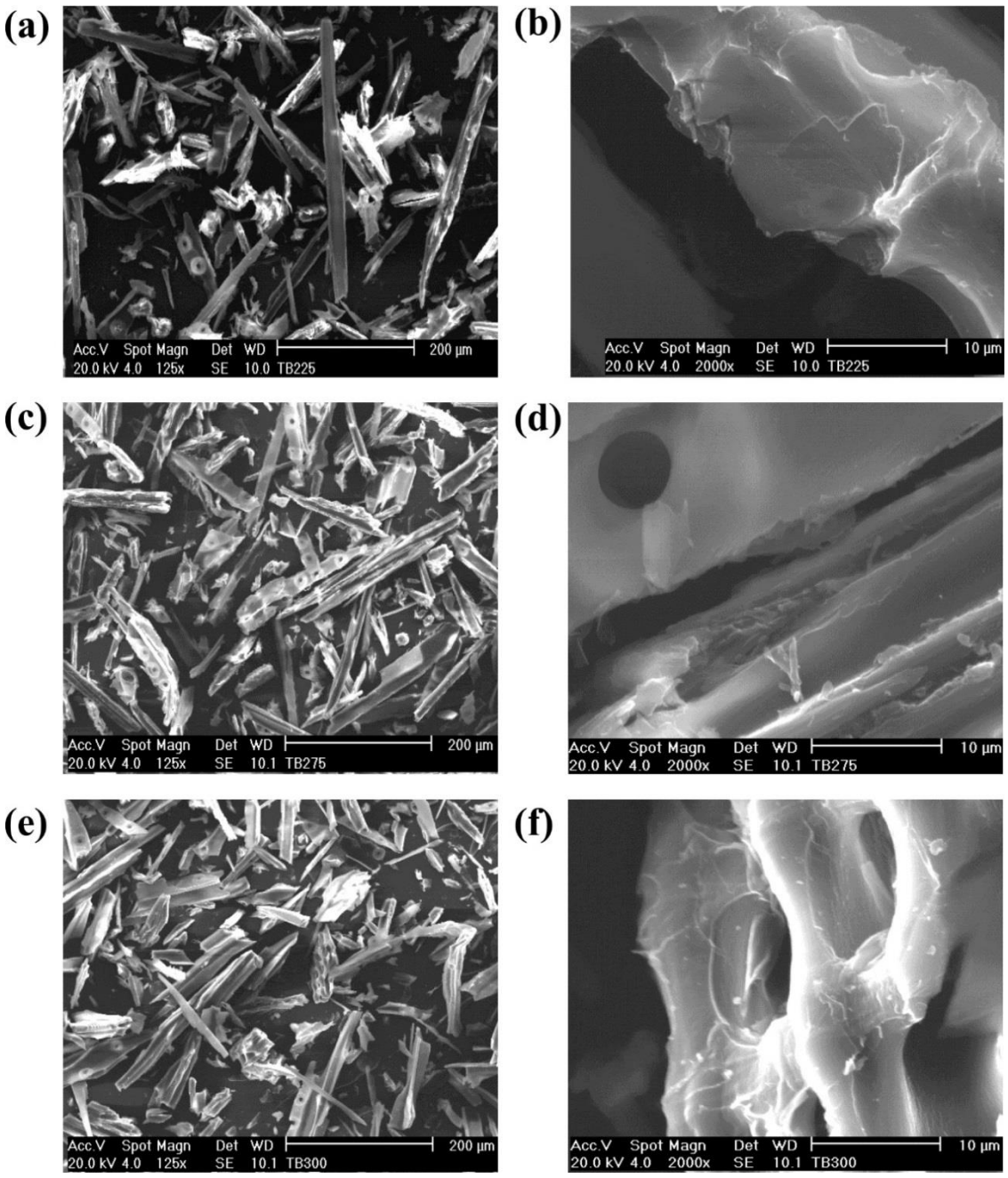

Fig. 5.1. Different resolution SEM images of torrefied biomass produced at different temperatures, (a - b) 225 ^{0}C, (c - d) 275 ^{0}C, (e – f) 300 ^{0}C. The red arrows show the pores within the torrefied biomass (paper III).

5.2.2 Characterization of torrefaction condensate

Torrefaction condensate contains number of different compounds. These are generally grouped into organic acids, aldehydes, and phenolic compounds. However, for this thesis, Table 5.2 shows the quantities of organic acids, methanol, aldehydes, acetol and water for pinewood torrefaction condensate. Apart from water, of the identified compounds, acetic acid is one of the most abundant compounds.

Table 5.1 Composition of torrefaction condensate produced at various temperatures (paper II).

Organic compounds		Compositions (wt.%)		
		225 °C	275 °C	300 °C
Organic acids	Acetic acid	3.08	5.60	5.40
	Lactic acid	0.62	1.30	1.80
	Formic acid	1.20	1.00	1.90
	Propionic acid	0.01	0.01	nd
Aldehydes	Formaldehyde	0.10	0.50	0.20
	Acetaldehyde	<0.01	0.16	0.02
	Furfural	0.26	0.79	0.55
	Hydroxymethylfurfural	0.31	0.37	0.50
Others	Methanol	0.44	1.59	1.35
	Acetol	<0.01	<0.01	<0.01
	Water	84	73	58
	Unidentified	9,94	15,7	30,28
	Total	100	100	100
	pH	2.21	2.19	2.26
	VS (%)	6.61	13.64	17.22

According to [30], the water in torrefaction condensate comes from two different sources, one from the evaporation of freely-bound water and the other from the water resulting from the dehydration and condensation reactions. In this study, the water content varied from 84, 73, and 58 wt.% for the torrefaction condensate produced at 225 ^{0}C, 275 ^{0}C and 300 ^{0}C respectively. Acetic acid is the main organic compound present in torrefaction condensate. It comes mainly from the cleavage of the acetoxy-methoxy groups present in the hemicellulose. In this study, the acetic acid concentration varied from 3 to 5 wt.%, over a temperature range of 225 ^{0}C to 300 ^{0}C. However, the concentration of acetic acid in torrefaction condensate varies significantly according to the type of biomass. For example [29] reported acetic acid concentration of 8.77 wt.% and 17.65 wt.% for pea hay and Arundo donax biomass

under the same torrefaction conditions i.e. 310 ^{0}C and 7.15 min. Of the aldehydes, furfural and 5-HMF are the major compounds. Their concentrations varied between 0.25 to 0.7 wt.% and 0.3 to 0.5 wt.% respectively. The methanol concentration was between 0.4 and 1.6 wt.%. The GC-MS analysis (paper III) showed that torrefaction condensate also contains several phenolic compounds, such as coniferyl aldehyde, guaiacol, vanillin and cresol.

The VS of the torrefaction condensate was around 7, 14, and 17% respectively for condensate produced at 225 ^{0}C, 275 ^{0}C and 300 ^{0}C. Previously, [28] has reported that increasing the torrefaction temperature from 240 ^{0}C to 300 ^{0}C resulted in an increase in total organic content from 2.4 to 29.2 wt.% respectively.

5.3 Influence of torrefaction treatment on biomass pyrolysis (paper I)

5.3.1 Thermogravimetric analysis of pyrolysis

The TG and DTG curves of dried and torrefied biomass pyrolysis at 20 ^{0}C/min are presented in Fig. 5.2. The major difference between dried and torrefied biomass pyrolysis was with the active pyrolysis temperature range. For torrefied biomass, the pyrolysis started at higher temperatures and the rise in temperature was directly proportional to the torrefaction temperature. The observed pyrolysis starting temperatures were 262, 308, 323 and 330 ^{0}C for DEC, TB250, TB275 and TB300 respectively at 20 ^{0}C/min heating rate. However, the end temperature of 400 ^{0}C was similar for all the samples. Fig. 5.2 shows that DEC pyrolysis has two peaks, at 301 ^{0}C and 307 ^{0}C. According to previous studies [108], the first peak at 301 ^{0}C represents the decomposition of the hemicellulose. However, for the pyrolysis of torrefied biomass the left-hand peak (at 310 ^{0}C) has disappeared. The reason for the difference in the DTG curves for dried and torrefied biomass can be attributed to the degradation of hemicellulose during the torrefaction process.

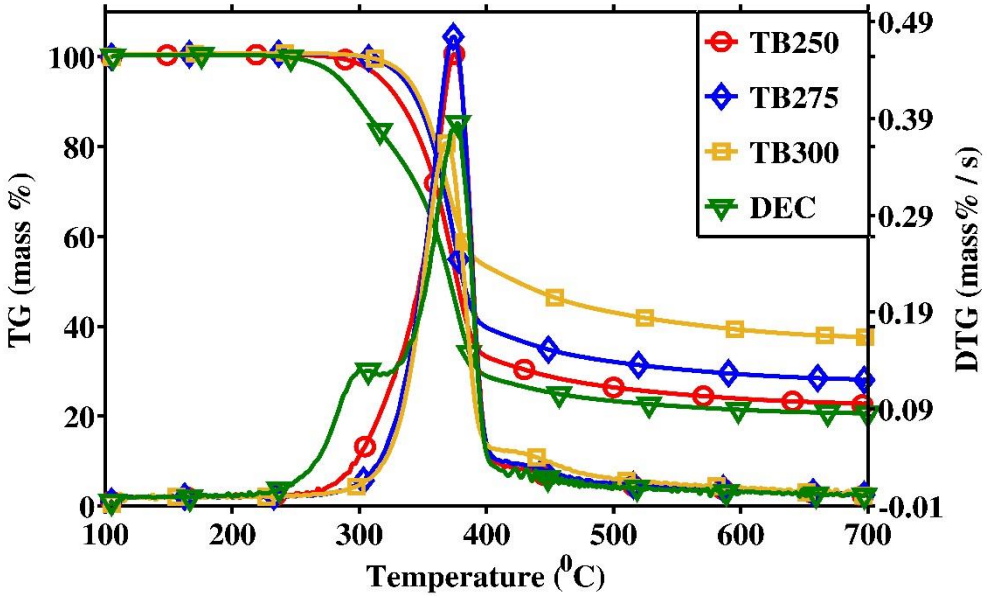

Fig. 5.2. TG and DTG curves of dried and torrefied pyrolysis at 20 ^{0}C/min (paper I).

5.3.2 Kinetic analysis

The apparent activation energy values for a conversion range of 0.1 – 0.8 for DEC and TB300 are reported in Fig. 5.3. The average E_a values for DEC were 184, 183 and 185 kJ/mol for FWO, KAS and Friedman respectively. In the case of the torrefied biomass, for TB300 the E_a values were 188, 193, 209 kJ/mol for FWO, KAS and Friedman respectively.

Fig 5.3 shows that dried biomass pyrolysis has lower E_a values than for the pyrolysis of TB300. For example, at α=0.1 the E_a values were 165 and 179 kJ/mol for DEC and TB300 respectively. This variation in the activation energy could be because of the degradation of the hemicellulose during torrefaction. As the highly reactive hemicellulose has already been degraded during torrefaction, the torrefied biomass requires more energy to start the pyrolysis reactions. Fig. 5.3 shows that there were considerable variations in the E_a values between DEC and TB300 at the end of the pyrolysis. This could be because of the degradation of the altered lignin structure. The lignin content in torrefied biomass increases significantly in comparison with dried biomass (because of the relative change in the concentration of the biomass components). In the literature, [34] reported that the lignin content increased from 17.6 % to 51.7% when biomass is torrefied at 300 ^{0}C. According to [122] the E_a values for lignin pyrolysis vary from 237 to 266 kJ/mol and in this study the observed E_a values at the end of the pyrolysis were 240 – 270 kJ/mol.

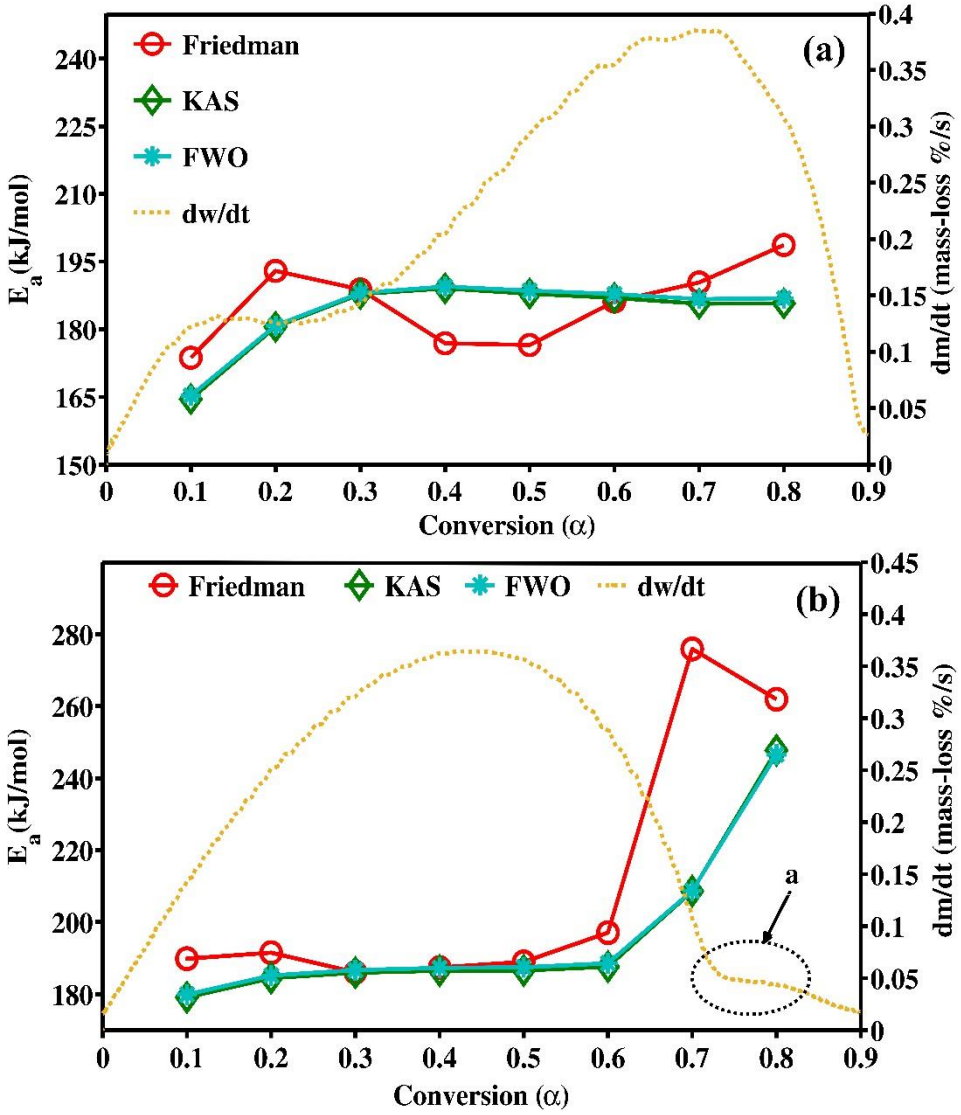

Fig. 5.3 Activation energy (Ea) vs. Conversion (α) for dried and torrefied biomass (a) DEC (b) TB300 (paper I).

In earlier studies, [88] reported E_a values in the range of 120 - 150 kJ/mol for the non-isothermal pyrolysis of the Eucalyptus clone. In another study [123] reported E_a values of 186 and 188 kJ/mol for raw and torrefied (270, 5 min) Douglas fir biomass pyrolysis respectively.

5.3.3 Influenced on the reaction mechanism

According to [124], the variation of E_a values with respect to α represents the presence of a multistep reaction mechanism. From Fig. 5.3 it can be observed that the E_a values vary with α, which shows that the pyrolysis of DEC and TB300 are proceeding with a multistep reaction mechanism. In this thesis, the influence of torrefaction treatment on the pyrolysis reaction mechanism was identified by making a comparative analysis between dried biomass and biomass torrefied at 300 ^{0}C.

Figure 5.4 shows the theoretical and experimental integral master plots of DEC and TB300. The plots are constructed using equation (21) with the average E_a values of the FWO method, i.e. 184 and 196 kJ/mol for dried and torrefied biomass respectively. The Fig. 5.4 shows that for DEC, the experimental curve is close to the theoretical plots of diffusion models (D1, D2 and D3) when $\alpha < 0.6$, and close to the reaction order models when $\alpha > 0.6$ respectively. For TB300, the experimental curve is close to the first order reaction model and the diffusion models when $\alpha < 0.5$ and $\alpha > 0.5$ respectively.

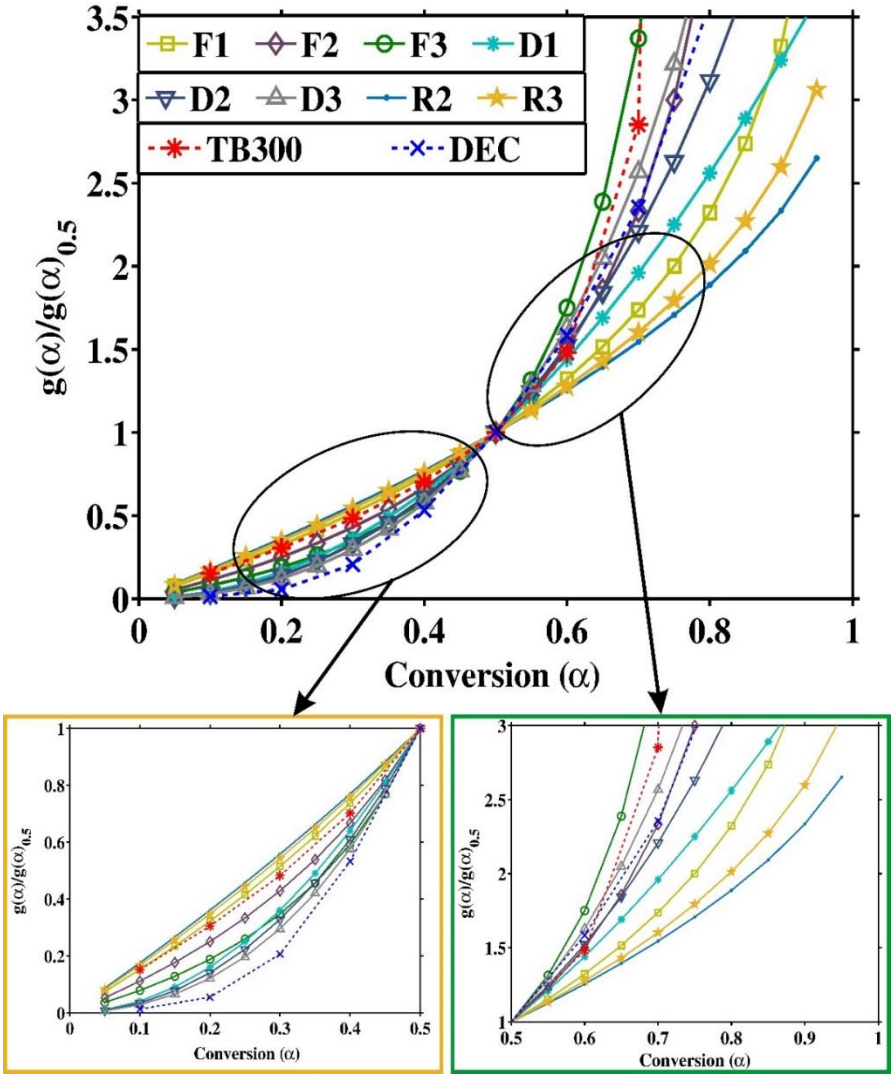

Fig. 5.4. Theoretical and experimental master plots (g (α)/g (α) 0.5 vs. conversion (α)) for DEC and TB300. (Check Table 4.8 for abbreviation) (paper I).

When the E_a values are broadly constant, the model fitting methods can be applied to the same conversion range[110]. Taking this into consideration, and using the information from Fig. 5.3, the Coats-Redfern plots for DEC and TB300 were divided into three regions as shown in Fig. 5.5.

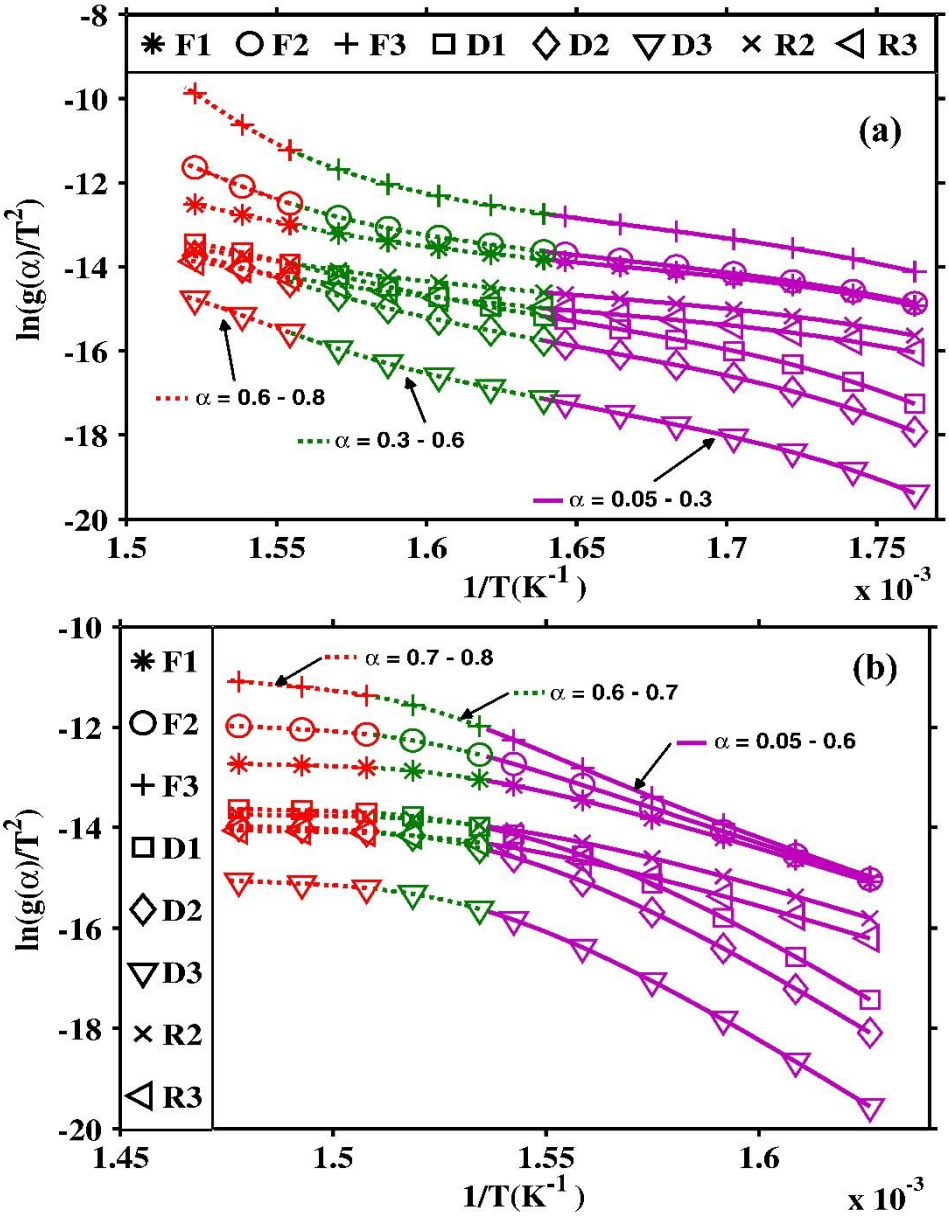

Fig. 5.5. Coats-Redfern plots of a) DEC and b) TB300 for different reaction models (paper I).

Fig. 5.6 shows the plot between ln A and E_a at different conversion stages for DEC and TB300 at 20 ^{0}C/min. The high linear relationship, i.e. R > 0.96 to 0.99 between the ln A and E_a plots shows the presence of the compensation effect.

Table 5.4 shows the kinetic compensation parameters at different stages of conversion for different heating rates for DEC and TB300. These values were used to evaluate 'A_α' and f_α as discussed in section 4.6.2. Fig. 5.7 shows a comparative analysis between the theoretical and experimental values. For DEC, the experimental curve is close to the 2D diffusional model when $\alpha < 0.3$ and for $\alpha > 0.3$, the reaction mechanism is close to the first order reaction model. For TB300, the experimental curve followed the first order reaction model when $\alpha < 0.6$ and the third order model when $\alpha > 0.6$.

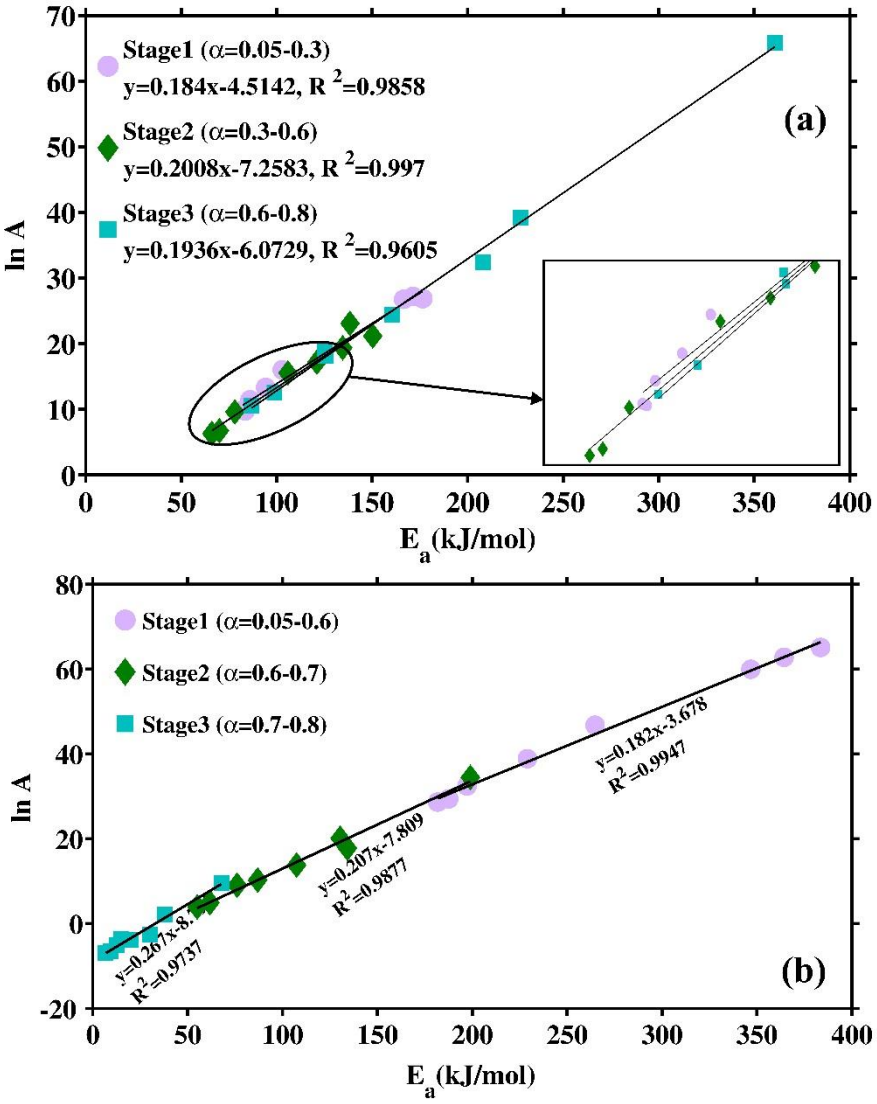

Fig. 5.6. Compensation plot (ln A vs. E_a) for (a) DEC and (b) TB300 samples at 20 °C/min heating rate (paper I).

Finally, from Fig. 5.4 and Fig. 5.7 it can be concluded that the thermal decomposition of DEC in the selected temperature range (105 to 700 ^{0}C) followed the diffusion models at the beginning and the reaction order models at the end of the pyrolysis. In previous studies, [112,125,126] the same order of reaction mechanism for the pyrolysis of different biomass types have been reported. However, the decomposition reaction mechanism is the opposite for torrefied biomass pyrolysis, in that the torrefied biomass followed the reaction order models at the beginning of pyrolysis and the diffusional models at the end.

Table 5.4 Kinetic compensation parameters at various heating rates for dried biomass (DEC) and Torrefied biomass (TB300) (paper I).

DEC									
	Stage 1 (α= 0.05 - 0.3)			Stage 2 (α= 0.3 - 0.6)			Stage 3 (α= 0.6 - 0.8)		
ß (°C/min)	b (mol kJ^{-1})	a	r^2	b (mol kJ^{-1})	A	r^2	b (mol kJ^{-1})	a	r^2
5	0.196	-5.066	0.9896	0.210	-6.857	0.9734	0.210	-7.280	0.9991
8	0.188	-4.513	0.9853	0.198	-5.988	0.9623	0.205	-7.195	0.9971
12	0.187	-4.498	0.9859	0.196	-6.022	0.9610	0.203	-7.223	0.9970
20	0.184	-4.517	0.9858	0.194	-6.076	0.9605	0.201	-7.262	0.9970
TB300									
	Stage 1 (α= 0.05 - 0.6)			Stage 2 (α= 0.6 - 0.7)			Stage 3 (α= 0.7 - 0.8)		
ß (°C/min)	b (mol kJ^{-1})	a	r^2	b (mol kJ^{-1})	A	r^2	b (mol kJ^{-1})	a	r^2
5	0.187	-3.988	0.9891	0.266	-8.989	0.9734	0.271	-8.762	0.9773
8	0.187	-3.669	0.9947	0.219	-8.022	0.9818	0.276	-8.831	0.972
12	0.185	-3.690	0.9947	0.218	-8.055	0.9812	0.272	-8.83	0.9723
20	0.182	-3.678	0.9947	0.207	-7.809	0.9877	0.267	-8.793	0.9737

The pyrolysis reactions in the initial stages of pyrolysis are related to the decomposition of the hemicellulose, cellulose and the partial decomposition of the lignin. The primary products formed during this stage are H_2O, CO_2, CO, levoglucosan, furfural, primary tar and char [125,126]. According to [125,126], during the initial stage of pyrolysis the transfer of the primary products and the heat through the biomass takes place through diffusion. The same phenomena can be observed from Fig. 5.4 and Fig. 5.7, where the initial stage of the pyrolysis followed the diffusion order models.

On the other hand, the torrefaction treatment increased the thermal stability of the biomass, as can be seen from Fig. 5.2. This shows that the pyrolysis starting temperature went up from 270 ^{0}C for DEC to 330 ^{0}C for TB300. The ordered-cellulose regions in the biomass increases with torrefaction treatment [38] which presumably inhibited the heat transfer through the biomass [125]. This could be the reason for the increased thermal stability with the torrefaction treatment.

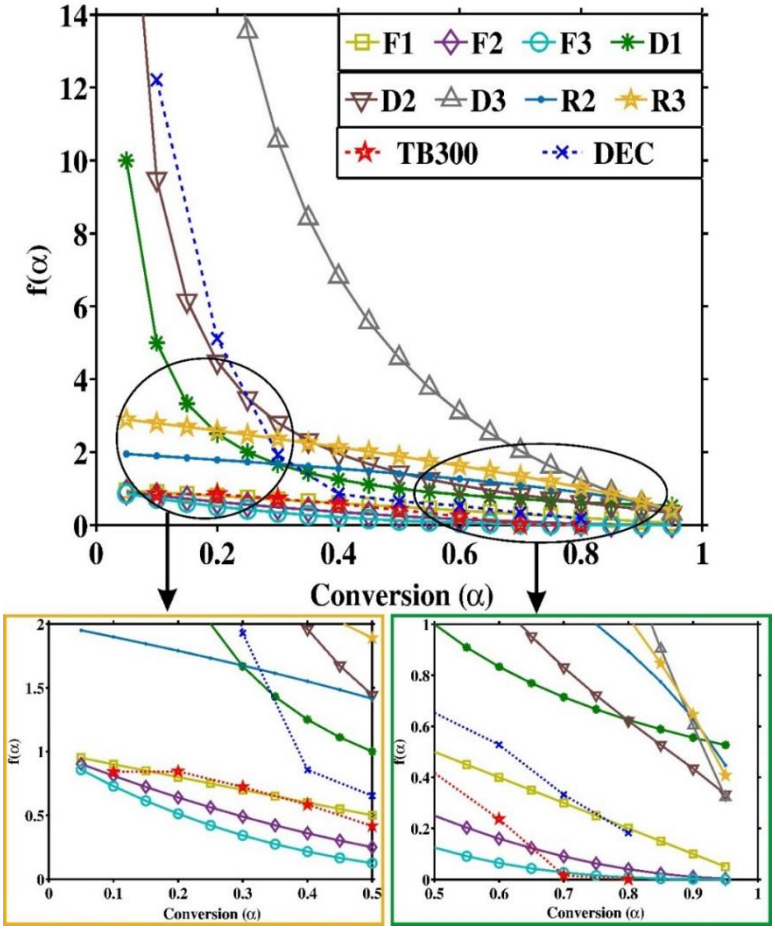

Fig. 5.7. Plot of theoretical and experimental f (α) vs. conversion (α) curves for DEC and TB300 (paper I). (Check Table 4.8 for abbreviation).

When the torrefaction temperature is higher than 300 ^{0}C, the primary products formed during the early stages are further converted into low-molecular-mass compounds and char through secondary cracking [127,128]. Lu et al. [126] reported that the formation of low-molecular-mass compounds could be the reason for the apparent first-order reaction mechanism in the temperature range of 300 to 500 ^{0}C. As the pyrolysis' starting temperature is higher than 300 ^{0}C, the primary products, for example levoglucosan, and the primary tar could easily be converted into low-molecular-mass compounds such as CO, CO_2, H_2 and CH_4 through secondary cracking reactions. This could be one possible reason for the observed first-order reaction model for the pyrolysis of torrefied biomass during the initial stage. In addition, the same phenomena could also be a reason for the increased CH_4 and H_2 concentrations and the reduced tar content in the volatiles from the torrefied biomass pyrolysis. Previous studies [51,129] have also observed a rise in the CH_4 and H_2 concentrations and a significant reduction in the tar content for torrefied biomass pyrolysis as compared to original biomass pyrolysis.

The diffusion-order reaction mechanism at the end of the torrefied biomass pyrolysis could be because of the altered structure of the lignin. According to [130], torrefaction treatment reduces the thermal stability of lignin. Because the

high-order cellulose degrades during the initial stage of pyrolysis and the thermal stability of the lignin is reduced, heat transfer through the biomass may occur unhindered.

This study has clearly shown that torrefaction has a significant influence on biomass pyrolysis in the form of, for example, the increased char yield, the altered reaction mechanisms and the increased heat flow. The kinetic parameters also vary significantly between dried and torrefied biomass. It is therefore important to take all these changes into account when designing pyrolysis for reactors and/or other processes aimed at optimizing the thermal conversion of torrefied biomass.

5.3.4 Influence on heat flow during pyrolysis

From the heat flow curves (Fig. 5.8, DSC data), it can be observed that the dried eucalyptus clone pyrolysis has exothermic reactions in the temperature range of 100 – 260 ^{0}C and 310 to 370 ^{0}C. These exothermic peaks are not there for biomass torrefied at 300 ^{0}C. Previous studies have reported that the thermal degradation of hemicellulose is exothermic and cellulose, endothermic. Towards the end of the pyrolysis, both the original and torrefied biomasses exhibited endothermic reactions. However, the TB300 had higher heat flow than DEC. The observed maximum heat flow in the temperature range of 400 to 500 ^{0}C were 2.5, 3.2 and 3.3 mW for DEC, TB250 and TB300 respectively. This analysis supports the conclusions made in a previous section that torrefied biomass requires a higher temperature and more energy in order to initiate pyrolysis reactions.

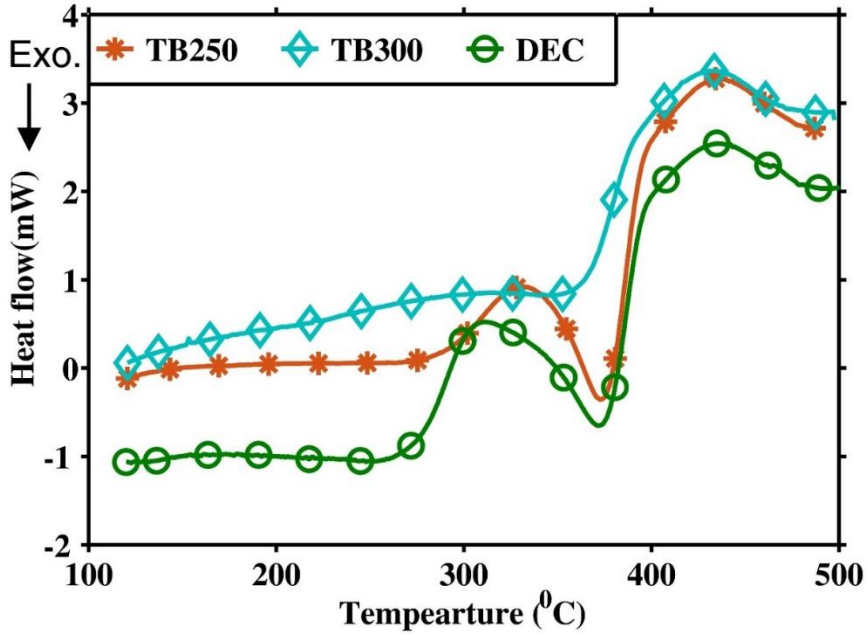

Fig. 5.8. DSC curves (heat flow) for the pyrolysis of DEC, TB250, TB300 samples at 20 °C/min (paper I).

5.4 Integrating torrefaction with AD (paper II)

5.4.1 Methane yield

Figure 5.9 shows the cumulative methane yield from the AD of torrefaction condensate produced at 225, 275 and 300 ^{0}C and loaded on various substrates to inoculum ratio, i.e. 0.1 and 0.2 at mesophilic (35 ^{0}C) and thermophilic (55 ^{0}C) conditions. The observed methane yield was in the range of 430 to 492 mL/g VS and 430 to 462 mL/g VS for mesophilic and thermophilic conditions respectively.

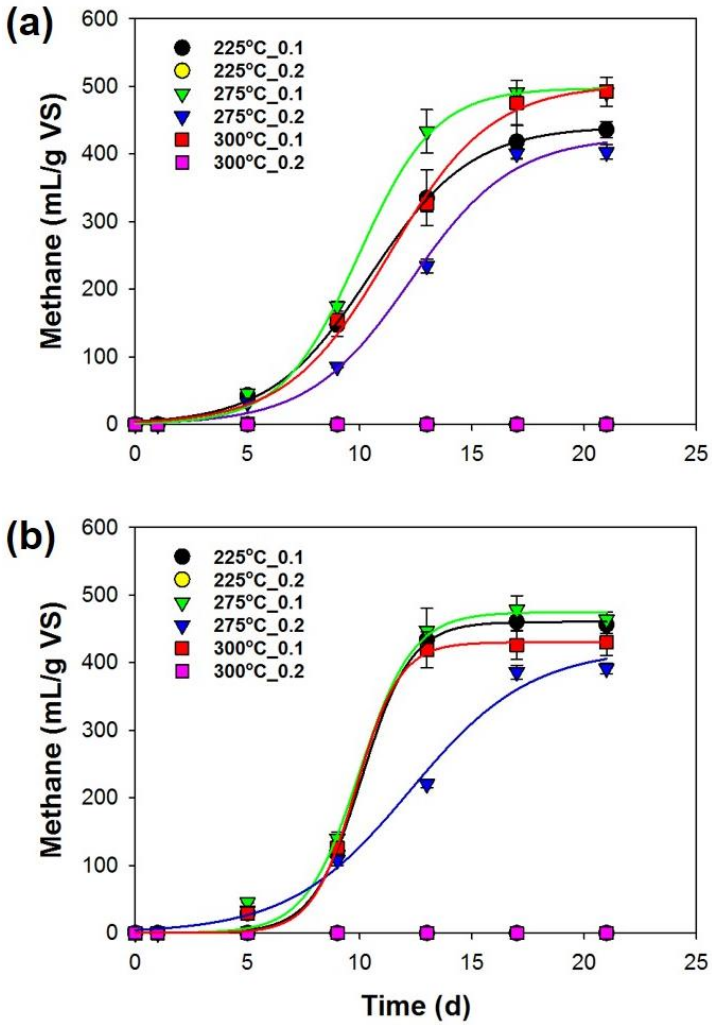

Fig. 5.9 shows the cumulative methane yield from AD of torrefaction condensate produced at 225, 275 and 300 ^{0}C and at 0.1 and 0.2 $VS_{substrate}$:$VS_{inoculum}$ loading (a) mesophilic (35 ^{o}C); (b) thermophilic (55 ^{o}C) conditions (paper II).

The cumulative methane yield for a period of 30 d at varied torrefaction condensate and substrate ratios is presented in Table 5.5. The methane yield at 0.1 $VS_{substrate}$:$VS_{inoculum}$ was 436, 490 and 492 mL/g VS for 225, 275 and 300 ^{0}C respectively in the mesophilic condition. The methane yield in the thermophilic condition was 456, 464 and 430 mL/g VS for 225, 275 and 300 ^{0}C respectively. The methane yield from the mesophilic condition was higher than for the thermophilic

condition. For torrefaction condensate produced at 225 and 300 ^{0}C, no methane production was observed at 0.2 $VS_{substrate}$:$VS_{inoculum}$ in either the mesophilic or thermophilic conditions. The reason that no methane was produced at the higher substrate to inoculum ratio could be the increased concentrations of inhibitory compounds.

Table 5.5 Cumulative methane yield for a period of 30 d at varied torrefaction condensate and substrate ratio (paper II).

Anaerobic digestion condition	Cumulative methane yield (mL/g of VS)					
	225 °C		275 °C		300 °C	
	0.1	0.2	0.1	0.2	0.1	0.2
Mesophilic	436±10	-	490±4	402±9	492±18	-
Thermophilic	456±11	-	463±9	391±7	429±16	-

In previous studies on the AD of the biomass-derived oil, such as pyrolysis oil and torrefaction condensate, it has been reported that the methane production could be inhibited because of the presence of phenols, aldehydes and other inhibitory compounds such as hydroxyacetaldehyde. One study [29] on the AD of model compounds found in biomass-derived oils showed that concentrations of more than > 0.01 wt.% of hydroxyacetaldehyde and guaiacol can significantly inhibit the AD process. The concentrations of hydroxyacetaldehyde and guaiacol in torrefaction condensate vary between 0.2 – 1.2 wt.% for the former, and 0.01 to 0.4 wt.% for the latter [28,29]. Torrefaction condensate also contains other strong microbial inhibitors such as furfural, 5-HMF and formaldehyde. According to [78] furfural and 5-HMF concentrations higher than 2 g/L and 0.5 g/L respectively can strongly inhibit the AD process. In this study, the concentrations of furfural and 5-HMF varied in the range of 2 – 6 g/L and 3 to 5 g/L respectively when the torrefaction temperature increased from 225 to 300 °C.

The torrefaction temperature has a significant influence on the overall AD process. In this study, no methane production was observed for torrefaction condensate produced at 225 °C and 300 °C at 0.2 $VS_{substrate}$:$VS_{inoculum}$, whereas with the same substrate loading, methane production was observed for torrefaction condensate produced at 275 °C. At the same time, there is a difference in the lag phase between the mesophilic (2 d) and thermophilic (5 d) conditions. The accumulation of VFA in the assays could be one possible reason for these differences in the methane yield. Previously, [131] reported that thermophilic condition could be more favorable for hydrolysis and acidogenesis, both of which lead to VFA accumulation and thereby inhibit the AD process.

5.4.2 Cyclic batch

The cumulative methane yield (mL) from the cyclic batch AD experiments on torrefaction condensate produced at 300 °C with various substrates to inoculum loading (0.1, 0.2 and 0.5) is presented in Fig. 5.10. Following the batch

experiments presented in the previous study, no methane production was observed for 0.2 and 0.5 $VS_{substrate}$:$VS_{inoculum}$ loading at both AD conditions for 30 d period. The methane yield for 0.1 $VS_{substrate}$:$VS_{inoculum}$ was 42 and 40 mL CH_4 for mesophilic and thermophilic respectively. After 30 d, the assays with 0.1 $VS_{substrate}$:$VS_{inoculum}$ were refed with substrate and 0.2 $VS_{substrate}$:$VS_{inoculum}$ was diluted as described in section 4.2.7. However, 0.5 $VS_{substrate}$:$VS_{inoculum}$ assays continued without any dilution.

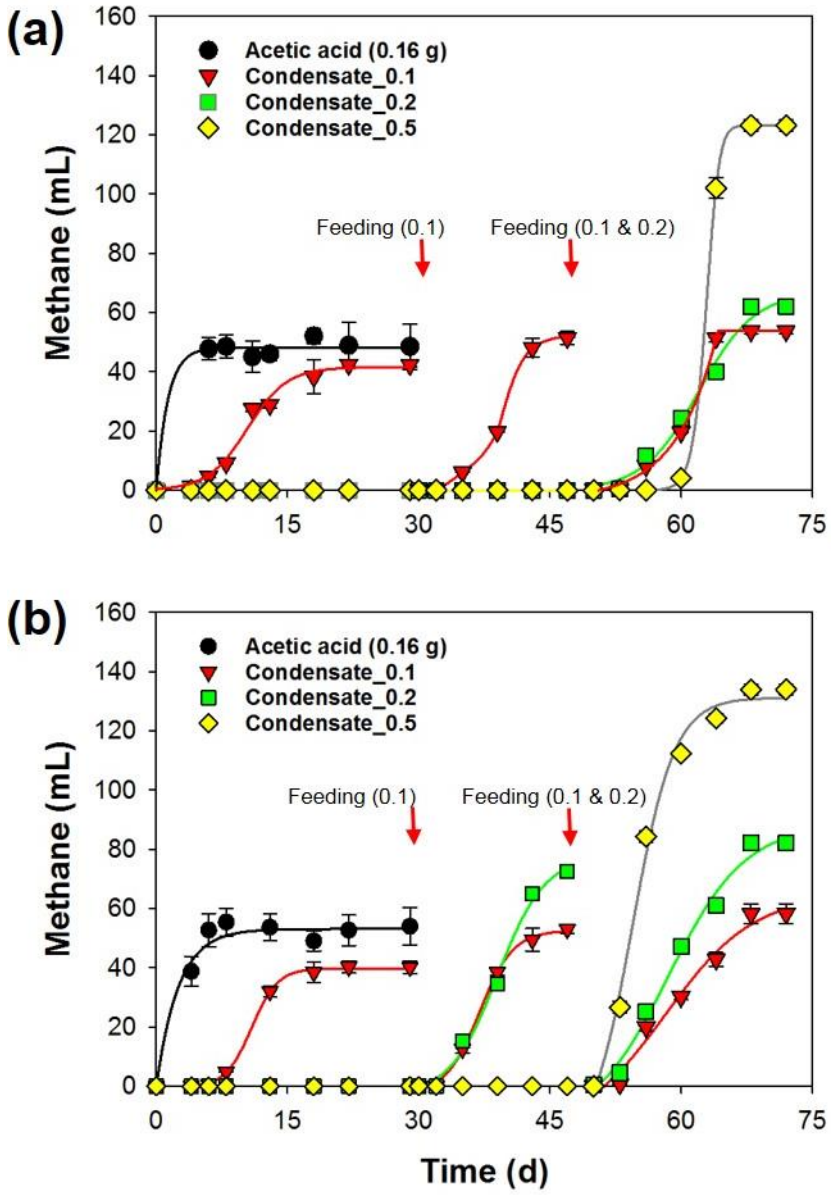

Fig. 5.10. Cumulative methane yield from the cyclic batch experiments of torrefaction condensate produced at 300 ^{0}C (a) mesophilic (35 ^{0}C); (b) thermophilic (55 ^{0}C) conditions (paper II).

After the first feed, the 0.1 $VS_{substrate}$:$VS_{inoculum}$ assays started producing methane immediately at a methane yield of 51 and 53 mL CH_4 for mesophilic and thermophilic respectively. The diluted 0.2 $VS_{substrate}$:$VS_{inoculum}$ assays also started producing the

gas in the thermophilic condition with a methane yield of 72± ml CH_4 after 18 days. Surprisingly, however, no methane production was observed for the diluted 0.2 $VS_{substrate}$:$VS_{inoculum}$ assays in the mesophilic condition. After 48 days, the assays of 0.1 and 0.2 $VS_{substrate}$:$VS_{inoculum}$ were refed with fresh torrefaction condensate and the assays with 0.5 $VS_{substrate}$:$VS_{inoculum}$ were diluted. After the second feed, all the bottles started producing methane. The methane yield for the diluted 0.5 $VS_{substrate}$:$VS_{inoculum}$ batch assays was 123 and 134 mL CH_4 for the mesophilic and thermophilic conditions respectively. Here, it is important to note that, after the first and second feeds the methane yield for the thermophilic condition was higher than for the mesophilic. At the same time, a rise of 60% in methane yield was observed at the end of three cycles. In the previous study [132] reported a rise of 40% in the methane yield at the end of the third cycle. According to [133], the reason for the increased methane yield with increasing number of feeding cycles could be because of the increased population of methane-producing microbes. The analysis with the cyclic batches shows that the inhibition of torrefaction condensate on the AD process is reversible.

5.4.3 Comparative analysis with other substrates

The previous study on the AD of torrefaction condensate produced at 315 °C reported the methane yield in the range of 50 – 100 mL/g of torrefaction condensate and at mesophilic condition. In this study, the observed methane yield was around 83 mL/g of torrefaction condensate produced at 300 °C. This analysis shows that torrefaction condensate is a promising feedstock for methane production. The comparative analysis presented in Table 5.6 shows that the methane potential of torrefaction condensate is comparable with other commonly used high-methane-potential substrates such as vegetable oils and cheese whey.

Table 5.6 Methane potential of the different substrates (*paper II).*

Substrate	Methane yield (mL /g VS)	References
Torrefaction condensate (mesophilic**)**	492	This study
Torrefaction condensate (thermophilic)	430	This study
Lipid extracted micro-algal biomass	240	[134]
Corn silage	296	[135]
Used vegetable oil	648	[135]
Cheese whey	423	[135]
Switch grass	122	[135]
Paper and pulp primary sludge	223	[136]
Aqueous pyrolysis liquid	72[a]	[5]
Organic fraction of municipal solid waste	80	[137]

a) In mL/g of aqueous pyrolysis liquid

5.5 Integrating torrefaction with adsorption and AD (paper III)

5.5.1 Influence of the torrefaction temperature on furfural adsorption

The influence of the torrefaction temperature on furfural adsorption is illustrated in Fig. 5.11. When the torrefaction temperature increased from 225 to 300 °C, the furfural adsorption (%) increased from 47 % to 77% at 150 g/L of torrefied biomass dosage and 12 h of residence time. The reason for the increased adsorption could be the enlarged pores and the consequent increase in the number of sites. As the temperature is increased from 225 to 300 °C the existing pores are enlarged thereby allowing the rapid diffusion of furfural solution into the torrefied biomass structure, which increases the surface contact.

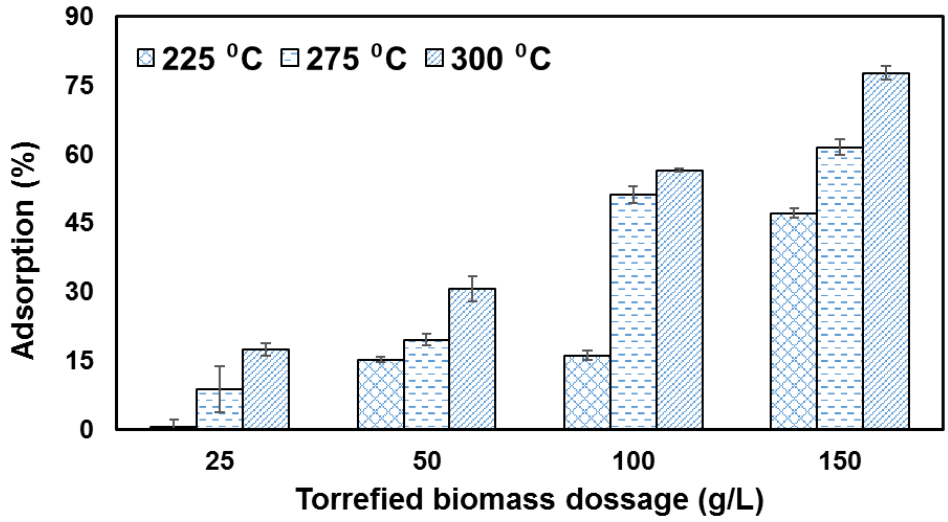

Fig. 5.11. Influence of torrefaction temperature on furfural adsorption. The initial concentration of furfural (C_0) = 6000 mg/L, and residence time = 12 h (paper III).

5.5.2 Effect of pH, dosage and contact time

This study has shown that the pH has a slight effect on furfural adsorption on torrefied biomass (Fig. 5.12a). For example, when the pH changes from 2 to 9, the q_e value (mg of furfural adsorbed per g of torrefied biomass) changed from 41±4.3 to 37± 2.6 respectively. The dosage of torrefied biomass does have a significant effect on the furfural adsorption (Fig. 5.12b). For example, the furfural adsorption was 17% at 25 g/L dosage and 77% at 150 g/L dosage. The q_e values were 41± 3.41 and 31±0.61 for 25 and 150 g/L dosage respectively at 12 h of contact time. Fig. 5.12c shows the influence of contact time on furfural adsorption. The furfural adsorption is relatively rapid in the first 2 hours, i.e. up to 85% of the total furfural is adsorbed. When the contact time was increased from 2 h to 12 h the furfural adsorption (%) at 150 g/L of loading increased from 54 to 77%.

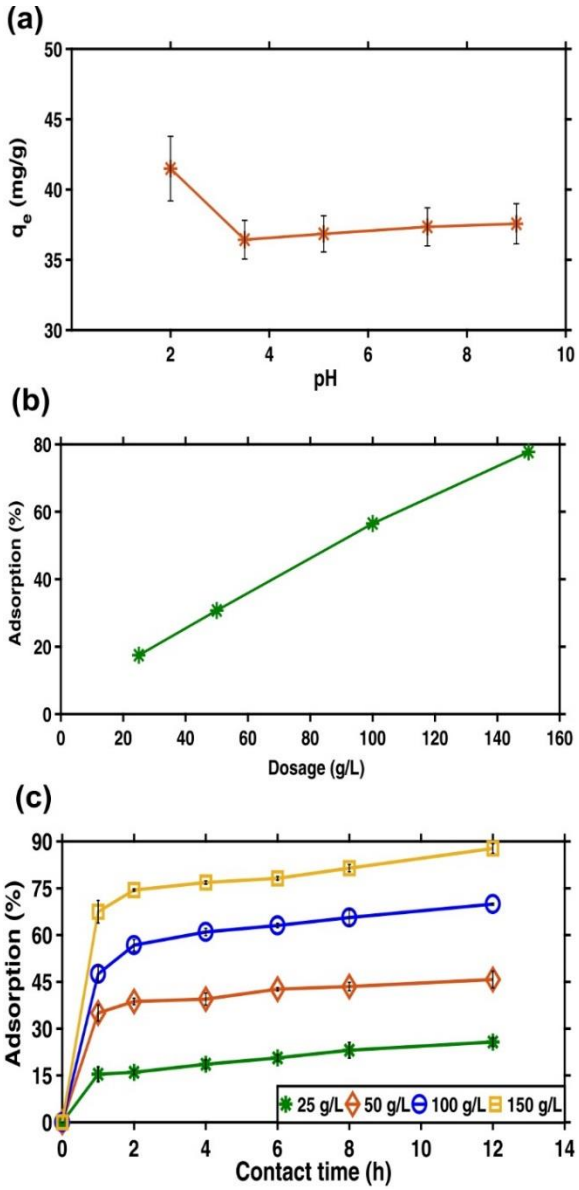

Fig. 5.12 (a) The influence of pH, (varied from 2 -9), (b) the influence of dosage (varied from 25 – 150 g/L) and (c) the influence of contact time (1 – 12 h) on the adsorption of furfural using torrefied biomass. The initial concentration of furfural: 6000 mg/L, contact time: 12 h (paper III).

5.5.3 Adsorption kinetics and mechanisms

The kinetics of furfural adsorption on torrefied biomass was studied using pseudo first- and second-order kinetic models following the equations presented in Table 4.10. Fig. 5.13 shows the plots of the pseudo first-order and second-order kinetic models. The evaluated kinetic rate constants (k_f) and (k_s) for the first and second order are 0.00230 and 0.0303 at 150 g/L of dosage. The pseudo second-order model fitted well with higher R^2 values, i.e. $R^2 > 0.99$.

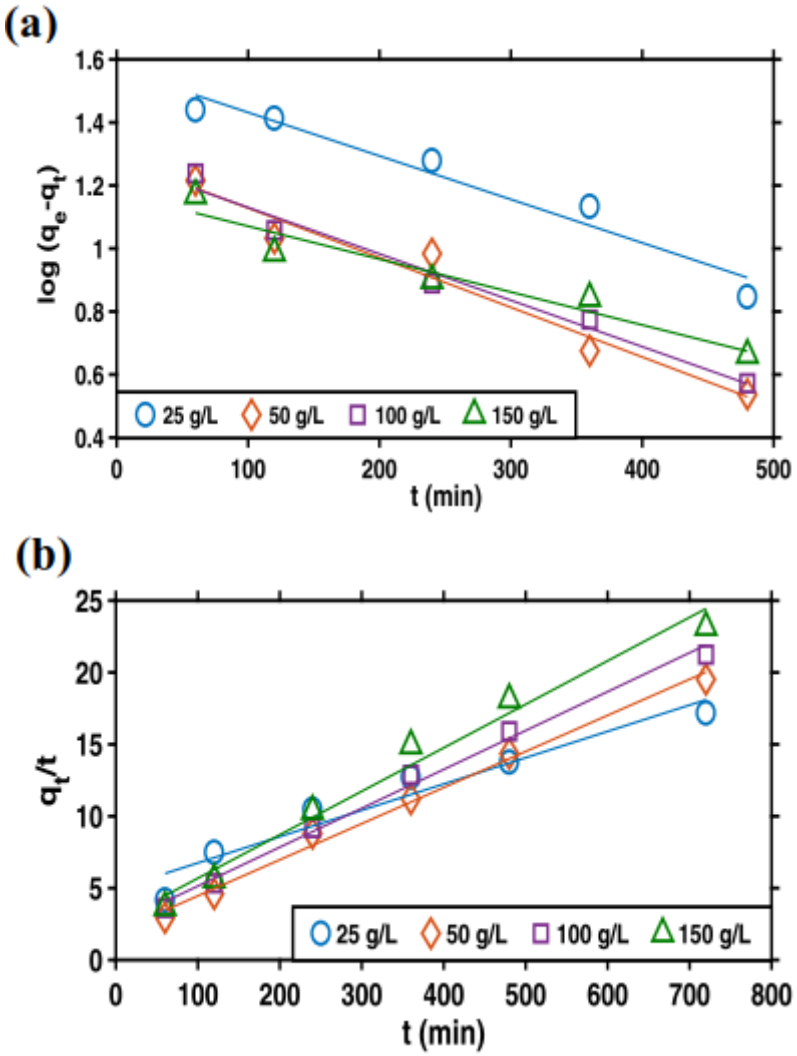

Fig. 5.13 Plots of pseudo first-order and second-order kinetic models.

The plots of the kinetic models presented in Table 4.11 are presented in Fig. 5.14. For the mass transfer model, the external mass transfer coefficient ($\beta_L S$) values varied from 4 to 22 x 10^{-4} min^{-1}. These were calculated from the slope of the plots shown in Fig. 5.14a. The 'S' values were calculated using BET surface area, i.e. 1.1 m^2/g, dosage (g) and total solution volume. The calculated β_L values varied from 1.3 to 1.6 x 10-8 m/min.

The multilinear plots of the intra-particle diffusional model with $R^2 > 0.97$ for the first and second zones presented in Fig. 5.14b show that the adsorption is controlled by two mechanisms. For the Boyd's diffusion model (Fig. 5.14c), the calculated average diffusional coefficient (De) was around 1.1 x 10^{-14} m^2/min. In a previous study, a diffusion coefficient of 2 x 10^{-11} m^2/min was reported for furfural adsorption. At the same time, the constant of Bangham's model (Fig. 5.14d) 'k_b' values varied from 3.14 to 7.9 x 10^{-4}.

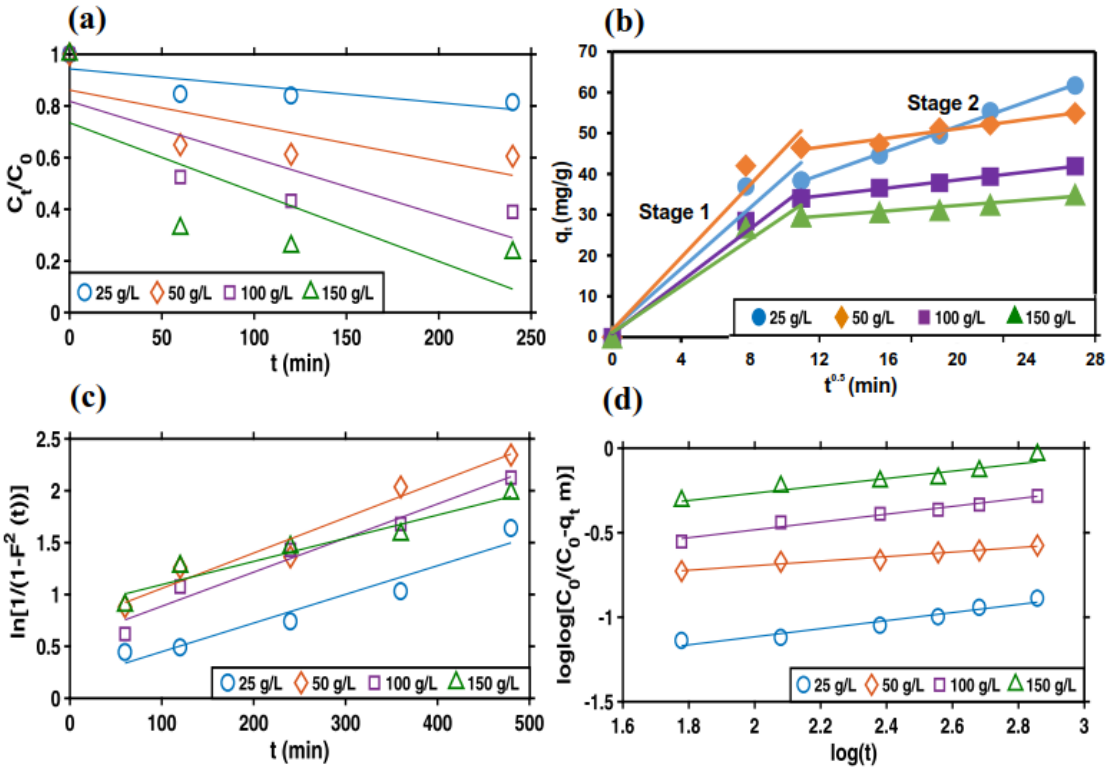

Fig. 5.14 Plots of kinetic models used to evaluate the rate-limiting step of adsorption process.

The intra-particle model showed that the furfural adsorption in torrefied biomass proceeds through two different stages. In general, the first stage represents the boundary layer effect and the second stage represents the intra-particle diffusion. At the same time, the high linear plots of Boyd's model (i.e. R^2 varies from 0.92 to 0.98) that are not passing through origin also suggests that film diffusion could be the rate-limiting step. On the other hand, the high linear plots (R > 0.97) of the second stage of the intra-particle model and Bangham's model (R^2 > 0.96) suggest that micropore diffusion could be the rate-limiting step. Based on kinetic analysis, it can be concluded that the rate-limiting steps for furfural adsorption in torrefied biomass were film diffusion at the initial stage (t < 2) and micro-pore diffusion at the second stage (t > 2).

The insignificant effect of pH suggests that furfural adsorption in torrefied biomass could be occurring because of hydrophobic interactions. Similarly, the adsorption of hydrophobic compounds such as furans and phenolics and the non-adsorption of hydrophilic compounds such as organic acids also points towards hydrophobic interactions. In addition, because of reduced OH groups, the surface of the torrefied biomass is hydrophobic in nature. A previous study [138] on the adsorption of furfural from pine needle hydrolysates using XAD-4 polymer also reported that furfural adsorption was through hydrophobic interactions.

5.5.4 Detoxification of torrefaction condensate

The adsorption (%) of different components present in torrefaction condensate at various torrefied biomass loadings are presented in Fig. 5.15. The phenolic and furan-aldehydes showed more affinity towards the torrefied biomass. The order of adsorption is phenolic > furan aldehydes > organic acids. At 250 g/L of dosage, the furfural adsorption was 54% and hydroxymethylfurfural (5-HMF) was reduced by 25%.

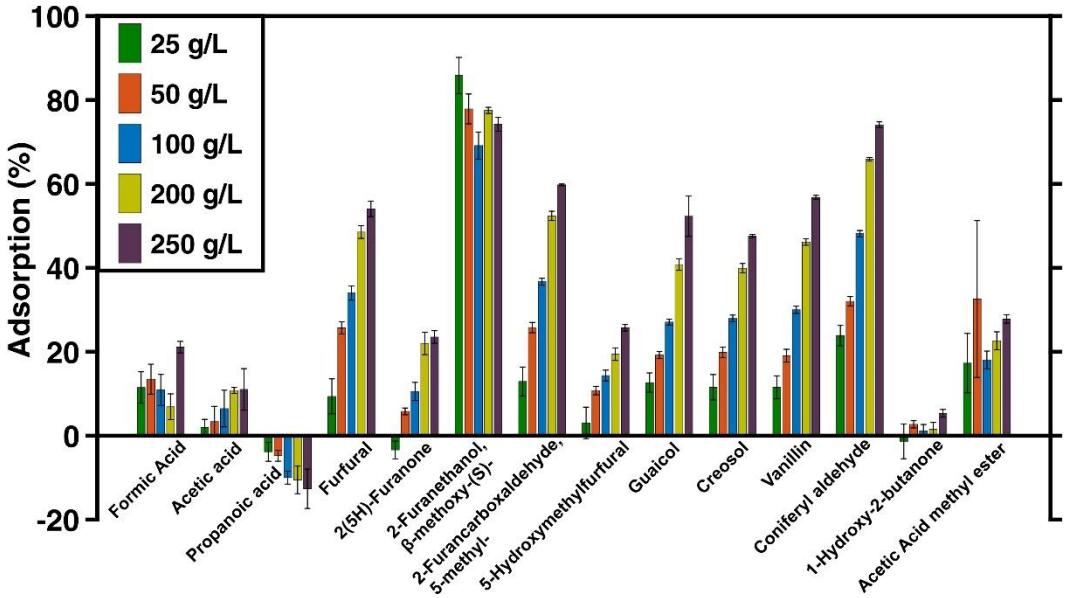

Fig. 5.15. Adsorption (%) of different compounds present in torrefaction condensate at varied torrefied biomass dosage (paper III).

At 250 g/L dosage, the adsorption (%) of other furans such as 2(5H)-furanone and 2-furancarboxaldehyde, 5-methyl- were 23 and 60% respectively. In the case of phenolic compounds, coniferyl aldehyde has the highest adsorption i.e. 74 % at 250 g/L. The adsorption of other phenolic compounds such as phenol, 2-methoxy-(guaiacol), creosol, and vanillin was 52, 47 and 56 % respectively at 250 g/L. For organic acids, the adsorption of formic acid and acetic acid was 21% and 11% respectively at 250 g/L. In contrast to other compounds, the propionic acid concentration was increased by 12 % at 250 g/L. The lower adsorption of acetic acid could be attributed to its polar characteristics and its consequent hydrophilic nature.

In the previous study, Björklund et al. [85] reported the removal of 36 % pf phenols, 27 % of 5-HMF and 49 % of furfural at 100 g/L of lignin dosage from spruce wood hydrolysis. Where, the initial concentration of those compounds was 2, 0.6 and 3.3 g/L. In this study, the adsorption of 33% of phenols, 14 % of 5-HMF and 34 % of furfural at 100 g/L of torrefied biomass dosage was observed. In the another study, Monlau et al. [139] used pyrolysis chars produced from solid anaerobic digestion digestate to remove furfural and 5-HMF from Douglas-fir wood hydrolysate where the initial concentration was 1000 mg/L. They reported that 99% of furfural and 95 % of 5-HMF was removed from the hydrolysate at 40 g/L dosage and 24 h contact time. The surface area of those chars were almost 50 times higher than the

surface area of the torrefied biomass reported in this study. It should be noted that in comparison with above referenced studies [85,139], higher amount of torrefied biomass was required to remove the inhibitory compounds. One reason for this could be the low surface area of the torrefied biomass, for example, the surface area of pyrolyzed chars was 50 times higher than the torrefied biomass. The other reason could be the high concentration of inhibitory compounds in torrefaction condensate, the concentration of inhibitory compounds in the torrefaction condensate is 9 times higher than the biomass hydrolysates reported in previous studies [85,139] . However, this will not have a negative impact on the overall process, as torrefied biomass after adsorption goes back into the pellets production (Fig. 4.3).

5.5.5 Influence of detoxification on the AD of torrefaction condensate

The AD batch assays were carried out using torrefaction condensate, detoxified with 250 g/L of torrefied biomass dosage. Fig. 5.16 shows the cumulative methane yield from the AD of torrefaction condensate before and after detoxification at the end of 35 d for 0.1 and 0.2 $VS_{substrate}$:$VS_{inoculum}$ loadings. The preliminary study on the AD of detoxified torrefaction condensate showed that the proposed adsorption process reduced the inhibition of torrefaction condensate and improved methane production. As expected, no inhibition was observed at 0.1 $VS_{substrate}$:$VS_{inoculum}$ loading and the methane yield was 689 and 695 mL/g VS for 0.1 $VS_{substrate}$:$VS_{inoculum}$ for the original and detoxified torrefaction condensates respectively. In case of 0.1 $VS_{substrate}$:$VS_{inoculum}$, for the initial 5 d the methane production followed the same trend for both the original and the detoxified torrefaction condensates. However, after 5 d the methane production from the detoxified torrefaction condensate started increasing, and after 20 d the methane yield for both set-ups was saturated. In case of 0.2 $VS_{substrate}$:$VS_{inoculum}$, the lag phase was reduced from 24 d to 16 d with detoxified torrefaction condensate.

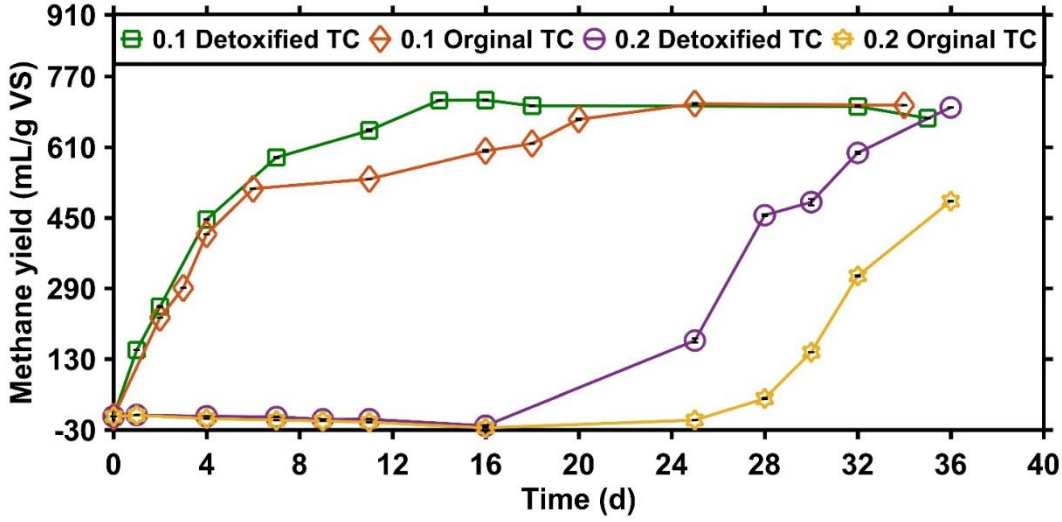

Fig. 5.16. Cumulated methane yield from AD of torrefaction condensate before and after detoxification at the end of 35 d for 0.1 and 0.2 $VS_{substrate}$:$VS_{inoculum}$ loadings (paper III).

5.6 Operational and economic feasibility of integrating torrefaction with AD (paper IV)

Although three different process configurations have been studied through experimental analysis, the techno-economic evaluation of integrating torrefaction with AD has been presented in this thesis. To better understand the benefits of process integration, it is worth studying the techno-economic feasibility of each process configuration individually. In this thesis, the techno-economic feasibility of integrating torrefaction with AD was considered in order to make a comparative analysis with commercial scale torrefaction operations where torrefied biomass is sold in the form of pellets. The main motive was to show the economic benefits of process integration of torrefaction with respect to the market price of the torrefied pellets. The techno-economic feasibility of integrating torrefaction with furfural adsorption and pyrolysis will be the subjects of future study.

5.6.1 Mass and energy balance

The mass and energy balances of stand-alone torrefaction and other integrated approaches is shown in Fig. 5.17. In the torrefaction process, drying was the major energy-consuming unit. The heat energy requirement at drying was 1372 kJ/kg of wet wood chips (40% of moisture), after which the moisture content is reduced from 40 to 10%. The energy balance in the torrefaction reactor showed that the overall torrefaction process is exothermic. However, it is important to consider the amount of heat energy required to raise the wood chips temperature to the torrefaction temperature and to remove the moisture. For that, the calculated heat energy requirement at torrefaction was 789 kJ/kg of dried biomass. A previous study [140] has shown that the energy required for the torrefaction of dry biomass at 280 °C was 714 kJ/kg. Finally, the total heat energy required for both drying and torrefaction was 2162 kJ/kg. The previous study, [141] reported an energy requirement of 2277 kJ/kg for a pilot plant operating at 260 °C.

The calculated heating value of the torrefaction volatiles was 4.3 MJ/kg of torrefaction volatiles (2 MJ/kg of dry biomass), which is within an acceptable range of the published data. For example, [32] reported a value of 3.5 MJ/kg of dry willow biomass and [61] reported a value of 6.3 MJ/kg of torrefaction volatiles.

At 10 t/h of torrefied biomass pellets production, the total amount of condensate produced was 4.54 t/h. The total methane yield was 9241 m^3/day at a digester volume of 7826 m3. The electrical energy production was 1.73 MW. However, the net electrical energy available after allowing 5% of electrical energy consumption for pumps and other controlling equipment was 1.64 MW (i.e. 13,016 MWh/year). The biomethane produced after upgrading for both HPWS and PSA units was 8871 m^3/d. The amount of digestate produced was 101 t/d. The total wastewater produced was 320 t/d (which includes saturated water vapor from drying and digestate).

Considering the heating value of torrefaction volatiles, the wet wood chips required to meet the total energy demand for the drying and torrefaction units was 0.83 t/h at a selected plant capacity for stand-alone torrefaction. However, for cases 2 and 3, the condensation of the torrefaction volatiles and the combustion of uncondensed gases was studied. In that scenario, the amount of wood chips required was 3.1 t/h at 10 t/h of torrefied pellets production.

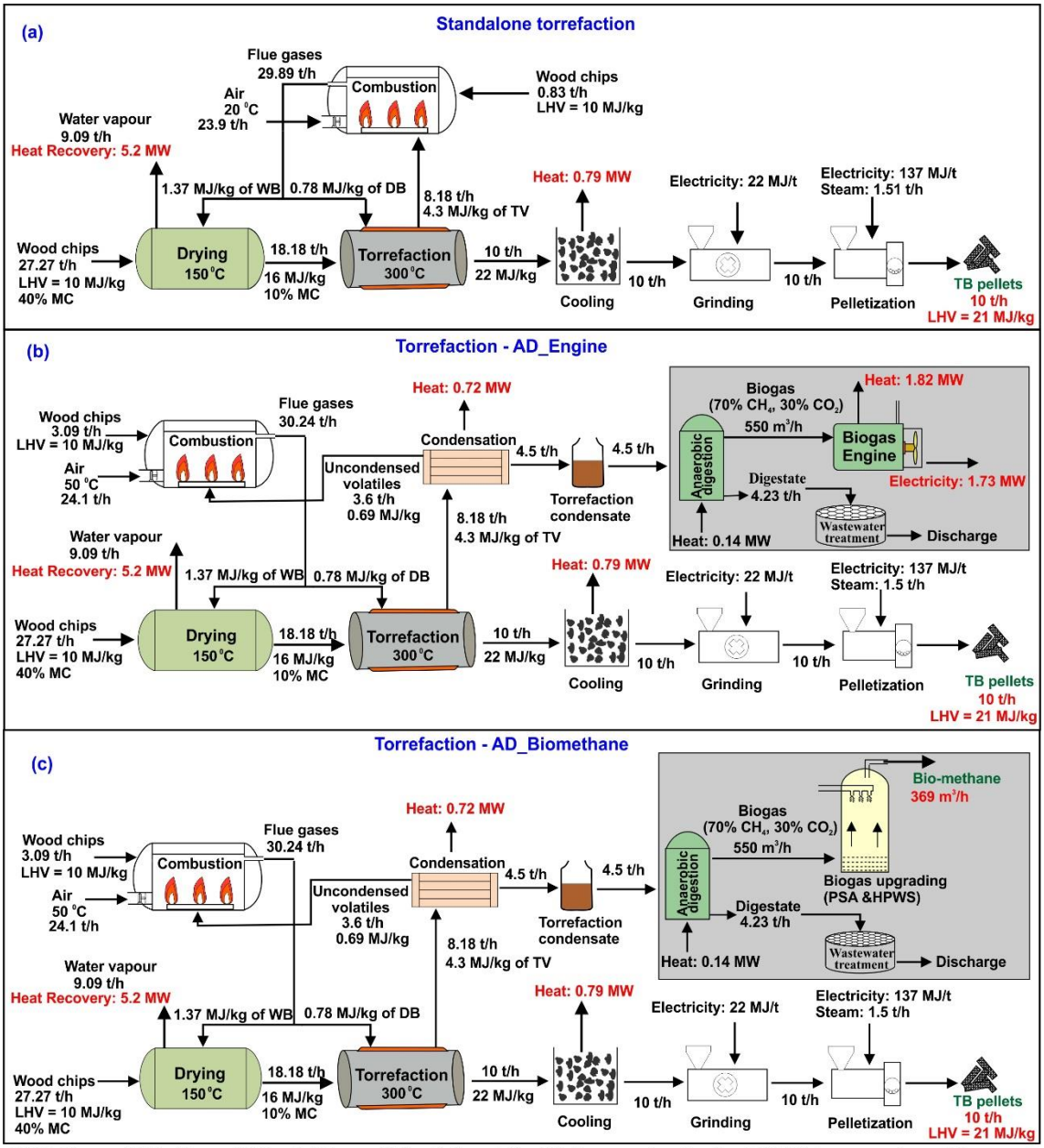

Fig. 5.17 Mass and energy balance for different cases, a) Case 1 (standalone torrefaction) (b) Case 2 (Torrefaction –AD_Engine), (c) Case 3 (Torrefaction – AD_Biomethane). TB = Torrefied biomass pellets, HPWS = High-pressure water scrubbing, PSA = Pressure swing adsorption (*paper IV*).

5.6.2 Energy recovery

The possible heat energy recovery options of an integrated torrefaction process was presented in Fig. 5.18. For all the cases, Most of the heat energy came from the dryer water vapor, 5245 kW. The heat energy available at the engine for DH was 1829 kW which includes heat energy from different stages of engine such as the exhaust gases (866 kW), the engine jacket water (712 kW), the intercooler stage 1 (154 kW) and the lube oil (96 kW). The maximum possible temperature raise for the DH water is different for different stages of the engine. For example, the possible temperature rise from the engine flue gas could be 130 °C, while the same at the inter cooler stage 1 was considered as 78 °C. However, the temperature for the DH water should be 90 °C, so the mass flow at each stage of the engine has to be adjusted in order to maintain the DH water exit temperature at 90 °C after mixing for different streams. The heat energy available from product cooling was 723 and 797 kW for volatiles and torrefied biomass cooling respectively. The total heat energy available was 6042, 8566 and 6737 kW for cases 1, 2 and 3 respectively.

5.6.3 Economic analysis

The total capital expenditure for different cases presented in Fig. 5.17 are shown in Table 5.7. The capital investment on torrefaction equipment (which includes feedstock handling, dryer, torrefaction unit and pelletizing unit) was around 21.85 M€ which is significantly higher than it is for other processes such as condensate production and AD. A major share of the capital investment goes on the torrefaction reactor. In this study, 50% of the total investment went on the torrefaction unit for stand-alone torrefaction. Previously [62] reported that 43% of the total investment went on a torrefaction unit at 100, 000 t/ year plant capacity. The total capital investment on AD was 6.5 M€ at a capacity of 369 m^3/h of biomethane and 1730 kW of electricity production. This was in the range reported by [142], i.e. 4 M€ for a plant capacity of 999 kW of electrical energy production. The total capital investment was 33.18, 42.61, 42.48 and 43.46 M€ for cases 1, 2, and 3-HPWS and 3-PSA respectively. In previous studies [22] and [27] have reported a capital investment of 49.46 and 28.2 Me for 100,000 t/y and 60,000 t/y plant capacity respectively.

Feedstock costs make up a major part of the total production costs, 73% for the stand-alone torrefaction process (Table 5.8). Based on the data presented in Table 5.8, the production costs were 189, 206, 213 and 221 €/t of torrefied biomass pellets for cases 1, 2, 3-HPWS and 3-PSA respectively. Previously, [62] reported a production cost of 160 €/t and 177 €/t for 100, 000 t/y and 80, 000 t/y plant capacities respectively.

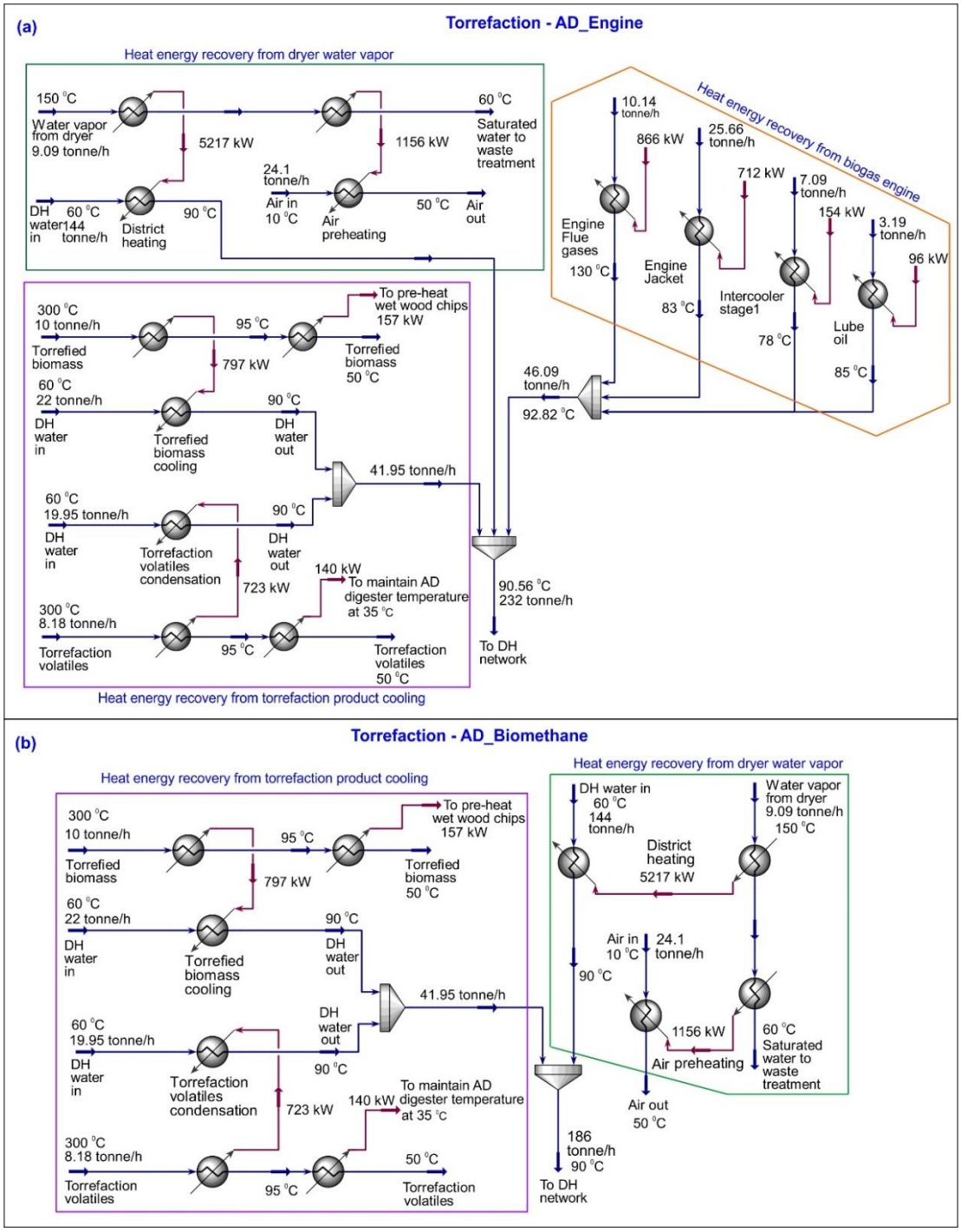

Fig. 5.18. Possible heat energy recovery for integrated torrefaction process (paper IV).

Table 5.7 Total capital invest on different processes and different cases.

Process	Case 1	Case 2	Case 3-HPWS	Case 3-PSA
Torrefied pellets production	22,156,067			
Condensate production	0	419,121		
Anaerobic digestion	0	4, 129, 437	3, 992, 162	4, 654, 166
Heat energy recovery	284, 100	538, 500		
Total capital investment (includes other capital expenses such as Startup expenses, Engineering and supervision, Contingency, Working Capital	33, 632, 910	41, 543, 858	41, 332, 318	42, 352, 465

Table 5.8 Summary of production costs for different cases (paper IV). .

Cost item	Production costs (€)			
	Case 1	Case 2	Case 3-HPWS	Case 3-PSA
Feedstock	10, 818, 500	11, 688, 600	11, 688, 600	11, 688, 600
Utilities	1, 120, 409	1, 120, 409	1, 120, 409	1, 120, 409
Maintenance and repair	877, 380	1, 083, 753	1, 078, 234	1, 473, 129
Manpower (operating labor + supervisors)	410, 997	410, 997	410, 997	410, 997
Factory overheads	1, 130, 411	1, 336, 784	1, 331, 266	1, 357, 878
Administration Costs	326, 472	388, 384	386, 728	394, 712
Waste treatment	86, 391	126, 593	126, 593	126, 593
Biogas upgrading			566, 366	740, 632
Distribution and selling	148, 107	161, 555	167, 091	173, 129
Total	**14, 958, 870**	**16, 317, 074**	**16, 876, 284**	**17, 486, 080**
Depreciation	2, 924, 600	3, 612, 509	3, 594, 114	3, 682, 823

The minimum selling price of torrefied biomass pellets in order to reach break-even point at a CRF of 10% was 199, 197, 185 and 194 for cases 1, 2, 3-HPWS and 3-PSA respectively. The minimum selling price of torrefied biomass pellets is lower for integrated approaches. The NPV and IRR are used to evaluate the economic viability of the process, which represents cumulative cash flow over a period and the rate of return on investment respectively. Fig. 5.19 shows NPA (a) and IRR (b) for all the cases studied. The NPV of stand-alone torrefaction was negative when the torrefied biomass pellets' price is less than 200 €/t. On the other hand, the integrated approaches for cases 3-HPWS has positive NPV value at a selling price of 190 €/t for the pellets. The IRR values were varied significantly for stand-alone torrefaction and the integrated approaches. For example, standalone torrefaction has a 5% return on investment at a pellet selling price of 220 €/t for the torrefied pellets, while at the same price, the case 3-HPWS has 14% of IRR.

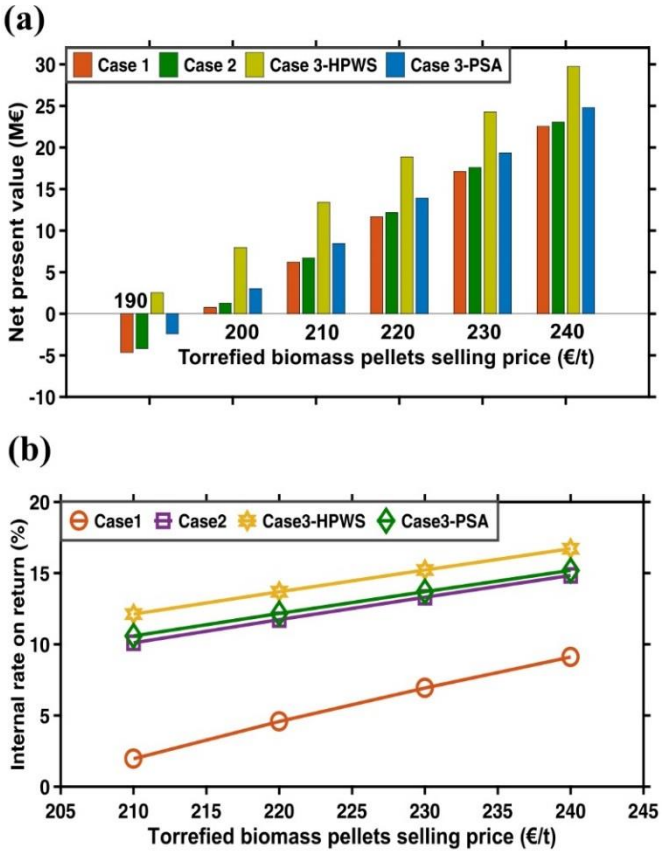

Fig. 5.19. Profitability analysis for different cases (a) NPV and (b) IRR (paper IV).

A sensitivity analysis of varying cost parameters on the minimum selling price and NPV of the torrefied pellets is presented in Figs. 5.20 and. 5.21 respectively. From Fig. 5.21 it can be observed that the feedstock cost significantly influences the economics of the process. For example, when the price of the wood chips rose by 25% then the minimum selling price was increased by 14, 15, 17 and 16% for cases 1, 2, 3-HPWS, and 3-PSA respectively. After the feedstock cost, the FCI also had a significant influence on the economics. For example, when the FCI was reduced by 25%, the NPV values for the case 3-HPWS rose by 41%.

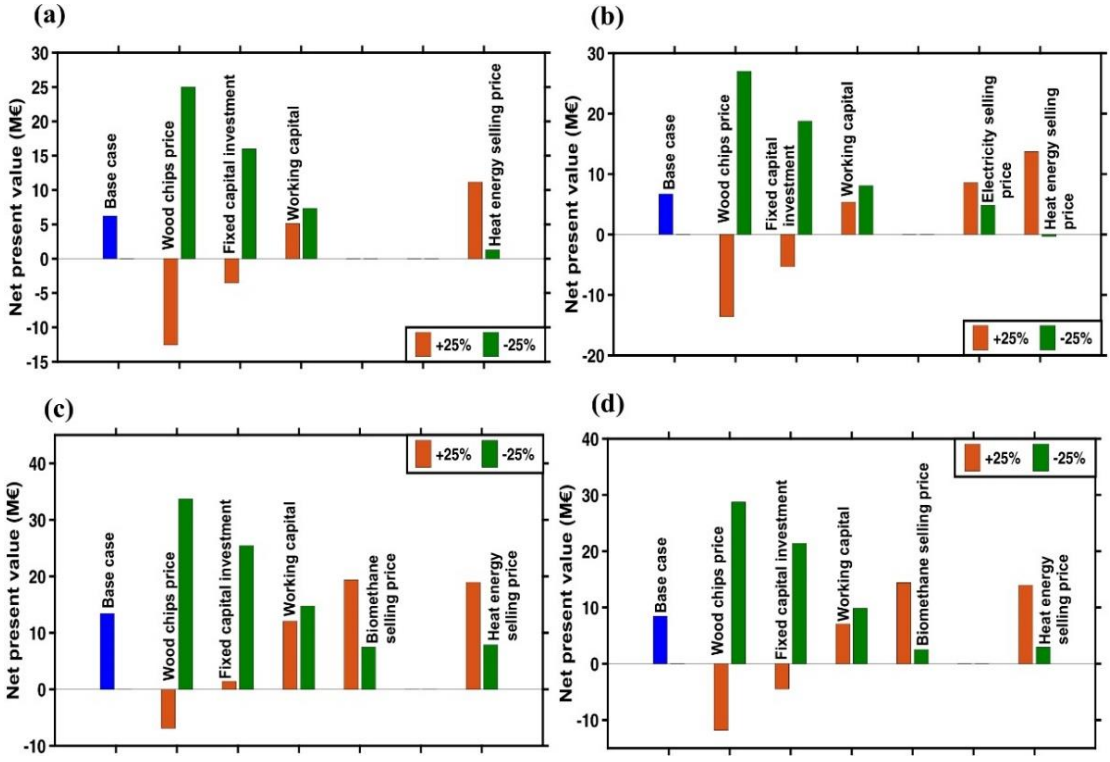

Fig. 5.20. Sensitivity analysis in terms of minimum selling price (at torrefied biomass selling price of 210 €/t) for different input parameters (a) Case 1 (b) Case 2 (c) Case 3-HPWS and (d) Case 3-PSA (paper IV).

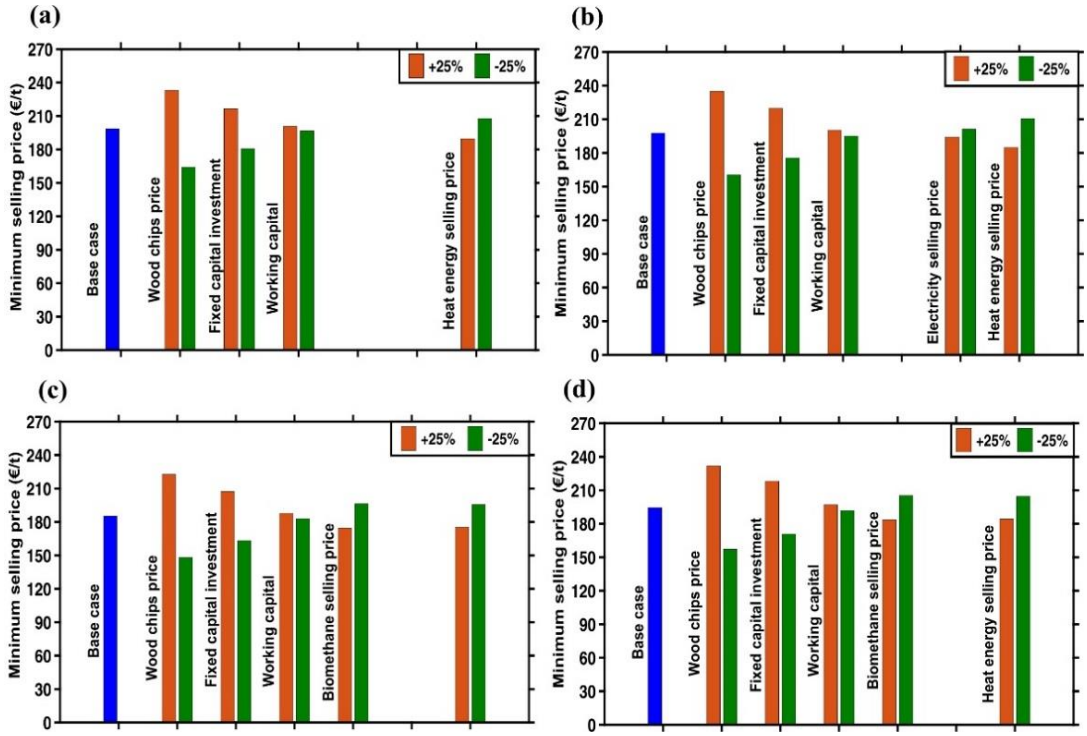

Fig. 5.21. Sensitivity analysis in terms of net present value (at torrefied biomass selling price of 210 €/t) for different input parameters (a) Case 1 (b) Case 2 (c) Case 3-HPWS and (d) Case 3-PSA (paper IV).

5.6.4 Summary of integrating torrefaction with AD

This study has shown that integrating torrefaction with AD is both technically and economically feasible. The methane production from AD at 10 t/h of torrefied biomass pellets production was comparable with industrial scale commercially operated biogas plants. The mass balance showed that condensing the volatiles to produce methane from the condensate, instead of just combusting the volatiles for heat energy production, increased the utility fuel requirement 2.8 times (wet wood chips in this study). At the same time, the investment costs for integrated approaches rose by 26% in comparison with the cost of a stand-alone torrefaction process. However, this was offset by additional revenue from the byproducts, such as biomethane, heat and electrical energy. This is reflected on the minimum selling price for torrefied biomass. For example, the minimum selling price of torrefied biomass fell from 199 €/t for stand-alone torrefaction to 183 €/t for case 3-HPWS.

The comparative analysis between the end applications for the biogas showed that upgrading the biogas and selling it as a vehicle fuel is more economically feasible than using it in a gas engine to produce electrical and heat energy. However, it should be noted that the economic feasibility of case 2 mainly depends on the heat energy demand, as much of the extra revenue comes from the sale of heat energy. If there is no demand for the heat energy, the heat energy from the engine flue gases could be diverted to the drying and/or torrefaction units, which would reduce the expenditure on utility fuels to some extent.

There are many opportunities for further reducing the selling price of torrefied biomass and thereby increasing its competitiveness with wood pellets and coal. For example, in this study, it was observed that the feedstock (wood chips) makes up 73% of the total production costs. Furthermore, the sensitivity analysis showed that the cost of the feedstock has a significant influence on the economics of the torrefaction process. Reducing the feedstock costs by 25 % can reduce the minimum selling price of torrefied pellets to 145 €/t for case 3-HPWS and 159 €/t for case 2. At such prices, torrefied wood pellets can compete with wood pellets, whose current price is 166 €/t [104]. Thus, for feasible economic operations low cost feedstock such as wood processing wastes, forest residues, saw dust and agricultural waste must be considered. However, their availability in large volumes for continuous operations should also be considered. The torrefaction reactor makes up a major part (43% for stand-alone torrefaction) of the total capital investment. However, with technological advances, the cost of investment in torrefaction should fall in the future. It has been predicted [22] that at a learning rate of 2%, the capital investment in the operational expenses of the torrefaction process will be significantly reduced by 2030.

Carbon credits is also an important option for generating addition revenue. According to [62], the torrefaction process can earn carbon credits of 25 to 72 €/t. When the torrefaction process is integrated with AD, the benefits from AD can also be taken into consideration. For example, there are investment subsidies

and/or feed-in-tariffs, which can help to further reduce the selling price of torrefied biomass pellets. In conclusion, taken altogether, a combination of low-cost feedstock (13 €/MWh), integrating the torrefaction with the AD, selling biomethane as a vehicle fuel, utilizing the heat energy recovery options and earning carbon credits (at 40 €/t) could reduce the selling price of torrefied pellets to 108 €/t.

5.7 A view on the process integration approaches to torrefaction

From the results of this thesis, and other previous studies [27,61], it is clear that integrating torrefaction with other biomass conversion processes could help to improve the techno-economic feasibility of the torrefaction process. Torrefaction can be integrated with pyrolysis with either a centralized or decentralized approach [143,144]. When it is integrated with centralized pyrolysis, the torrefaction process can benefited from heat energy integration with the whole process. In that, way the costs of the torrefaction process can be reduced significantly. Conversely, the pyrolysis process can also benefit through the energy savings in the biomass grinding, and a reduction in the investment of the biomass storage facilities. In addition, high quality pyrolysis oil can be produced from torrefied biomass pyrolysis [143,144].

When integrating torrefaction with AD, this study clearly shows that the torrefied pellets' selling price could be reduced significantly. Condensing the torrefaction volatiles and subsequent methane production through AD is more operationally and economically feasible than combusting them for energy production. It is important to note that torrefaction condensate contains several microbial inhibitory compounds, so new process configurations are required to remove or reduce these. When integrated with AD, the torrefaction process can also benefit from additional subsidies available specifically for AD technology.

When the production of torrefied pellets is integrated with adsorption and AD, not only is the methane yield improved, but so is the quality of the pellets. This approach also enables the extraction of high-demand chemical feedstock from the torrefaction condensate, such as furfural. In addition, this process eliminates the need for binders during pelletization. All of these factors can further improve the economic feasibility of the torrefaction process.

Heat energy integration and recovery is can also have a significant effect on the techno-economic feasibility of the torrefaction process. Although torrefaction is carried out at low temperatures, and the heat energy recovery possibilities are limited, one potential application in Nordic regions is district heating. If there is no heat energy demand, then preheating the biomass prior to drying is also a viable option.

Process integration approaches to torrefaction can significantly increase the investment and operational costs. However, these can be offset by the additional revenue from the by-products of the process, and through savings on fuel/energy costs. Nevertheless, further research is still required to better understand the pros and cons of the suggested process integration approaches.

6 Conclusion

Different process configuration were developed in order to improve the operational and economic feasibility of the torrefaction process for this thesis. Their feasibility was tested through laboratory experiments and process modeling.

The study on the pyrolysis of torrefied biomass showed that torrefaction had a significant effect on the kinetics, reaction mechanism and heat flow parameters of biomass decomposition during the pyrolysis process. The reported variation in the decomposition mechanism between dried and torrefied biomass could be due to the altered structure of the biomass during torrefaction, and the consequent formation of smaller molecules during the pyrolysis of torrefied biomass. It was also observed that the active pyrolysis temperature zone was shifted into a higher temperature range with torrefaction treatment. In addition, DSC analysis showed that the pyrolysis of torrefied biomass requires more energy than dried biomass pyrolysis. It can be concluded that the pyrolysis of torrefied biomass has different reaction mechanisms and it requires more heat energy to proceed with pyrolysis reactions than it does for dried biomass.

The issues raised in Chapter 2, indicate that combusting torrefaction volatiles to produce heat energy may not be a feasible option. Therefore, this thesis has investigated the feasibility of condensing the volatiles to produce torrefaction condensate and then using the condensate in anaerobic digestion to produce biogas. The experimental results on the anaerobic digestion of torrefaction condensate revealed that torrefaction condensate has a higher bio-methane potential (430–490 mL/g) than other substrates like waste vegetable oils and cheese whey. It should be noted, however, that methane production was inhibited at higher substrate to inoculum loading. However, the preliminary study with cyclic batch experiments showed that this is a reversible inhibition. On the other hand, because of the increased brittleness of torrefied biomass, it requires binding materials during pelletization. A new process configuration was developed in this study in order to reduce the binder requirement during pelletization and for the detoxification of torrefaction condensate in an integrated approach. The experimental results showed that torrefied biomass could remove significant quantities of furfural and other inhibitory compounds from the torrefaction condensate. At the same time, the lower adsorption of organic acids looks like an interesting avenue of exploration.

The techno-economic analysis showed that the selling price of torrefied biomass pellets could be significantly reduced when torrefaction is integrated with AD. However, the end application for the produced biogas also has a significant effect on the economics of the overall process for the integrated approaches. The waste-heat energy recovery options could also significantly influence the viability of an integrated torrefaction process. In this study, it was observed that upgrading the biomethane to use it, as a vehicle fuel is more feasible than using the biogas in a gas engine to produce electrical and heat energy. The cost of the feedstock also has a

significant influence on the torrefaction economics. This study showed that the combination of low-cost feedstock, integrated torrefaction and waste heat recovery could reduce the selling price of torrefied pellets to a level at which it is extremely competitive with wood pellets.

This thesis work contributed to the scientific knowledge of the torrefaction process by developing new process configurations to improve its techno-economic feasibility.

7 Future prospects

In this study, preliminary analysis was carried out to understand the influence of torrefaction treatment on heat flow during biomass pyrolysis. However, in-depth analysis is required to better understand the change in the heat flow pattern for torrefied biomass pyrolysis. In this study, it was observed that the thermal stability of the torrefied biomass is increasing with increasing torrefaction severity. Thus, extending this study to evaluate the influence of torrefaction treatment on thermal constants could be interesting.

The experimental results of batch assays showed that torrefaction condensate is a feasible feedstock for anaerobic digestion process. However, evaluating the anaerobic digestion of torrefaction condensate through continuous reactor experiments must be carried out to better understand the overall process feasibility. The torrefied biomass was able to remove the inhibitory compounds from torrefaction condensate partially. However, considering other methods for complete removal of inhibitory compounds could be interesting. Torrefaction condensate contains high concentration of furfural which is a high value industrial chemical. Thus, exploring the possibilities for furfural recovery from torrefaction condensate could be interesting.

In this thesis work, using the torrefaction condensate in anaerobic digestion for methane production was considered. However, considering it as a feedstock for other microbial conversion processes to produce high value products such as waxesters, bioplastics and other biochemicals could be very interesting for future studies.

In this thesis work, it was observed that feedstock cost has significant influence on torrefaction process economics. Thus, integrating the torrefaction with the processes that generates low cost feedstock could be interesting.

Bibliography

[1] Pires JCM. COP21: The algae opportunity? Renewable and Sustainable Energy Reviews 2017;79:867–77. doi:10.1016/j.rser.2017.05.197.

[2] Liobikienė G, Butkus M. The European Union possibilities to achieve targets of Europe 2020 and Paris agreement climate policy. Renewable Energy 2017;106:298–309. doi:10.1016/j.renene.2017.01.036.

[3] Thrän D, Witt J, Schaubach K, Kiel J, Carbo M, Maier J, et al. Moving torrefaction towards market introduction – Technical improvements and economic-environmental assessment along the overall torrefaction supply chain through the SECTOR project. Biomass and Bioenergy 2016;Volume 89:184–200. doi:10.1016/j.biombioe.2016.03.004.

[4] Eurostat. Energy statistics 2016.

[5] Fabbri D, Torri C. Linking pyrolysis and anaerobic digestion (Py-AD) for the conversion of lignocellulosic biomass. Current Opinion in Biotechnology 2016;38:167–73. doi:10.1016/j.copbio.2016.02.004.

[6] Zanchi G, Pena N, Bird N. Is woody bioenergy carbon neutral? A comparative assessment of emissions from consumption of woody bioenergy and fossil fuel. GCB Bioenergy 2012;4:761–72. doi:10.1111/j.1757-1707.2011.01149.x.

[7] Koppejan J, Sokhansanj S, Melin S, Madrali S. Status overview of torrefaction technologies (IEA Bioenergy Task 32). 2012.

[8] Doddapaneni TRKC, Konttinen J, Hukka TI, Moilanen A. Influence of torrefaction pretreatment on the pyrolysis of Eucalyptus clone: A study on kinetics, reaction mechanism and heat flow. Industrial Crops and Products 2016;92:244–54. doi:10.1016/j.indcrop.2016.08.013.

[9] Agar DA. A comparative economic analysis of torrefied pellet production based on state-of-the-art pellets. Biomass and Bioenergy 2017;97:155–61. doi:10.1016/j.biombioe.2016.12.019.

[10] Bulkowska K, Gusiatin ZM, Klimiuk E, Pawlowski A, Pokoj T. Biomass for Biofuels. CRC Press; 2016.

[11] Senneca O. Kinetics of pyrolysis, combustion and gasification of three biomass fuels. Fuel Processing Technology 2007;88:87–97. doi:10.1016/j.fuproc.2006.09.002.

[12] REN21: Renewable Energy Policy Network for the 21st Century. Renewables 2016. Global status report. 2016.

[13] World Energy Council. World Energy Resources Bioenergy 2016 2016:60. doi:10.1016/0165-232X(80)90063-4.

[14] Davis, S.C., Hay, W. & Pierce J. Biomass in the energy industry: an introduction. 2014.

[15] Spliethoff H. Power Generation from Solid Fuels. Springer Berlin Heidelberg; 2010.

[16] Crocker M. Thermochemical Conversion of Biomass to Liquid Fuels and Chemicals. Royal Society of Chemistry; 2010.

[17] Alén R. Biorefining of forest resources. Paperi ja Puu Oy; 2011.

[18] Brown RC, Stevens C. Thermochemical Processing of Biomass: Conversion into Fuels, Chemicals and Power. Wiley; 2011.

[19] Gent S, Twedt M, Gerometta C, Almberg E. Theoretical and Applied Aspects of Biomass Torrefaction: For Biofuels and Value-Added Products. Elsevier Science; 2017.

[20] Sermyagina E, Saari J, Kaikko J, Vakkilainen E. Integration of torrefaction and CHP plant: Operational and economic analysis. Applied Energy 2016;183:88–99. doi:10.1016/j.apenergy.2016.08.151.

[21] Thrän D. Global Wood Pellet Industry and Trade Study 2017 (IEA Bioenergy Task 40). IEA; 2017.

[22] Batidzirai B, Mignot APR, Schakel WB, Junginger HM, Faaij APC. Biomass torrefaction technology: Techno-economic status and future prospects. Energy 2013;62:196–214. doi:10.1016/j.energy.2013.09.035.

[23] Chen WH, Peng J, Bi XT. A state-of-the-art review of biomass torrefaction, densification and applications. Renewable and Sustainable Energy Reviews 2015;44:847–66. doi:10.1016/j.rser.2014.12.039.

[24] Pandey A, Negi S, Binod P, Larroche C. Pretreatment of Biomass: Processes and Technologies. Elsevier Science; 2014.

[25] Chen WH, Peng J, Bi XT. A state-of-the-art review of biomass torrefaction, densification and applications. Renewable and Sustainable Energy Reviews 2015;44:847–66. doi:10.1016/j.rser.2014.12.039.

[26] Lu KM, Lee WJ, Chen WH, Liu SH, Lin TC. Torrefaction and low temperature carbonization of oil palm fiber and eucalyptus in nitrogen and air atmospheres. Bioresource Technology 2012;123:98–105. doi:10.1016/j.biortech.2012.07.096.

[27] Kumar L, Koukoulas AA, Mani S, Satyavolu J. Integrating torrefaction in the wood pellet industry: A critical review. Energy and Fuels 2017;31:37–54. doi:10.1021/acs.energyfuels.6b02803.

[28] Fagernas L, Kuoppala E, Arpiainen V. Composition, utilization and economic assessment of torrefaction condensates. Energy and Fuels 2015;29:3134–42. doi:10.1021/acs.energyfuels.5b00004.

[29] Liaw SS, Frear C, Lei W, Zhang S, Garcia-Perez M. Anaerobic digestion of C1-C4 light oxygenated organic compounds derived from the torrefaction of lignocellulosic materials. Fuel Processing Technology 2015;131:150–8. doi:10.1016/j.fuproc.2014.11.012.

[30] Tumuluru JS, Sokhansanj S, Hess JR, Wright CT, Boardman RD. A review on biomass torrefcation process and product properties for energy applications. Industrial Biotechnology 2011;7:384–401. doi:10.1089/ind.2011.0014.

[31] Bates RB, Ghoniem AF. Biomass torrefaction: Modeling of reaction

thermochemistry. Bioresource Technology 2013;134:331–40. doi:10.1016/j.biortech.2013.01.158.

[32] Prins MJ, Ptasinski KJ, Janssen FJJG. More efficient biomass gasification via torrefaction. Energy 2006;31:3458–70. doi:10.1016/j.energy.2006.03.008.

[33] Zheng A, Zhao Z, Chang S, Huang Z, Wang X, He F, et al. Effect of torrefaction on structure and fast pyrolysis behavior of corncobs. Bioresource Technology 2013;128:370–7. doi:10.1016/j.biortech.2012.10.067.

[34] Ru B, Wang S, Dai G, Zhang L. Effect of Torrefaction on Biomass Physicochemical Characteristics and the Resulting Pyrolysis Behavior. Energy and Fuels 2015;29:5865–74. doi:10.1021/acs.energyfuels.5b01263.

[35] Wang S, Luo Z. Pyrolysis of Biomass. Walter de Gruyter GmbH & Co KG, 2017; 2017.

[36] Khazraie Shoulaifar T, Demartini N, Willför S, Pranovich A, Smeds AI, Virtanen TAP, et al. Impact of torrefaction on the chemical structure of birch wood. Energy and Fuels 2014;28:3863–72. doi:10.1021/ef5004683.

[37] Doddapaneni, Praveenkumar R, Tolvanen H, Palmroth MRT, Konttinen J, Rintala J. Anaerobic batch conversion of pine wood torrefaction condensate. Bioresource Technology 2017;225:299–307. doi:10.1016/j.biortech.2016.11.073

[38] Park J, Meng J, Lim KH, Rojas OJ, Park S. Transformation of lignocellulosic biomass during torrefaction. Journal of Analytical and Applied Pyrolysis 2013;100:199–206. doi:10.1016/j.jaap.2012.12.024.

[39] Melkior T, Jacob S, Gerbaud G, Hediger S, Le Pape L, Bonnefois L, et al. NMR analysis of the transformation of wood constituents by torrefaction. Fuel 2012;92:271–80. doi:10.1016/j.fuel.2011.06.042.

[40] Kiel JHA, Janssen AHH, Joshi Y. Thermochemical Conversion. Biomass as a Sustainable Energy Source for the Future, John Wiley & Sons, Inc; 2014, p. 388–402. doi:10.1002/9781118916643.ch12.

[41] Bates RB, Ghoniem AF. Modeling kinetics-transport interactions during biomass torrefaction: The effects of temperature, particle size, and moisture content. Fuel 2014;137:216–29. doi:10.1016/j.fuel.2014.07.047.

[42] Stelt MJC Van Der. Chemistry and reaction kinetics of biowaste torrefaction. 2010. doi:978-90-386-2435-8.

[43] Anca-couce A, Mehrabian R, Scharler R. Kinetic Scheme to Predict Product Composition of Biomass Torrefaction. Chemical Engineering Transactions 2014;37:43–8. doi:10.3303/CET1437008.

[44] Blasi C Di, Lanzetta M. Intrinsic kinetics of isothermal xylan degradation in inert atmosphere. Journal of Analytical and Applied Pyrolysis 1997;41:287–303.

[45] Anca-Couce A. Reaction mechanisms and multi-scale modelling of lignocellulosic biomass pyrolysis. Progress in Energy and Combustion Science 2016;53:41–79. doi:10.1016/j.pecs.2015.10.002.

[46] Lasek JA, Kopczyński M, Janusz M, Iluk A, Zuwała J. Combustion properties

of torrefied biomass obtained from flue gas-enhanced reactor. Energy 2017;119:362–8. doi:10.1016/j.energy.2016.12.079.

[47] Haykiri-Acma H, Yaman S, Kucukbayrak S. Combustion characteristics of torrefied biomass materials to generate power. 2016 4th IEEE International Conference on Smart Energy Grid Engineering, SEGE 2016 2016:226–30. doi:10.1109/SEGE.2016.7589530.

[48] Ndibe C, Grathwohl S, Paneru M, Maier J, Scheffknecht G. Emissions reduction and deposits characteristics during cofiring of high shares of torrefied biomass in a 500 kW pulverized coal furnace. Fuel 2015;156:177–89. doi:10.1016/j.fuel.2015.04.017.

[49] Lu Z, Jian J, Jensen PA, Wu H, Glarborg P. Influence of Torrefaction on Single Particle Combustion of Wood. Energy and Fuels 2016;30:5772–8. doi:10.1021/acs.energyfuels.6b00806.

[50] Doddapaneni TRKC, Konttinen J, Hukka TI, Moilanen A. Influence of torrefaction pretreatment on the pyrolysis of Eucalyptus clone: A study on kinetics, reaction mechanism and heat flow. Industrial Crops and Products 2016;92:244–54. doi:10.1016/j.indcrop.2016.08.013.

[51] Worasuwannarak N, Wannapeera J, Fungtammasan B. Pyrolysis behaviors of woody biomass torrefied at temperatures below 300°C. 2011 IEEE 1st Conference on Clean Energy and Technology, CET 2011 2011:287–90. doi:10.1109/CET.2011.6041498.

[52] Wannapeera J, Fungtammasan B, Worasuwannarak N. Effects of temperature and holding time during torrefaction on the pyrolysis behaviors of woody biomass. Journal of Analytical and Applied Pyrolysis 2011;92:99–105. doi:10.1016/j.jaap.2011.04.010.

[53] Meng J, Park J, Tilotta D, Park S. The effect of torrefaction on the chemistry of fast-pyrolysis bio-oil. Bioresource Technology 2012;111:439–46. doi:10.1016/j.biortech.2012.01.159.

[54] Dudyński M, Van Dyk JC, Kwiatkowski K, Sosnowska M. Biomass gasification: Influence of torrefaction on syngas production and tar formation. Fuel Processing Technology 2015;131:203–12. doi:10.1016/j.fuproc.2014.11.018.

[55] Pinto F, Gominho J, André RN, Gonçalves D, Miranda M, Varela F, et al. Effect of Rice Husk Torrefaction on Syngas Production and Quality. Energy & Fuels 2017;31:5183–92. doi:10.1021/acs.energyfuels.7b00259.

[56] Xiao L, Zhu X, Li X, Zhang Z, Ashida R, Miura K, et al. Effect of Pressurized Torrefaction Pretreatments on Biomass CO2 Gasification. Energy and Fuels 2015;29:7309–16. doi:10.1021/acs.energyfuels.5b01485.

[57] Zhang Y, Geng P, Liu R. Synergistic combination of biomass torrefaction and co-gasification: 1. Reactivity studies. Bioresource Technology 2017;245:225–33. doi:10.1016/j.biortech.2017.08.197.

[58] Couhert C, Salvador S, Commandre JM. Impact of torrefaction on syngas production from wood. Fuel 2009;88:2286–90. doi:10.1016/j.fuel.2009.05.003.

[59] Hawkins Wright. Global demand for torrefied biomass 2012.

http://www.forestbusinessnetwork.com/13392/global-demand-for-torrefied-biomass-could-exceed-70-million-tonnes-a-year-by-the-end-of-the-decade/ (accessed July 22, 2017).

[60] Proskurina S, Heinimö J, Schipfer F, Vakkilainen E. Biomass for industrial applications: The role of torrefaction. Renewable Energy 2017;111:265–74. doi:10.1016/j.renene.2017.04.015.

[61] Arpiainen V, Wilen C. Production of Solid Sustainable Energy Carriers from Biomass by Means of Torrefaction Report on requirements of end users on densified and torrefied materials. VTT 2014:1–18.

[62] Pirraglia A, Gonzalez R, Saloni D, Denig J. Technical and economic assessment for the production of torrefied ligno-cellulosic biomass pellets in the US. Energy Conversion and Management 2013;66:153–64. doi:10.1016/j.enconman.2012.09.024.

[63] Koppejan J, Sokhansanj S, Melin S, Madrali S. Status overview of torrefaction technologies (IEA Bioenergy Task 32). IEA Bioenergy Task 32 2012:1–54.

[64] Ghiasi B, Kumar L, Furubayashi T, Lim CJ, Bi X, Kim CS, et al. Densified biocoal from woodchips: Is it better to do torrefaction before or after densification? Applied Energy 2014;134:133–42. doi:10.1016/j.apenergy.2014.07.076.

[65] Li H, Liu X, Legros R, Bi XT, Jim Lim C, Sokhansanj S. Pelletization of torrefied sawdust and properties of torrefied pellets. Applied Energy 2012;93:680–5. doi:10.1016/j.apenergy.2012.01.002.

[66] Peng JH, Bi HT, Lim CJ, Sokhansanj S. Study on Density, Hardness, and Moisture Uptake of Torrefied Wood Pellets. Energy Fuels 2013;27:967–974. doi:10.1021/ef301928q.

[67] Hu Q, Shao J, Yang H, Yao D, Wang X, Chen H. Effects of binders on the properties of bio-char pellets. Applied Energy 2015;157:508–16. doi:10.1016/j.apenergy.2015.05.019.

[68] Reza MT, Uddin MH, Lynam JG, Coronella CJ. Engineered pellets from dry torrefied and HTC biochar blends. Biomass and Bioenergy 2014;63:229–38. doi:10.1016/j.biombioe.2014.01.038.

[69] Winjobi O, Zhou W, Kulas D, Nowicki J, Shonnard DR. Production of Hydrocarbon Fuel Using Two-Step Torrefaction and Fast Pyrolysis of Pine. Part 2: Life-Cycle Carbon Footprint. ACS Sustainable Chemistry and Engineering 2017;5:4541–51. doi:10.1021/acssuschemeng.7b00373.

[70] Sermyagina E, Saari J, Zakeri B, Kaikko J, Vakkilainen E. Effect of heat integration method and torrefaction temperature on the performance of an integrated CHP-torrefaction plant. Applied Energy 2015;149:24–34. doi:10.1016/j.apenergy.2015.03.102.

[71] Sermyagina E, Saari J, Kaikko J, Vakkilainen E. Integration of torrefaction and CHP plant: Operational and economic analysis. Applied Energy 2016;183:88–99. doi:10.1016/j.apenergy.2016.08.151.

[72] Clausen LR. Integrated torrefaction vs. external torrefaction - A thermodynamic analysis for the case of a thermochemical biorefinery. Energy

2014;77:597–607. doi:10.1016/j.energy.2014.09.042.

[73] Ping FHH, Tong Z. Anaerobic Biotechnology: Environmental Protection And Resource Recovery. World Scientific Publishing Company; 2015.

[74] Nayono SE. Anaerobic Digestion of Organic Solid Waste for Energy Production. KIT Scientific Publ.; 2010.

[75] Henze M, van Loosdrecht MCM, Ekama GA, Brdjanovic D. Biological Wastewater Treatment. IWA Publishing; 2008.

[76] Hübner T, Mumme J. Integration of pyrolysis and anaerobic digestion - Use of aqueous liquor from digestate pyrolysis for biogas production. Bioresource Technology 2015;183:86–92. doi:10.1016/j.biortech.2015.02.037.

[77] Torri C, Fabbri D. Biochar enables anaerobic digestion of aqueous phase from intermediate pyrolysis of biomass. Bioresource Technology 2014;172:335–41. doi:10.1016/j.biortech.2014.09.021.

[78] Pekařová S, Dvořáčková M, Stloukal P, Ingr M, Šerá J, Koutny M. Quantitation of the Inhibition Effect of Model Compounds Representing Plant Biomass Degradation Products on Methane Production. BioResources 2017;12:2421–32.

[79] Chan JKS, Duff SJB. Methods for mitigation of bio-oil extract toxicity. Bioresource Technology 2010;101:3755–9. doi:10.1016/j.biortech.2009.12.054.

[80] Zhao X, Chi Z, Rover M, Brown R, Jarboe L, Wen Z. Microalgae Fermentation of Acetic Acid-Rich Pyrolytic Bio-Oil : Reducing Bio-Oil Toxicity by Alkali Treatment 2013;32:955–61. doi:10.1002/ep.

[81] Lian J, Garcia-Perez M, Coates R, Wu H, Chen S. Yeast fermentation of carboxylic acids obtained from pyrolytic aqueous phases for lipid production. Bioresource Technology 2012;118:177–86. doi:10.1016/j.biortech.2012.05.010.

[82] Weil JR, Dien B, Bothast R, Hendrickson R, Mosier NS, Ladisch MR. Removal of fermentation inhibitors formed during pretreatment of biomass by polymeric adsorbents. Industrial and Engineering Chemistry Research 2002;41:6132–8. doi:10.1021/ie0201056.

[83] Lee JM, Venditti RA, Jameel H, Kenealy WR. Detoxification of woody hydrolyzates with activated carbon for bioconversion to ethanol by the thermophilic anaerobic bacterium Thermoanaerobacterium saccharolyticum. Biomass and Bioenergy 2011;35:626–36. doi:10.1016/j.biombioe.2010.10.021.

[84] Soleimani M, Tabil L, Niu C. Adsorptive Isotherms and Removal of Microbial Inhibitors in a Bio-Based Hydrolysate for Xylitol Production. Chemical Engineering Communications 2015;202:787–98. doi:10.1080/00986445.2013.867258.

[85] Björklund L, Larsson S, Jönsson LJ, Reimann E, Nilvebrant N-O. Treatment with lignin residue: a novel method for detoxification of lignocellulose hydrolysates. Applied Biochemistry and Biotechnology 2002;98–100:563–75. doi:10.1385/ABAB:98-100:1-9:563.

[86] Cavka A, Jönsson LJ. Detoxification of lignocellulosic hydrolysates using sodium borohydride. Bioresource Technology 2013;136:368–76.

doi:10.1016/j.biortech.2013.03.014.

[87] Zwart RWR, Pels JR. Use of torrefaction condensate 2013.

[88] Rocha EPA, Sermyagina E, Cardoso M, Vakkilainen E, Colodette JL. Pyrolysis of brazilian eucalyptus clones: non-isothermal thermogravimetric kinetic analysis. IWBLCM 2015, 1st International Workshop on Biorefinery of Lignocelulosic Materials, 2015, p. 291–5.

[89] Gomes FJB, Colodette JL, Burnet A, Batalha LAR, Santos FA, Demuner IF. Thorough Characterization of Brazilian New Generation of Eucalypt Clones and Grass for Pulp Production. International Journal of Forestry Research 2015:1–10. doi:http://dx.doi.org/10.1155/2015/814071.

[90] Garcia R, Pizarro C, Lavin AG, Bueno JL. Biomass proximate analysis using thermogravimetry. Bioresource Technology 2013;139:1–4. doi:10.1016/j.biortech.2013.03.197.

[91] Keipi T, Tolvanen H, Kokko L, Raiko R. The effect of torrefaction on the chlorine content and heating value of eight woody biomass samples. Biomass and Bioenergy 2014;66:232–9. doi:10.1016/j.biombioe.2014.02.015.

[92] Kramb J, Gomez-Barea A, DeMartini N, Romar H, Doddapaneni TRKC, Konttinen J. The effects of calcium and potassium on CO2 gasification of birch wood in a fluidized bed. Fuel 2017;196:398–407. doi:10.1016/j.fuel.2017.01.101.

[93] Nocquet T, Dupont C, Commandre JM, Grateau M, Thiery S, Salvador S. Volatile species release during torrefaction of wood and its macromolecular constituents: Part 1 - Experimental study. Energy 2014;72:180–7. doi:10.1016/j.energy.2014.02.061.

[94] Christensen T. Solid Waste Technology and Management. Wiley; 2011.

[95] Deublein D, Steinhauser A. Typical Design Calculation for an Agricultural Biogas Plant. Biogas from Waste and Renewable Resources 2010:357–64. doi:10.1002/9783527632794.ch35.

[96] Lehto J, Oasmaa A, Solantausta Y, Kytö M, Chiaramonti D. Fuel oil quality and combustion of fast pyrolysis bio-oils. VTT Technology n.d.;87:79.

[97] Akbulut A. Techno-economic analysis of electricity and heat generation from ı case study farm-scale biogas plant : Çiçekdagi case study. Energy 2012;44:381–90.

[98] Firdaus N, Prasetyo BT, Sofyan Y, Siregar F. Part II of II: Palm Oil Mill Effluent (POME): Biogas Power Plant. Distributed Generation & Alternative Energy Journal 2017;32:6–18. doi:10.1080/21563306.2017.11878943.

[99] Chen H, Chen X, Qiao Z, Liu H. Release and transformation characteristics of K and Cl during straw torrefaction and mild pyrolysis. Fuel 2016;167:31–9. doi:10.1016/j.fuel.2015.11.059.

[100] Azuara M, Kersten SRA, Kootstra AMJ. Recycling phosphorus by fast pyrolysis of pig manure: Concentration and extraction of phosphorus combined with formation of value-added pyrolysis products. Biomass and Bioenergy 2013;49:171–80. doi:10.1016/j.biombioe.2012.12.010.

[101] Svoboda K, Martinec J, Poho\vrelý M, Baxter D. Integration of biomass drying with combustion/gasification technologies and minimization of emissions of organic compounds. Chemical Papers 2009;63:15–25. doi:10.2478/s11696-008-0080-5.

[102] Deublein D, Steinhauser A. Attachment II: Economy of Biogas Plants for the Year 2007 (Calculation on the Basis of the Example of Attachment I). Biogas from Waste and Renewable Resources 2008;2007:415–7. doi:10.1002/9783527621705.app2.

[103] Turton R. Analysis, Synthesis, and Design of Chemical Processes. Prentice Hall; 2012.

[104] FOEX Indexes Ltd, Bioenergy and Wood Indices n.d. http://www.foex.fi/biomass/ (accessed July 15, 2017).

[105] Buyukkamaci N, Koken E. Economic evaluation of alternative wastewater treatment plant options for pulp and paper industry. Science of the Total Environment 2010;408:6070–8. doi:10.1016/j.scitotenv.2010.08.045.

[106] Uusitalo V, Soukka R, Horttanainen M, Niskanen A, Havukainen J. Economics and greenhouse gas balance of biogas use systems in the Finnish transportation sector. Renewable Energy 2013;51:132–40. doi:10.1016/j.renene.2012.09.002.

[107] Biogas price n.d. https://www.gasum.com/en/About-gasum/for-the-media/News/2016/Natural-gas-price-reduced-at-Gasum-filling-stations-as-from-July-1-2016/ (accessed August 20, 2017).

[108] White JE, Catallo WJ, Legendre BL. Biomass pyrolysis kinetics: A comparative critical review with relevant agricultural residue case studies. Journal of Analytical and Applied Pyrolysis 2011;91:1–33. doi:10.1016/j.jaap.2011.01.004.

[109] Khawam A, Flanagan DR. Basics and applications of solid-state kinetics: A pharmaceutical perspective. Journal of Pharmaceutical Sciences 2006;95:472–498. doi:10.1002/jps.

[110] Sbirrazzuoli N. Determination of pre-exponential factors and of the mathematical functions f(??) or G(??) that describe the reaction mechanism in a model-free way. Thermochimica Acta 2013;564:59–69. doi:10.1016/j.tca.2013.04.015.

[111] Cadenato A, Morancho JM, Fernández-Francos X, Salla JM, Ramis X. Comparative kinetic study of the non-isothermal thermal curing of bis-GMA/TEGDMA systems. Journal of Thermal Analysis and Calorimetry 2007;89:233–44. doi:10.1007/s10973-006-7567-5.

[112] Mishra G, Bhaskar T. Non isothermal model free kinetics for pyrolysis of rice straw. Bioresource Technology 2014;169:614–21. doi:10.1016/j.biortech.2014.07.045.

[113] Fierro V, Torné-Fernández V, Montané D, Celzard A. Adsorption of phenol onto activated carbons having different textural and surface properties. Microporous and Mesoporous Materials 2008;111:276–84. doi:10.1016/j.micromeso.2007.08.002.

[114] Teng TT, Low LW. Removal of Dyes and Pigments from Industrial Effluents BT - Advances in Water Treatment and Pollution Prevention. In: Sharma SK, Sanghi R, editors., Dordrecht: Springer Netherlands; 2012, p. 65–93. doi:10.1007/978-94-007-4204-8_4.

[115] Suresh S, Sundaramoorthy S. Green Chemical Engineering: An Introduction to Catalysis, Kinetics, and Chemical Processes. CRC Press; 2014.

[116] Jain R, Dominic D, Jordan N, Rene ER, Weiss S, van Hullebusch ED, et al. Higher Cd adsorption on biogenic elemental selenium nanoparticles. Environmental Chemistry Letters 2016;14:381–6. doi:10.1007/s10311-016-0560-8.

[117] Louwes AC, Basile L, Yukananto R, Bhagwandas JC, Bramer EA, Brem G. Torrefied biomass as feed for fast pyrolysis: An experimental study and chain analysis. Biomass and Bioenergy 2017. doi:10.1016/j.biombioe.2017.06.009.

[118] Zheng A, Zhao Z, Chang S, Huang Z, He F, Li H. Effect of torrefaction temperature on product distribution from two-staged pyrolysis of biomass. Energy and Fuels, 2012. doi:10.1021/ef201872y.

[119] Chen Q, Zhou JS, Liu BJ, Mei QF, Luo ZY. Influence of torrefaction pretreatment on biomass gasification technology. Chinese Science Bulletin 2011;56:1449–56. doi:10.1007/s11434-010-4292-z.

[120] Pohlmann JG, Osório E, Vilela ACF, Diez MA, Borrego AG. Integrating physicochemical information to follow the transformations of biomass upon torrefaction and low-temperature carbonization. Fuel 2014;131:17–27. doi:10.1016/j.fuel.2014.04.067.

[121] Chen H, Chen X, Qin Y, Wei J, Liu H. Effect of torrefaction on the properties of rice straw high temperature pyrolysis char: Pore structure, aromaticity and gasification activity. Bioresource Technology 2017;228:241–9. doi:10.1016/j.biortech.2016.12.074.

[122] Cai J, Wu W, Liu R, Huber GW. A distributed activation energy model for the pyrolysis of lignocellulosic biomass. Green Chemistry 2013;15:1331. doi:10.1039/c3gc36958g.

[123] Das O, Sarmah AK. Mechanism of waste biomass pyrolysis: Effect of physical and chemical pre-treatments. Science of the Total Environment 2015;537:323–34. doi:10.1016/j.scitotenv.2015.07.076.

[124] Janković B, Adnadević B, Jovanović J. Application of model-fitting and model-free kinetics to the study of non-isothermal dehydration of equilibrium swollen poly (acrylic acid) hydrogel: Thermogravimetric analysis. Thermochimica Acta 2007;452:106–15. doi:10.1016/j.tca.2006.07.022.

[125] Poletto M, Zattera AJ, Santana RMC. Thermal decomposition of wood: Kinetics and degradation mechanisms. Bioresource Technology 2012;126:7–12. doi:10.1016/j.biortech.2012.08.133.

[126] Lu C, Song W, Lin W. Kinetics of biomass catalytic pyrolysis. Biotechnology Advances 2009;27:583–7. doi:10.1016/j.biotechadv.2009.04.014.

[127] Patwardhan P. Understanding the product distribution from biomass fast pyrolysis. Iowa State University 2010;PhD Thesis.

[128] Anthony Dufour. Thermochemical Conversion of Biomass for the Production of Energy and Chemicals. John Wiley & Sons; 2016.

[129] Ren S, Lei H, Wang L, Bu Q, Chen S, Wu J, et al. The effects of torrefaction on compositions of bio-oil and syngas from biomass pyrolysis by microwave heating. Bioresource Technology 2013;135:659–64. doi:10.1016/j.biortech.2012.06.091.

[130] Arshanitsa A, Dizhbite T, Bikovens O, Pavlovich G, Andersone A, Telysheva G. Effects of Microwave Treatment on the Chemical Structure of Lignocarbohydrate Matrix of Softwood and Hardwood. Energy & Fuels 2016;30:457–64. doi:10.1021/acs.energyfuels.5b02462.

[131] Franke-Whittle IH, Walter A, Ebner C, Insam H. Investigation into the effect of high concentrations of volatile fatty acids in anaerobic digestion on methanogenic communities. Waste Management 2014;34:2080–9. doi:10.1016/j.wasman.2014.07.020.

[132] Gyenge L, Crognale S, Lányi S, Ábrahám B, Ráduly B. Anaerobic digestion of corn-DDGS: Effect of pH-control, agiTation and batch repetition. UPB Scientific Bulletin, Series B: Chemistry and Materials Science 2014;76:163–72.

[133] Kim J, Lee C. Changes in Microbial Community Structure During Anaerobic Repeated-Batch Treatment of Cheese-Processing Wastewater. APCBEE Procedia 2013;5:520–6. doi:10.1016/j.apcbee.2013.05.088.

[134] Kinnunen H V., Koskinen PEP, Rintala J. Mesophilic and thermophilic anaerobic laboratory-scale digestion of Nannochloropsis microalga residues. Bioresource Technology 2014;155:314–22. doi:10.1016/j.biortech.2013.12.115.

[135] Labatut RA, Angenent LT, Scott NR. Biochemical methane potential and biodegradability of complex organic substrates. Bioresource Technology 2011;102:2255–64. doi:10.1016/j.biortech.2010.10.035.

[136] Bayr S, Rintala J. Thermophilic anaerobic digestion of pulp and paper mill primary sludge and co-digestion of primary and secondary sludge. Water Research 2012;46:4713–20. doi:10.1016/j.watres.2012.06.033.

[137] Forster-Carneiro T, P??rez M, Romero LI. Thermophilic anaerobic digestion of source-sorted organic fraction of municipal solid waste. Bioresource Technology 2008;99:6763–70. doi:10.1016/j.biortech.2008.01.052.

[138] Negi S. Pretreatment Strategies of Lignocellulosic Biomass Towards Ethanol Yield: Case Study of Pine Needles, in: Biofuels: Technology, Challenges and Prospects. In: Agarwal AK, Agarwal RA, Gupta T, Gurjar BR, editors., Singapore: Springer Singapore; 2017, p. 85–102. doi:10.1007/978-981-10-3791-7_6.

[139] Monlau F, Sambusiti C, Antoniou N, Zabaniotou A, Solhy A, Barakat A. Pyrochars from bioenergy residue as novel bio-adsorbents for lignocellulosic hydrolysate detoxification. Bioresource Technology 2015;187:379–86. doi:10.1016/j.biortech.2015.03.137.

[140] Kohl T, Laukkanen T, Järvinen M, Fogelholm CJ. Energetic and environmental performance of three biomass upgrading processes integrated

with a CHP plant. Applied Energy 2013;107:124–34. doi:10.1016/j.apenergy.2013.02.021.

[141] Ranta T, Föhr J, Soininen H. Evaluation of a pilot-scale wood torrefcaction plant based on pellet properties and Finnish market economics. International Journal of Energy and Environment 2016;7:159–68.

[142] Sgroi F, Foderà M, Di Trapani AM, Tudisca S, Testa R. Economic evaluation of biogas plant size utilizing giant reed. Renewable and Sustainable Energy Reviews 2015;49:403–9. doi:10.1016/j.rser.2015.04.142.

[143] Winjobi O, Shonnard DR, Zhou W. Production of Hydrocarbon Fuel Using Two-Step Torrefaction and Fast Pyrolysis of Pine. Part 1: Techno-economic Analysis. ACS Sustainable Chemistry and Engineering 2017;5:4529–40. doi:10.1021/acssuschemeng.7b00372.

[144] Chai L, Saffron CM, Yang Y, Zhang Z, Munro RW, Kriegel RM. Integration of decentralized torrefaction with centralized catalytic pyrolysis to produce green aromatics from coffee grounds. Bioresource Technology 2016;201:287–92. doi:10.1016/j.biortech.2015.11.065.

Appendix Original papers

Publication I

Tharaka Rama Krishna C Doddapaneni, Jukka Konttinen, Terttu I. Hukka, Antero Moilanen

"Influence of torrefaction pretreatment on the pyrolysis of Eucalyptus clone: A study on kinetics, reaction mechanism and heat flow".

Industrial Crops Products 2016; 92 :244–54.

Industrial Crops and Products 92 (2016) 244–254

Contents lists available at ScienceDirect

Industrial Crops and Products

journal homepage: www.elsevier.com/locate/indcrop

Influence of torrefaction pretreatment on the pyrolysis of Eucalyptus clone: A study on kinetics, reaction mechanism and heat flow

Tharaka Rama Krishna C. Doddapaneni[a,b,*], Jukka Konttinen[a], Terttu I. Hukka[a], Antero Moilanen[a]

[a] Department of Chemistry and Bioengineering, Tampere University of Technology, Korkeakoulunkatu 1, 33720 Tampere, Finland
[b] Department of Chemistry, University of Jyväskylä, P.O. Box 35, 40014 Jyväskylä, Finland

ARTICLE INFO

Article history:
Received 3 February 2016
Received in revised form 3 August 2016
Accepted 7 August 2016

Keywords:
Eucalyptus clone torrefaction
Torrefied biomass
Non-isothermal kinetics
Torrefied biomass pyrolysis
Pyrolysis
Reaction mechanism

ABSTRACT

The adverse nature of biomass requires specific pretreatment processes to better utilize it in bioenergy applications, and torrefaction is one of the most recognized thermal pretreatment methods. In this regard, we studied the effect of torrefaction pretreatment on kinetics, reaction mechanism and heat flow during the pyrolysis of biomass by making a comparative analysis between the pyrolysis of dried and torrefied Eucalyptus wood. Torrefied biomass was produced at three temperatures, namely 250, 275 and 300 °C. Pyrolysis was performed at 700 °C. The char yield during pyrolysis increased from 22.39 percent to 36.34 percent when the torrefaction temperature was increased from 250 to 300 °C. Kinetic analysis showed that torrefied biomass has higher activation energy values than dried biomass. The reported activation energy values for dried biomass were within the range of 165–185 kJ/mol, and for the biomass torrefied at 300 °C they were within the range of 180–245 kJ/mol. We used two different approaches, namely master plots and kinetic compensation parameters, to identify the reaction mechanism. The results showed that torrefaction treatment had an effect on the reaction mechanism of the biomass pyrolysis. The reason could be the degradation of hemicellulose during torrefaction, and thereby the formation of smaller molecules during the pyrolysis of torrefied biomass. The heat flow data from differential scanning calorimetry (DSC) showed that pyrolysis started with exothermic reactions for dried samples, and endothermic reactions for torrefied samples. The results presented provide valuable insights into increasing the understanding of the pyrolysis of torrefied biomass.

1. Introduction

Some of the most concerning environment-related issues include global warming, and the increasing usage and depletion of fossil fuels. Researchers from around the world are increasingly focusing on these issues, and are trying to resolve them with various approaches, of which biomass usage for energy production is one. At the moment, biomass acts as a primary energy source in rural areas of Asia and Africa, where its use is restricted to domestic applications. Because of its attractive characteristics, such as being carbon dioxide neutral, and being a renewable energy source, the interest in biomass energy is also increasing in the Western world (Senneca, 2007). Biomass fuels include wood, short rotation energy crops, grass, agricultural waste, aquatic plants, sawdust, herbaceous shrubs, and so on. According to Alén et al. (1996), biomass mainly comprises cellulose, hemicellulose, lignin and a small amount of extractives.

Biomass-to-energy conversion processes are grouped into three categories based on the approach used—physical, thermochemical, and biological. Of these, thermochemical conversion is the most commonly employed on the industrial scale. The thermal conversion processes are further subdivided into combustion, pyrolysis, torrefaction, and gasification. Compared with other processes pyrolysis is interesting due to its characteristic of producing multiple products (gaseous, bio-oils and char). Pyrolysis is typically defined as the thermal decomposition and devolatilization of organic materials in an inert environment.

However, because of their heterogeneous structure, and their diverse physical and chemical properties, biomass fuels are associated with several issues during their conversion. Commonly reported issues are: their high moisture content, their low energy density, their fibrous and hydrophilic nature, ash and inorganic

* Corresponding author at: Department of Chemistry and Bioengineering, Tampere University of Technology, Korkeakoulunkatu 1, 33720 Tampere, Finland.
E-mail addresses: tharaka.doddapaneni@tut.fi, dtrk09@gmail.com (T.R.K.C. Doddapaneni).

http://dx.doi.org/10.1016/j.indcrop.2016.08.013
0926-6690/

elements and tars. Because of these issues, the thermal conversion of biomass is often considered to be a complex process. To achieve better conversion efficiency, it is equally important to pretreat biomass, and several technologies have been developed in that regard. Torrefaction is one such pretreatment method, which is considered as a mild form of the pyrolysis process where biomass is heated slowly in an inert environment to a temperature in the range 200–300 °C (Tran et al., 2014). Torrefaction enhances the biomass utilization by altering the physical and chemical properties discussed above.

As pyrolysis occurs simultaneously with biomass combustion and gasification, it is important to understand the decomposition characteristics of the fuels for the better design and optimization of the thermochemical processes (Poletto et al., 2012). Important characteristics that need to be evaluated in order to better understand the pyrolysis process are kinetics, the reaction mechanism, and heat flow data of the devolatilization process.

Eucalyptus, which has a high rate of production with an average yield of 45–60 m3/ha/year, is the most widely planted hardwood in the world. In addition to most commonly planted species such as Eucalyptus grandis (EG), E. urophylla (EU), E. camaldulensis, and E. globulus, several hybrids have also been developed under a project called the Brazilian Genolyptus, with the aim of improving the wood quality and productivity (Gomes et al., 2015). These new biomass materials are used in the paper and pulp industry but another interesting option is bioenergy applications. In this regard, it is essential to have a detailed understanding of the thermal decomposition of Eucalyptus clones.

On the other hand, a considerable amount of research data is available on the effects of torrefaction on the physical and chemical properties of the biomass. Also, there are numerous studies available on the pyrolysis of biomass, but very few studies are available on the pyrolysis of torrefied biomass. To the knowledge of the author, no research data is available on the pyrolysis of torrefied Eucalyptus clones. Tolvanen et al. (2013) studied the fast pyrolysis of torrefied wood using a drop tube reactor. Ren et al. (2013a) studied the pyrolysis of torrefied Douglas fir sawdust using the Friedman method; they observed the trend that activation energy decreased as torrefaction temperature increased. Tran et al. (2014) studied the pyrolysis of torrefied stump materials using the Distributed Activation Energy Model (DAEM) and three pseudo-component models, and observed that torrefied stump has a higher level of activation energy than the original stump. In the study of co-pyrolysis of torrefied wood with coal blends, Lu et al. (2013) reported that biomass torrefied at 300 °C contained more lignin than raw biomass. Worasuwannarak et al. (2011) studied the pyrolysis of torrefied Leucaena biomass using the thermal gravimetric mass spectrometry (TG-MS) technique, and concluded that the product distribution between raw and torrefied biomass pyrolysis was significantly different. These studies focused mainly on kinetic parameters but to better understand torrefied biomass pyrolysis, it is equally important to study the reaction mechanism and heat flow.

The aim of the present works was to identify the effect of torrefaction pretreatment on biomass pyrolysis characteristics—kinetics, reaction mechanism and heat flow. In the present study, we employed thermogravimetric analysis (TGA) and differential scanning calorimetry (DSC) to investigate the pyrolysis of Eucalyptus biomass. The biomass was torrefied at three different temperatures, that is, 250, 275 and 300 °C. Torrefied biomass pyrolysis is carried out at 700 °C, with heating rates of 5, 8, 12 and 20 °C/min. For the kinetic analysis, we used the methods of Flynn-Wall-Ozawa (FWO) and Kissinger-Akahira-Sunose (KAS), and the Friedman model free method. The model-fitting method, called the Coats-Redfern method, was used to identify the reaction mechanism during the pyrolysis of torrefied biomass. We carried out a preliminary analysis on DSC data to support the findings of the TGA. The presented results provide valuable insights into increasing the understanding of the pyrolysis of torrefied biomass.

2. Materials and method

2.1. Materials

The biomass sample selected for this study was Eucalyptus clone E. urophylla (Timor) × E. camaldulensis (VM1). The selected material is also known as “urocam”. The debarked stems of the selected Eucalyptus biomass samples were supplied by the Department of Forest Engineering, Federal University of Vicosa, Minas Gerais, Brazil. The detailed compositional analysis of the selected biomass was presented by Rocha et al., 2015a and Gomes et al., 2015. Prior to the experimental analysis, the biomass samples used in the experiments were ground using a Retsch ZM 200 centrifugal mill. To avoid the internal heat transfer effects, the ground biomass was sieved to a mesh size of 100–125 μm. Biomass of the same particle size was used for all the experiments.

2.2. Experimental plan

2.2.1. Thermogravimetric analysis

Both torrefaction and pyrolysis of the Eucalyptus samples were carried out in a Mettler Toledo TGA850. To create the inert environment around the sample, and also to remove the released volatile gases, we used nitrogen gas at a flow rate of 80 ml/min. For each test, we used a sample size of about 7.5 mg in a 70 μl aluminum oxide crucible. To make sure that an inert environment was achieved in the TGA furnace, we allowed a purging time of 20 min at the beginning of each experiment. For each experiment, we raised the furnace temperature from room temperature to 105 °C at 20 °C/min., and maintained the temperature of 105 °C for an isothermal period of 30 min to ensure the drying was complete. To produce the torrefied biomass, the furnace temperature was increased from 105 °C to the selected torrefaction temperature (250, 275 or 300 °C) at 50 °C/min., and kept at that temperature for 1 h. Later, we used the same crucible with the torrefied biomass for the subsequent pyrolysis process. For pyrolysis, the furnace temperature was increased from 105 °C to 700 °C at selected heating rates, and the samples were kept at 700 °C for 40 min. The selected heating rates (β) were 5, 8, 12 and 20 °C/min. All experiments were conducted twice to check the reproducibility. The sample temperature and the corresponding mass were automatically recorded simultaneously by the TGA equipment. Hereafter, the torrefied biomass is represented by TB250, TB275 and TB300 for a torrefaction temperature of 250, 275 and 300 °C, respectively, and the dried Eucalyptus clone is abbreviated to DEC.

2.2.2. Differential scanning calorimetry

The torrefied biomass for the DSC experiments was produced in a tube furnace, located at the Material Science Department, Tampere University of Technology, Tampere, Finland. Torrefied biomass was produced by increasing the furnace temperature from 105 °C to the selected torrefaction temperature (250 and 300 °C) at 20 °C/min., and kept at that temperature for 1 h. For each test, a sample size of about 10 mg in ceramic crucible was used. The DSC experiments were carried out in a Mettler Toledo DSC821e differential scanning calorimeter. The dried biomass and torrefied biomass samples of 3.5–4 mg were each loaded into 40 μl aluminum crucibles, and later closed with a pierced lid. An empty 40 μl aluminum crucible with a pierced lid was used for the reference. The relative mass difference between the sample and the reference was approximately one percent. At the beginning of each test, a purging time of

20 min at 50 °C was allowed. The operating conditions for the drying zone were the same as in the case of the TGA measurements. The pyrolysis temperature range was 105–500 °C at a selected heating rate of 20 °C/min. We used 99.9995 percent nitrogen at a flow rate of 50 cm3/min as an inert gas flowing into the furnace.

2.3. Kinetic modeling

As per, White et al. (2011) pyrolysis of lignocellulosic biomass can be represented with a single-step endothermic reaction i.e. lumping of all reactions together as shown in the reaction (R1)

$$Solid\ \ Biomass \xrightarrow{k} Char + Volatiles \qquad (R1)$$

where k is the global apparent rate constant and its temperature dependency can be represented by Arrhenius equation as,

$$k(T) = A\ \ exp\left(\frac{-E_a}{RT}\right) \qquad (1)$$

where 'T' is the absolute temperature (K), 'R' is the universal gas constant (J/K mol), 'A' is the frequency factor or pre-exponential factor (min-1), and 'E_a' is the activation energy.

Single step solid-state reactions under isothermal conditions can be expressed by the first order differential equation as,

$$\frac{d\alpha}{dt} = k(T)\cdot f(\alpha) \qquad (2)$$

where $\frac{d\alpha}{dt}$ is the reaction rate, $k(T)$ is the above discussed rate constant and $f(\alpha)$ is a conversion function which represents the controlling reaction mechanism. The conversion functions of commonly used solid state reaction models are presented in Table 1. α is the extent of reaction (−) and it can be defined as the amount of material decomposed in mass fraction as,

$$\alpha = \frac{m_o - m_t}{m_o - m_f}$$

where, m_0 is the initial mass of the sample, m_t is the mass of the material present at time 't' and m_f is the final residual mass of the material.

After substituting Eq. (1) in (2), Eq. (2) becomes

$$\frac{d\alpha}{dt} = A\exp\left(-\frac{E_a}{RT}\right)\cdot f(\alpha) \qquad (3)$$

For non-isothermal experiments the rate equation can be expressed as Eq. (4)

$$\frac{d\alpha}{dT} = \left(\frac{A}{\beta}\right)\cdot \exp\left(-\frac{E_a}{RT}\right)\cdot f(\alpha) \qquad (4)$$

where β is the linear heating rate $\left(\frac{dT}{dt}\right)$.

Different mathematical models which are listed at (Brown et al., 2000; Khawam and Flanagan, 2006) have been developed to solve the Eq. (4)

Integrating the Eq. (4) within the limits of 0 *to* α and T_0 *to* T gives Eq. (5)

$$g(\alpha) = \frac{A}{\beta}\int_0^T e^{-\frac{E_a}{RT}}dT \qquad (5)$$

Table 1
Differential $f(\alpha)$ and integral form $g(\alpha)$ of usually employed solid state reaction models (Khawam and Flanagan, 2006).

Model	$f(\alpha) = \frac{1}{k}\left(\frac{d\alpha}{dt}\right)$	$g(\alpha) = kt$
Reaction order models		
First order (F1)	$1-\alpha$	$-\ln(1-\alpha)$
Second order (F2)	$(1-\alpha)^2$	$(1-\alpha)^{-1}-1$
Third order (F3)	$(1-\alpha)^3$	$0.5[(1-\alpha)^{-1}-1]$
Diffusion models		
1-D diffusion (D1)	$1/2\alpha$	α^2
2-D diffusion (D2)	$[-\ln(1-\alpha)]^{-1}$	$[(1-\alpha)\ln(1-\alpha)]+\alpha$
3-D diffusion (D3)	$3(1-\alpha)^{\frac{2}{3}}/2\left(1-(1-\alpha)^{\frac{1}{3}}\right)$	$[1-(1-\alpha)^{\frac{1}{3}})]^2$
Geometrical contraction models		
Contracting area (R2)	$2(1-\alpha)^{1/2}$	$1-(1-\alpha)^{1/2}$
Contracting volume (R3)	$3(1-\alpha)^{2/3}$	$1-(1-\alpha)^{1/3}$

In the Eq. (5) the term $\int_0^T e^{-\frac{E_a}{RT}}dT$ represents the temperature integral which does not have an analytical solution. If the term $\frac{E_a}{RT}$ is replaced with 'x', then the Eq. (5) can be transformed as equation.

$$g(\alpha) = \frac{AE_a}{\beta R}\int_0^\infty (e^{-x}/x^2)dx \qquad (6)$$

which can be presented as

$$g(\alpha) = \frac{AE_a}{\beta R}p(x). \qquad (7)$$

2.3.1. Coats & Redfern method

The Coats & Redfern method is the most widely used model-fitting method in the non-isothermal analysis of biomass. It uses the integral approach to the rate equations and asymptotic series expansion for approximating the temperature integral $p(x)$ giving Eq. (8).

$$\ln\left(\frac{g(\alpha)}{T^2}\right) = \ln\left[\frac{AR}{\beta E}\left(1-\frac{2RT}{E_a}\right)\right] - \frac{E_a}{RT} \qquad (8)$$

Plotting a graph of the left-hand side versus $\frac{1}{T}$ yields a straight line; the values of '$-E_a$' and 'A' can be determined from its slope and intercept, respectively.

2.3.2. Friedman

Friedman uses the differential form of the non-isothermal rate equation. Applying the natural logarithm to the non-isothermal rate law, the Eq. (4) gives Eq. (9)

$$\ln\left[\beta\left(\frac{d\alpha}{dT}\right)\right]_\alpha = \ln[Af(\alpha)] - \frac{E_a}{RT_\alpha} \qquad (9)$$

A plot between $\ln\left[\left(\frac{d\alpha}{dt}\right)\right]_\alpha$ versus $1/T\alpha$ gives a straight line; the values of '$-E_a$' and 'A' can be determined by its slope and intercept, respectively (Khawam and Flanagan, 2006).

2.3.3. Flynn-Wall-Ozawa method (FWO)

FWO method uses the integral form of the non-isothermal rate equation. Applying the logarithm to the non-isothermal rate law and by solving the temperature integral $p(x)$ using Doyle's approximation the Eq. (7) gives Eq. (10).

$$(\log\beta)_\alpha = \log\left(\frac{AE_a}{Rg(\alpha)}\right) - 2.315 - 0.4567\frac{E_a}{RT_\alpha} \qquad (10)$$

A plot of $\left(\log\beta\right)_{\alpha}$ versus $1/T_{\alpha}$ gives a straight line; the values of '$-E_a$' and 'A' can be determined from its slope and intercept respectively (Khawam and Flanagan, 2006).

2.3.4. Kissinger-Akahira-Sunose (KAS)

KAS method is an integral iso-conversional method which uses Doyle's approximation to solve the temperature integral. Applying the Doyle's approximation to the temperature integral and taking the natural logarithm on both sides gives the Eq. (11).

$$\ln\left(\frac{\beta}{T_{\alpha}^{2}}\right) = \frac{-E_a}{R}\left(\frac{1}{T_{\alpha}}\right) - \ln\left[\left(\frac{E_a}{AR}\right)\int_{0}^{\alpha}\frac{d\alpha}{f(\alpha)}\right] \quad (11)$$

The kinetic parameters can be evaluated graphically by plotting $\ln\left(\frac{\beta}{T_{\alpha}^{2}}\right)$ as a function of $\frac{1}{T_{\alpha}}$ (White et al., 2011).

2.3.5. Evaluation of pre-exponential factor and reaction mechanism

Model free methods can be used to study the E_a values and to find out their dependency on the conversion (α). As the, kinetic parameters are computed without having the knowledge on the reaction mechanism, using iso-conversional methods is not suggested in order to evaluate the pre-exponential factor. There are several approaches to predict the reaction mechanism and pre-exponential factor and some of them are explained in (Sbirrazzuoli, 2013; Cadenato et al., 2007). In the present study two different approaches, i.e. master plots and kinetic compensation effect (KCE), were used to evaluate the reaction mechanism.

2.3.5.1. Integral master plots. The solid state degradation reaction mechanism can be determined using the master plots method, where the reduced theoretical curves of each reaction model are compared with the experimental curves. Using a reference point at α = 0.5, the following Eq. (12) can be determined from Eq. (6).

$$\frac{g(\alpha)}{g(0.5)} = \frac{p(x)}{p(x)_{0.5}} \quad (12)$$

where $p(x)_{0.5}$ is the temperature integral at α = 0.5.

Eq. (13) can be obtained upon applying the Coats-Redfern approximation to the Eq. (12).

$$\frac{g(\alpha)}{g(0.5)} = \frac{exp\left(-E_a/RT\right)T^2}{exp\left(-E_a/RT_{0.5}\right){T_{0.5}}^2} \quad (13)$$

The left side of Eq. (13) represents the reduced theoretical curve of each reaction model. If the activation energy value is known, the right side term can be calculated from the experimental data (Cadenato et al., 2007).

2.3.5.2. Kinetic compensation effect (KCE). The kinetic compensation effect can be described as the correlation between the kinetic parameters i.e. if a variation in the activation energy E_a is observed, and then there will be a change also in the pre-exponential factor A. The variation in E_a and A values may be because of the temperature program or reaction model used. An apparent compensation effect exists when a model changes in the model fitting method, where the kinetic parameters are evaluated from a single heating rate. The KCE can be explained mathematically by transforming the Eq. (2) to Eq. (14)

$$\ln A_i = \frac{E_i}{RT} + \ln\left[\frac{\left(d\alpha/dt\right)}{f(\alpha)}\right]_i \quad (14)$$

$$\ln A_i = a + bE_i \quad (15)$$

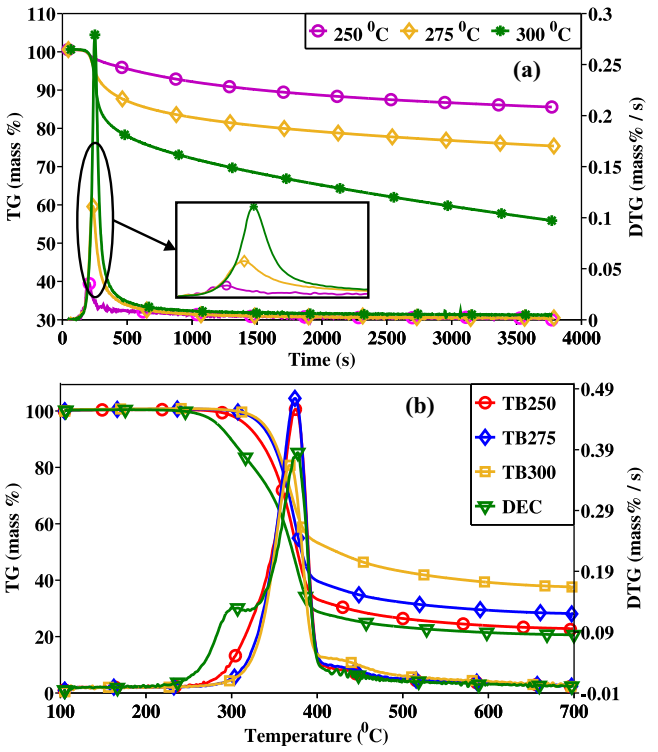

Fig 1. TG and DTG Curves of torrefaction and pyrolysis processes (a) torrefaction curves at various temperatures (b) pyrolysis of dried and torrefied biomass at 20 °C/min.

where a and b are the compensation parameters and i refers to a factor producing variation in E_a and A values.

Model-fitting methods like Coats-Redfern can be used to produce a set of E_a and A values for each reaction model at different heating rates. The parameters E_a and A obtained by model-fitting method are used to present the compensation effect and there by evaluating the compensation parameters a and b. Once the compensation parameters are evaluated, the pre-exponential factor $\ln A$ can be obtained from Eq. (15) using E_α values from iso-conversional methods. When E_α and A_α values are obtained, the conversion function f(α) can be evaluated by substituting terms into Eq. (2). Finally, the suitable reaction mechanism can be identified by comparing the theoretical f(α) curves with experimental f(α) curves (Mishra and Bhaskar, 2014; Sbirrazzuoli, 2013). Totally eight reaction models (Table 1) which are frequently used in biomass decomposition processes were studied.

TGA data was primarily processed using MS Excel and kinetic analysis was made with a specially designed program in MATLAB.

3. Results and discussion

3.1. Thermogravimetric analysis of Eucalyptus clone torrefaction

TG analysis of torrefaction of the DEC biomass is presented in Fig. 1a. Temperature shows a significant effect on the mass loss during torrefaction. From Fig. 1a, it can be seen that the torrefied biomass yields were 85.57, 75.35 and 44.36 wt.% for torrefaction temperatures of 250, 275 and 300 °C, respectively. For the 250 °C and 275 °C the mass-loss curve is almost becomes linear, but in the case of 300 °C it can be seen that the mass-loss curve continues to go down because of the degradation of cellulose and lignin in addition to the hemicellulose degradation. According to White et al. (2011), the left and right shoulders of the DTG curves represent the hemicellulose and cellulose, and the long tail represents the lignin

degradation. From Fig. 1a, for the 300 °C case, the left and right shoulders are both clearly visible. For the 275 °C case, a very small right shoulder is observed and for the 250 °C case, there is no right shoulder. This indicates that cellulose thermal degradation needs a higher temperature than 250 °C. This analysis was in accordance with the work done by Chen and Kuo (2011).

3.2. Thermogravimetric analysis of pyrolysis

The TG and DTG curves of dried and torrefied biomass measured at a heating rate of 20 °C/min. are presented in Fig. 1b as an example to make a comparative analysis between dried and torrefied biomass. Compared with the dried biomass, the active pyrolysis temperature range of the torrefied biomass was increased to higher temperatures, and this rise was directly proportional to the torrefaction temperature. The same trend was reported by Ren et al. (2013a) for the pyrolysis of torrefied Douglas fir sawdust. The residual char yield increased significantly with the torrefaction temperature. For the dry biomass, the char yield was 19.85 wt.%, and for the torrefied biomass samples TB250, TB275 and TB300 the char yields were 22.39, 29.92, and 36.34 wt.%, respectively. The increased char yield for the torrefied biomass in the TB300 sample was due to the relative loss of the cellulose, and crosslinking reactions (Park et al., 2013).

The DTG curves of DEC pyrolysis (Fig. 1b) shows two peaks. Published data (Rocha et al., 2015b) suggests that the first peak represents the hemicellulose degradation, and that the second peak represents the cellulose degradation. For the heating rate of 20 °C/min., the first and second peaks for DEC were observed at 301 and 377 °C, respectively. From Fig. 1b, it can be clearly seen that the first peak has disappeared in the case of torrefied biomass pyrolysis. The shoulder on the left has shifted towards the second peak, and the degree of the shift increases with the increasing torrefaction temperature. The reason was most likely the large mass loss of hemicellulose and cellulose during the torrefaction process. Fig. 1b shows that, when the torrefaction temperature was increased, the pyrolysis started at a higher temperature. The pyrolysis starting temperatures at a 20 °C/min. heating rate for DEC, TB250, TB275 and TB300, were 262, 308, 323 and 330 °C, respectively. The temperature at the end of the pyrolysis was around 400 °C, which was about the same for both the dried and all the torrefied biomass samples. From the DTG curves (Fig. 1b), it can be seen that the peak temperature for both the TB250 and TB275 cases was very close to that of the dried biomass, but a slight change in the peak temperature was observed in the case of TB300. In contrast to the dried biomass, the higher peak was observed for the torrefaction temperatures of 250 and 275 °C. But in the 300 °C case, the peak was below that of the dried biomass. The observed peak heights as a percent of

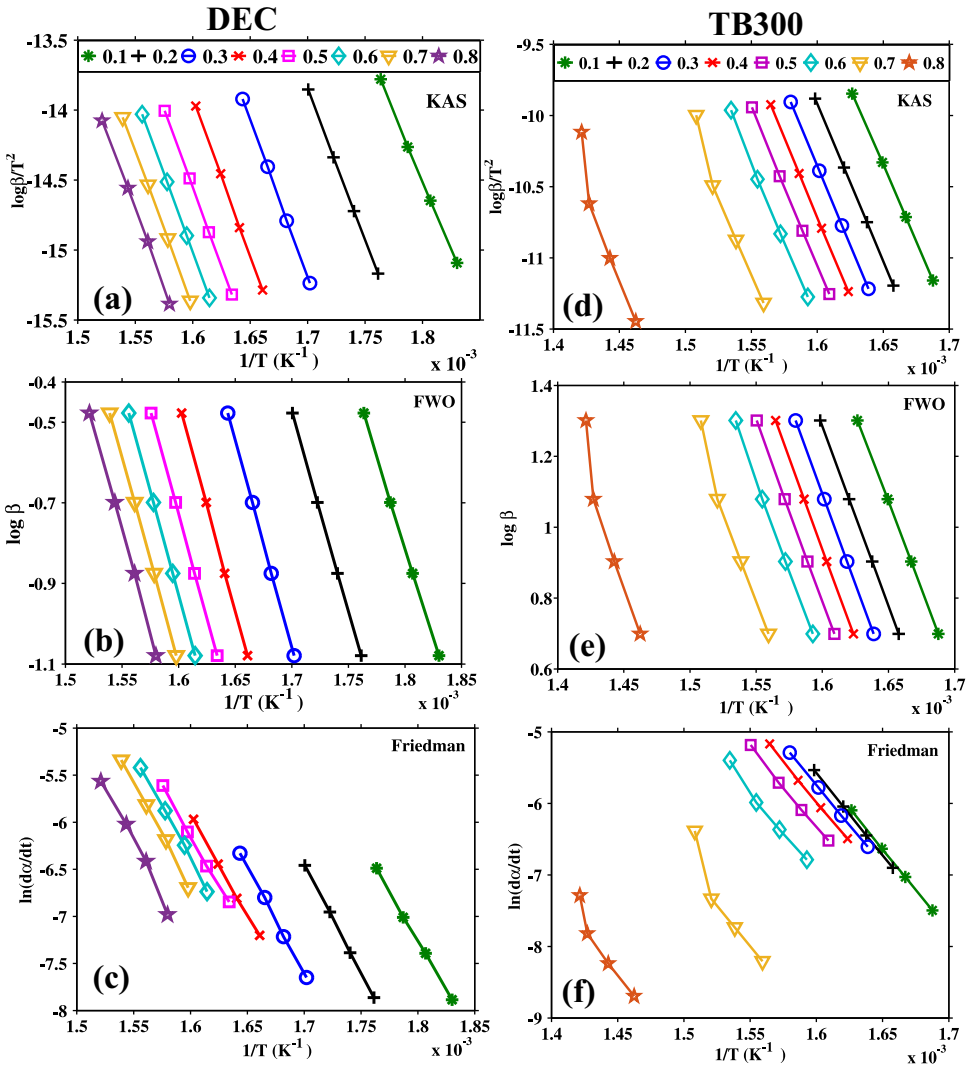

Fig. 2. Iso-conversional plots of KAS, FWO and Friedman methods at various conversions (a-c) dried biomass (DEC) (d-f) Torrefied biomass (TB300).

Table 2
Iso-conversional kinetic parameters for DEC and TB300 at various conversion values.

DEC						
	FWO		KAS		Friedman	
α	E_a (kJ/mol)	R^2	E_a (kJ/mol)	R^2	E_a (kJ/mol)	R^2
0.1	165	0.9999	164	0.9989	173	0.9988
0.2	180	0.9993	180	0.9996	192	0.9996
0.3	188	0.9998	187	0.9999	188	0.9999
0.4	189	0.9991	189	0.9999	176	0.9999
0.5	188	0.9999	187	0.9999	176	0.9999
0.6	187	0.9982	186	1	186	1
0.7	186	0.9982	185	1	190	1
0.8	186	0.9974	185	0.9999	198	0.9999
Average	184		183		185	
TB300						
0.1	179	0.9999	179	0.9999	189	0.9999
0.2	185	1	184	1	191	1
0.3	186	1	185	1	186	0.9999
0.4	187	1	186	1	187	0.9994
0.5	187	0.9999	186	0.9999	188	0.9981
0.6	188	0.9992	187	0.9991	197	0.9912
0.7	208	0.9808	208	0.9789	275	0.9063
0.8	246	0.9369	247	0.9313	261	0.9295
Average	196		195		209	

the mass-loss per second, for dried biomass and TB250, TB275 and TB300 at a 20 °C/min heating rate, were 0.38, 0.45, 0.47 and 0.36, respectively. From the same DTG curve (Fig. 1b), at the end of the active pyrolysis at 430 °C for TB300, a mild pyrolysis was observed in addition to the cellulose pyrolysis. Lu et al. (2013) attributed the mild pyrolysis to the lignin reaction. Based on their fiber analysis, the biomass torrefied at 300 °C contains more lignin (69 percent) than the biomass torrefied at 250 °C (42 percent).

3.3. Kinetic analysis

3.3.1. Model-free methods

The iso-conversional FWO, KAS and Friedman plots for DEC and TB300 are presented in Fig. 2. The fitted lines are nearly parallel for DEC (Fig. 2a–c), but for TB300, the fitted lines were not parallel at the end of the conversion, that is for values greater than 0.7 (Fig. 2d–f). This variation increased according to the severity of the torrefaction. Table 2 records the apparent activation energy (E_a) and the exponential factor (A) for DEC and TB300, for a conversion range of 0.1–0.8. From Table 2, the values of the average apparent activation energy of DEC for the FWO, KAS, and Friedman methods were 184, 183 and 185 kJ/mol, respectively. In the case of torrefied biomass, for TB250, TB275 and TB300, the respective reported values were 183, 184 and 196 kJ/mol for FWO, 182, 183 and 195 kJ/mol for KAS, and 188, 193 and 209 kJ/mol for Friedman.

Fig. 3 shows the activation energy (E_a) as a function of the conversion rate (α) for dried and torrefied biomass. From the same figure, for torrefied biomass it can be observed that the E_a values were stable with little variation in the conversion range of 0.1–0.6. In the case of dried biomass, the E_a values at the start of the pyrolysis were lower than those of the torrefied biomass. The variation in the activation energy values increased as the torrefaction temperature increased. This can be attributed to the depletion of hemicellulose during the torrefaction. According to Chen and Kuo (2011), and also as reported in this study from Fig. 1b (the first peak) and Fig. 3a, hemicellulose starts degrading at low temperatures and with low activation energy values. Since the highly reactive hemicellulose is already degraded, the pyrolysis of torrefied biomass requires more energy to start the pyrolysis reactions. The same phenomenon can be observed from Fig. 1b (TG curve), where the mass loss of DEC started earlier than that of the torrefied biomass. In the conversion

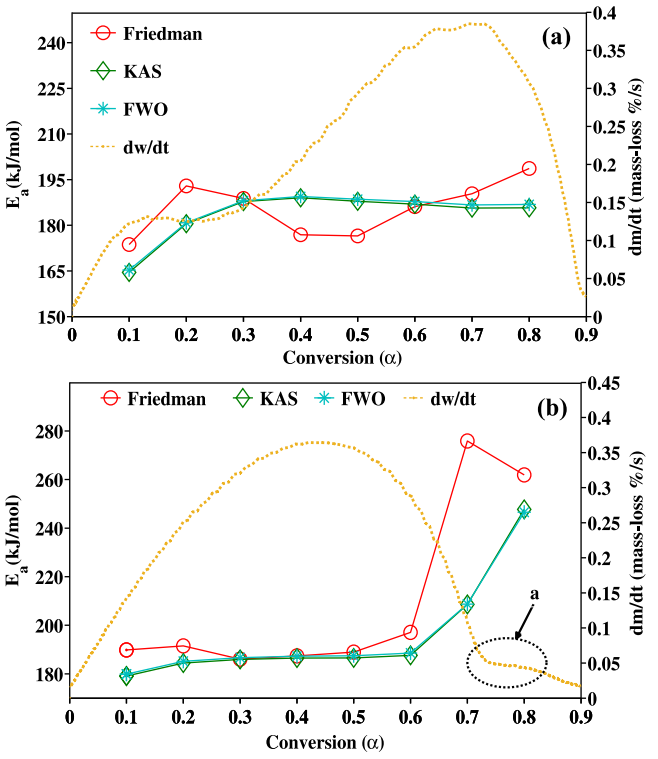

Fig. 3. Activation energy (E_a) vs. Conversion (α) for dried and torrefied biomass (a) DEC (b) TB300.

range of 0.3–0.5, slight decreases were observed in the activation energy values in the case of the Friedman method, whereas no changes in the activation energy values were observed for the FWO and KAS methods. At the end of the pyrolysis, that is, for values of α greater than 0.7, the E_a values showed an increasing trend for both dried and torrefied biomass, but the variation is higher for the torrefied biomass. This huge variation in the E_a values at the end of the torrefied biomass pyrolysis can be attributed to the altered biomass structure, and the degradation of lignin. This was discussed in Section 3.2, and corresponds to the marked area '*a*' in Fig. 3b. It shows that the selected Eucalyptus clone torrefied at higher temperatures, especially at 300 °C, has higher activation energies than those of the dried biomass. Tran et al. (2014) observed the same trend during their study on torrefied stump materials.

Rocha et al., 2015b worked with the non-isothermal pyrolysis of Eucalyptus clones. Their reported values of activation energy varied from 120 kJ/mol to 150 kJ/mol, which were a little lower than the values observed (185 kJ/mol) in the present study. This variation in the kinetic parameters could be attributed to the difference in the experimental procedures adopted. Poletto et al. (2012) reported an E_a value of 200 kJ/mol for the non-isothermal pyrolysis of *Eucalyptus grandis*, which is very close to the value (185 kJ/mol) observed for the Eucalyptus clone pyrolysis in this work.

The activation energy values reported by Jin et al. (2013) for the non-isothermal pyrolysis of cellulose and hemicellulose are in the range of 208–381 and 88–348 kJ/mol respectively. Amutio et al. (2015) studied the fast pyrolysis of eucalyptus wood waste and reported the activation energy values of 103 and 172 kJ/mol for cellulose and hemicellulose respectively. Literature survey shows that the difference in the activation energy values between hemicellulose and cellulose is very high. But, considering that hemicellulose is mainly degraded during the torrefaction, the observed difference in the activation energy values of dried and torrefied biomass pyrolysis is not as high as the difference in

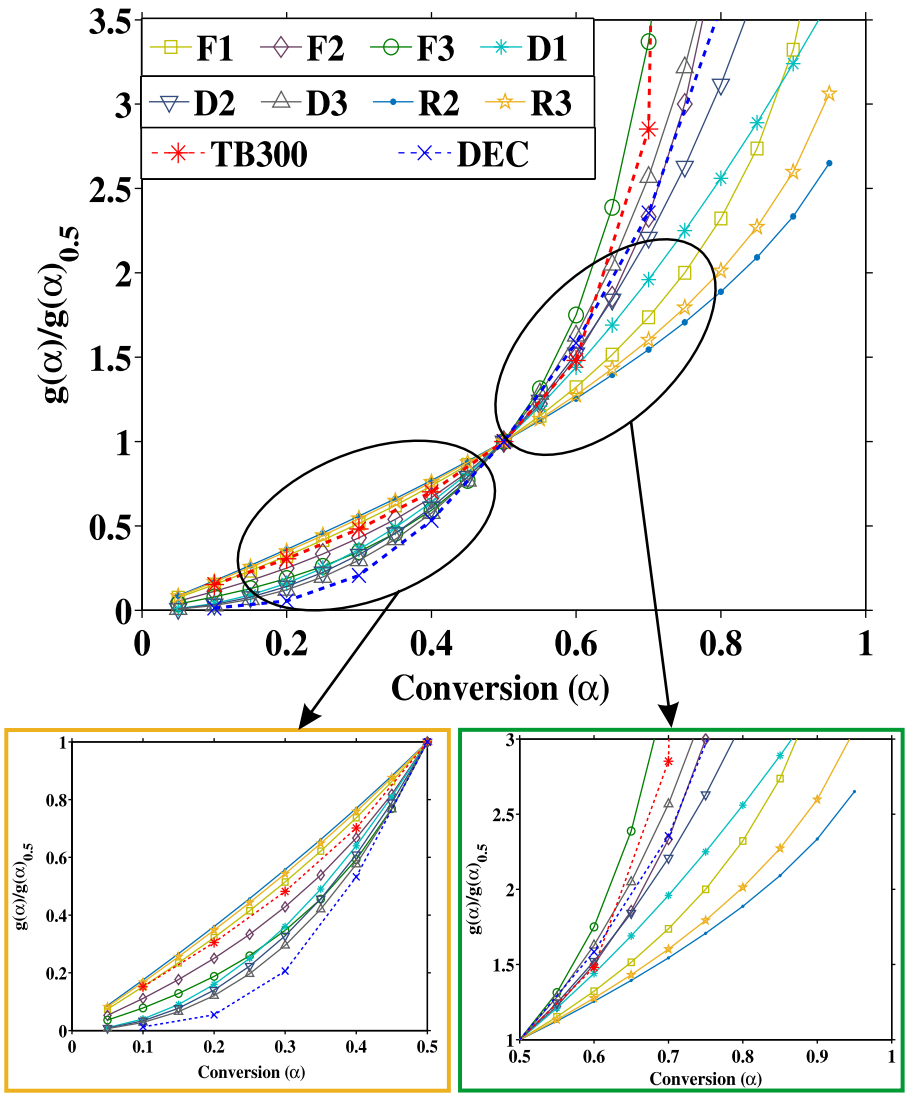

Fig. 4. Theoretical and experimental master plots ($g(\alpha)/g(\alpha)_{0.5}$ vs. conversion (α)) for both DEC and TB300. (Check Table 1 for abbreviation).

the activation energy values of the individual biomass components. This variation in the activation energy values between dried and torrefied biomass pyrolysis could be attributed to the structural changes in the biomass. Ru et al. (2015) reported that the structures of hemicellulose and cellulose becomes similar after the torrefaction. When the results from this study are compared with published data, the difference in the activation energy values (184 and 196 kJ/mol for DEC and TB300 respectively) are in the same range with the published data. For example, Das and Sarmah, (2015) reported the activation energy values of 186 and 188 kJ/mol for raw and torrefied (270 °C, 5 min) Douglas fir biomass respectively.

3.4. Identifying the reaction mechanism

According to Janković et al. (2007), the dependence of E_a values on the conversion represents the presence of a multistep reaction mechanism. From observing Fig. 3, it can be stated that the pyrolysis of both dried and torrefied biomass proceeds with a multistep reaction mechanism. The E_a values obtained from the FWO method are used to evaluate the reaction mechanism. A comparative analysis was conducted between dried biomass and the biomass torrefied at 300 °C (TB300) in order to identify the effect of torrefaction on the reaction mechanism during biomass pyrolysis.

3.4.1. Integral master plots

The theoretical and experimental $g(\alpha)$ curves plotted as a function of the conversion rate (α) are presented in Fig. 4 for both the DEC and the TB300 samples. The experimental master plots were constructed using Eq. (13), and the predetermined average activation energy values from the FWO method, that is, 184 and 196 kJ/mol for DEC and TB300, respectively. From Fig. 4, it can be observed for DEC that, if the conversion rate (α) is less than 0.6, then the experimental curve is close to the theoretical master plots of diffusion order models (D1, D2 and D3). When α is greater than 0.6, the same experimental curve is close to the second order reaction model. Similar results were reported by Mishra and Bhaskar (2014); Poletto et al. (2012) and Vlaev et al. (2003). In the case of the torrefied biomass (TB300), when the conversion rate (α) is less than 0.5, the experimental curve is close to the first order reaction model and for conversion values greater than 0.5 the decomposition mechanism is controlled by diffusion reactions. The results show that the decomposition process for both dried and torrefied Eucalyptus clone proceeds with complex multistep reactions.

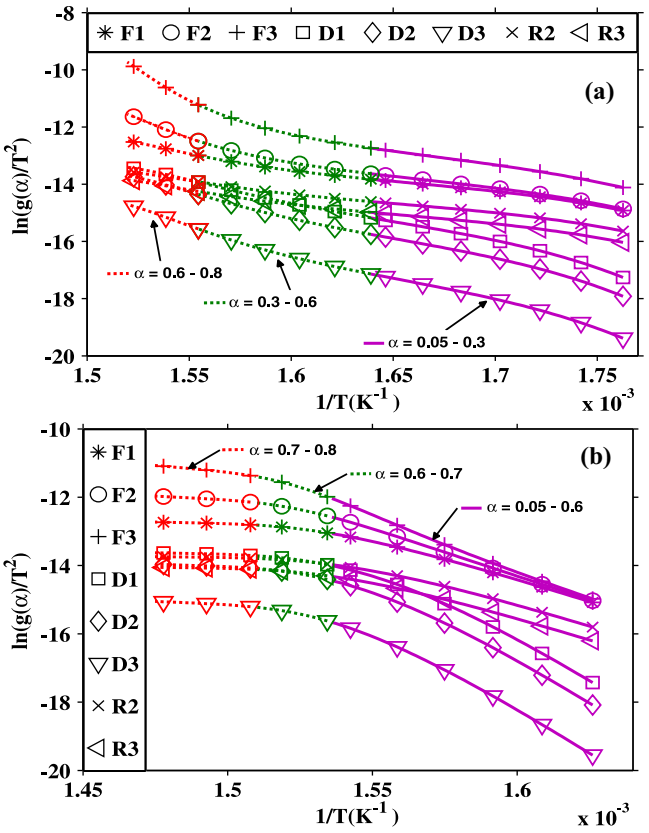

Fig. 5. Coats-Redfern graphs for dried and torrefied biomass (TB300) at various reaction models (a) DEC (b) TB300. (Check Table 1 for abbreviation).

Table 3
Kinetic parameters of Coats-Redfern method for Torrefied biomass (TB300) at different stages of conversion.

Reaction Model	α	E_a (kJ/mol)	A (sec^{-1})	R^2
First order (F1)				
	0.05–0.6	197	1.25E + 14	0.9968
	0.6–0.7	76	8.39E + 03	0.9815
	0.7–0.8	15	2.54E − 02	0.9936
Second order (F2)				
	0.05–0.6	229	7.69E + 16	0.9999
	0.6–0.7	130	5.25E + 08	0.9873
	0.7–0.8	37	7.83E + 00	0.9982
Third order (F3)				
	0.05–0.6	264	2.00E + 20	0.9984
	0.6–0.7	198	8.99E + 14	0.9901
	0.7–0.8	67	1.38E + 04	0.9988
1D-difussional (D1)				
	0.05–0.6	346	1.08E + 26	0.9879
	0.6–0.7	86	2.79E + 04	0.9751
	0.7–0.8	12	5.84E − 03	0.9807
2D-difussional (D2)				
	0.05–0.6	364	1.79E + 27	0.9913
	0.6–0.7	107	9.87E + 05	0.9784
	0.7–0.8	19	2.27E − 02	0.99
3D-difussional (D3)				
	0.05–0.6	383	1.87E + 28	0.9944
	0.6–0.7	134	5.15E + 07	0.9816
	0.7–0.8	30	7.08E − 02	0.9948
Contracting area (R2)				
	0.05–0.6	181	2.74E + 12	0.9926
	0.6–0.7	55	4.99E + 01	0.9762
	0.7–0.8	6	9.78E − 04	0.9759
Contracting volume (R3)				
	0.05–0.6	187	5.87E + 12	0.9945
	0.6–0.7	61	1.37E + 02	0.9783
	0.7–0.8	9	1.55E − 03	0.986

3.4.2. *Kinetic compensation effect*

The model fitting methods can be applied to the region where the activation energy (E_a) is approximately constant. In this study, Coats-Redfern method was used to find a set of E_a and A values for all the reaction models presented in Table 1 at different heating rates. Based on Fig. 3, the Coats-Redfern graphs are divided into three stages, as shown in Fig. 5a–b, where model-free analysis indicates constant activation energy values. The evaluated kinetic parameters for TB300 at β = 20 °C/min. are presented in Table 3, and for DEC they are presented in Table S1in the Supplementary information.

The kinetic compensation parameters (a, b) at different stages of the conversion for four heating rates for DEC and TB300 samples are presented in Table 4. Fig. 6 shows the relationship between E_a and $ln\ A$ at different stages of conversion of TB300 for β = 20 °C/min. The linear relationship between $ln\ A$ and E_a shows the presence of a compensation effect. It can be seen that the values of a and b are close to each other for different heating rates. Once the compensation parameters are evaluated, the pre-exponential factor, (A_α), and the conversion function, f(α), are evaluated for different Eα values, as discussed in Section 2.3.5.2. Fig. 7 shows a comparison between the theoretical f(α) and the experimental f(α) curves for the DEC and TB300 samples. For the DEC, when the conversion rate (α) is less than 0.3, the experimental curve is close to the 2D diffusional model, and when α is greater than 0.3, the reaction mechanism is shifted towards the first order reaction model. In the case of torrefied biomass (TB300), when the conversion rate (α) is less than 0.6, the experimental curve is close to the first order reaction model and for the conversion value greater than 0.6, the curve is shifted towards the third order model.

The experimental curves for the master plots and the kinetic compensation effect methods both show the same overall trend. The results showed that torrefaction pretreatment has a significant effect on the reaction mechanism of the biomass pyrolysis. Finally, from Figs. 4 and 6, it can be concluded that the pyrolysis of DEC follows diffusional models at the initial stages, and reaction-order models towards the end. The same order of reaction mechanisms were also observed by Poletto et al. (2012), Lu et al. (2009) and Mishra and Bhaskar, (2014). In the case of TB300, a reaction-order model was observed at the start of the pyrolysis, and a diffusional model at the end. At higher conversion rates, that is, when α is greater than 0.7, the reaction mechanism shifted to a third order model.

According to Lu et al. (2009) and Poletto et al. (2012), at the initial stage of the pyrolysis, the heat transfer through the biomass sample and the release of the volatile products from the inside layers of the biomass takes place through the diffusion. The pyrolysis reactions at this stage are related to the decomposition of cellulose, hemicellulose and lignin, and the formation of primary products such as H_2O, CO, CO_2, primary tar, levoglucosan, Furfural and char etc. Torrefaction treatment increases the ordered cellulose regions in the biomass (Park et al., 2013), and these high-ordered cellulose regions create the difficulty to the heat transfer during the pyrolysis (Poletto et al., 2012). In other words, it can be said that the thermal stability of the biomass increases with torrefaction treatment. The same can be seen in Fig. 1b, where the pyrolysis starting temperatures of DEC and TB300 are 270 and 330 °C respectively. According to Poletto et al. (2012), at temperatures higher than 350 °C the ordered cellulose, which are low-molecular-mass chains, acts as a centers for random nucleation and growth. Lu et al., 2009; reported that the apparent first-order reaction mechanism in the temperature range of 300–500 °C is because of the formation of small molecules from the secondary cracking of the products. At

Table 4
Kinetic compensation parameters for dried biomass (DEC) and Torrefied biomass (TB300).

DEC									
β (°C/min)	Stage 1 (α = 0.05 – 0.3)			Stage 2 (α = 0.3 – 0.6)			Stage 3 (α = 0.6 – 0.8)		
	b (mol kJ^{-1})	A	r^2	b (mol kJ^{-1})	A	r^2	b (mol kJ^{-1})	a	r^2
5	0.196	−5.066	0.9896	0.210	−6.857	0.9734	0.210	−7.280	0.9991
8	0.188	−4.513	0.9853	0.198	−5.988	0.9623	0.205	−7.195	0.9971
12	0.187	−4.498	0.9859	0.196	−6.022	0.9610	0.203	−7.223	0.9970
20	0.184	−4.517	0.9858	0.194	−6.076	0.9605	0.201	−7.262	0.9970
TB300									
β (°C/min)	Stage 1 (α = 0.05 – 0.6)			Stage 2 (α = 0.6 – 0.7)			Stage 3 (α = 0.7 – 0.8)		
	b (mol kJ^{-1})	A	r^2	b (mol kJ^{-1})	A	r^2	b (mol kJ^{-1})	a	r^2
5	0.187	−3.988	0.9891	0.266	−8.989	0.9734	0.271	−8.762	0.9773
8	0.187	−3.669	0.9947	0.219	−8.022	0.9818	0.276	−8.831	0.972
12	0.185	−3.690	0.9947	0.218	−8.055	0.9812	0.272	−8.83	0.9723
20	0.182	−3.678	0.9947	0.207	−7.809	0.9877	0.267	−8.793	0.9737

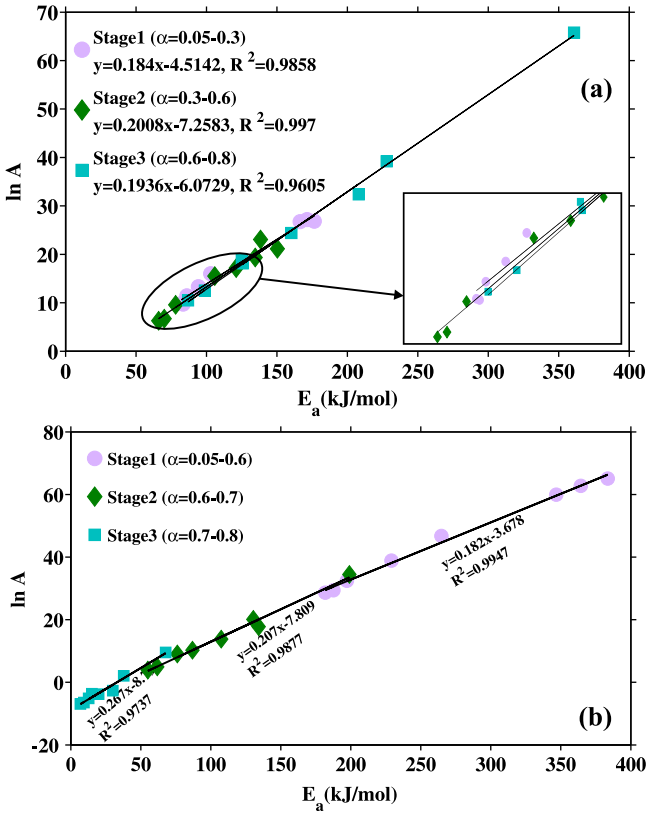

Fig. 6. Compensation plot (ln A vs. E_a) of model-fitting kinetic parameters for (a) DEC and (b) TB300 samples at 20 °C/min heating rate.

elevated temperatures i.e. >300 °C, the primary products from the cellulose pyrolysis, such as levoglucosan and primary tar are further converted into low molecular mass compounds and char through secondary cracking reactions (Patwardhan, 2010) (Anthony Dufour, 2016). As the pyrolysis starting temperature is higher for torrefied biomass compared to raw biomass (i.e. >300 °C), levoglucosan and primary tar could be readily converted into small molecular mass compounds (CO, CO_2, H_2, CH_4 etc.) and char through secondary cracking reactions. This could also be one possible reason for the increased CH_4 and H_2 and the reduced tar content in the product distribution of torrefied biomass pyrolysis. Ren et al. (2013b) observed the rise in the CH_4 and H_2 content in the volatiles and Wannapeera et al. (2011) observed the significant reduction in the tar content in case of torrefied biomass pyrolysis in comparison with raw biomass pyrolysis. Based on the above discussion, the observed reaction order models for the torrefied biomass pyrolysis could be attributed to the formation of low molecular mass products. Torrefaction treatment also alters the lignin structure and reduces its thermal stability (Arshanitsa et al., 2016). As the high-ordered cellulose is already degraded during the initial stage and the lignin thermal stability is low, there is no difficulty for the heat transfer through diffusion. This could be the reason for the observed diffusion mechanism at the end of the torrefied biomass pyrolysis. In their study, Poletto et al. (2012), discussed the details of the diffusion order and the random nucleation models and related them to the biomass pyrolysis.

As the pyrolysis reaction mechanism is different between raw and torrefied biomass, and the major portion of hemicellulose is already degraded, a significant variation in the composition of pyrolysis products between raw and torrefied biomass is expected. Ren et al., 2013b; reported that torrefaction treatment increased the content of sugars, phenols and hydrocarbons and reduced the organic acids. At the same time torrefaction treatment reduces CO_2 and tar content (Wannapeera et al., 2011).

3.5. Differential scanning calorimetry analysis

The impact of the torrefaction can also be studied from the DSC curves. Fig. 8 shows the heat flow during the pyrolysis of DEC and of torrefied biomass. The heat flow of Eucalyptus biomass is exothermic in the temperature ranges 100–260 °C and 310–370 °C. In the case of TB300, however, the heat flow curves differ significantly compared with dried biomass. From Fig. 8, it can be clearly seen that the exothermic peak has disappeared in the case of the pyrolysis of biomass torrefied at TB300. The exothermic peak was still present for TB250. The existing literature (Shen et al., 2015; Stenseng et al., 2001) suggests that hemicellulose and lignin pyrolysis are exothermal, whereas cellulose pyrolysis is endothermal. Based on this premise, the absence of the exothermic peak for TB300 supports the belief that hemicellulose is the main biomass component degraded during the torrefaction. At the end of the pyrolysis process, that is, between 400 and 500 °C, all the samples exhibited endothermic behavior. However, the heat flow in the case of the torrefied biomass was higher than with the dried biomass. The observed maximum heat flows for the dried biomass, and for TB250 and TB300, in the temperature range of 400–500 °C were 2.5, 3.2 and 3.3 mW, respectively. This shows that heat flow increased as the torrefaction temperature increased. This may be attributed to the difference in the char yield, and to the structural differences in the produced char. This analysis suggests that heat flows

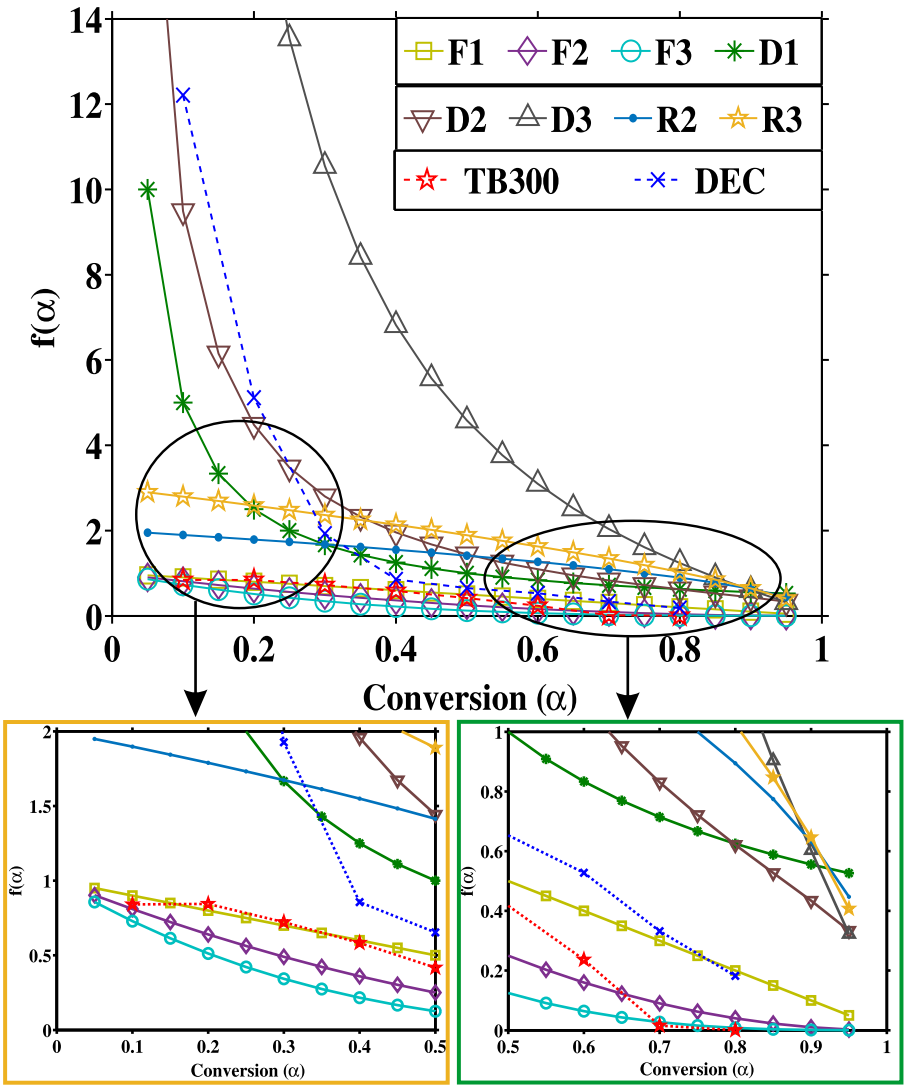

Fig. 7. Plot of Theoretical and experimental curves of f(α) vs. conversion (α) for both DEC and TB300. (Check Table 1 for abbreviation).

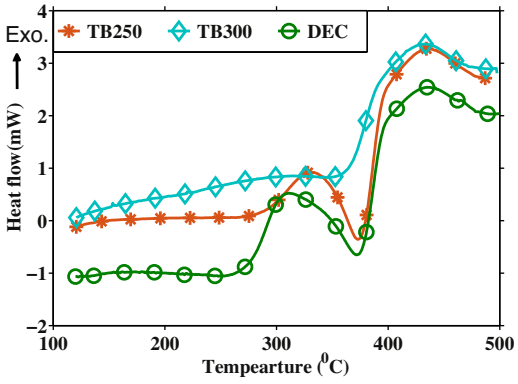

Fig. 8. DSC curves (heat flow) for the pyrolysis of DEC, TB250, TB300 samples at 20 °C/min.

during the pyrolysis of the torrefied biomass were more strongly influenced by the torrefaction temperature. In Section 3.3.1, it was reported that torrefied biomass requires more energy to proceed with pyrolysis reactions, and this statement is supported by the DSC analysis.

The higher activation energy values of torrefied biomass decomposition represent the need for more energy for the cleavage of the chemical bonds. The reason may be the altered structure, and thereby the altered heat transfer properties, of the biomass during torrefaction. When designing the pyrolysis reactors, for the optimal conversion of the pretreated biomass, it is important to consider that kinetic parameters (E_a, A, and f(α)) are varying between raw and torrefied biomass. A detailed study on the influence of torrefaction treatment on the heat of biomass pyrolysis could be interesting for future studies.

4. Conclusion

The following conclusions can be drawn from the present study on the effect of the torrefaction pretreatment on Eucalyptus clone during its subsequent pyrolysis:

Torrefaction pretreatment had a significant effect on the kinetics, reaction mechanism and heat flow parameters of biomass decomposition during the pyrolysis process. Kinetic analysis showed that torrefied biomass has higher activation energy values than the dried biomass. We also observed the kinetic compensation effect for both dried and torrefied biomass at various heating rates. The reported variation in the decomposition mechanism between

dried and torrefied biomass could be due to the degradation of hemicellulose during torrefaction, and thereby the formation of smaller molecules during the pyrolysis of torrefied biomass.

The DSC analysis showed that dried Eucalyptus biomass pyrolysis was exothermic at the beginning of the process, that is, for temperatures less than 260 °C, whereas the torrefied Eucalyptus exhibited endothermic behavior.

Finally, the reported variation in the reaction parameter and heat flow data of dried and torrefied biomass pyrolysis can be attributed to the altered chemical structure of the biomass during torrefaction.

The information provided in this work could provide valuable insights into increasing the understanding of the pyrolysis of torrefied biomass.

Acknowledgements

The authors gratefully acknowledge the financial support by the Academy of Finland for the IMUSTBC project.

Appendix A. Supplementary data

Supplementary data associated with this article can be found, in the online version, at http://dx.doi.org/10.1016/j.indcrop.2016.08.013.

References

Alén, R., Kuoppala, E., Oesch, P., 1996. Formation of the main degradation compound groups from wood and its components during pyrolysis. J. Anal. Appl. Pyrolysis 36, 137–148, http://dx.doi.org/10.1016/0165-2370(96)00932-1.

Amutio, M., Lopez, G., Alvarez, J., Olazar, M., Bilbao, J., 2015. Fast pyrolysis of eucalyptus waste in a conical spouted bed reactor. Bioresour. Technol. 194, 225–232, http://dx.doi.org/10.1016/j.biortech.2015.07.030.

Anthony Dufour, 2016. Thermochemical Conversion of Biomass for the Production of Energy and Chemicals. John Wiley & Sons.

Arshanitsa, A., Dizhbite, T., Bikovens, O., Pavlovich, G., Andersone, A., Telysheva, G., 2016. Effects of microwave treatment on the chemical structure of lignocarbohydrate matrix of softwood and hardwood. Energy Fuels 30, 457–464, http://dx.doi.org/10.1021/acs.energyfuels.5b02462.

Brown, M.E., Maciejewski, M., Vyazovkin, S., Nomen, R., Sempere, J., Burnham, a., Opfermann, J., Strey, R., Anderson, H.L., Kemmler, a., Keuleers, R., Janssens, J., Desseyn, H.O., Li, C.-R., Tang, T.B., Roduit, B., Malek, J., Mitsuhashi, T., 2000. Computational aspects of kinetic analysis. Thermochim. Acta 355, 125–143, http://dx.doi.org/10.1016/S0040-6031(00)00443-3.

Cadenato, A., Morancho, J.M., Fernández-Francos, X., Salla, J.M., Ramis, X., 2007. Comparative kinetic study of the non-isothermal thermal curing of bis-GMA/TEGDMA systems. J. Therm. Anal. Calorim. 89, 233–244, http://dx.doi.org/10.1007/s10973-006-7567-5.

Chen, W.H., Kuo, P.C., 2011. Torrefaction and co-torrefaction characterization of hemicellulose, cellulose and lignin as well as torrefaction of some basic constituents in biomass. Energy 36, 803–811, http://dx.doi.org/10.1016/j.energy.2010.12.036.

Das, O., Sarmah, A.K., 2015. Mechanism of waste biomass pyrolysis: effect of physical and chemical pre-treatments. Sci. Total Environ. 537, 323–334, http://dx.doi.org/10.1016/j.scitotenv.2015.07.076.

Gomes, F.J.B., Colodette, J.L., Burnet, A., Batalha, L.A.R., Santos, F.A., Demuner, I.F., 2015. Thorough characterization of Brazilian new generation of eucalypt clones and grass for pulp production. Int. J. For. Res., 1–10, http://dx.doi.org/10.1155/2015/814071.

Janković, B., Adnadević, B., Jovanović, J., 2007. Application of model-fitting and model-free kinetics to the study of non-isothermal dehydration of equilibrium swollen poly (acrylic acid) hydrogel: thermogravimetric analysis. Thermochim. Acta 452, 106–115, http://dx.doi.org/10.1016/j.tca.2006.07.022.

Jin, W., Singh, K., Zondlo, J., 2013. Pyrolysis kinetics of physical components of wood and wood-polymers using isoconversion method. Agriculture 3, 12–32, http://dx.doi.org/10.3390/agriculture3010012.

Khawam, A., Flanagan, D.R., 2006. Basics and applications of solid-state kinetics: a pharmaceutical perspective. J. Pharm. Sci. 95, 472–498, http://dx.doi.org/10.1002/jps.

Lu, C., Song, W., Lin, W., 2009. Kinetics of biomass catalytic pyrolysis. Biotechnol. Adv. 27, 583–587, http://dx.doi.org/10.1016/j.biotechadv.2009.04.014.

Lu, K.M., Lee, W.J., Chen, W.H., Lin, T.C., 2013. Thermogravimetric analysis and kinetics of co-pyrolysis of raw/torrefied wood and coal blends. Appl. Energy 105, 57–65, http://dx.doi.org/10.1016/j.apenergy.2012.12.050.

Mishra, G., Bhaskar, T., 2014. Non isothermal model free kinetics for pyrolysis of rice straw. Bioresour. Technol. 169, 614–621, http://dx.doi.org/10.1016/j.biortech.2014.07.045.

Park, J., Meng, J., Lim, K.H., Rojas, O.J., Park, S., 2013. Transformation of lignocellulosic biomass during torrefaction. J. Anal. Appl. Pyrolysis 100, 199–206, http://dx.doi.org/10.1016/j.jaap.2012.12.024.

Patwardhan, P., 2010. Understanding the Product Distribution from Biomass Fast Pyrolysis. Iowa State Univ. PhD Thesis.

Poletto, M., Zattera, A.J., Santana, R.M.C., 2012. Thermal decomposition of wood: kinetics and degradation mechanisms. Bioresour. Technol. 126, 7–12, http://dx.doi.org/10.1016/j.biortech.2012.08.133.

Ren, S., Lei, H., Wang, L., Bu, Q., Chen, S., Wu, J., 2013a. Thermal behaviour and kinetic study for woody biomass torrefaction and torrefied biomass pyrolysis by TGA. Biosyst. Eng. 116, 420–426, http://dx.doi.org/10.1016/j.biosystemseng.2013.10.003.

Ren, S., Lei, H., Wang, L., Bu, Q., Chen, S., Wu, J., Julson, J., Ruan, R., 2013b. The effects of torrefaction on compositions of bio-oil and syngas from biomass pyrolysis by microwave heating. Bioresour. Technol. 135, 659–664, http://dx.doi.org/10.1016/j.biortech.2012.06.091.

Rocha, E.P.A., Gomes, F.J.B., Sermyagina, E., Cardoso, M., Colodette, J.L., 2015a. Analysis of Brazilian biomass focusing on thermochemical conversion for energy production. Energy Fuels acs. Energyfuels, 5b01945, http://dx.doi.org/10.1021/acs.energyfuels.5b01945.

Rocha, E.P.A., Sermyagina, E., Cardoso, M., Vakkilainen, E., Colodette, J.L., 2015b. Pyrolysis of brazilian eucalyptus clones: non-isothermal thermogravimetric kinetic analysis. IWBLCM 2015, 1st International Workshop on Biorefinery of Lignocelulosic Materials, 291–295.

Ru, B., Wang, S., Dai, G., Zhang, L., 2015. Effect of torrefaction on biomass physicochemical characteristics and the resulting pyrolysis behavior. Energy Fuels 29, 5865–5874, http://dx.doi.org/10.1021/acs.energyfuels.5b01263.

Sbirrazzuoli, N., 2013. Determination of pre-exponential factors and of the mathematical functions f(??) or G(??) that describe the reaction mechanism in a model-free way. Thermochim. Acta 564, 59–69, http://dx.doi.org/10.1016/j.tca.2013.04.015.

Senneca, O., 2007. Kinetics of pyrolysis, combustion and gasification of three biomass fuels. Fuel Process. Technol. 88, 87–97, http://dx.doi.org/10.1016/j.fuproc.2006.09.002.

Shen, J., Igathinathane, C., Yu, M., Pothula, A.K., 2015. Biomass pyrolysis and combustion integral and differential reaction heats with temperatures using thermogravimetric analysis/differential scanning calorimetry. Bioresour. Technol. 185, 89–98, http://dx.doi.org/10.1016/j.biortech.2015.02.079.

Stenseng, M., Jensen, a., Dam-Johansen, K., 2001. Investigation of biomass pyrolysis by thermogravimetric analysis and differential scanning calorimetry. J. Anal. Appl. Pyrolysis 58, 765–780, http://dx.doi.org/10.1016/s0165-2370(00)00200-x.

Tolvanen, H., Kokko, L., Raiko, R., 2013. Fast pyrolysis of coal, peat, and torrefied wood: mass loss study with a drop-tube reactor, particle geometry analysis, and kinetics modeling. Fuel 111, 148–156, http://dx.doi.org/10.1016/j.fuel.2013.04.030.

Tran, K.-Q., Bach, Q.-V., Trinh, T.T., Seisenbaeva, G., 2014. Non-isothermal pyrolysis of torrefied stump – A comparative kinetic evaluation. Appl. Energy 136, 759–766, http://dx.doi.org/10.1016/j.apenergy.2014.08.026.

Vlaev, L.T., Markovska, I.G., Lyubchev, L.a., 2003. Non-isothermal kinetics of pyrolysis of rice husk. Thermochim. Acta 406, 1–7, http://dx.doi.org/10.1016/S0040-6031(03)00222-3.

Wannapeera, J., Fungtammasan, B., Worasuwannarak, N., 2011. Effects of temperature and holding time during torrefaction on the pyrolysis behaviors of woody biomass. J. Anal. Appl. Pyrolysis 92, 99–105, http://dx.doi.org/10.1016/j.jaap.2011.04.010.

White, J.E., Catallo, W.J., Legendre, B.L., 2011. Biomass pyrolysis kinetics: a comparative critical review with relevant agricultural residue case studies. J. Anal. Appl. Pyrolysis 91, 1–33, http://dx.doi.org/10.1016/j.jaap.2011.01.004.

Worasuwannarak, N., Wannapeera, J., Fungtammasan, B., 2011. Pyrolysis behaviors of woody biomass torrefied at temperatures below 300 °C. 2011 IEEE 1st Conf. Clean Energy Technol. CET 2011, 287–290, http://dx.doi.org/10.1109/CET.2011.6041498.

Publication II

Tharaka Rama Krishna C Doddapaneni, Ramasamy Praveenkumar, Henrik Tolvanen, Marja R T Palmroth, Jukka Konttinen, Jukka Rintala

"Anaerobic batch conversion of pine wood torrefaction condensate"

Bioresource Technology 2017; 225: 299–307.

Bioresource Technology 225 (2017) 299–307

Contents lists available at ScienceDirect

Bioresource Technology

journal homepage: www.elsevier.com/locate/biortech

Anaerobic batch conversion of pine wood torrefaction condensate

Tharaka Rama Krishna C. Doddapaneni [1,*], Ramasamy Praveenkumar [1], Henrik Tolvanen, Marja R.T. Palmroth, Jukka Konttinen, Jukka Rintala

Department of Chemistry and Bioengineering, Tampere University of Technology, P.O. Box 541, FI-33101 Tampere, Finland

HIGHLIGHTS

- Torrefaction condensate is a good substrate for anaerobic digestion.
- Torrefaction temperature affects both condensate composition and the methane yield.
- Anaerobic digestion under mesophilic conditions yielded better methane yield.
- Under optimized conditions, a maximum methane yield of 492 mL/g VS was observed.

GRAPHICAL ABSTRACT

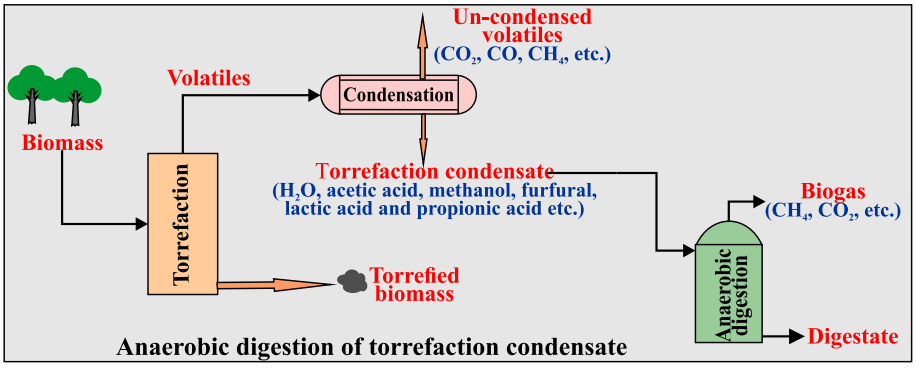

ARTICLE INFO

Article history:
Received 8 September 2016
Received in revised form 15 November 2016
Accepted 19 November 2016
Available online 22 November 2016

Keywords:
Torrefaction
Condensate
Anaerobic digestion
Acetic acid
Methane

ABSTRACT

Organic compound rich torrefaction condensate, owing to their high water content and acidic nature, have yet to be exploited for practical application. In this study, microbial conversion of torrefaction condensate from pine wood through anaerobic batch digestion (AD) to produce methane was evaluated. Torrefaction condensate exhibited high methane potentials in the range of 430–492 mL/g volatile solids (VS) and 430–460 mL/g VS under mesophilic and thermophilic conditions, respectively. Owing to the changes in the composition, the methane yields differed with the torrefaction condensates produced at different temperatures (225, 275 and 300 °C), with a maximum of 492 ± 18 mL/g VS with the condensate produced at 300 °C under mesophilic condition. The cyclic batch AD experiments showed that 0.1 $VS_{substrate}$:$VS_{inoculum}$ is optimum, whereas the higher substrate loading (0.2–0.5) resulted in a reversible inhibition of the methane production. The results suggest that torrefaction condensate could be practically valorized through AD.

1. Introduction

The European Union has set the political targets of increasing the primary energy consumption from renewable resources up to 20% by 2020 and 27% by 2030 (Thrän et al., 2016). Co-firing biomass in existing coal power plants is being considered as one option to achieve these renewable energy targets. In order to enhance the fuel properties, biomass needs to be pre-treated before being fed into the existing coal-firing power plants. Torrefaction is one such pre-treatment process, which enhances fuel properties of the biomass by increasing the energy density and hydrophobicity and by reducing the moisture content and the required grinding energy (Doddapaneni et al., 2016). Torrefaction is carried out in the range of 200–300 °C. The degradation mainly occurs between 275–300 °C and the product distribution also significantly varies in this temperature range. The thermal devolatilization of biomass proceeds with

* Corresponding author.
E-mail address: tharaka.doddapaneni@tut.fi (T.R.K.C. Doddapaneni).
[1] These authors have contributed equally to the manuscript.

http://dx.doi.org/10.1016/j.biortech.2016.11.073
0960-8524/

strong exothermic reactions in the range of 270–290 °C (Fagernas et al., 2015). According to Thrän et al. (2016), the quality of the torrefied biomass depends on its degree of torrefaction and the degree of torrefaction depends on the temperature and the residence time. To maximize the solid product yield, generally torrefaction is carried-out at low temperature and long residence time in commercial torrefaction equipment.

Torrefied biomass is being considered for a variety of industrial processes such as pyrolysis, gasification, cement kilns, as a substitute for coke in the steel industry and, in addition to all of this, it can be used as a fuel for co-firing in coal-fired power plants (Thrän et al., 2016). In spite of these advantages, still torrefaction needs to be proved for its technical and economic feasibility (Koppejan et al., 2012). As listed by Koppejan et al. (2012), several issues in the development of the torrefaction technologies, for example, energy integration, volatile gases handling and applicability of multi feedstock are need to be addressed. To improve the technical and economic feasibility, the energy integration within the process must be optimized and at the same time additional value should be generated through the byproducts like the torrefaction condensate.

Torrefaction condensate produced from different feedstock and at different operating conditions have been characterized in the past e.g. (Liaw et al., 2015; Tumuluru et al., 2011b, and Fagernas et al., 2015). The majority of the compounds (i.e. acids, alcohols, aldehydes, furans and phenols) at the concentration as present in the torrefaction condensate are water-soluble (Fagernas et al., 2015). Among the water soluble compounds, acetic acid, methanol, furfural, formaldehyde, hydroxymethylfurfural and phenol contributes to 80–90 wt.% of the total organic fraction of the condensate (Fagernas et al., 2015).

In general, the torrefaction volatiles are combusted to meet the heat energy requirements within the process (both drying and torrefaction units), and according to Liaw et al. (2015), it has very little effect on the process integration and overall economic viability of the process. In spite of having several valuable chemicals, owing to their complex composition, the torrefaction condensate has not yet been studied for its actual potential (Fagernas et al., 2015).

Biochemical conversion of torrefaction condensate into useful products could be one potential option for its valorization. Anaerobic digestion (AD) is a biochemical process of converting complex organic material into methane and carbon dioxide using a consortium of microorganism. AD comprises of different stages, initially the complex organic material is converted into volatile fatty acids (VFA) through hydrolysis and acidogenesis. In the later stage VFAs are further converted to acetic acid, CO_2, H_2, NH+ etc. through acetogenesis. In the final stage, the intermediate products are further converted into CH_4 and CO_2 by methanogens (Fabbri and Torri, 2016). As torrefaction condensate has high water content (50–85%), and acetic acid (5–15%) and other organic acids like formic acid and lactic acid (Tumuluru et al., 2011a and Liaw et al., 2015), which are readily anaerobically converted, torrefaction condensate could be an optimum feedstock for AD process and it is expected that the methane yields could be higher in comparison with other complex substrates. However, at the same time the inhibitory effects on AD by the presence of compounds such as furfural and phenolics in the torrefaction condensate should also be considered (Liaw et al., 2015).

On the other hand, the earlier studies on bio-oils are mainly focused on the biochemical conversion of pyrolysis oil. Fabbri and Torri (2016), studied linking the pyrolysis with AD and suggested that AD of pyrolysis volatile fractions is one of the best approaches to increase the energy recovery but there is a knowledge gap in these kinds of process integration in terms of multidisciplinary interface. Hübner and Mumme (2015), studied the AD of the aqueous liquors from the pyrolysis of digestate obtained from on-farm biogas plant and reported that volatile organic compounds (VOCs) except cresols present in the pyrolysis aqueous phase where degraded below the detection limit. Lian et al. (2012), studied the yeast fermentation of carboxylic acids separated from pyrolysis aqueous phase and proved its feasibility for lipid production through oleaginous yeast. In their study, Lian et al. (2013) reported that, the fermentation of levoglucosan obtained from the pyrolysis oil is one possible approach for the biofuel production. Torri and Fabbri (2014) studied the AD of aqueous pyrolysis liquid and reported that addition of bio-char increased the methane yield by reducing the inhibition level of the pyrolysis oil to the microorganism.

Even though there is a significant difference in the composition between torrefaction condensate and pyrolysis oil, the earlier knowledge on the biochemical conversion of pyrolysis oil could be useful while working with torrefaction condensate. At the same time, to our knowledge there is only one study reported on the AD of torrefaction condensate. Liaw et al. (2015), studied the mesophilic batch AD of the torrefaction condensate (310 °C, the residence time 7.5 and 10.8 min) from different biomass spices (i.e. corn stover, pea hay, sorghum etc.) They concluded that the methane yield from this process depends on the concentration of hydroxyl-acetate and phenols in the torrefaction condensate, owing to their inhibitory effects.

For the better understanding and optimizing the process integration between torrefaction and AD, the AD of torrefaction condensate produced at different temperatures should be studied. The influence of the varied concentration of the torrefaction condensate on the methane production should also be studied; it helps to understand better the potential level and type of the inhibition to the microorganism. In the earlier studies, it was reported that torrefaction (Liaw et al., 2015) and pyrolysis condensates (Fabbri and Torri, 2016 and Hübner and Mumme, 2015) are inhibitory to the microorganisms at higher concentration. However, it was not clear whether the inhibition is reversible or irreversible, which is essential to be understood when the process is to be scaled up. Furthermore, the methane production and inhibition may be affected by the temperature of AD as it influences the dynamics of microbial population and the chemistry of the condensate (Franke-Whittle et al., 2014 and Diebold, 2000).

The objective of this study was to assess initially the feasibility of AD of the torrefaction condensate from pine wood. Pine is a soft wood, which is widely used in industrial applications like pulp and paper, bioenergy and construction sectors (South and Smidt, 2014), and there is interest to find new uses in various biorefinery applications. For this purpose, AD of the torrefaction condensate produced at different temperatures i.e. 225, 275 and 300 °C, was studied using the bio-methane potential (BMP) batch assays under mesophilic and thermophilic conditions. Furthermore, in order to understand the potential inhibitory effects of the condensate, different organic loading and cyclic batch AD were carried out.

2. Materials and methods

2.1. Biomass

Finnish pine wood was used as a raw material to produce the torrefaction condensate. The selected biomass was a debarked stem wood and received in the form of wood chips (Kuljetusliike Viikari Oy, Narva, Finland). The proximate analysis of the biomass was carried out using thermogravimetric analyzer (TGA; Mettler Toledo TGA 850) following the method as reported elsewhere with little modification (Garcia et al., 2013). Considering the restrictions with TGA operating parameters, the end temperature was set at 800 °C. The proximate analysis of the selected biomass is presented in Table S1.

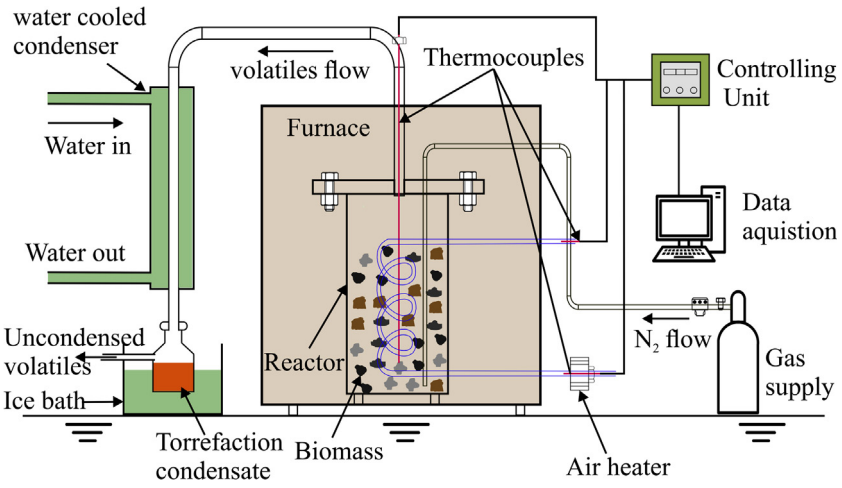

Fig. 1. Torrefaction reactor system.

2.2. Torrefaction and condensate collection

Initially, the biomass was dried at 105 °C for at least 24 h in an air driven furnace and stored in air tight plastic containers. The schematic of torrefaction reactor system used in this study is presented in Fig. 1. The reactor was made up of stainless steel with an electrically heating furnace. The detailed information about the torrefaction reactor can be found in the literature (Keipi et al., 2014). The temperature of the reactor was increased from room temperature (~20 °C) to the selected torrefaction temperature i.e. 225, 275 and 300 °C at around 5 °C/min and maintained for an isothermal period of 1 h. The volatiles from the biomass were condensed using a water circulated tube condenser and collected using a glass bottle submerged in an ice bath. The un-condensed gases were left to the exhaust system.

For each run, 1 kg of dried biomass was loaded in the reactor. Initially, 20 L/min of N_2 flow was used to maintain the inert environment in the reactor and later the N_2 flow was reduced to 5 L/min once the reactor temperature reached to the set temperature. The temperature at different locations of the system was recorded using thermocouples connected with controlling unit as shown in the Fig. 1. The reactor temperature was also controlled by altering the mass flow and temperature of the air circulated through the closed coils. The sample temperature was measured using a thermocouple located in the center of the reactor. The temperature fluctuations were maintained within ±5 °C limit of the selected torrefaction temperature. Because of the large reactor size and relatively large sample volume, the temperature of the sample could be deviating more from the measured thermocouple reading at some places of the reactor. The collected torrefaction condensate was stored at 4 °C to prevent the ageing reactions. However, the formation of bottom settled tar-like substances, which are viscous carbonaceous substances formed mainly from lignin derived compounds (Diebold, 2000), was observed during the storage. As tars are known to clog the processing equipment (Milne et al., 1998) in the present study these tar-like compounds were separated through separating flask before the condensate was used in AD experiments. Further, the pH of the torrefaction condensate was adjusted from 2.0 to 7.0 by adding NaOH.

2.3. Bio-methane potential (BMP) assay

The inoculums used in this study were the pre-collected and stored (at 4 °C) sludge from the existing mesophilic and thermophilic anaerobic digesters, respectively, operated in our laboratory with pulp and paper industry sludge. The inoculums were adapted to the mesophilic (35 °C) and thermophilic (55 °C) conditions for 48 h in an electrically heated oven before using them for BMP assays.

The batch BMP assays of the torrefaction condensate (substrate), produced at different temperatures (i.e. 225, 275 and 300 °C) were studied using 120 mL serum bottles with a 60 mL of working volume at 35 and 55 °C as described by Kinnunen et al. (2014). The volatile solids (VS), $VS_{substrate}$:$VS_{inoculum}$ ratios of 0.1 and 0.2 were tested. A serum bottle with water and inoculum only served as a blank. The methane yields of inoculum were subtracted from the methane yields measured in the test bottles with the substrate. All the experiments and analyses were carried out in duplicates and the results were represented as mean and standard deviation. Fig. 2 gives the process flow and basic understanding about the experimental plan.

2.4. Cyclic batch AD experiments

In the cyclic batch AD experiments, the initial set-up was as in BMP assays but after a certain time, a volume of liquid phase was removed and the same amount of water and/or substrate was added (Keshtkar et al., 2001). Cyclic batch AD experiments were carried out starting with three batch set-ups containing, 0.1, 0.2, and 0.5 $VS_{substrate}$:$VS_{inoculum}$ following the BMP assay procedure (Section 2.3) using torrefaction condensate produced at 300 °C. The experiment was carried out for 72 d with two intermittent feeding points at 30 and 50 d. In the first feeding, no gas production was observed in case of 0.2 and 0.5 $VS_{substrate}$:$VS_{inoculum}$ loading. To understand the inhibition type of torrefaction condensate on the inoculum, the 0.2 and 0.5 $VS_{substrate}$:$VS_{inoculum}$ set-ups were diluted to match approximately the 0.1 $VS_{substrate}$:$VS_{inoculum}$ loading during the first and second feeding, respectively. For this purpose, a part of the liquid phase in the bottles were removed and the same amount of distilled water was added to maintain liquid volume of 60 mL. During each feeding cycles, the aqueous fractions were removed from the bottles contained 0.1 $VS_{substrate}$:$VS_{inoculum}$ through gravity settling and fed again with 0.1 VS ratio of substrate along with distilled water to make up the volume to 60 mL.

2.5. Analytical methods

For the analysis of the chemical composition of the torrefaction condensate organic acids, aldehydes, methanol and acetol, the organic fraction of the condensate was extracted with water and

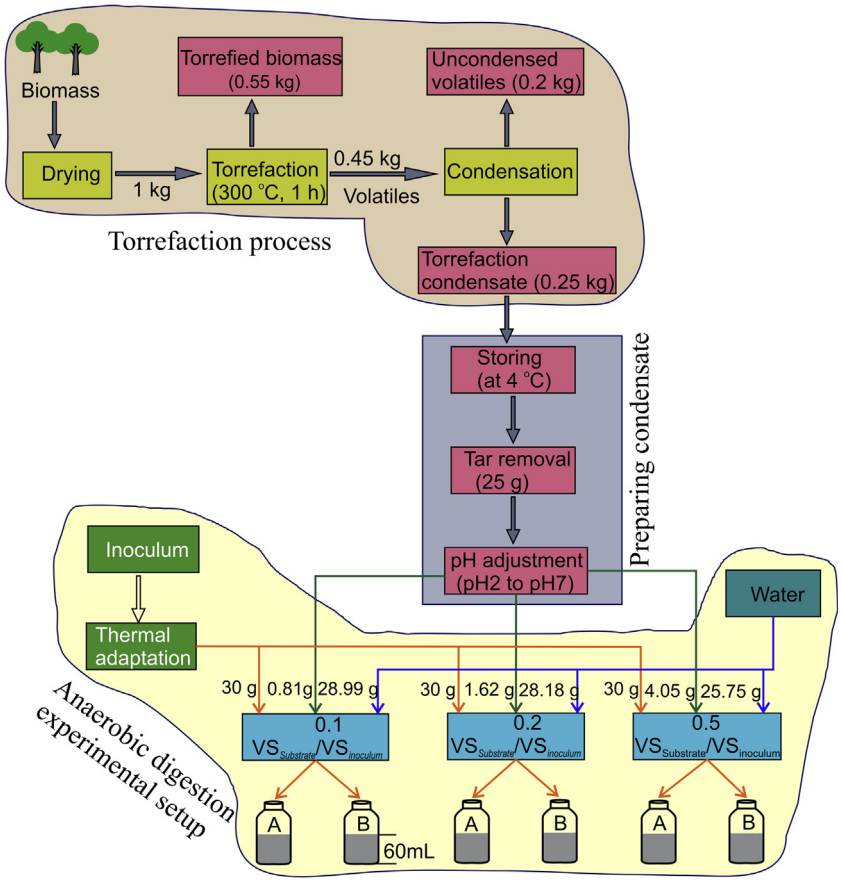

Fig. 2. Process flow adopted in this study for the AD of torrefaction condensate.

the extract was used for the analysis of organic analytes (analyzed at Nablabs oy, Oulu, Finland). Water content was analyzed with Karl Fischer titration. Organic acids, formaldehyde, acetaldehyde, furfural and hydroxymethylfurfural were analyzed with high pressure liquid chromatographic method based on EPA method (EPA 8315A). Methanol and acetol 2-hydroxyacetaldehyde were analyzed with internal method using gas chromatography and headspace gas chromatography mass spectrometry.

The total solids (TS) and VS (APHA 2540) and chemical oxygen demand (COD) (APHA 5220 D), were analyzed according to standard protocols. Soluble COD (sCOD) were measured after filtration through a 0.45 μm membrane filter. The pH was measured using a TPS WP-81 pH meter.

Methane concentrations were measured in gas chromatography equipped with flame ionization detector (Perkin Elmer, Clarus 500, USA) by comparing against control gas samples containing 30% CH_4 and 30% CO_2. Helium was used as a carrier gas and operation conditions were: oven 100 °C, detector 225 °C and injector 230 °C (Kinnunen et al., 2015). Methane concentration results were converted to standard temperature and pressure conditions (STP, T = 273 K, p = 1 bar) The methane production was calculated as cumulative methane yield (L CH_4) and specific methane yield per VS of substrate added (L CH_4/g VS).

2.6. Heating value of torrefaction condensate

The theoretical heating value of the torrefaction condensate was evaluated by the summation of the heating value of all major compounds present in the torrefaction condensate, as presented in the Eq. (1) (Khartchenko and Kharchenko, 2013).

$$LHV = \sum_{i=1}^{n} HHV_i - (h_{fg}.m_{H_2O}) \quad (1)$$

where, '*i*' represents the major compounds present in the torrefaction condensate (i.e. acetic acid, lactic acid, furfural, methanol and formaldehyde etc.), h_{fg} is the heat of vaporization of water (i.e. 2257 kJ/kg) and m_{H_2O} is the mass of water vapor in kg.

3. Results and discussion

3.1. Torrefaction process

3.1.1. Product distribution

The product distribution from the torrefaction process of the studied pine wood is presented in Fig. S1. The torrefied biomass yield was around 82, 75 and 55 wt.% and the condensate yield was around 7, 18 and 25 wt.% when torrefaction (1 h) was carried out at 225, 257 and 300 °C respectively. This shows that the temperature has a significant effect on the product distribution with torrefaction process. The un-condensed gas yield (mainly CO and CO_2) was calculated through the difference (100% – [solid product% + condensate%]). The product distribution observed in this study was in agreement with the torrefaction product of other woody spices like beech, poplar and spruce (Verhoeff et al., 2011). For example, during torrefaction (at 300 °C for 1 h) of spruce biomass, a yield of 29 wt.% of torrefaction condensate was reported (Fagernas et al. (2015).

3.1.2. Torrefaction condensate composition

The studied torrefaction condensate from pine wood contains several water soluble compounds among which organic acids,

Table 1
Composition of the torrefaction condensate produced at various temperatures.

Organic compounds		Compositions (wt%)		
		225 °C	275 °C	300 °C
Organic acids	Acetic acid	3.08	5.60	5.40
	Lactic acid	0.62	1.30	1.80
	Formic acid	1.20	1.00	1.90
	Propionic acid	0.01	0.01	nd
Aldehydes	Formaldehyde	0.10	0.50	0.20
	Acetaldehyde	<0.01	0.16	0.02
	Furfural	0.26	0.79	0.55
	Hydroxymethylfurfural	0.31	0.37	0.50
Others	Methanol	0.44	1.59	1.35
	Acetol	<0.01	<0.01	<0.01
	Water	84	73	58
	Unidentified	9,94	15,7	30,28
	Total	100	100	100
	pH	2.21	2.19	2.26
	VS (%)	6.61	13.64	17.22

aldehydes, methanol, acetol and water are quantified and presented in Table 1. Acetic acid is the major organic compound present in the condensate irrespective of torrefaction temperature. During torrefaction, acetic acid is mainly produced as a result of cleavage of acetoxy-methoxy groups present in the hemicellulose fractions (Tumuluru et al., 2011b). The composition of the torrefaction condensate varies with the biomass species, Liaw et al. (2015) reported that, at same torrefaction conditions (310 °C and 7.5 min residence time) acetic acid content raised from 6.5 to 14.2 wt.% between corn stover and red fir wood chips respectively. Fagernas et al. (2015) reported that, at same torrefaction conditions (300 °C and 3 h residence time), methanol content varied from 2.6 to 5.3 wt.% for spruce and bamboo respectively. In this study, acetic acid content in the torrefaction condensate from pine wood varied from 3 to 5% with temperature changes from 225 to 300 °C. Similarly, methanol yield was also increased from 0.4 to 1.5% when torrefaction temperature was raised from 225 to 275 °C. Water is the major component in the torrefaction condensate and the observed quantities are around 84, 73, 58 wt.% for the torrefaction temperature of 225, 275 and 300 °C respectively. According to Tumuluru et al. (2011a) water in the torrefaction condensate results from the evaporation of freely bounded water in the biomass and also from the dehydration and condensation reactions.

The VS of the torrefaction condensate from the studied pine wood increased with the increasing torrefaction temperature, which is likely due to increasing degree of hemicellulose and cellulose degradation (Tumuluru et al., 2011a). Similarly, in case of spruce wood, which is another largely used softwood, increase in torrefaction temperature from 240 to 300 °C resulted an increase in COD, a measure of organic content, from 37 to 810 g/L, while the total organic content was increased from 2.4 to 29.2 wt.%, respectively (Fagernas et al., 2015).

3.2. AD of torrefaction condensate

3.2.1. Methane yield

Fig. 3 shows the cumulative methane yield from the anaerobic digestion of pine wood torrefaction condensate produced at different temperatures (225, 275 and 300 °C) loaded at different substrate to inoculum ratio (0.1 and 0.2 $VS_{substrate}$:$VS_{inoculum}$) at mesophilic (35 °C) and thermophilic (55 °C) condition. Torrefaction condensate produced at all studied temperatures appeared as a promising substrate for AD. The methane yield of 430–492 mL/g VS and 430–460 mL/g VS was obtained with the torrefaction condensate in mesophilic and thermophilic AD conditions, respectively. The only previous study on AD of torrefaction condensate reported methane yield, under mesophilic conditions, in the range of 50–100 mL/g of condensate produced at 315 °C with different agricultural crop residues (Liaw et al., 2015), while in the present study the methane yield for condensate produced at 300 °C was around 83 mL/g of condensate. Table 2 shows the comparison of

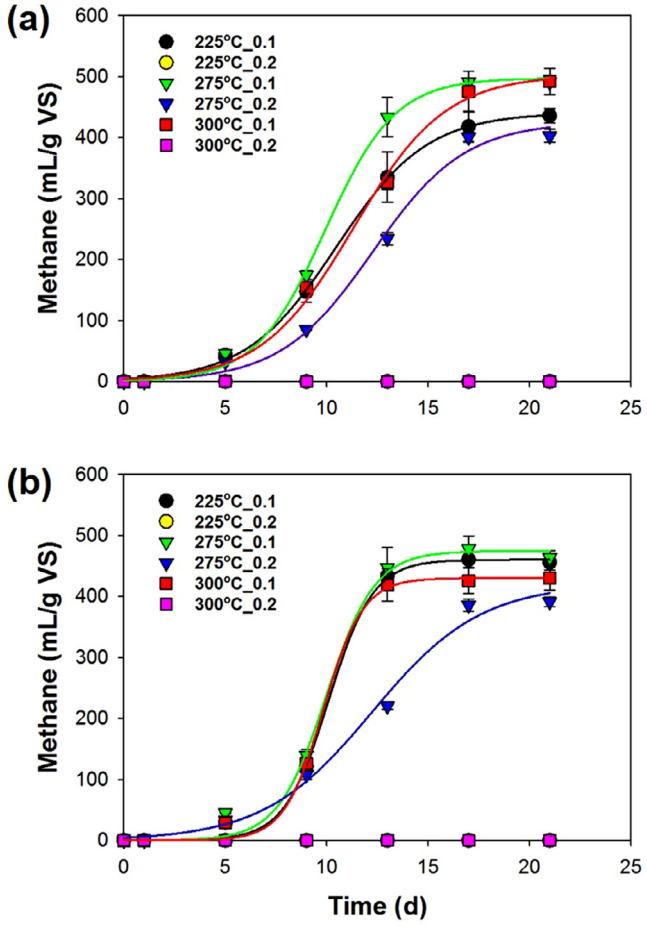

Fig. 3. Cumulative methane yield during batch experiments with condensate prepared at different temperatures (225, 275 and 300 °C) and at various $VS_{substrate}$:$VS_{inoculum}$ loading (0.1 and 0.2) (a) mesophilic (35 °C); (b) thermophilic (55 °C) conditions.

Table 2
Methane potential of the various substrates.

Substrate	Methane yield (mL/g VS)	References
Torrefaction condensate (mesophilic)	492	This study
Torrefaction condensate (thermophilic)	430	This study
Lipid extracted micro-algal biomass	240	Kinnunen et al. (2014)
Corn silage	296	Labatut et al. (2011)
Used vegetable oil	648	Labatut et al. (2011)
Cheese whey	423	Labatut et al. (2011)
Switch grass	122	Labatut et al. (2011)
Paper and pulp primary sludge	223	Bayr and Rintala (2012)
Aqueous pyrolysis liquid	72[a]	Torri and Fabbri (2014)
Organic fraction of municipal solid waste	80	Forster-Carneiro et al. (2008)

[a] in mL/g of Aqueous pyrolysis liquid.

the methane yields of the different substrates with that of the present torrefaction condensate. The methane yield from the torrefaction condensate is well in comparison with the best AD substrates such as used vegetable oils and cheese whey.

The torrefaction temperature had a significant effect on the methane yield during the AD process. With the torrefaction condensates produced at 225 and 300 °C, the methane production was observed only at 0.1 $VS_{substrate}$:$VS_{inoculum}$ ratio in case of both thermophilic and mesophilic conditions. Whereas, for 275 °C the methane production was observed at both 0.1 and 0.2 $VS_{substrate}$:$VS_{inoculum}$ loading. Irrespective of torrefaction temperatures, no methane production was observed with 0.5 $VS_{substrate}$:$VS_{inoculum}$ loading.

Table 3 reports the cumulative methane yield for a period of 30 d. The observed methane yield at 0.1 $VS_{substrate}$:$VS_{inoculum}$ loading and at mesophilic condition was around 436 ± 10, 490 ± 9 and 492 ± 18 mL/g VS for 225, 275 and 300 °C respectively. The methane yield was higher for the torrefaction condensate produced at 275 and 300 °C than the condensate produced at 225 °C. In case of thermophilic condition, the methane yield was around 456 ± 11, 464 ± 9 and 430 ± 16 mL/g VS for 225, 275 and 300 °C respectively.

Earlier studies on the AD of biomass and biomass derived oils reported that aldehydes, phenols, and furfurals are the main inhibitory compounds for methane production, (Liaw et al., 2015 and Hübner and Mumme, 2015). Previous study with AD of the condensate model inhibitory compounds such as hydroxyacetaldehyde and guaiacol shows that a concentration of >0.01 wt.% would deteriorate the AD process (Liaw et al., 2015). Another group reported the inhibitory effects of phenols and their derivatives present in the pyrolysis oil on the AD process (Hübner and Mumme, 2015). In this study, the concentration of these inhibitory compounds in the condensate varied with torrefaction temperature. For example, furfural varied from 0.29 to 0.55 wt.%, while formaldehyde, which is a strong inhibitor to the AD process (Omil et al., 1999), varied between 0.10 and 0.20 wt.% for torrefaction temperature of 225 and 300 °C respectively. At the same time, the increased $VS_{substrate}$:$VS_{inoculum}$ ratio also increases the concentration of these inhibitory compounds in the AD assays. Based on these information, no methane production at 0.2 and 0.5 $VS_{substrate}$:$VS_{inoculum}$ loadings could be attributed to the increased concentration of inhibitory compounds when compared to the 0.1 $VS_{substrate}$:$VS_{inoculum}$ ratio.

From Fig. 3 it can be observed that there was a difference in lag phase for the methane production between mesophilic and thermophilic conditions. In case of thermophilic the methane production lag phase was around 5 d, whereas in case of mesophilic it was reduced to 2 d. At the same time, higher methane yield was observed in case of mesophilic (Table 3), when compared with the thermophilic AD conditions, for the condensate produced at 275 and 300 °C. The reason for the less methane yield in case of thermophilic could be the accumulation of VFA in the assays (Fig. S2). Thermophilic condition could be more suitable for the hydrolysis and acidogenesis of the substrate, which leads to the increased VFA concentration and thereby reducing the pH of the reactor and ultimately leads to the inhibition of methanogens (Franke-Whittle et al., 2014). According to Diebold (2000), organic acids present in the bio-oils reacts with methanol and form esters, for example acetic acid forms methyl acetate. At elevated temperatures under the presence of strong base (i.e. NaOH) methyl acetate would converted back into acetic acid and methanol, and because of this major portion of the organic acids present in the torrefaction condensate are in their original from and not in the ester form (Stoker, 2015). This could be one of the reasons for the delay in the startup of the methane production in case of thermophilic conditions.

3.2.2. Cyclic batch AD experiments

Cyclic batch AD experiments were carried out in order to understand the inhibition exerted by the torrefaction condensate on the AD process and to optimize the conditions to overcome the inhibition. Fig. 4 shows the cumulative methane production (mL) from cyclic batch AD experiments using torrefaction condensate prepared at 300 °C at different $VS_{substrate}$:$VS_{inoculum}$ loadings (0.1, 0.2 and 0.5). In spite of better performances of torrefaction condensate prepared at 275 °C, the condensate produced at 300 °C was selected for this experiment owing to their higher volumes of condensate production, 28% higher than that from the former, and at the same time the later shows higher degree of inhibition towards the AD process, which needs to be optimized. The inoculum was

Table 3
Cumulative methane yield of torrefaction condensate produced at different temperatures (225, 275 and 300 °C) at 0.1 and 0.2 $VS_{substrate}$:$VS_{inoculum}$ loading at mesophilic (35 °C) and thermophilic (55 °C) conditions.

Anaerobic digestion condition	Cumulative methane yield (mL/g of VS)					
	225 °C		275 °C		300 °C	
	0.1	0.2	0.1	0.2	0.1	0.2
Mesophilic	436 ± 10	–	490 ± 4	402 ± 9	492 ± 18	–
Thermophilic	456 ± 11	–	463 ± 9	391 ± 7	429 ± 16	–

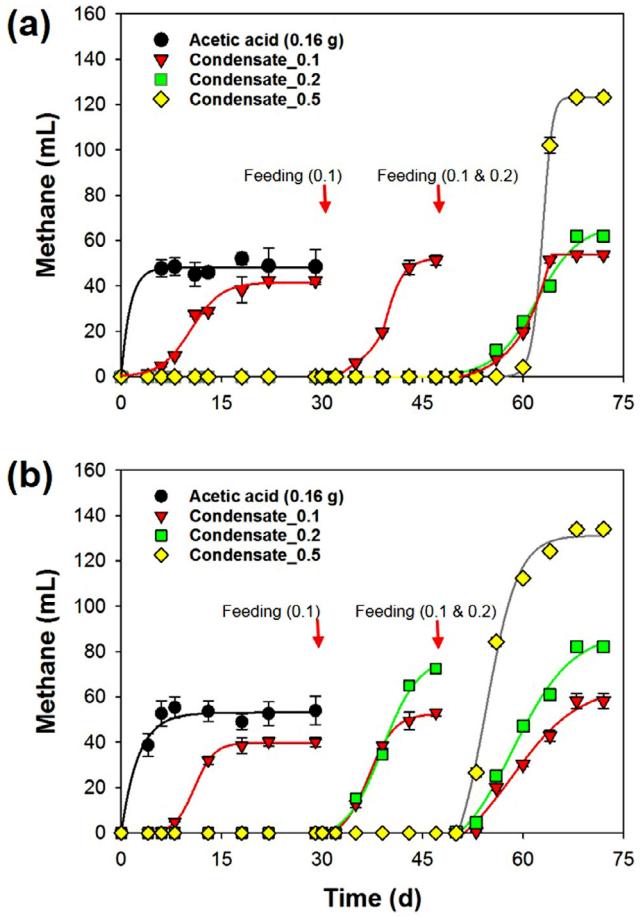

Fig. 4. Methane yield during the cyclic batch experiments with torrefaction condensate produced at 300 °C (a) mesophilic (35 °C); (b) thermophilic (55 °C) conditions.

tested with acetic acid for its methane production potential and used as a standard to compare the methane potentials of the torrefaction condensate. The inoculum performance when tested with acetic acid, yielded a maximum of 50 ± 1 and 54 ± 5 mL CH_4 with 0.16 g of acetic acid (the initial amount in the assay), under mesophilic and thermophilic conditions, respectively. This is on par with the theoretical BMP of acetic acid (370 ml/g [Capareda, 2013]), showing that the inoculum used in this study is well adapted to the operating conditions

As expected, during the first batch of the experiments, the methane production was observed only with the lowest substrate loading tested (0.1 $VS_{substrate}$:$VS_{inoculum}$). At this loading, the torrefaction condensate yielded, 42 ± 1 and 40 ± 2 mL CH_4 under mesophilic and thermophilic AD conditions, respectively. No methane production was observed with 0.2 and 0.5 $VS_{substrate}$:$VS_{inoculum}$ loadings under both AD conditions during the 30 d incubation.

During the 1st feeding experiment (Fig. 4; 30 d), the assays with 0.1 $VS_{substrate}$:$VS_{inoculum}$ were re-fed with fresh condensate substrate, the assays with 0.2 $VS_{substrate}$:$VS_{inoculum}$ were diluted to approximately match the COD values as that of 0.1 $VS_{substrate}$:$VS_{inoculum}$ loading (refer Table 4) and the assays with 0.5 $VS_{substrate}$:$VS_{inoculum}$ loading were left untreated. The re-fed assays with 0.1 $VS_{substrate}$:$VS_{inoculum}$ straight away started producing methane and yielded 51 ± 2 and 53 ± 1 mL CH_4 under mesophilic and thermophilic AD conditions, respectively. It is important to note here that the methane yields were almost similar under both AD conditions unlike the initial batch experiments where mesophilic conditions yielded higher methane than under thermophilic conditions with the condensate produced at 300 °C. Surprisingly, under thermophilic conditions, the assays with 0.2 $VS_{substrate}$:$VS_{inoculum}$, that has been diluted, produced methane and yielded 72 ± 1 mL CH_4 at the end of 18 d. Whereas, no methane production was observed under the mesophilic conditions. This might be attributed to the better adaption of microorganisms under thermophilic conditions with time. Thermophilic conditions promote the biochemical reaction rate of the microorganisms to hydrolyze the substrate at faster rates when compared to the mesophilic conditions, which would faster adaptation of microorganism to tough conditions (Franke-Whittle et al., 2014 and Gebreeyessus and Jenicek, 2016).

During the 2nd feeding experiments (Fig. 4; 48 d), the assays with 0.1 $VS_{substrate}$:$VS_{inoculum}$ and the 0.2 $VS_{substrate}$:$VS_{inoculum}$ assays that were previously diluted were re-fed with fresh substrate. At the same time, the assays with 0.5 $VS_{substrate}$:$VS_{inoculum}$ were diluted to approximately match the COD as that of 0.1 $VS_{substrate}$:$VS_{inoculum}$ loading (refer Table 4). During this phase of experiment all the assays started producing methane under both mesophilic and thermophilic conditions. This clearly showed that the inhibition caused by higher concentrations of torrefaction condensate are reversible and they do not permanently deteriorate the methane production capacity of microorganisms in the

Table 4
Methane yield, VS and COD during the cyclic batch AD experiments with torrefaction condensate (300 °C) with different substrate to inoculum ratio.

Mesophilic AD	Initial			1st feeding			2nd feeding			Final		
Substrate:inoculum	0.1	0.2	0.5	0.1	0.2 → 0.1	0.5	0.1	0.2 → 0.1	0.5 → 0.1	0.1	0.2 → 0.1	0.5 → 0.1
pH	7,3	7,2	7,1	7,4	7,4	7,1	7,1	7,0	7,0	7,1	7,1	7,1
TS%	1.8	2.0	2.4	na	na	na	na	na	na	1.8	2.0	2.0
VS%	1.5	1.6	2.0	na	na	na	na	na	na	1.2	1.2	1.1
COD (g/L)	3.4 ± 0.1	7.7 ± 0.2	16.9 ± 0.2	3.8 ± 0.1	4.2 ± 0.1	14.7 ± 0.2	3.9 ± 0.1	4.2 ± 0.1	6.1 ± 0.1	3.1 ± 0.2	3.6 ± 0.3	4.9 ± 0.3
Methane (mL)	42 ± 1	nd	nd	51 ± 2	nd	nd	53 ± 1	62 ± 1	123 ± 1	–	–	–
Thermophilic AD	Initial			1st feeding			2nd feeding			Final		
Substrate:Inoculum	0.1	0.2	0.5	0.1	0.2 → 0.1	0.5	0.1	0.2 → 0.1	0.5 → 0.1	0.1	0.2 → 0.1	0.5 → 0.1
pH	7,1	7,1	7,2	7,1	7,3	7,2	7,1	7,0	7,2	7,2	7,2	7,3
TS%	1.8	1.9	2.3	na	na	na	na	na	na	1.7	1.9	2.1
VS%	1.4	1.6	2.0	na	na	na	na	na	na	1.2	1.1	1.0
COD (g/L)	3.3 ± 0.1	7.6 ± 0.1	16.5 ± 0.1	3.9 ± 0.1	4.4 ± 0.2	13.2 ± 0.3	4.1 ± 0.2	4.9 ± 0.2	6.3 ± 0.2	3.9 ± 0.3	4.1 ± 0.3	4.7 ± 0.2
Methane (mL)	40 ± 2	nd	nd	53 ± 1	72 ± 1	nd	58 ± 3	82 ± 1	134 ± 1	–	–	–

na, not available; nd, not detected.
0.2 → 0.1, the set up with initial substrate to inoculum ratio of 0.2 was diluted using dH2O by removing ~15 g of aqueous fractions to approximate bring it to 0.1 ratio during the first feeding experiments. Later during the second feeding experiments, the entire aqueous fractions (~20.5 g) were removed after gravity settling and fed with 0.1 VS ratio of substrate along with dH2O to make up the volume to 60 mL.
0.5 → 0.1, the set up with initial substrate to inoculum ratio of 0.5 was diluted using dH2O by removing ~20 g of aqueous fractions to approximately bring it to 0.1 ratio during the second feeding experiments.

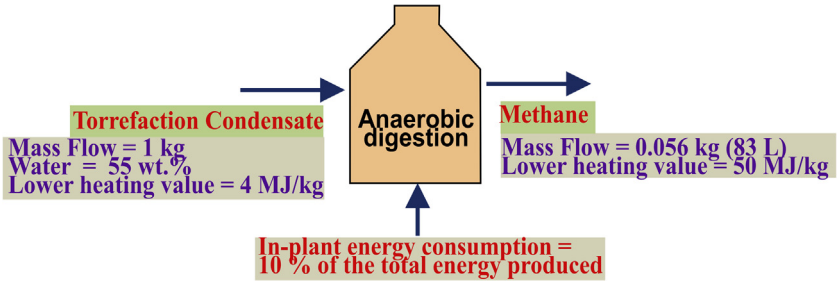

Fig. 5. Basic energy balance of the anaerobic digestion of torrefaction condensate.

inoculum. Moreover, the methane production capacity has been increased with time, finally yielding a maximum of 123 ± 1 and 134 ± 1 mL CH_4 in the case of diluted 0.5 $VS_{substrate}$:$VS_{inoculum}$ assays under mesophilic and thermophilic conditions, respectively. After three cycles of loading, a rise of 60% in the methane yield was observed in case of mesophilic condition in this study. In a similar type of cyclic batch AD of corn distiller's dried grain, Gyenge et al. (2014) reported a rise of 40% in the methane yield after the third cycle. The previous studies (Kim and Lee, 2013) on the changes of microbial community structure during repeated batch experiments shows that, the reason for the raise in the methane yield with increasing feeding cycle is because of the increased population of methanogens. In general, thermophilic conditions showed better revival of methane production capacity when compared to the mesophilic conditions. These results suggest that a pre-adaptation of the inoculum with higher concentration of torrefaction condensate before the AD process would improve the methane production capacity and at the same time fasten the methane production rates.

3.2.3. Energy balance of the process

Fig. 5 shows the basic energy balance of anaerobic digestion of torrefaction condensate. The theoretical heating value of the torrefaction condensate was evaluated, according to the Eq. (1).

The calculated lower heating value (LHV) of the torrefaction condensate is around 4 MJ/kg, which is low in comparison with LHV of pyrolysis oil (i.e. 14–18 MJ/kg [Lu et al., 2009]), mainly because of the high water content (i.e. 55 wt.%) in the torrefaction condensate. Owing to this high water content, the torrefaction condensate would have poor ignition property during combustion (Torri and Fabbri, 2014). Earlier studies reported that 8.5–13% of the total energy production is utilized for in-plant energy consumption during AD process (Acton, 2013 and Sørensen, 2007). For this study, it is considered that 10% of the total energy production is utilized within the AD process. The basic energy balance shows that the energy efficiency of AD of torrefaction condensate is approximately 60%. However, the overall energy and economics of the AD system depends on several factors like type of substrate loaded, type of reactor employed, the operating conditions of the digester and the end use of the produced bio-methane. So, a detailed process study and optimization need to be made to better understand the process feasibility of the anaerobic digestion of torrefaction condensate and it is the subject of our future study.

As the methane yield is comparable with other substrates, the torrefaction condensate could be a good choice as a feedstock to produce methane through AD. Even though, the better methane production was demonstrated at lower loading, there is room for improving the substrate loading through detoxification of torrefaction condensate by selectively removing the toxic compounds such as furfurals and phenols through methods such as selective evaporation, activated carbon-based filtration. Moreover, torrefaction condensate could also be an interesting option for co-digestion with other substrates such as pulp and paper industry wastewater sludge, and sludge from municipal wastewater treatment plants, which could also minimize the inhibitory impacts. Research on this could be instigated in future.

4. Conclusions

To our knowledge this is the first comprehensive study on AD of torrefaction condensate from pine wood reporting methane yields around 430–492 mL/g VS and 430–460 mL/g VS for mesophilic and thermophilic conditions, respectively. Methane yield of the torrefaction condensate differs (436–492 mL/g VS) with torrefaction temperatures (225–300 °C). Torrefaction condensate inhibits batch AD at high substrate loading (0.2–0.5). The cyclic batch experiment shows that this inhibition is reversible and the methane production can be rapidly restored by diluting the loading. In practice this could be realized through co-digestion with mixture of non-inhibitory substrates.

Acknowledgement

The authors gratefully acknowledge the financial support by the Academy of Finland for the IMUSTBC -271117 (Improving process understanding and widening of the feedstock of thermal biomass conversion) project, and the TUT Postdoc funding program.

Appendix A. Supplementary data

Supplementary data associated with this article can be found, in the online version, at http://dx.doi.org/10.1016/j.biortech.2016.11.073.

References

Acton, Q.A., 2013. Issues in Energy Research and Application: 2013 Edition. ScholarlyEditions, Atalanta.
Bayr, S., Rintala, J., 2012. Thermophilic anaerobic digestion of pulp and paper mill primary sludge and co-digestion of primary and secondary sludge. Water Res. 46, 4713–4720. http://dx.doi.org/10.1016/j.watres.2012.06.033.
Capareda, S., 2013. Introduction to Biomass Energy Conversions. CRC Press, Florida.
Diebold, J.P., 2000. A Review of the Chemical and Physical Mechanisms of the Storage Stability of Fast Pyrolysis Bio-Oils. Nrel/Sr-570-27613 59. NREL/SR-570-27613.
Doddapaneni, T.R.K.C., Konttinen, J., Hukka, T.I., Moilanen, A., 2016. Influence of torrefaction pretreatment on the pyrolysis of Eucalyptus clone: a study on kinetics, reaction mechanism and heat flow. Ind. Crops Prod. 92, 244–254. http://dx.doi.org/10.1016/j.indcrop.2016.08.013.
Fabbri, D., Torri, C., 2016. Linking pyrolysis and anaerobic digestion (Py-AD) for the conversion of lignocellulosic biomass. Curr. Opin. Biotechnol. 38, 167–173. http://dx.doi.org/10.1016/j.copbio.2016.02.004.
Fagernas, L., Kuoppala, E., Arpiainen, V., 2015. Composition, utilization and economic assessment of torrefaction condensates. Energy Fuels 29, 3134–3142. http://dx.doi.org/10.1021/acs.energyfuels.5b00004.
Forster-Carneiro, T., Prez, M., Romero, L.I., 2008. Thermophilic anaerobic digestion of source-sorted organic fraction of municipal solid waste. Bioresour. Technol. 99, 6763–6770. http://dx.doi.org/10.1016/j.biortech.2008.01.052.

Franke-Whittle, I.H., Walter, A., Ebner, C., Insam, H., 2014. Investigation into the effect of high concentrations of volatile fatty acids in anaerobic digestion on methanogenic communities. Waste Manage. 34, 2080–2089. http://dx.doi.org/10.1016/j.wasman.2014.07.020.

Garcia, R., Pizarro, C., Lavin, A.G., Bueno, J.L., 2013. Biomass proximate analysis using thermogravimetry. Bioresour. Technol. 139, 1–4. http://dx.doi.org/10.1016/j.biortech.2013.03.197.

Gebreeyessus, G., Jenicek, P., 2016. Thermophilic versus mesophilic anaerobic digestion of sewage sludge: a comparative review. Bioengineering 3, 15. http://dx.doi.org/10.3390/bioengineering3020015.

Gyenge, L., Crognale, S., Lányi, S., Ábrahám, B., Ráduly, B., 2014. Anaerobic digestion of corn-DDGS: effect of pH-control, agiTation and batch repetition. UPB Sci. Bull. Ser. B Chem. Mater. Sci. 76, 163–172.

Hübner, T., Mumme, J., 2015. Integration of pyrolysis and anaerobic digestion – use of aqueous liquor from digestate pyrolysis for biogas production. Bioresour. Technol. 183, 86–92. http://dx.doi.org/10.1016/j.biortech.2015.02.037.

Keipi, T., Tolvanen, H., Kokko, L., Raiko, R., 2014. The effect of torrefaction on the chlorine content and heating value of eight woody biomass samples. Biomass Bioenergy 66, 232–239. http://dx.doi.org/10.1016/j.biombioe.2014.02.015.

Keshtkar, A., Ghaforian, H., Abolhamd, G., Meyssami, B., 2001. Dynamic simulation of cyclic batch anaerobic digestion of cattle manure. Bioresour. Technol. 80, 9–17.

Khartchenko, N.V., Kharchenko, V.M., 2013. Advanced energy systems. Energy Technology Series,. CRC Press, Florida.

Kim, J., Lee, C., 2013. Changes in microbial community structure during anaerobic repeated-batch treatment of cheese-processing wastewater. APCBEE Procedia 5, 520–526. http://dx.doi.org/10.1016/j.apcbee.2013.05.088.

Kinnunen, H.V., Koskinen, P.E.P., Rintala, J., 2014. Mesophilic and thermophilic anaerobic laboratory-scale digestion of Nannochloropsis microalga residues. Bioresour. Technol. 155, 314–322. http://dx.doi.org/10.1016/j.biortech.2013.12.115.

Kinnunen, V., Ylä-Outinen, A., Rintala, J., 2015. Mesophilic anaerobic digestion of pulp and paper industry biosludge-long-term reactor performance and effects of thermal pretreatment. Water Res. 87, 105–111. http://dx.doi.org/10.1016/j.watres.2015.08.053.

Koppejan, J., Sokhansanj, S., Melin, S., Madrali, S., 2012. Status overview of torrefaction technologies. IEA Bioenergy Task 32, 1–54.

Labatut, R.A., Angenent, L.T., Scott, N.R., 2011. Biochemical methane potential and biodegradability of complex organic substrates. Bioresour. Technol. 102, 2255–2264. http://dx.doi.org/10.1016/j.biortech.2010.10.035.

Lian, J., Garcia-Perez, M., Coates, R., Wu, H., Chen, S., 2012. Yeast fermentation of carboxylic acids obtained from pyrolytic aqueous phases for lipid production. Bioresour. Technol. 118, 177–186. http://dx.doi.org/10.1016/j.biortech.2012.05.010.

Lian, J., Garcia-Perez, M., Chen, S., 2013. Fermentation of levoglucosan with oleaginous yeasts for lipid production. Bioresour. Technol. 133, 183–189. http://dx.doi.org/10.1016/j.biortech.2013.01.031.

Liaw, S.S., Frear, C., Lei, W., Zhang, S., Garcia-Perez, M., 2015. Anaerobic digestion of C1–C4 light oxygenated organic compounds derived from the torrefaction of lignocellulosic materials. Fuel Process. Technol. 131, 150–158. http://dx.doi.org/10.1016/j.fuproc.2014.11.012.

Lu, Q., Li, W.Z., Zhu, X.F., 2009. Overview of fuel properties of biomass fast pyrolysis oils. Energy Convers. Manage. 50, 1376–1383. http://dx.doi.org/10.1016/j.enconman.2009.01.001.

Milne, T.A., Evans, R.J., Abatzoglou, N., 1998. Biomass Gasifier " Tars ": Their Nature, Formation, and Conversion. National Renewable Energy Laboratory, Golden, CO.. 10.2172/3726.

Omil, F., Méndez, D., Vidal, G., Méndez, R., Lema, J.M., 1999. Biodegradation of formaldehyde under anaerobic conditions. Enzyme Microbiol. Technol. 24, 255–262. http://dx.doi.org/10.1016/S0141-0229(98)00119-7.

Sørensen, B., 2007. Renewable Energy Conversion, Transmission and Storage, Renewable Energy Conversion, Transmission and Storage. Academic press, London. 10.1016/B978-012374262-9.50024-0.

South, D.B., Smidt, M., 2014. Pine. Cellulosic Energy Cropping Systems. John Wiley Sons Ltd, Hoboken, New Jersey, pp. 161–181. http://dx.doi.org/10.1002/9781118676332.ch10.

Stoker, H.S., 2015. Organic and Biological Chemistry. Cengage Learning, Boston.

Thrän, D., Witt, J., Schaubach, K., Kiel, J., Carbo, M., Maier, J., Ndibe, C., Koppejan, J., Alakangas, E., Majer, S., Schipfer, F., 2016. Moving torrefaction towards market introduction – technical improvements and economic-environmental assessment along the overall torrefaction supply chain through the SECTOR project. Biomass Bioenergy 89, 184–200. http://dx.doi.org/10.1016/j.biombioe.2016.03.004.

Torri, C., Fabbri, D., 2014. Biochar enables anaerobic digestion of aqueous phase from intermediate pyrolysis of biomass. Bioresour. Technol. 172, 335–341. http://dx.doi.org/10.1016/j.biortech.2014.09.021.

Tumuluru, J.S., Sokhansanj, S., Hess, J.R., Wright, C.T., Boardman, R.D., 2011a. A review on biomass torrefaction process and product properties for energy applications. Ind. Biotechnol. 7, 384–401. http://dx.doi.org/10.1089/ind.2011.0014.

Tumuluru, J.S., Wright, C.T., Richard D. Boardman, Richard J. Hess, Shahab Sokhansanj, 2011b. Review on biomass torrefaction process and product properties and design of moving bed torrefaction system model development, in: ASABE Annual International Meeting (2011). Louisville, Kentucky.

Verhoeff, F., Boersma, A.R., Pels, J.R., Lensselink, J., 2011. Torrefaction Technology for the production of solid bioenergy carriers from biomass and waste. Energy Res. Cent. Netherlands, 75.

Publication III

Tharaka Rama Krishna C Doddapaneni, Rohan Jain, Ramasamy Praveenkumar, Henrik Romar, Jukka Konttinen, Jukka Rintala

"Adsorption of furfural from torrefaction condensate using torrefied biomass"

Chemical Engineering Journal 2018; 334: 558–68.

Chemical Engineering Journal 334 (2018) 558–568

Contents lists available at ScienceDirect

Chemical Engineering Journal

journal homepage: www.elsevier.com/locate/cej

Adsorption of furfural from torrefaction condensate using torrefied biomass

Tharaka Rama Krishna C. Doddapaneni[a,*], Rohan Jain[a,b], Ramasamy Praveenkumar[a], Jukka Rintala[a], Henrik Romar[c], Jukka Konttinen[a]

[a] Laboratory of Chemistry and Bioengineering, Tampere University of Technology, P.O. Box 541, FI-33101 Tampere, Finland
[b] Helmholtz-Zentrum Dresden-Rossendorf, Helmholtz Institute Freiberg for Resource Technology, Bautzner Landstrasse 400, 01328 Dresden, Germany
[c] University of Oulu, Research Unit of Sustainable Chemistry, P.O. Box 3000, FI-90014 Oulu, Finland

GRAPHICAL ABSTRACT

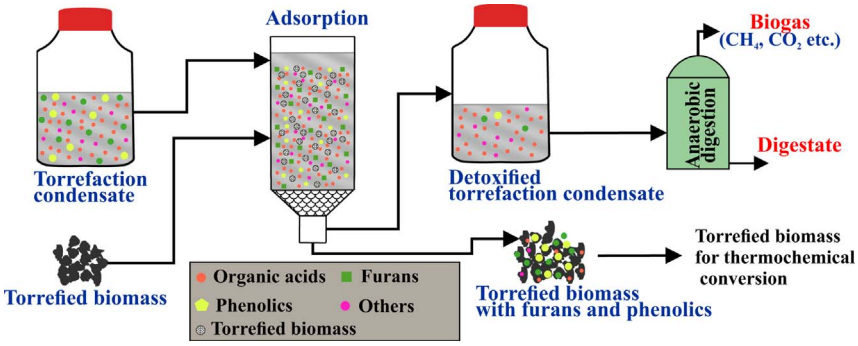

ARTICLE INFO

Keywords:
Detoxification
Anaerobic digestion
Pellets
Torrefaction volatiles
Energy densification

ABSTRACT

Torrefaction is a biomass energy densification process that generates a major byproduct in the form of torrefaction condensate. Microbial conversion of torrefaction condensate could be an attractive option for energy integration within torrefaction process. However, torrefaction condensate contains several compounds, such as furfural, 5-hydroxymethylfurfural and guaiacol that are inhibitory to microbes. In this study, for the first time, we reported detoxification of torrefaction condensate, by removing the major inhibitory compound furfural, using torrefied biomass and later used the detoxified torrefaction condensate for anaerobic digestion. The effect of varying torrefaction temperature (225–300 °C), torrefied biomass dosage (25–250 g/L), initial pH (2.0–9.0), and contact time (1–12 h) on furfural adsorption was studied with batch adsorption experiments. The furfural adsorption on torrefied biomass was best represented by pseudo second order kinetic model. The adsorption of furfural and other inhibitory compounds on torrefied biomass was likely a hydrophobic interaction. A maximum of 60% of furfural was adsorbed from torrefaction condensate containing 9000 mg furfural/L using 250 g/L of torrefied biomass in batch adsorption. For, column (20 mm internal diameter and 200 mm bed height), the saturation time for furfural adsorption was around 50 min. Anaerobic digestion of the detoxified torrefaction condensate shows that the lag phase in methane production was reduced from 25 d to 15 d for 0.2 volatile solid $(VS)_{substrate}$:$VS_{inoculum}$ loading. The study shows that torrefaction condensate can be effectively detoxified using torrefied biomass for microbial conversion and can be integrated within the torrefied biomass pellet production process.

* Corresponding author.
E-mail address: tharaka.doddapaneni@tut.fi (T.R.K.C. Doddapaneni).

http://dx.doi.org/10.1016/j.cej.2017.10.053
Received 25 July 2017; Received in revised form 7 October 2017; Accepted 11 October 2017
Available online 12 October 2017

1. Introduction

Torrefaction is a pretreatment method for biomass upgradation, where the biomass is heated slowly at a temperature range of 200–300 °C in an inert environment in order to increase the energy density and hydrophobicity by lowering the moisture content of the biomass [1,2]. In the recent days the research interest on torrefaction process is increasing owing to high commercial demand of torrefied biomass, projected to be 70 million tons per year by 2020 globally [3].

The two major technical challenges in commercialization of torrefaction technology are handling the volatile gases that are produced during the torrefaction and the energy integration within the process [1]. At present, the volatile gases produced are combusted back to meet the energy requirements for biomass drying and torrefaction. However, owing to their high water and CO_2 content, the torrefaction volatiles have low heating value. In addition, presence of different types of organic acids makes them very corrosive to the combusting equipment [1,4,5] Hence, advanced process integration approaches are required for better utilization of torrefaction volatiles and thereby improving the overall efficiency and economic viability of the torrefaction system [4,5]

The torrefaction condensate (obtained by condensing the volatiles) mainly contains water and acetic acid. Recently, Doddapaneni et al. [5] reported that torrefaction condensate, with ~50 g/L of acetic acid, can be used as substrate for anaerobic digestion (AD) for bio-methane production. However, owing to the presence of inhibitory compounds such as furfural, 5-Hydroxymethylfurfural (5-HMF) and guaiacol, the methane production was inhibited at higher substrate loading [4]. In order to improve the methane production, concentration of these inhibitory compounds should be significantly decreased in the torrefaction condensate.

Adsorption is a cost-effective method for removal of inhibitory compounds from the pyrolysis oil and biomass hydrolysate [6,7]. Polymeric adsorbents such as XAD-4 and XAD-7 was shown to adsorb 90 and 80 mg of furfural per g of adsorbent from corn fiber hydrolysate [6]. Other study [8] reported that the adsorption of phenol and furfural from oat hull hydrolysate using powdered activated carbon improved the bioproduction of xylitol by 10%. However, due to the large concentration of furfural (6000–11,000 mg/L) in the torrefaction condensate [4,5,9], a cheap and readily available adsorbent with reasonable adsorption capacity is required. Torrefied biomass could be an alternative adsorbent due to their hydrophobic nature as furfural is also hydrophobic, cost-effectiveness and easy availability. However, there are no studies on the removal of furfural from torrefaction condensate using torrefied biomass and the further application of detoxified torrefaction condensate for bioconversion.

Torrefaction process reduces the energy required for biomass grinding but subsequently, it increases the energy requirement for pelletization owing to the increase in the biomass brittleness [10]. The energy required to pelletize the raw biomass and torrefied biomass are in the range of 757 kJ/kg and 1164 kJ/kg respectively [11]. Preconditioning of torrefied biomass with water to a moisture content of 10% [12] or addition of binding materials, such as wheat flour [11], lignin, starch, calcium hydroxide and sodium hydroxide [13,14] has been reported to improve the properties of the pellets. However, this external addition of binders would add to the production cost and also sourcing binders for large production volumes would be challenging [15].

Fig. 1 illustrates an integrated process to address the above-discussed issues i.e. (i) microbial inhibition with torrefaction condensate: through torrefied biomass based adsorption of inhibitory compounds, and (ii) the supply of binders for torrefied biomass pelletization: through adsorbed compounds from torrefaction condensate. The proposed approach is to use a part of torrefied biomass as an adsorbent for removal of the inhibitory compounds from the condensate. Following adsorption, the water content and compounds adsorbed on the biomass will themselves add binding effects and thereby could reduce the energy requirement in pelletization [16]. Moreover, the torrefied biomass with compounds adsorbed to them could be mixed with rest of the torrefied biomass before pelletizing, which will improve the quality and durability of the pellets. The torrefaction condensate after adsorption (detoxified condensate) can be used in AD process.

This study focuses on the adsorption and anaerobic digestion stages presented in Fig. 1. Here we used torrefied biomass, for the first time, to adsorb furfural from the torrefaction condensate in order to improve the prospects of utilizing torrefaction condensate in anaerobic digestion. Adsorption of furfural was studied in detail, as it is the major inhibitory compound present in torrefaction condensate [4,5]. The adsorption efficiency of torrefied biomass was tested using standard furfural solution by means of batch experiments by varying pH and biomass dosage and further evaluated through kinetic modelling. Further, the batch adsorption experiments were also carried out using actual torrefaction condensate. Later, column experiments were conducted with both standard furfural solution and torrefaction condensate. The break-through curves were determined for furfural and other inhibitory compounds. The empirical models were investigated to decipher the mechanisms of adsorption. Finally, the anaerobic digestion experiments were carried out with both original and detoxified torrefaction condensate.

2. Materials and methods

2.1. Torrefaction process

Torrefied biomass and torrefaction condensate were produced as described by Doddapaneni et al. [5]. Briefly, Finnish pine wood chips were air dried at 105 °C for 24 h in an electrically heated oven. The reactor (Fig. S1) temperature was raised from room temperature (20 °C) to a final torrefaction temperature i.e. 225, 275 or 300 °C and maintained at that temperature for 2 h. The fluctuation in the reactor temperature was maintained within ± 5 °C during the isothermal period by circulating water through the coils wrapped around the reactor. In each run, one kg of biomass was loaded into the reactor. The volatiles released during the torrefaction process were condensed using water circulated condenser and a glass bottle submerged in an ice bath. The condensate was stored at 4 °C to prevent further aging reactions. The torrefaction condensate has a tendency to form settled tar that is viscous and sticky in nature. This viscous tar (~5 vol%) was removed by simple decantation and the torrefied biomass was grinded using Restsch ZM200 centrifugal mill prior to the adsorption experiments. The grinded biomass was sieved to a particle size of < 100 μm.

2.2. Characterization of torrefied biomass

Torrefied biomass was characterized using scanning electron microscopy (SEM) and Brunauer–Emmett–Teller (BET) analysis. Pore size distribution and surface area measurements were evaluated according to Barrett-Joyner-Halenda (BJH) and BET model, respectively.

2.3. Batch adsorption experiments

All the batch adsorption experiments were carried out in a total volume of 20 mL, with continuous mixing at 150 rpm and room temperature (≈20 °C). The kinetics of furfural adsorption using torrefied biomass was studied for 12 h at an initial furfural concentration of 6000 mg/L and pH 3.6, and torrefied biomass concentration varying from 25 to 150 g/L. All the subsequent batch adsorption experiments were carried out for the duration of 12 h as the equilibrium was achieved. For the isotherm study, the initial furfural concentration was varied from 300 to 6000 mg/L with pH of 3.6 and torrefied biomass concentration of 50 g/L. The effect of pH on furfural adsorption was studied by varying the initial furfural solution pH from 2.0 to 9.0, with

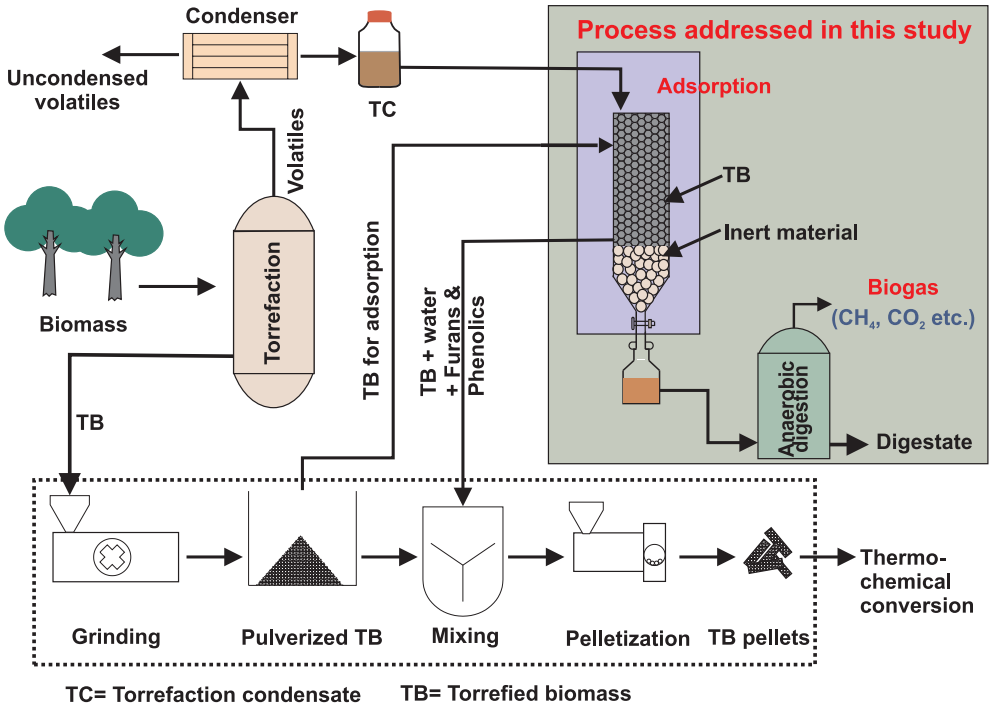

Fig. 1. A biorefinery process involving detoxification of torrefaction condensate and anaerobic digestion for efficient energy integration within torrefied biomass pellet production.

initial furfural concentration of 6000 mg/L and torrefied biomass concentration of 100 g/L. The effect of biomass dosage on furfural adsorption was studied by varying torrefied biomass concentration from 25 to 150 g/L, with initial furfural concentration of 6000 mg/L and pH of 3.6. In case of batch adsorption studies with torrefaction condensate, the torrefied biomass dosage of 25, 50, 100, 200 and 250 g/L was added to 10 mL of torrefaction condensate. Torrefaction condensate was used at its original pH in all adsorption tests carried out in this study. The solid-liquid separation was achieved by centrifuging the samples at $5018 \times g$ for 5 min. Supernatants were filtered using 0.45 µm (Chromafill® – PET 45/25) prior to gas chromatography mass spectrometer (GC-MS) analysis. All the batch adsorption experiments were carried out in duplicates and if the difference was more than 10%, the experiments were repeated.

2.4. Column adsorption experiments

The column experiments were carried out in glass column of internal diameter of 10 and 20 mm and the length of 300 mm. Borosilicate glass beads (2 mm dia) were used to pack torrefied biomass from top and bottom in the column. This glass bead packing (2 cm height) was also helpful in allowing uniform distribution of the adsorbate in the column by preventing backlash. The effective bed height of adsorbent (i.e. torrefied biomass) was 200 mm. The amount of torrefied biomass filled in 10 and 20 mm columns was 6 g and 20 g, respectively. Either the standard furfural solution with 6000 mg/L with initial pH of 3.6 or the torrefaction condensate were loaded into column using peristaltic pump at 1 mL/min. Aliquots from the column were collected every 5 min for GC-MS analysis. Control experiments with borosilicate glass beads were carried out to rule out adsorption of furfural on them.

2.5. Anaerobic digestion (AD) batch assay

The AD batch assays of torrefaction condensate before and after detoxification was studied, using 120 mL serum bottles at mesophilic condition i.e. 35 °C for 35 d. The operating volume was 60 mL. The substrate (condensate) to inoculum volatile solids (VS) ratio ($VS_{substrate}$:$VS_{inoculum}$) of 0.1 (non-inhibitory concentration) and 0.2 (inhibitory concentration) were tested. Granular sludge collected from the mesophilic upflow anaerobic sludge blanket (USAB) reactor that treats waste water from an integrated beta-amylase and ethanol plant (Jokioinen, Finland) was used as inoculum for AD batch assays. Detailed methodology has been previously reported [5].

2.6. Analytical methods

Surface characteristics of torrefied biomass was analyzed using scanning electron microscopy JSM–T10 (Jeol, USA). Specific surface area (SSA) and pore size distributions were measured using a Micrometrics ASAP 2020 (Norcross, USA) by physical adsorption of nitrogen. For adsorption tests, about 100 mg of sample was loaded into a quartz tube. Prior to adsorption tests, contaminating gases from samples were removed using 10 µm Hg at a temperature of 150 °C. Detailed methodology has been reported by Kramb et al. [17].

Gas chromatograph (GC; Agilent series 6890) equipped with mass spectrometry (MS) detector (Agilent 5975B) and the capillary column HP-5MS (30 m, 0.25 mm ID, 0.25 µm film thickness; Agilent) was used to analyze both standard furfural solution and torrefaction condensate before and after adsorption experiments. In case of standard furfural solution, initially the GC column was held for 2 min at 50 °C, and followed by a ramp of 5 °C/min to a temperature of 250 °C. Later, the oven was heated to a final temperature of 280 °C at 10 °C/min and held for 10 min. The helium gas with a flow rate of 1 mL/min was used as a carrier gas. The injection temperature was 250 °C. The injection volume was 0.2 µL with a split ratio of 20:1. In case of torrefaction condensate analysis, the oven temperature was raised at a heating rate of 2 °C/min to a temperature of 180 °C and then to a final temperature of 280 °C at 10 °C/min. The oven was held at final temperature for 5 min. The MS temperature was maintained at 250 °C.

The total solids (TS) and VS of the inoculum and the torrefaction condensate was tested as described by Doddapaneni et al. [5]. The methane production was tested using GC following the procedure described in our earlier study [5].

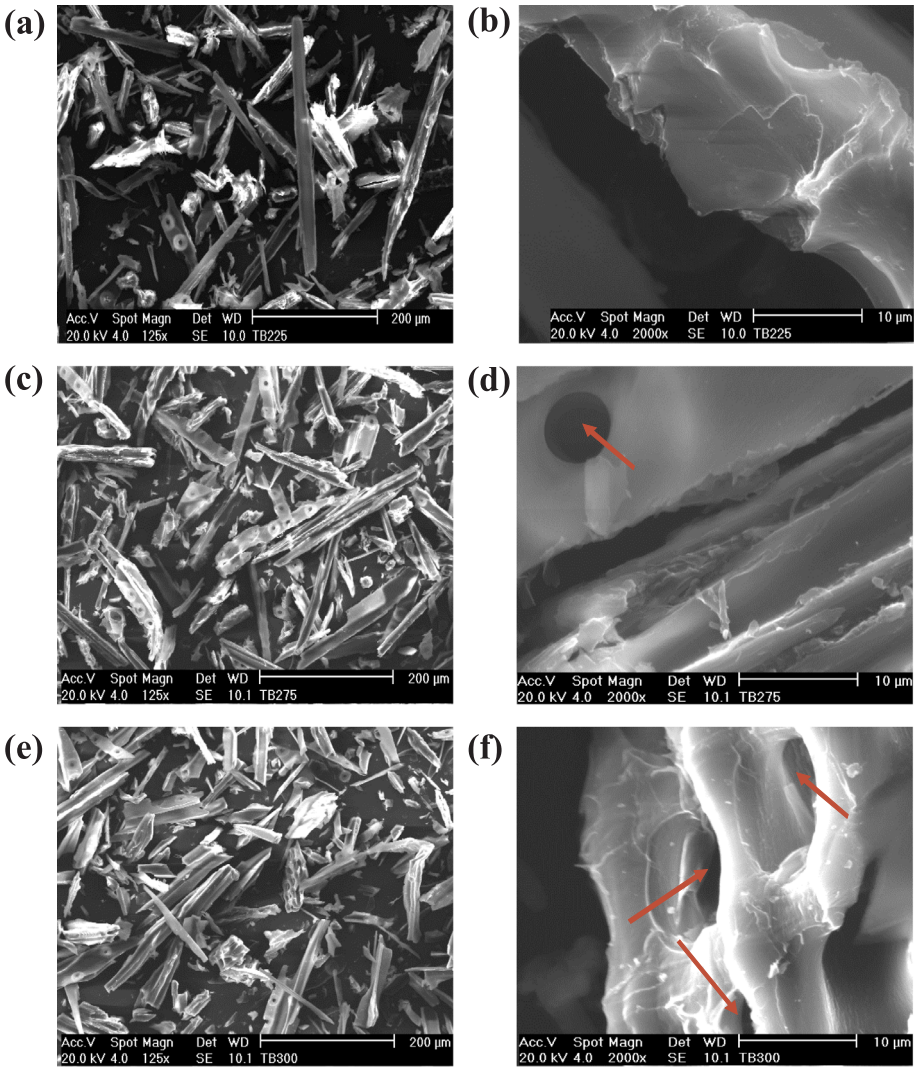

Fig. 2. SEM images of torrefied biomass produced at different temperatures (a and b) 225 °C, (c and d) 275 °C, (e and f) 300 °C at different resolution. The red arrows represent pores within the torrefied biomass.

3. Results

3.1. Characterization of the adsorbent (torrefied biomass)

Fig. 2 shows SEM images of the pine wood biomass torrefied at 225, 275 and 300 °C. It can be observed that the porosity of biomass is increasing with increasing torrefaction temperature. At temperature 225 °C, no specific surface area (SSA) and pore diameter was detected by the BET analysis (Table 1). The further increase in temperature to 275 °C led to increase in SSA (1.47 m^2/g). However, SSA (1.10 m^2/g) decreased with further raise in temperature to 300 °C.

3.2. Characterization of torrefaction condensate

Torrefaction condensate mainly contains water, organic acids, aldehydes and phenolic compounds. The pH of torrefaction condensate was around 2.1. The concentration of acetic acid and furfural were, 80 and 9 g/L, respectively for the torrefaction condensate produced at 300 °C. The VS was around 11%.

Table 1
BET surface analysis of torrefied biomass produced at different torrefaction temperatures.

Sample	Specific surface area (m^2/g)	Pore volume (cm^3/g)	Mean pore diameter (nm)
TB225	Nd	No pores	–
TB275	1.47	0.0065	17.8
TB300	1.10	0.0043	15.7

3.3. Influence of torrefaction temperature on furfural adsorption

The influence of torrefaction temperature to produce torrefied biomass on furfural adsorption was studied (Fig. S2 in supplementary information). Furfural adsorption (%) increased from 47% at 225 °C to 77% at 300 °C with 150 g torrefied biomass/L at 12 h of residence time. Because of the higher adsorption, the torrefied biomass produced at 300 °C was used in all our adsorption experiments.

3.4. Batch adsorption of furfural

3.4.1. Kinetic study

The influence of contact time was studied by varying the reaction duration from 1 to 12 h (Fig. 3a). The adsorption of furfural was relatively fast and more than 85% of maximum q_e (mg of furfural adsorbed per g of torrefied biomass) was achieved in first 2 h. The kinetic analysis of the adsorption of furfural on torrefied biomass was made using pseudo first order and second order kinetic models [18] (more details in supplementary information).

The plot of log ($q_e - q_t$) versus t and the plot of q_t/t versus t represents the first order and second order kinetic models respectively. The rate constants (k_f), and (k_s), for first and second order kinetic

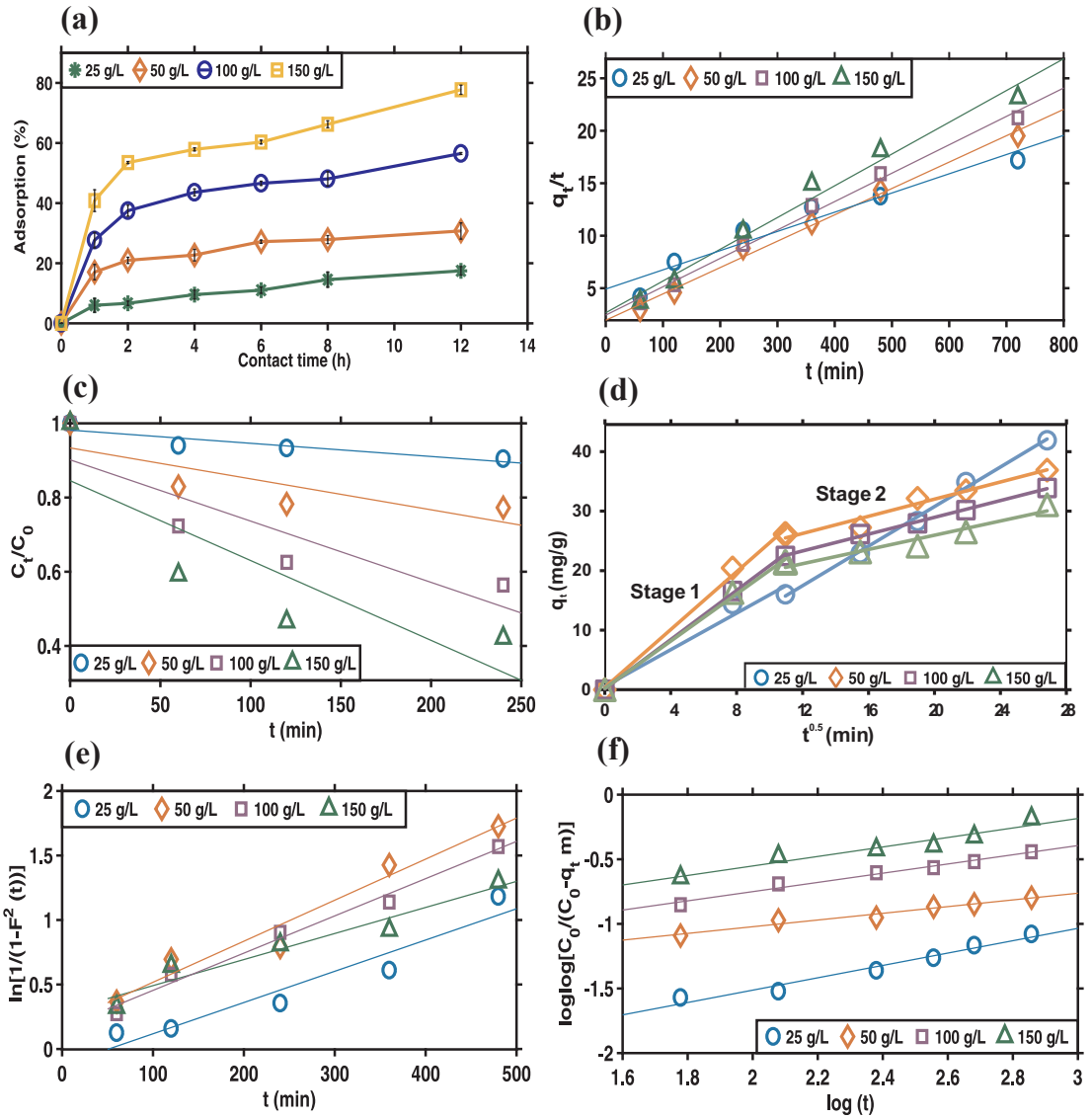

Fig. 3. Adsorption kinetics plot for (a) contact time vs adsorption (%), (b) pseudo second-order, (c) mass transfer model, (d) intra-particle diffusion model, (e) film diffusion model, and (f) pore diffusion model. The initial concentration of furfural: 6000 mg/L; pH of furfural solution: 3.6; torrefied biomass dosage: 25–150 g/L; and contact time: 1–12 h.

models, respectively were presented in Table 2. From Fig. 3b and Table 2 it can be observed that the pseudo second order model fits well with the R^2 values greater than 0.99. The variation between the calculated $q_{e\ cal.}$ and the experimental q_e values were varying between 11–52% and 6–8% for pseudo first order and second order kinetic models, respectively further suggesting better fit for pseudo second order kinetic model.

The adsorption process consist of four steps such as 1) bulk solution transport (i.e. external mass transfer) 2) external diffusion (i.e. boundary layer diffusion), 3) intra-particle diffusion and 4) adsorption [19]. Either one or a combination of these steps can control the overall adsorption process [20]. Thus, the adsorption of furfural on to torrefied biomass was further studied to identify the rate-limiting step in the process. The external mass transfer model, furfural transfer across the boundary layer (Boyd's film diffusion model), intra-particle diffusion (Webber-Morris) and pore diffusion model (Bangham's model) were tested.

The mass transfer of adsorbate from the bulk solution to the boundary layer could be a rate-limiting step and this was analyzed using the mass transfer model represented by Eq. (1) [21,22].

$$\frac{d\left(\frac{C_t}{C_0}\right)}{dt} = -\beta_L S \tag{1}$$

where β_L is the external mass transfer coefficient. Fig. 3c represents the plot of mass transfer model i.e. C_t/C_o versus t. The external mass transfer coefficient (β_L) was calculated from the slope of the same plot. The $\beta_L S$ values varied from 4 to 22 × 10^{-4} min^{-1}. The S, which is specific surface area (surface area per unit volume of adsorption), was calculated by taking the BET specific surface area value of 1.1 m^2/g. The BET specific surface area was multiplied by dosage (g) and divided by total volume of reaction to get S. Using the calculated values of S, the β_L values varied from 1.3 to 1.6 × 10^{-8} m min^{-1}.

The intra-particle diffusion model (Eq. (2)) was used to identify the transfer of furfural from the external surface of the adsorbate to sites through pores of the torrefied biomass.

$$q_t = k_{id} t^{1/2} + C \tag{2}$$

where q_t is the equilibrium adsorption (mg/g) at time t and k_{id} is the intra-particle diffusion rate constant. The multi-linear plots (with average $R^2 > 0.97$ for the first and second zone) represents that the adsorption is controlled by two mechanisms (Fig. 3d, Table 2). The first

Table 2
Kinetic parameters. The initial concentration of furfural: 6000 mg/L; pH of standard furfural solution: 3.6; torrefied biomass dosage: 25–150 g/L; contact time: 1–12 h.

Dosage (g/L)	k_f	$q_{e\ Cal}$	R^2	Error%
Pseduo first-order model				
25	0.00322	37.14	0.9523	0.11
50	0.00368	19.32	0.9593	0.47
100	0.00345	18.95	0.9764	0.44
150	0.00230	14.98	0.929	0.52
Dosage (g/L)	k_s	$q_{e\ Cal.}$	R^2	Error%
Pseduo second-order model				
25	0.0183	54.64	0.933	0.303
50	0.0251	39.84	0.992	0.07
100	0.0271	36.90	0.993	0.08
150	0.0303	33.00	0.979	0.06
Dosage (g/L)		$-\beta_L$		R^2
Mass transfer model				
25		-1.45×10^{-8}		0.8240
50		-1.45×10^{-8}		0.6557
100		-1.55×10^{-8}		0.7709
150		-1.33×10^{-8}		0.6987
Dosage (g/L)		D_e (m^2/min)		R^2
Film diffusion model (Boyd)				
25		1.01×10^{-14}		0.9195
50		1.34×10^{-14}		0.9597
100		1.22×10^{-14}		0.9846
150		8.41×10^{-15}		0.939
Dosage (g/L)	k_{id1}	R^2	k_{id2}	R^2
Intra particle diffusion model				
25	1.537	0.9621	1.612	0.9939
50	2.431	0.9934	0.721	0.957
100	2.068	0.9988	0.706	0.9964
150	1.982	0.9963	0.598	0.9345
Dosage (g/L)	α	K_{0B}		R^2
Pore diffusion model (Bangham's)				
25	0.478	3.13×10^{-4}		0.9647
50	0.259	1.33×10^{-3}		0.967
100	0.356	7.92×10^{-4}		0.982
150	0.368	7.93×10^{-4}		0.932

linear phase lasted for 2 h while the second linear phase lasted for another 10 h (Fig. 3d). The previous study [23] on the furfural adsorption on to the activated carbon also reported the multilinear plots for intra-particle diffusion model.

Film diffusion model or Boyd's kinetic model (Eq. (3)) was used to identify whether the diffusion of adsorbate across the boundary layer was a rate-limiting step.

$$ln\left[\frac{1}{(1-F^2(t))}\right] = \frac{\pi^2 D_e t}{r^2} \quad (3)$$

where F(t) = q_t/q_e; D_e is the effective diffusion coefficient (m^2/s); r is the radius of the spherical adsorbent particle [20]. If the plot of $ln\left[\frac{1}{(1-F^2(t))}\right]$ vs t is a straight line and passing through the origin then the film diffusion is the rate limiting step [20]. Previous study [24] reported that the spherical equivalent diameter of the torrefied biomass sieved to a particle size of 112–125 μm was 200 μm According to that, it was assumed that the torrefied biomass particle is spherical with a particle diameter of 150 μm. The internal diffusion coefficient (D) was calculated from the slope of the plot presented in Fig. 3e. The average diffusion coefficient (De) was around 1.1×10^{-14} m^2/min. The previous study [23] on the furfural adsorption reported a diffusion coefficient (De) of 2×10^{-11} m^2/min.

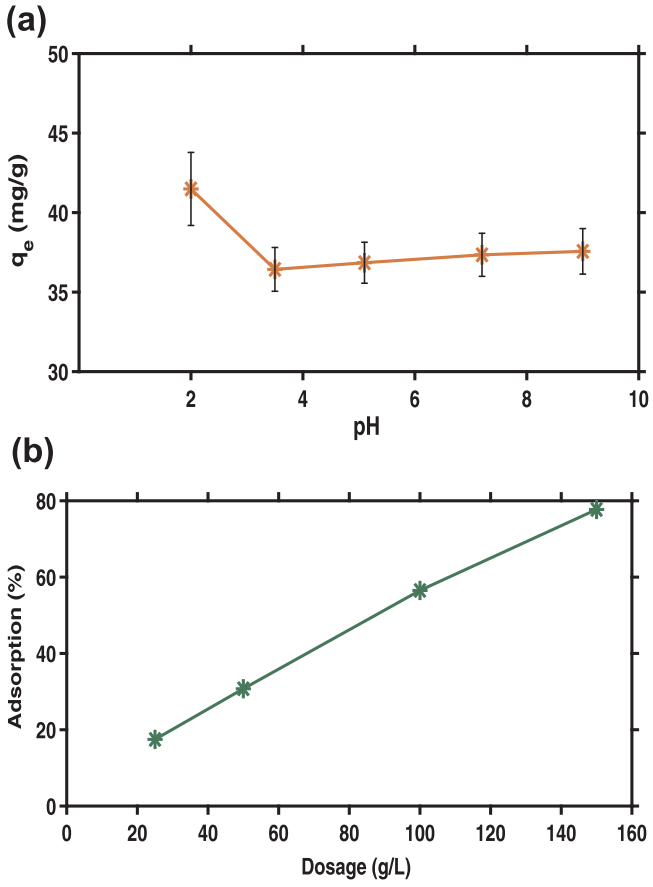

Fig. 4. (a) The influence of pH, (varied from 2 to 9), and (b) influence of dosage (varied from 25 to 150 g/L) on adsorption of furfural using torrefied biomass. The initial concentration of furfural: 6000 mg/L, contact time: 12 h.

The rate-limiting step of intraparticle diffusion was also evaluated by Bangham's kinetic model represented by Eq. (4).

$$log\ log\left[\frac{C_o}{C_0 - q_t m}\right] = \log\left(\frac{k_b m}{2.303V}\right) + \alpha \log(t) \quad (4)$$

where C_o is the initial concentration of the adsorbate (mg/L), V is the volume of solution (L), m is the mass of the adsorbent (g/L), and k_b and α are the constants [20]. The average $R^2 > 0.96$ was observed for all the dosage experiments (Fig. 3f).

3.4.2. Effect of pH and dosage

The influence of pH on the adsorption was studied by varying pH from 2.0 to 9.0 (Fig. 4a). The q_e (mg of furfural adsorbed per g of torrefied biomass) value did not vary significantly (< 10%) i.e. from 41 (± 4.3) to 37 (± 2.6) when the pH was increased from 2.0 to 9.0, respectively. The effect of dosage on furfural adsorption was studied by increasing the dosage from 25 to 150 g/L of torrefied biomass, at 12 h of residence time. The furfural removal increased from 17 (at 25 g/L) to 77% (150 g/L) (Fig. 4b). The q_e values were 41 (± 3.41) and 31 (± 0.61) (mg of furfural adsorbed per g of torrefied biomass) for 25 and 150 g/L dosage, respectively, at 12 h of residence time.

3.4.3. Adsorption isotherms

Fig. 5a represents the variation of q_e (mg of furfural adsorbed per g of torrefied biomass) with the equilibrium concentration of furfural. When the initial concentration was varied from 300 to 6000 mg/L the q_e of furfural onto torrefied biomass was increased from 4.1 (± 0.13)

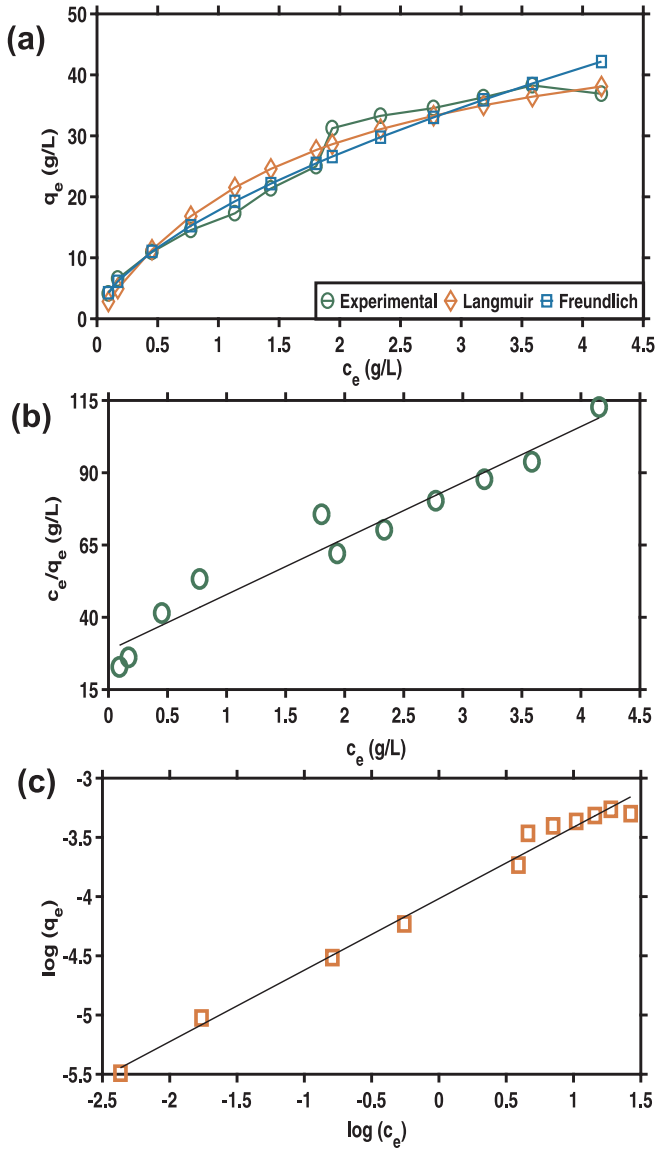

Fig. 5. Adsorption isotherm plots: (a) isotherm, (b) Langmuir, (c) Freundlich. The initial concentration of furfural (C_0): 300–6000 mg/L; torrefied biomass dosage: 50 g/L; and contact time:12 h.

to 36.9 (± 3.2) (mg of furfural adsorbed per g of torrefied biomass), respectively. The maximum q_e value (i.e. 38 mg of furfural adsorbed per g of torrefied biomass) was observed at an initial concentration of 5500 mg/L.

The isotherms were modeled using the linearized Langmuir (Eq. (5)) and Freundlich models (Eq. (6)).

$$\frac{C_e}{q_e} = \frac{C_e}{q_m} + \frac{1}{k_L q_m} \tag{5}$$

C_e is the equilibrium concentration of the furfural (mg/L), q_e (mg of furfural adsorbed per g of torrefied biomass) is the amount of furfural adsorbed at equilibrium (mg/g), q_m is the monolayer adsorption capacity or the maximum adsorption capacity (mg of furfural adsorbed per g of torrefied biomass). k_L is the Langmuir constant which represents adsorption energy (L/g) [18].

$$ln\, q_e = ln\, k_f + \left(\frac{1}{n}\right) ln\, C_e \tag{6}$$

where k_f is adsorbent capacity ((mg/g) (L/mg))$^{1/n}$) and n is the intensity of the adsorption [18].

Table 3
Isotherm model constants. The initial concentration of furfural (C_0): 300–6000 mg/L; contact time:12 h; torrefied biomass dosage: 50 g/L.

Langmuir			Freundlich		
q_m (mg/g)	KL (L/mg)	R^2	n	K_f ((g/g) (L/g)$^{1/n}$)	R^2
52	0.000679	0.9476	1.657	0.278	0.9886

Fig. 5b and c shows the linear fitting between concentration (q_e) and the equilibrium concentration (c_e) for Langmuir and Freundlich models respectively. The evaluated constants are presented in Table 3. It was observed that Freundlich model fitted better with R^2 of 0.988 compared to 0.947 for Langmuir model. The monolayer adsorption capacity (q_m) of the torrefied biomass, which is calculated from the Langmuir plot was around 52 mg/g. The Freundlich constants k_f and n were 0.278 (mg/g) (L/g) and 1.657 respectively suggesting favorable adsorption.

3.5. Batch adsorption of torrefaction condensate

Fig. 6 shows adsorption (%) of different compounds from torrefaction condensate at 250 g/L of torrefied biomass dosage. The torrefied biomass adsorbed up to 54% of furfural from the torrefaction condensate. Hydroxymethylfurfural (5-HMF), another important inhibitor present in torrefaction condensate, was also adsorbed up to 25%. Around 23% and 60% of furans such as 2(5H)-furanone and 5-methyl-2-furancarboxaldehyde were adsorbed, respectively. In case of phenolic compounds, 74% of coniferyl aldehyde was adsorbed. Around 52, 47 and 56% of other phenolics such as guaiacol, creosol, and vanillin were adsorbed, respectively. In case of organic acids, 21% of formic acid and just 11% of acetic acid was adsorbed. In contrast, concentration of propionic acid was increased by 12%. However, it should be noted that it is not possible to reliable measure the volume change during the adsorption as the torrefaction condensate is trapped within the torrefied biomass that can be recovered after stirring and resulting in false adsorption. From our control experiments, the volume change with maximum concentration of torrefied biomass would be less than 15% during the adsorption. Thus, the adsorption capacity of the torrefied biomass maybe increased by less than 10% than the values reported in this study.

3.6. Column adsorption study

3.6.1. Column adsorption of standard furfural solution

Column adsorption studies of aqueous furfural solution was carried out at two different column diameters i.e. 10 and 20 mm. The furfural uptake and the time required to reach adsorption saturation was increased with increasing column diameter.

In case of 10 mm diameter column (Fig. S4a in supplementary information) the breakthrough time (i.e. C/C_0 > 2%) was 10 min and the saturation time (i.e. C/C_0 > 95%) was around 80 min. The breakthrough and saturation time of 20 mm diameter column (Fig. S4b) was 150 and 380 min respectively. This analysis shows that 20 mm diameter column will be more effective for adsorption of inhibitory compounds from torrefaction condensate in comparison with 10 mm diameter column because of the higher quantity of the torrefied biomass in the column leading to the increased number of active sites and the adsorption surface area. Hence, the column with 20 mm diameter and 200 mm bed length was considered for the column adsorption of torrefaction condensate.

3.6.2. Column adsorption of torrefaction condensate

Fig. 7 represents the breakthrough curves of different compounds present in torrefaction condensate. The adsorption (%) presented in Fig. 7 were based on the differences in GC-MS peak area of the

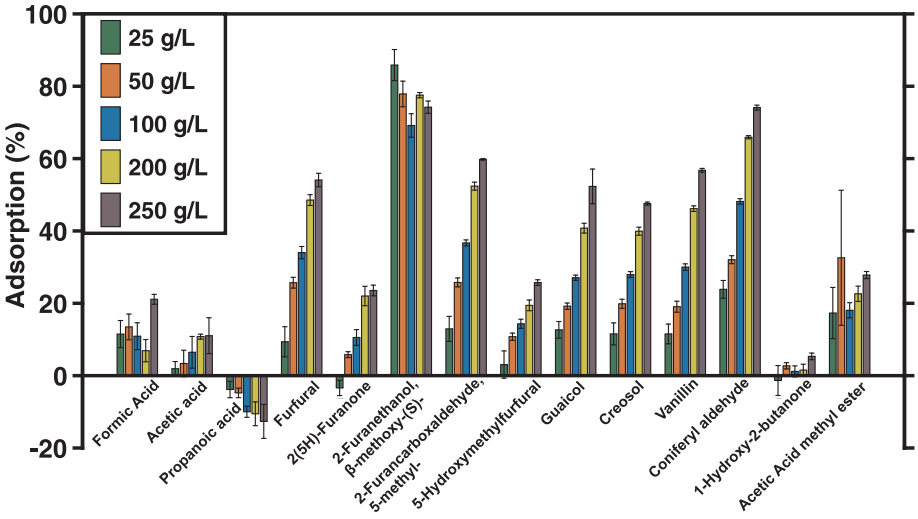

Fig. 6. Adsorption (%) of different compounds in torrefaction condensate with different torrefied biomass dosage (25–250 g/L) during batch experiments. Torrefaction temperature: 300 °C and contact time: 12 h.

respective compounds before and after adsorption.

The maximum adsorption of furfural observed was 52% and the saturation time was 50 min. From Fig. 7a, it can be observed that 5-HMF reached saturation within 5 min. The maximum adsorption for other furans such as 5-methyl-2-Furancarboxaldehyde, and 2(5H)-Furanone was 61 and 28% and the saturation time was 50 and 30 min, respectively.

All the phenolic compounds followed similar adsorption pattern (Fig. 7b). Similar to the batch experiments, coniferyl aldehyde had highest adsorption of 64%. At the same time, vanillin has the least adsorption (30%). Coniferyl aldehyde has the highest saturation time (90 min) than other compounds reported in this study. The maximum adsorption of other phenolic compounds such as guaiacol, cresol and vanillin was 48, 43 and 30% and the saturation was around 50, 30 and 15 min, respectively.

The breakthrough curves of organic acids in torrefaction condensate such as formic, acetic and propionic acids were shown in Fig. 7c. The maximum adsorption of formic acid was around 54%, which was higher than in batch adsorption (20%). Whereas, only around 5% of acetic acid has been adsorbed. The changes in the concentration of acetic acid during time course (between 50 and 150 min) could be possibly due to a tradeoff between their methyl ester counterparts (as seen in Fig. 7d) and not because of actual adsorption on to the torrefied biomass. Moreover, finally we were able to retain 95% of acetic acid in the condensate after 180 min of column adsorption. In case of propionic acid; the column adsorption study followed the batch adsorption by resulting in slight increase in their concentration (~17% after 180 min) possibly due to decrease in water content.

The concentrations of other compounds (Fig. 7d) such as 2-propanone, 1-hydroxy- (acetol) and 1-hydroxy-2-butanone were more stable

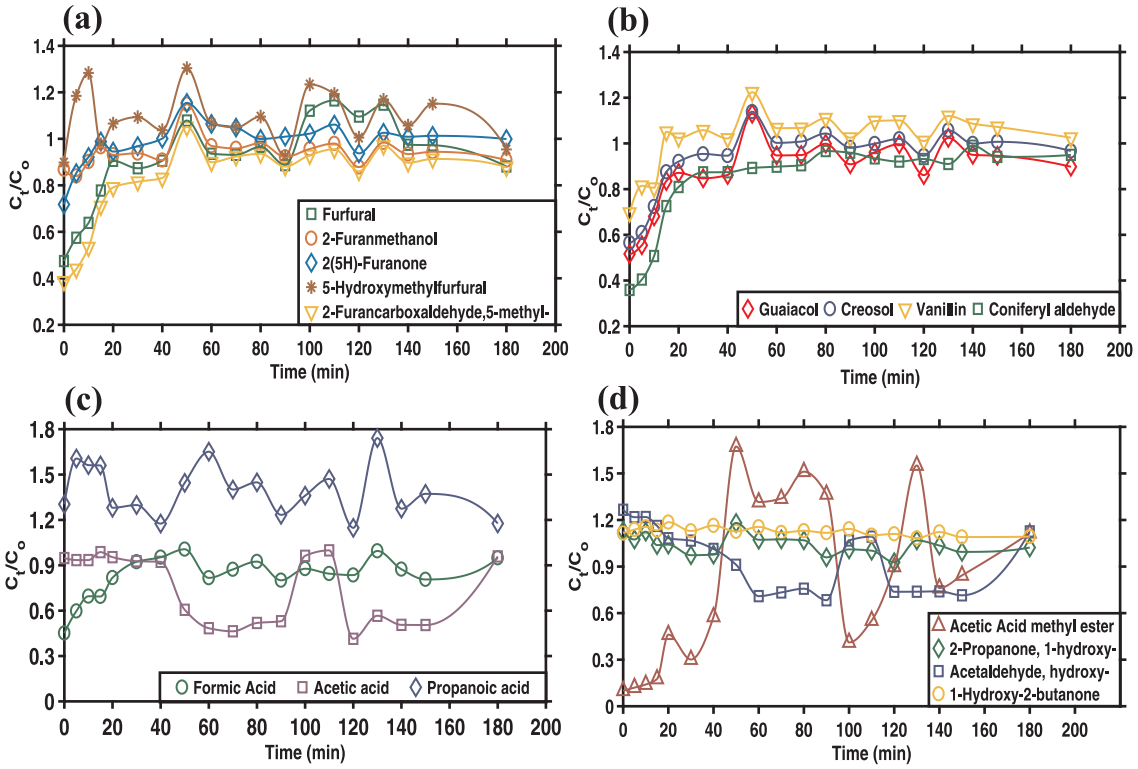

Fig. 7. Breakthrough curves of column adsorption of torrefaction condensate (a) furans (b) phenolics (c) acids and (d) others organic compounds. Column diameter: 20 mm; bed height: 200 mm; flow rate: 1 mL/min.

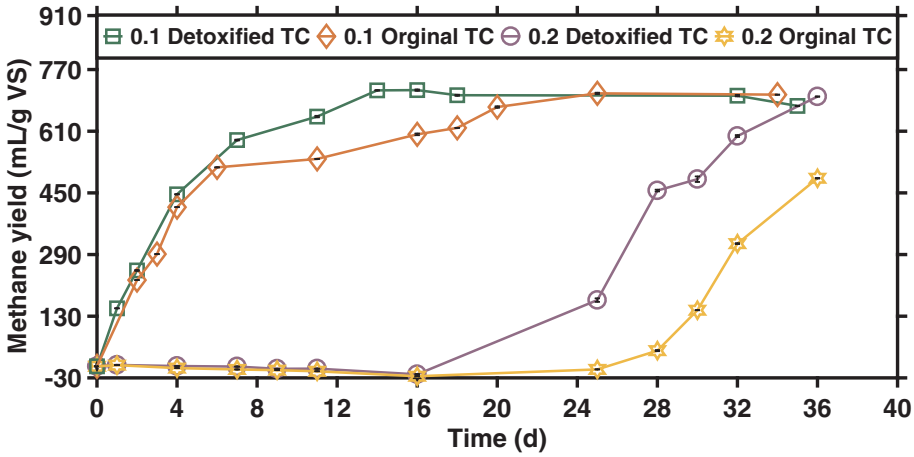

Fig. 8. Cumulative methane yield during AD batch assays with detoxified and original torrefaction condensate at 0.1 and 0.2 $VS_{substrate}$:$VS_{inoculum}$ loading. TC = torrefaction condensate.

and no adsorption of these compounds was observed. In addition to these two compounds, hydroxy-acetaldehyde was least adsorbed (< 1% at 50 min) by torrefied biomass.

3.7. Anaerobic digestion batch assay

The torrefaction condensate, detoxified with 250 g/L of torrefied biomass dosage was used in AD batch assays. Fig. 8 shows the cumulative methane yield from AD of torrefaction condensate before and after adsorption at the end of 35 d for 0.1 and 0.2 $VS_{substrate}$:$VS_{inoculum}$ loadings. The respective methane yield (mL/g VS) for torrefaction condensate before and after detoxification was 689 and 695 for 0.1 $VS_{substrate}$:$VS_{inoculum}$ and 699 and 487 for 0.2 $VS_{substrate}$:$VS_{inoculum}$.

4. Discussion

4.1. Effect of adsorption of furfural on to torrefied biomass

This study, for the first time, demonstrated adsorption of furfural from torrefaction condensate using torrefied biomass in order to make torrefaction condensate less toxic for microbial bioconversion. About 60% of furfural has been adsorbed from the torrefaction condensate, meaning the reduction in furfural from 9000 to 3600 mg/L at 250 g/L dosage. We have handled very high concentrations of furfural when compared to the studies dealing with biomass hydrolysates, typically in range of 200–3000 mg-furfural/L [6–8,25]. Eventhough we have used high dosage of torrefied biomass as adsorbent, this will not have a negative impact on the overall process considering the fact that the adsorbent is from the same streamline (torrefied biomass pellet production) and following adsorption, they will be mixed back with the rest of the torrefied biomass and taken for regular application. Moreover, thus all the materials are used in an integrated approach no wastes will be generated out of this process.

Björklund et al. [25] studied the removal of fermentation inhibitors from spruce wood hydrolysate using the lignin as an adsorbent and was able to remove 49% of furfural, 27% of 5-HMF and 36% of phenols at 100 g/L of lignin dosage where the initial concentration of the inhibitory compounds was 2, 0.6 and 3.3 g/L respectively. These values were close to the ones reported in this study for example, removal of 34% of furfural, 14% of 5-HMF and 33% of phenols with 100 g/L torrefied biomass. These values have been achieved in this study in spite of having the initial concentrations around 10 times higher than the ones reported in the earlier study [25]. Monlau et al. [7] studied the applicability of pyrolysis chars produced from solid anaerobic digestion digestate to remove the inhibitory compounds from Douglas-fir wood hydrolysate. They reported that 100% of furfural and 94% of 5-HMF was removed from the hydrolysate at 40 g/L dosage and 24 h contact time where initial concentration of both the compounds was 1000 mg/L suggesting q_e (mg of furfural adsorbed per g of adsorbent) of 48 mg/g. This value is higher than the one obtained for torrefied biomass (36.9 ± 3.2 mg/g) at 50 g/L. Such high removal efficiencies were achieved owing to the very high surface area of pyrolysis chars, about 50 times higher than the torrefied biomass and the lower initial concentration, about 9 times lower than torrefaction condensate. However, further, using torrefied biomass for adsorption of these compounds would have multiple benefits within the refinery. Firstly, removing inhibitory compounds from the condensate will allow them to be utilize for biomethane production. Secondly, increasing moisture content of the biomass and compounds adsorbed onto the biomass would be useful in later stages of refinery in improving the biomass pelletization.

4.2. Mechanism of furfural adsorption on to torrified biomass

The adsorption of main inhibitory compound furfural on to torrefied biomass is likely due to hydrophobic interaction. The insignificant effect of pH on the adsorption of furfural points in the direction of hydrophobic interaction (Fig. 4a). As the pH varies from 2.0 to 9.0, the deprotonation of the biomass would take place and thus, increasing the number of charged sites. However, the increase in the number of charged sites had no effect on the adsorption of furfural on the torrefied biomass suggesting non-electrostatic mechanisms. Furthermore, adsorption of hydrophobic compounds such as furfural and phenols while non-adsorption of hydrophilic compounds such as acids suggest the adsorption by means of hydrophobic interaction. In addition, the surface of the torrefied biomass is hydrophobic because of the reduced OH-groups [1], further suggesting the hydrophobic interaction between furfural and torrefied biomass. Indeed, the adsorption of furfural from pine needle hydrolysates on to polystyrene-divinylbenzene (XAD-4) copolymers has described as a hydrophobic interaction [26]. As the hydrophobic interactions are spontaneous, the adsorption of furfural on to the hydrophobic sites on the torrefied biomass would be quite fast.

Prior to the adsorption of furfural to the hydrophobic sites in the torrefied biomass, furfural has to reach in close proximity of the sites from the bulk solution. This is done in three steps – arriving of furfural from the bulk solution to the boundary layer, transfer of furfural from the boundary layer to the external surface of torrefied biomass passing through the film or boundary layer and diffusion of furfural to the hydrophobic adsorption site [27]. The low β_L values ($1.3–1.6 \times 10^{-8}$ m/min) and poorer R^2 values (Fig. 3c, varying between 0.78 and 0.82) shows that external mass transfer of the furfural from the bulk solution to the boundary layer is quite fast, thus mass transfer is not a rate limiting step [21,28]. It is important to note that the external mass transfer here refers to the transfer of the adsorbate from the bulk solution to the external part of the layer formed on the surface of the torrefied biomass. This layer is gradient of the furfural concentration varying from the bulk solution to the surface of the

torrefied biomass.

The first stage of the intraparticle diffusion model (webber-Morris graph) represents the boundary layer effect and the second stage represents the intra-particle diffusion or micropore diffusion (Fig. 3d) [29]. The intercept of the first zone (varying between 1.5 and 2.4) of intraparticle diffusion plot (Fig. 3d) represents the boundary layer thickness and thus suggesting that the film diffusion is playing a significant role in the adsorption of furfural onto torrefied biomass [22]. Further that the linear plots of Boyd's model (R^2 varies from 0.92 to 0.98) that are not passing through the origin (Fig. 3e) points out that film diffusion is the rate-limiting step [30]. However, the linearity of the second stage intraparticle diffusion model (Fig. 3d) (average $R^2 > 0.97$) and Bangham model (Fig. 3f) (average $R^2 > 0.96$) points out that the furfural passage through micropore diffusion in the torrefied biomass is rate-limiting step. All the above evidence suggests that the film diffusion at the initial stage of the adsorption ($t < 2$ h) and the micropore diffusion at the later stage ($t > 2$ h) are the rate limiting step in the adsorption of furfural on the torrefied biomass. However, further controlled experiments are required to confirm this finding.

The reason for both the film diffusion and micropore diffusion to be the rate limiting step can be due to the hydrophobic nature of both furfural and torrefied biomass. As the torrefaction condensate is predominantly made of water (water content > 50%), the furfural molecule, being hydrophobic, will be in cluster. Further, the torrefied biomass would have minimized the hydrophobic sites present on the surface or most likely only hydrophilic sites would be present on the surface. These sites would be interacting with water molecules and thus, creating a layer of waterfilm. This would lead to difficulty in passing of furfural, a hydrophobic molecule, through the film layer made of hydrophilic components resulting in film diffusion a rate-limiting step [31]. As the bulk of the hydrophobic sites would be present more deep in the torrefied biomass, resulting in the need for furfural to diffuse from the external site to internal hydrophobic sites whose passage might be blocked by water molecules. This is well reflected in diffusion being rate-limiting step in intraparticle diffusion model and Bangham model. Indeed, such mechanism was also observed for adsorption of phenol on carbon [31].

4.3. Effect of torrefaction temperature on to the adsorption property of torrefied biomass

At a temperature of 225 °C, a minor portion of hemicellulose is degraded and the volatiles are mainly H_2O and CO_2, which could have caused the low pore distribution on torrefied biomass [32]. As the severity of the torrefaction increases (for example at 275 °C) the further degradation of hemicellulose and minor portion of cellulose and lignin occurs, which increases the release of volatiles and there by increases the micro pores. According to Reza et al. [14] and Chen et al. [32], it is because the precipitated tar plugs the existing pores to generate new pores and thereby results in the decreased pore size and increased surface area. However, as the temperature further increases to 300 °C, the existing pores are widen and enlarged which results in the decreased surface area (Fig. 1 and Table 1). The adsorption of furfural increases with the increasing torrefaction temperature and this could be mainly because of the enlarged pores or increase in number of sites or both. Further, as the severity of the torrefaction increases, the existing pores on the biomass will enlarge and these enlarged pores allows the furfural solution to diffuse more rapidly into torrefied biomass structures and there by increases the surface contact. The higher adsorption of furfural by torrefied biomass produced at 300 °C with larger pore size and increased diffusion also reflect that the micropore diffusion is involved in adsorption mechanism. In general, the removal of oxygen containing hydrophilic sites at higher temperatures results in higher adsorption of hydrophobic material. This was very well reflected in furfural adsorption on torrefied biomass produced at different torrefaction temperature (Fig. S2).

4.4. Anaerobic digestion of torrefaction condensate

The preliminary study on AD of detoxified torrefaction condensate showed that the proposed adsorption process has improved the methane production. As expected, no inhibition was observed at 0.1 $VS_{substrate}$:$VS_{inoculum}$ loading and the methane production was similar for both detoxified and original torrefaction condensate for the initial 5 d. However, the methane production with detoxified torrefaction condensate started increasing rapidly after 5 d in comparison with original condensate. After 20 d, methane production saturated for both the setups with around 700 mL/g VS. In case of 0.2 $VS_{substrate}$:$VS_{inoculum}$ loading, owing to the inhibitory concentrations of compounds in torrefaction condensate, there was a prolonged lag phase (25 d) for methane production in case of original condensate. Whereas, as a result of adsorption, the detoxified condensate started producing methane just within 15 d, ie. 10 d faster than with the original condensate. At the same time methane production was higher in case of detoxified condensate (699 mL/g VS) than with original condensate (487 mL/g VS) at the end of 35 d. The methane yield from torrefaction condensate reported in this study (700 mL/g VS) is comparable with substates such as used vegetable oil (648 mL/g VS) [33] and co-digestion of 60% of grease trapped sludge with 40% sewage sludge (845 mL/g VS) [34].

Eventhough, methane production is better with detoxified condensate, the lag phase for methane production is still longer with 0.2 $VS_{substrate}$:$VS_{inoculum}$ loading when compared with 0.1 $VS_{substrate}$:$VS_{inoculum}$ loading. This could be because of only partial removal of inhibitory compounds from the torrefaction condensate. For example, around 3600 mg/L of furfural was present in the condensate even after adsorption. According to [35], the furfural concentration at 2000 mg/L could inhibit the AD process and increases the lag phase. Further decrease in the furfural concentration could be possibly achieved through a sequential batch/column adsorption. Nevertheless, Doddapaneni et al. [5] reported that microorganism could be adapted through cyclic batch AD to decrease the lag phase in methane production. Thus, improving the methane production with little or no lag phase, with higher dosages of torrefaction condensate, is possible and this could be a subject of further investigation.

4.5. Adsorption scale-up

The torrefaction plant capacity proposed by Pirragila et al. [15] i.e. 200,000 ton of torrefied biomass/annum with 8400 operating hours was considered here to understand the flow rate of torrefied biomass in an industrial scale torrefied biomass plant. The previous study [5] shows that 0.25 kg of torrefaction condensate can be produced per 1 kg of biomass input. Based on that ~250 ton/day of torrefaction condensate will be generated at selected plant capacity. At the same time, column experiments results (internal dia of 20 mm and 200 mm bed height) from this study shows that furfural adsorption would be achieved in 60–100 min of the largescale column operations. Based on that, 100 ton of biomass is required for the column adsorption everyday. The bulk density of torrefied wood is between 200 and 400 kg/m^3 [36]. Considering the bulk density of 300 kg/m^3, a total volume of 333 m^3 is required for column adsorption for everyday operation. The low saturation time of torrefied biomass would result in frequent loading and unloading of the torrefied biomass in column. As the torrefied biomass pellets are continuously produced, the low saturation times of the column is a challenge for the proposed integrated approach (Fig. 1). So, the conventional column adsorption for the detoxification of torrefaction condensate could be difficult to integrate with torrefied biomass pellets production.

In general adsorption column requires piping, valves and other control units which may increase the capital, operational and maintenance expenses of the torrefaction unit. In contrast, batch adsorption could be carried out with a conventional mixing tank [37,38]. The loading and unloading of the torrefied biomass to the adsorption vessel

could be easier in comparison with column. At the same time the operational expenses for batch adsorption are lower in comparison with column operation [39]. Thus, the batch adsorption could be more feasible to integrate with torrefaction process in the proposed approach (Fig. 1).

5. Conclusion

In this study, for the first time, torrefaction condensate was detoxified using torrefied biomass in order to use it as a substrate for methane production. The removal of furfural and other inhibitory compounds was achieved and better methane production by detoxified torrefaction condensate was demonstrated. The pseudo second order kinetics suggesting a hydrophobic interaction between furfural and torrefied biomass was argued. Intraparticle diffusion model and Bangham model combined with effect of torrefaction temperature on furfural adsorption onto torrefied biomass points to micropore diffusion as a rate limiting step in later stages. Further, a continuous column detoxification of torrefaction condensate was operated and a way for process integration of this was discussed .

Acknowledgement

The authors gratefully acknowledge the TUT Postdoc funding program. The authors would like to thank Suniti Singh, Marja R.T and Leo Hyvärinen from Tampere University of Technology for providing inoculum for AD tests, helping with GC-MS analyses and SEM images, respectively.

Appendix A. Supplementary data

Supplementary data associated with this article can be found, in the online version, at http://dx.doi.org/10.1016/j.cej.2017.10.053.

References

[1] J. Koppejan, S. Sokhansanj, S. Melin, S. Madrali, Status overview of torrefaction technologies, 2012.
[2] T.R.K.C. Doddapaneni, J. Konttinen, T.I. Hukka, A. Moilanen, Influence of torrefaction pretreatment on the pyrolysis of Eucalyptus clone: a study on kinetics, reaction mechanism and heat flow, Ind. Crops Prod. 92 (2016) 244–254, http://dx.doi.org/10.1016/j.indcrop.2016.08.013.
[3] Hawkins Wright, Global demand for torrefied biomass, (2012). http://www.forestbusinessnetwork.com/13392/global-demand-for-torrefied-biomass-could-exceed-70-million-tonnes-a-year-by-the-end-of-the-decade/ (accessed July 22, 2017).
[4] S.S. Liaw, C. Frear, W. Lei, S. Zhang, M. Garcia-Perez, Anaerobic digestion of C1–C4 light oxygenated organic compounds derived from the torrefaction of lignocellulosic materials, Fuel Process. Technol. 131 (2015) 150–158, http://dx.doi.org/10.1016/j.fuproc.2014.11.012.
[5] T.R.K.C. Doddapaneni, R. Praveenkumar, H. Tolvanen, M.R.T. Palmroth, J. Konttinen, J. Rintala, Anaerobic batch conversion of pine wood torrefaction condensate, Bioresour. Technol. 225 (2017) 299–307, http://dx.doi.org/10.1016/j.biortech.2016.11.073.
[6] J.R. Weil, B. Dien, R. Bothast, R. Hendrickson, N.S. Mosier, M.R. Ladisch, Removal of fermentation inhibitors formed during pretreatment of biomass by polymeric adsorbents, Ind. Eng. Chem. Res. 41 (2002) 6132–6138, http://dx.doi.org/10.1021/ie0201056.
[7] F. Monlau, C. Sambusiti, N. Antoniou, A. Zabaniotou, A. Solhy, A. Barakat, Pyrochars from bioenergy residue as novel bio-adsorbents for lignocellulosic hydrolysate detoxification, Bioresour. Technol. 187 (2015) 379–386, http://dx.doi.org/10.1016/j.biortech.2015.03.137.
[8] M. Soleimani, L. Tabil, C. Niu, Adsorptive isotherms and removal of microbial inhibitors in a bio-based hydrolysate for xylitol production, Chem. Eng. Commun. 202 (2015) 787–798, http://dx.doi.org/10.1080/00986445.2013.867258.
[9] L. Fagernas, E. Kuoppala, V. Arpiainen, Composition, utilization and economic assessment of torrefaction condensates, Energy Fuels 29 (2015) 3134–3142, http://dx.doi.org/10.1021/acs.energyfuels.5b00004.
[10] W.H. Chen, J. Peng, X.T. Bi, A state-of-the-art review of biomass torrefaction, densification and applications, Renewable Sustainable Energy Rev. 44 (2015) 847–866, http://dx.doi.org/10.1016/j.rser.2014.12.039.
[11] B. Ghiasi, L. Kumar, T. Furubayashi, C.J. Lim, X. Bi, C.S. Kim, S. Sokhansanj, Densified biocoal from woodchips: is it better to do torrefaction before or after densification? Appl. Energy 134 (2014) 133–142, http://dx.doi.org/10.1016/j.apenergy.2014.07.076.
[12] J.H. Peng, H.T. Bi, C.J. Lim, S. Sokhansanj, Study on Density, Hardness, and Moisture Uptake of Torrefied Wood Pellets, Energy Fuels 27 (2013) 967–974. doi:10.1021/ef301928q.
[13] Q. Hu, J. Shao, H. Yang, D. Yao, X. Wang, H. Chen, Effects of binders on the properties of bio-char pellets, Appl. Energy 157 (2015) 508–516, http://dx.doi.org/10.1016/j.apenergy.2015.05.019.
[14] M.T. Reza, M.H. Uddin, J.G. Lynam, C.J. Coronella, Engineered pellets from dry torrefied and HTC biochar blends, Biomass Bioenergy 63 (2014) 229–238, http://dx.doi.org/10.1016/j.biombioe.2014.01.038.
[15] A. Pirraglia, R. Gonzalez, D. Saloni, J. Denig, Technical and economic assessment for the production of torrefied ligno-cellulosic biomass pellets in the US, Energy Convers. Manage. 66 (2013) 153–164, http://dx.doi.org/10.1016/j.enconman.2012.09.024.
[16] R.W.R. Zwart, J.R. Pels, Use of torrefaction condensate, (2013), http://www.google.com/patents/WO2013019111A1?cl=en.
[17] J. Kramb, A. Gomez-Barea, N. DeMartini, H. Romar, T.R.K.C. Doddapaneni, J. Konttinen, The effects of calcium and potassium on CO_2 gasification of birch wood in a fluidized bed, Fuel 196 (2017) 398–407, http://dx.doi.org/10.1016/j.fuel.2017.01.101.
[18] V. Fierro, V. Torné-Fernández, D. Montané, A. Celzard, Adsorption of phenol onto activated carbons having different textural and surface properties, Microporous Mesoporous Mater. 111 (2008) 276–284, http://dx.doi.org/10.1016/j.micromeso.2007.08.002.
[19] T.T. Teng, L.W. Low, Removal of Dyes and Pigments from Industrial Effluents BT - Advances in Water Treatment and Pollution Prevention, 65–93 Springer Netherlands, Dordrecht, 2012 10.1007/978-94-007-4204-8_4.
[20] S. Suresh, S. Sundaramoorthy, Green Chemical Engineering: An Introduction to Catalysis, Kinetics, and Chemical Processes, CRC Press, 2014.
[21] R. Jain, D. Dominic, N. Jordan, E.R. Rene, S. Weiss, E.D. van Hullebusch, R. Hubner, P.N.L. Lens, Higher Cd adsorption on biogenic elemental selenium nanoparticles, Environ. Chem. Lett. 14 (2016) 381–386, http://dx.doi.org/10.1007/s10311-016-0560-8.
[22] H. Benaïssa, Influence of ionic strength on methylene blue removal by sorption from synthetic aqueous solution using almond peel as a sorbent material: experimental and modelling studies, J. Taibah Univ. Sci. 4 (2010) 31–38, http://dx.doi.org/10.1016/S1658-3655(12)60024-7.
[23] A.K. Sahu, V.C. Srivastava, I.D. Mall, D.H. Lataye, Adsorption of furfural from aqueous solution onto activated carbon: kinetic, equilibrium and thermodynamic study, Sep. Sci. Technol. 43 (2008) 1239–1259, http://dx.doi.org/10.1080/01496390701885711.
[24] H. Tolvanen, T. Keipi, R. Raiko, A study on raw, torrefied, and steam-exploded wood: fine grinding, drop-tube reactor combustion tests in N_2/O_2 and CO_2/O_2 atmospheres, particle geometry analysis, and numerical kinetics modeling, Fuel 176 (2016) 153–164, http://dx.doi.org/10.1016/j.fuel.2016.02.071.
[25] L. Björklund, S. Larsson, L.J. Jönsson, E. Reimann, N.-O. Nilvebrant, Treatment with lignin residue: a novel method for detoxification of lignocellulose hydrolysates, Appl. Biochem. Biotechnol. 98–100 (2002) 563–575, http://dx.doi.org/10.1385/ABAB:98-100:1-9:563.
[26] S. Negi, Pretreatment Strategies of Lignocellulosic Biomass Towards Ethanol Yield: Case Study of Pine Needles, in: Biofuels: Technology, Challenges and Prospects, in: A.K. Agarwal, R.A. Agarwal, T. Gupta, B.R. Gurjar (Eds.), Springer Singapore, Singapore, 2017: pp. 85–102. doi:10.1007/978-981-10-3791-7_6.
[27] T. Furusawa, J.M. Smith, Fluid-particle and intraparticle mass transport rates in slurries, Ind. Eng. Chem. Fundam. 12 (1973) 197–203, http://dx.doi.org/10.1021/i160046a009.
[28] M.a. Acheampong, J.P.C. Pereira, R.J.W. Meulepas, P.N.L. Lens, Kinetics modelling of Cu(II) biosorption on to coconut shell and Moringa oleifera seeds from tropical regions, Environ. Technol 33 (2012) 409–417, http://dx.doi.org/10.1080/09593330.2011.576705.
[29] W.J. Weber, J.C. Morris, Removal of biologically resistant pollutants from waste waters by adsorption, Adv. Water Pollut. Res. 2 (1962) 231–266.
[30] D. Suteu, C. Zaharia, T. Malutan, Equilibrium, kinetic, and thermodynamic studies of basic blue 9 dye sorption on agro-industrial lignocellulosic materials, Cent. Eur. J. Chem. 10 (2012) 1913–1926, http://dx.doi.org/10.2478/s11532-012-0122-2.
[31] B.G. Tsyntsarski, B.N. Petrova, T.K. Budinova, N.V. Petrov, D.K. Teodosiev, Removal of phenol from contaminated water by activated carbon, produced from waste coal material, Bulg. Chem. Commun. 46 (2014) 353–361.
[32] Q. Chen, J.S. Zhou, B.J. Liu, Q.F. Mei, Z.Y. Luo, Influence of torrefaction pretreatment on biomass gasification technology, Chin. Sci. Bull. 56 (2011) 1449–1456, http://dx.doi.org/10.1007/s11434-010-4292-z.
[33] R.A. Labatut, L.T. Angenent, N.R. Scott, Biochemical methane potential and biodegradability of complex organic substrates, Bioresour. Technol. 102 (2011) 2255–2264, http://dx.doi.org/10.1016/j.biortech.2010.10.035.
[34] Å. Davidsson, C. Lövstedt, J. la Cour Jansen, C. Gruvberger, H. Aspegren, Co-digestion of grease trap sludge and sewage sludge, Waste Manage. 28 (2008) 986–992, http://dx.doi.org/10.1016/j.wasman.2007.03.024.
[35] S. Pekařová, M. Dvořáčková, P. Stloukal, M. Ingr, J. Šerá, M. Koutny, Quantitation of the inhibition effect of model compounds representing plant biomass degradation products on methane production, BioResources 12 (2017) 2421–2432.
[36] W. Stelte, Optimization of product specific processing parameters for the production of fuel pellets from torrefied biomass, Danish Technol. Inst. Cent. Biomass Biorefinery, 2014.
[37] J. Korkisch, Modern Methods for the Separation of Rarer Metal Ions, Elsevier Science, 2013.
[38] G. Crini, P.M. Badot, Sorption Processes and Pollution: Conventional and Non-conventional Sorbents for Pollutant Removal from Wastewaters, Presses universitaires de Franche-Comté, 2010. https://books.google.fi/books?id=y06b_mOOrVwC.
[39] S.C. Lee, S. Park, Removal of furan and phenolic compounds from simulated biomass hydrolysates by batch adsorption and continuous fixed-bed column adsorption methods, Bioresour. Technol. 216 (2016) 661–668, http://dx.doi.org/10.1016/j.biortech.2016.06.007.

Publication IV

Tharaka Rama Krishna C Doddapaneni*, Ramasamy Praveenkumar, Henrik Tolvanen, Jukka Rintala, Jukka Konttinen

"Techno-economic evaluation of integrating torrefaction with anaerobic digestion"

Applied Energy 2018; 213: 272–284.

Applied Energy 213 (2018) 272–284

Contents lists available at ScienceDirect

Applied Energy

journal homepage: www.elsevier.com/locate/apenergy

Techno-economic evaluation of integrating torrefaction with anaerobic digestion

Tharaka Rama Krishna C. Doddapaneni*, Ramasamy Praveenkumar, Henrik Tolvanen, Jukka Rintala, Jukka Konttinen

Laboratory of Chemistry and Bioengineering, Tampere University of Technology, P.O. Box 541, FI-33101 Tampere, Finland

HIGHLIGHTS

- Integrating torrefaction with anaerobic digestion has better process economics.
- Selling price of torrefied pellets reduced with proposed process integration.
- Pellets selling price reduced by 15 €/t with proposed process integration.
- Torrefaction process economics are significantly influenced by feedstock price.

ARTICLE INFO

Keywords:
Techno-economic analysis
Torrefaction – anaerobic digestion
Minimum selling price
Energy recovery
Process integration
Torrefied pellets

ABSTRACT

In recent days, the interest on torrefaction is increasing owing to its ability to improve biomass properties to a level of competing with coal. However, its techno-economic feasibility still need to be optimized. Integrating torrefaction with other thermochemical and biochemical processes could be a feasible option to improve the performance of the torrefaction process. In that regard, this study evaluates the techno-economic feasibility of integrating the torrefaction with anaerobic digestion (AD). In addition, new process configurations were studied to identify the possible heat energy recovery options. Technical feasibility was tested through mass and energy balance at each process unit. The economic indicators such as net present value (€), minimum selling price and internal rate on return (%) were used to evaluate the economic performance. At 10 t/h of torrefied biomass pellets production capacity, the estimated bio-methane production from AD was 369 m^3/h. The economic evaluation shows that the minimum selling price of the torrefied biomass to reach the breakeven could be reduced from 199 €/t for standalone torrefaction to 185 €/t in case of torrefaction integrated with AD. The sensitivity analysis shows that feedstock and total capital investment were the most sensitive input parameters. This study shows that integrating the torrefaction with AD has better technical and economic feasibility than standalone torrefaction.

1. Introduction

The main aim of the Paris climate change agreement was maintaining the global average temperature 2 °C below the pre-industrial level and reducing the greenhouse gas emissions by 40% compared with 1990 level by 2030 [1]. At the same time the European union energy targets are, 20% of the primary energy consumption from renewable resources by 2020 and 27% by 2030 [2]. By 2014, fossil fuels (i.e. coal, oil and natural gas) are accounted for 80% of world primary energy supply [3]. Among the other fuels, coal combustion is the major source of CO_2 emissions, and according to IEA statistics, 45% of the global CO_2 emissions are from coal combustion in 2014 [3]. Replacing or reducing the coal with renewable materials in the industrial applications and electrical energy production could be one option to achieve the above said environmental and energy targets.

Biomass could be one such a renewable material, which can be considered as an alternative to coal. However, biomass has several challenges like high moisture content, fibrous, hydrophilic nature and low heating value [4]. To overcome these issues, biomass should be pretreated. Several pretreatment methods have been proposed, torrefaction being one of them [2]. During torrefaction, the biomass is heated slowly in the temperature range of 200–300 °C in an inert environment. Torrefaction treatment allows biomass to compete with coal by altering its physiochemical properties for example, energy density

* Corresponding author.
E-mail address: tharaka.doddapaneni@tut.fi (T.R.K.C. Doddapaneni).

https://doi.org/10.1016/j.apenergy.2018.01.045
Received 9 October 2017; Received in revised form 21 December 2017; Accepted 13 January 2018

and hydrophobicity [5]. In the recent days the research interest and commercial demand on the torrefied biomass is increasing globally. The market forecast shows that global demand for torrefied wood pellets will be around 70 million tons a year by 2020 [6].

However, the techno-economic optimization of the torrefaction process is required to remain competitive with conventional wood pellets production. According Koppejan et al. [5], the two major technical challenges to the commercialization of torrefaction technology are handling the volatile gases and energy integration within the process. According to Batidzirai et al. [7], torrefaction process still need to be optimized with respect to heat integration and waste heat utilization. Thus, the integration of torrefaction process with other thermochemical and/or biochemical processes could be useful for the improved technical and economic performance. Previously, Ekaterina et al. [8] studied the integration of torrefaction with combined heat and power (CHP) plant and reported that higher utilization of CHP boiler was achieved during part-load operations. In other study, Kumar et al. [9] studied the integration of torrefaction as a downstream operation in a conventional biomass pelletization process. The results show that capital investment can be reduced in an integrated approach in comparison with standalone torrefaction process. Clausen [10] studied the integration of torrefaction with gasification through thermodynamic modeling and reported that the biomass to syngas conversion efficiency increased from 63 to 86% in an integrated approach. Arpiainen et al. [11] analyzed the feasibility of integrating the torrefaction with CHP, saw mill and pulp and paper industry and concluded that integrating the torrefaction with CHP does not reduced the costs significantly. However, these studies were mainly focused on the integration of torrefaction with thermochemical processes. Fagernas et al. [12] studied the possibility of condensing the volatiles and selling the torrefaction condensate as a feedstock for pesticides production, and reported that the increased selling price of the torrefaction condensate reduces the selling price of the torrefied biomass.

Previously, Doddapaneni et al. [13] and Liaw et al. [14] studied the integration of torrefaction process with anaerobic digestion (AD) for the effective utilization of torrefaction condensate. The results from these studied [13,14] shows that torrefaction condensate can be effectively converted into biogas though AD. Although, the experimental results are promising, the techno-economic analysis and process modeling at an industrial scale operation, is required to better-understand the feasibility of such a process.

This study focuses on analyzing the operational and economic feasibility of integrating the torrefaction with AD. In addition, the possible heat energy recovery options from torrefaction process were also studied. The techno-economic performance of the standalone torrefaction process was compared with two different integrated process configurations. These two process configurations are using the biogas in a gas engine to produce electrical and heat energy and biogas upgrading into bio-methane using high-pressure water scrubbing (HPWS) and pressure swing adsorption (PSA). The technical feasibility of the process was analyzed through energy and mass balance at each process step. The comparative economic analysis between different process configurations was studied in terms of minimum selling price, net present value (NPV) and internal rate of return (IRR). A sensitivity analysis was carried out in order to understand the influence of different input values of the operating parameters on the economics of the studied process configurations. To the best of our knowledge, this is the first study on the techno-economic analysis of torrefaction process integrating with AD.

2. Methods

2.1. Process description

Fig. 1 shows three different process configurations considered in this study. The major difference between different cases presented in Fig. 1 are given below.

Case 1: This case represents the standalone torrefaction process, where the volatiles from the torrefaction process were combusted along with wood chips to meet the heat energy demand.
Case 2: In this case, the condensation of torrefaction volatiles to produce torrefaction condensate and later, the AD of torrefaction condensate to produce biogas was considered. Finally, utilizing the biogas in a biogas engine to produce electrical energy was also considered in this case.
Case 3: The difference between case 2 and case 3 was with the application of produced biogas. In contrast to case 2, the biogas upgrading to bio-methane using high-pressure water scrubbing (HPWS) and pressure swing adsorption (PSA) was considered in case 3.

The pellets production process was common for all the cases. In case 2 and case 3, it was assumed that, the uncondensed gases are combusted along with wood chips to produce the heat energy required for drying and torrefaction units. For all the cases, the possibilities for heat energy recovery was also studied.

2.2. Process parameters

The mass and energy balances for torrefaction and AD were carried out based on the experimental results from our previous study [13]. A plant capacity of 10 ton/h of torrefied biomass pellets production was considered for all the cases presented in Fig. 1.

2.2.1. Drying and torrefaction process

Operating conditions of drying and torrefaction units are presented in Table 1. The forestry wood chips with a moisture content of 40% and heating value of 10 MJ/kg were considered as feedstock material [8]. It was assumed that in the drying section, moisture content of the wood chips is reduced from 40 to 10% and the products i.e. dried wood chips and water vapor leaves the dryer at its operating temperature (i.e. 150 °C). The energy required at drying unit was calculated from the latent heat of evaporation of water (2260 kJ/kg) and the sensible heat of wood chips (kJ/kg) at dryer operating temperature.

The torrefaction temperature was selected as 300 °C. The product flow information of the torrefaction unit was selected from our previous experimental data [13] which represents the mass yield of 0.55 and 0.45 kg/kg of dry wood chips for torrefied biomass and torrefaction volatiles, respectively. The energy required for torrefaction process was calculated by using Eq. (1), which represents the overall energy balance between input and output energy flows [7].

$$[m_{DB} \times (LHV_{DB} + (Cp_{DB} \times T_{DB}))] + Q_{in} = [m_{TB} \times (LHV_{TB} + (Cp_{TB} \times T_{TB}))] + [m_{TV} \times (LHV_{TV} + (Cp_{TV} \times T_{TV}))] + Q_{loss} \quad (1)$$

where m, LHV, C_p and T are the mass, lower heating value, specific heat capacity and temperature and DB, TB and TV are the dried biomass, torrefied biomass and torrefaction volatiles respectively. Q_{in} is the heat energy input to the torrefaction reactor and Q_{loss} is the heat energy loss from the torrefaction reactor. In this study, the radiative heat loss was considered as 3% on the LHV of the dried biomass [15]. The specific heating values for dried biomass (Cp_{TB}) and torrefied biomass (Cp_{DB}) was selected as 1.2 and 1.4 kJ/kg·K respectively [16]. The thermal properties of the torrefaction volatiles selected from [17] and National Institute of Standards and Technology's web directory [18] was used in Eq. (1).

2.2.2. Product properties

The heating value of the torrefied biomass varies between 19 and 24 MJ/kg depending on the severity of torrefaction [8] and in this study

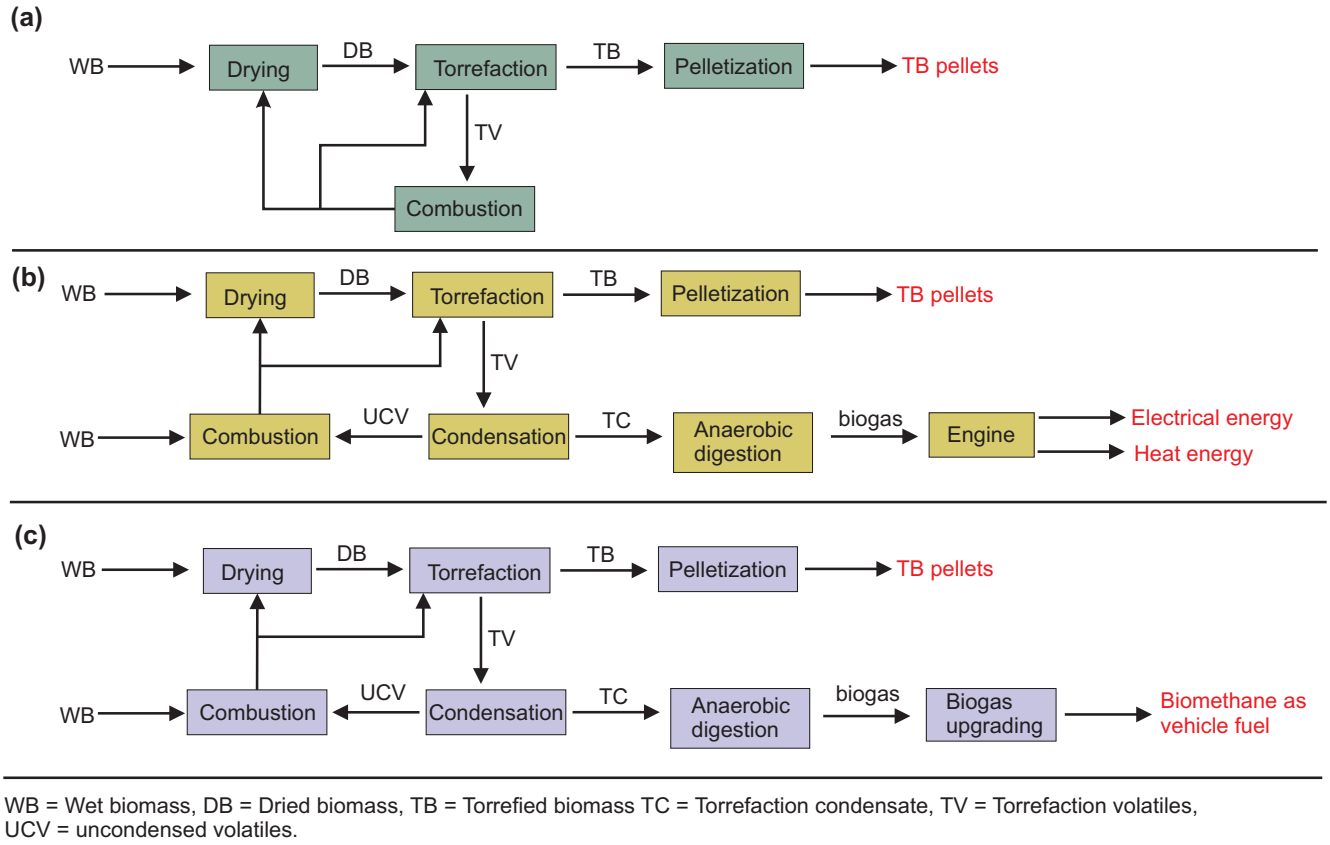

Fig. 1. Process flow for different cases considered in this study, (a) Case 1 (standalone torrefaction), (b) Case 2 (Torrefaction –AD_Engine), (c) Case 3 (Torrefaction –AD_Biomethane).

Table 1
Properties and operating characteristics.

Feedstock properties	Raw wood chips	After drying	After torrefaction
Moisture content (%)	40	10	0
Lower heating value (LHV) (MJ/kg)	10	16	22
Operating characteristics			
Dryer operating temperature (°C)	150		
Torrefaction temperature (°C)	300		
AD operating temperature (°C)	35		
Engine exhaust gases temperature (°C)	485		

heating value of 22 MJ/kg of torrefied biomass was selected. Torrefaction volatiles mainly contains water, acetic acid, furfural, methanol, acetol, phenolic compounds, tar, CO_2 and CO. In this study the composition of condensable volatile gases was selected from our previous study [13]. The Heating value of the volatile gases was calculated by adding LHV of major compounds as presented in Eq. (2). The uncondensed volatiles yield at 300 °C was 0.20 [13] which mainly contains CO_2 and CO. The yield of CO_2 and CO was calculated using the correlation that the ratio of CO_2 to CO was 2.5 [19]. The condensate yield and other properties such as volatile solid content (VS) and biomethane potential was selected as 0.25 kg/kg of dried wood, 17% and 83 mL/g of torrefaction condensate respectively [13].

$$LHV = \sum_{i=1}^{n} m_i \cdot LHV_i \quad (2)$$

where '*i*' represents the major compounds present in the torrefaction volatiles.

2.2.3. Process flow for pellets production

The operational procedure for pellets production reported by Kumar et al. [9] was considered in this study for pellets production from torrefied biomass. Initially, the torrefied biomass from the reactor is cooled to a temperature of 95 °C and later cooled to a final temperature of 50 °C. The cooled torrefied biomass is then ground before preconditioning. Because of the increased brittleness and the reduced water content, pelletizing the torrefied biomass is difficult and it requires more energy [20]. Thus, torrefied biomass pelletization requires external binders. In the literature researchers studied the feasibility of different binders such as, steam, saw dust, vegetable oils and corn [21]. In this study, preconditioning the torrefied biomass with low-pressure steam at 15 wt% (i.e. 0.15 kg of steam/kg of torrefied biomass) was considered. The material loss during pelletization was considered as negligible. The energy required for grinding, pelletizing, and screening unit of pelletizing section was selected as 22,137, and 101 MJ/t as suggested by Kumar et al. [9].

2.2.4. Anaerobic digestion (AD)

The experimental data for batch assay of AD of torrefaction condensate presented in our previous study [13] was used for mass and energy balance at AD digester. The operating temperature of the digester was considered as 35 °C. The volume of the digester was calculated considering the organic loading rate of 3 kg VS/m^3·day and the methodology presented by [22]. According to [22] the organic loading rate varies 4–5 kg VS/m^3·day for industrial scale reactors that are operating at mesophilic conditions. However, in this study organic loading rate of 3 kg VS/m^3·day was selected because of the inhibitory effects associated with the torrefaction condensate. A design factor of 1.25 was used to accommodate the calculation errors and safety measures. The heat energy required to maintain the digester temperature was calculated using the Eq. (3) [23].

$$Q_{AD} = [m_{TC} \times Cp \times (T_2 - T_1)] + Q_{AD-loss} \quad (3)$$

where Q_{AD}, is the heat energy demand for AD, m_{TC} is the mass of the torrefaction condensate, Cp is the specific heat capacity of the torrefaction condensate, T_2 is AD operating temperature, and T_1 is the torrefaction condensate inlet temperature. The Cp of the torrefaction condensate was selected as 2.8 kJ/kg-K [24]. The inlet temperature of the torrefaction condensate was selected as 20 °C.

The heat loss at digester was calculated following the methodology presented by [23] and the Eq. (4).

$$Q_{AD-loss} = k_d \times A_D \times \Delta T_D \quad (4)$$

where $Q_{AD-loss}$ is the heat loss at digester. k_d is the k-factor of the digester material, A_D is the surface area of the digester, and ΔT_D is the average temperature difference between heating medium and the substrate (torrefaction condensate). The k-factor of the digester material and the outside temperature was selected as 0.5 W/m^2 °C and −10 °C respectively [23]. The surface area of the digester was calculated considering the height to diameter ratio of 0.5.

For case 2, using produced biogas in a gas engine to produce electrical and heat energy was considered. The amount of electrical energy produced was calculated using the Eq. (5). For that, it was considered that 1 m^3 of bio-methane is equal to 10 kWh of energy potential (heating value) [25].

$$E_{elc.} = V_m \times 10 \times \eta_{elc.} \quad (5)$$

where V_m is the volume of the methane produced, $\eta_{elc.}$ is the electrical efficiency of the biogas engine that was considered as 45% in this study.

For case 3, the upgrading of biogas as bio-methane was considered. The CH_4 and CO_2 concentration was selected as 70 and 30 vol% respectively, based on theoretical methane yield from fat containing substrate [26]. The HPWS and PSA methods were considered for the biogas upgrading through CO_2 removal. The previous studies [27] reported that the total methane loss from biogas upgrading processes is < 2%. In this study, the methane yield of 96% was considered for both HPWS and PSA [28]. Finally, the application of upgraded bio-methane as vehicle fuel was considered.

At present, no research data is available on the properties of the digestate produced from the AD of the torrefaction condensate. The nutrients (nitrogen (N), phosphorous (P) & potassium (K) in the digestate comes from the raw material used for the AD process [29]. The biomass derived oils, for example pyrolysis oil contain low amount of nitrogen (below 0.4 wt%) and ash (0.01–0.1 wt%) [24]. At the same time, according to [30,31] the release of P and K to the gas phase is very low at torrefaction temperature of 300 °C. Thus, the feasibility of using the digestate as fertilizer could be limited. In this study, the digestate is considered as an industrial wastewater that needs to be treated before releasing to the environment.

2.2.5. Energy recovery

In this study, in addition to the integration of torrefaction and AD, the possibilities for heat energy recovery was also studied with an aim of improving the thermal efficiency of the torrefaction process. Three different possibilities as listed below were considered for heat energy recovery.

- From engine flue gases, water jacket and from lube oil cooler (only for case 2).
- From dryer exhaust gases, which contains water, dust and volatile organic compounds (VOC).
- From torrefaction products cooling.

In this study, the application of recovered heat energy for district heating (DH) was considered. For case 1, heat energy recovery from torrefied biomass cooling only was considered. As the combustion of torrefaction volatiles was considered for case 1 (standalone torrefaction process), it was assumed that torrefaction volatiles enter boiler combustion chamber at torrefaction reactor temperature. However, for case 2 and 3, the heat energy recovery from both torrefied biomass and volatiles cooling was considered. It was assumed that initially, both torrefied biomass and volatiles are cooled to 95 °C and later cooled to a final temperature of 50 °C. The high-grade heat energy recovered during the initial stage of the torrefaction product cooling i.e. when torrefaction products are cooled from 300 °C to 95 °C was considered for district heating. The low-grade heat energy recovered from torrefaction products cooling (when cooled from 95 °C to 50 °C) was considered for AD digester heat energy requirement and wood chips preheating.

The possible heat energy recovery at engine was calculated based on the data reported by [32,33]. The heat energy recovery from engine exhaust gases, engine water jacket and lube oil cooling was considered. The engine exhaust gases temperature was selected as 485 °C [33] and these exhaust gases can be reduced to a stack temperature of 135 °C.

The water vapor from the dryer contains volatile organic compound (VOC) and dust, thus it must be treated before releasing to the environment. The water vapor leaves the dryer at 150 °C and contains high amount of heat energy, thus heat energy recovery from water vapor coming out from dryer was also considered in this study. In the previous study Svoboda et al. [34] reported different approaches for the heat energy recovery from biomass drying exhaust gases. However, in this study using the heat energy recovered from drying exhaust gases for air preheating and district heating was considered for all the cases studied. It was considered that, the heat energy from water vapor is initially used for district heating and later for preheating the combustion air from 10 to 50 °C. Finally, the water vapor is released at 60 °C for further treatment at wastewater treatment plant. It was also assumed that the inlet and outlet temperatures of water for district heating was 60 °C and 90 °C respectively. The energy recovery was simulated using Aspen hysys®.

2.3. Economic analysis

2.3.1. Total capital investment

The economic analysis of all the cases presented in Fig. 1 were carried out to make a comparative analysis and to identify the economic feasibility of integrating torrefaction with AD. The mass and energy balances established through previous sections were used to scale up the equipment to a level of selected plant capacity and thereby to establish the capital investment. The cost of the equipment was selected from previous literature [9,21]. However, the size of the equipment varies with plant operating capacity, thus the final cost specific to this study were established through scaling factor as presented in Eq. (6) [8,35].

$$C = C_0 \times \left(\frac{A}{A_0}\right)^n \quad (6)$$

where C and A are the cost and capacity of the present equipment and C_0 and A_0 are the cost and capacity of the base equipment respectively; n represents the scaling factor. In general, the n values varies between 0.6 and 0.8 [7,35] and in this study an n value of 0.6 was considered.

The equipment cost varies year to year, thus the cost data available in the literature must be converted to the present year. This was done using chemical engineering plant cost index (CEPCI) [35] data using Eq. (7). In this study, the cost index data of June-2017 was used for present year.

$$Cost_{year\ X} = Cost_{Year\ Y} \times \frac{CEPCI_Y}{CEPCI_X} \quad (7)$$

In the present study, the cost data of drying, torrefaction and pelletizing units was selected from Kumar et al. [9]. The cost of heat exchangers and volatiles condensation units were selected from [36]. The cost data for boiler was taken from [21]. In case of AD digester, the

Table 2
Cost parameters considered for the calculation of production costs and revenue.

Utility	Cost (€)	Reference
Wet wood chips (forest) (€/kWh)	17.5	[40]
Electrical energy purchasing price (€/MWh)	100	[8]
Steam as binding agent (€/t)	22	[35]
Wages (€/h)	14	
Electrical energy selling price (€/MWh)	83.5	[41]
District heat selling price (€/MWh)	60	[8]
Biomethane selling price (€/m^3)	1.18	[42]
Biometahne upgrading costs for HPWS (€/m^3 of biogas)	0.13	[38]
Biometahne upgrading costs for PSA (€/m^3 of biogas)	0.17	[43]

literature shows that, the digester cost varies from 300 to 500 USD/m^3 [37] and in this study a value of 400 USD/m^3 was considered. The cost information of the biogas engine was selected based on internal communication. The capital investment required for biogas upgrading was selected from de Hullu et al. [38]. The fixed capital investment on the equipment (CIE) was calculated by the summation of all the major equipment present in respective cases presented in Fig. 1. The total fixed capital (FCI) was calculated by adding capital investment on equipment and other capital costs such as startup expenses (10% of CIE), engineering and supervision (12% of CIE) and contingency (10% of CIE) [8,9].

In addition to FCI, working capital is required in order to start the plant and operate it until the time the first income received. According to the previous studies [35] the working capital for chemical plants varies from 15 to 20% of FCI and in this study 15% was selected. Finally, the total capital investment (TCI) was calculated by adding FCI and working capital.

2.3.2. Production costs

The utility and other specific costs were presented in Table 2. The manpower required to operate the plant was calculated using the methodology presented in the literature [35]. It was considered that the factory operates for 330 days, 24 h a day, i.e. 7920 working hours. Three 8 h working shifts per day was considered. The expenses on the supervising staff was calculated as 15% on the operating labor expenses [35]. The maintenance and repair costs were selected as 3% of FCI. The other operating costs such as factory overheads, administration costs and distribution and selling cots, were calculated based on correlations presented by [35]. The factory overheads includes payroll overheads, employ benefits, medical, accounting and safety services. The wastewater treatment cost i.e. 1.2 €/m^3, reported for pulp and paper industry effluents [39] was used to calculate waste water treatment costs [35]. The depreciation amount was calculated using straight line method for a period of 10 years.

2.3.3. Profitability and sensitivity analysis

The economic performance of the standalone torrefaction unit and the considered integration approaches were evaluated based on internal rate of return (IRR), net present value (NPV). The net present value was calculated using the Eq. (8) [8,44].

$$NPV = \left(\frac{(1+i)^n - 1}{i \times (1+i)^n} \times net\ cash\ flow\right) - TCI \quad (8)$$

where i is the interest rate (8%), n is the lifetime of the plant (20 years) and TCI is the total capital investment. The net cash flow can be calculated by Eq. (9).

$$net\ cash\ flow = ((TR - PC) * (1 - tax\ rate)) + D \quad (9)$$

where TR is the total revenue (€), which includes the revenue from all the sources in the process. PC is the total production cost (€) and D is the depreciation. The income tax rate was selected as 30% in this study.

The IRR (%) value was calculated by solving iteratively, at such i value the NPV becomes zero in the Eq. (8) [8].

The influence of integrating the torrefaction with AD on the selling price of torrefied biomass was evaluated using minimum selling price information. The minimum selling price of the torrefied biomass was calculated using the methodology presented by [45]. To reach the breakeven point, the total costs must be equal to the total revenue as presented in Eq. (10).

$$TR = PC + ROI + IT \quad (10)$$

$$ROI = CRF \times TCI \quad (11)$$

$$IT = \text{taxation rate} \times (TR - PC - D) \quad (12)$$

where TR is the total revenue (€), PC is the total production cost (€), ROI is the return on investment (€), IT is the income tax (€), CRF is the capital recovery factor calculated using Eq. (13) and TCI is the total capital investment and D is the depreciation amount (€).

$$CRF = \frac{i \times (1+i)^n}{(1+i)^n - 1} \quad (13)$$

Sensitivity analysis was carried out to understand the influence of different cost parameters on the economic performance of all the cases presented in Fig. 1. For this, the input parameters such as TCI, working capital, cost of wood chips, selling price of the products were varied in the range of ± 25% to the base values.

3. Results and discussion

3.1. Mass and energy balance

Fig. 2 shows the mass and energy flows for different cases studied. In the torrefaction process, drying and torrefaction are major energy consuming units. The calculated energy requirement for drying was 1372 kJ/kg of wet wood chips. Ghiasi et al. [46] reported the energy requirement for drying as 1328 kJ/kg of wood, when reduced moisture content from 45 to 15%. For torrefaction, a wide range of heat of reaction values have been reported in the literature. Bates et al. [17] predicted that the heat of reaction varies from 350 kJ/kg of dry biomass at 200 °C to −630 kJ/kg of dry biomass at 300 °C. Prins et al. [47] reported a value of 124 ± 400 kJ/kg of wood, for torrefaction at 300 °C for 10 min. In this study, the calculated heat energy required for torrefaction was −419 kJ/kg of dry wood (10% moisture). This shows that the overall torrefaction reactions are exothermic and no external heat is required for the torrefaction reaction however, the energy required at torrefaction depends on the type of reactor considered. Thus, it is optimistic to consider the energy required for the remaining moisture removal (in this study 10%) and to raise the wood chips temperature to the operating temperature (300 °C) [9]. The calculated energy requirement for torrefaction was 789 kJ/kg of dried wood. The heat loss at torrefaction reactor was considered as 10% of total heat exchanged as suggested by [48]. Kohl et al. [49] reported the energy requirement of 714 kJ/kg of dry biomass at torrefaction operating temperature of 280 °C. The calculated total energy required for both drying and torrefaction was around 2162 kJ/kg of wood. In an another study, Ranta et al. [50] reported a value of 2277 kJ/kg for a pilot plant operation at a torrefaction temperature of 260 °C. The energy required for grinding, sieving and pelletizing was selected as 260 MJ/t of torrefied pellets [9].

The calculated lower heating value of torrefaction volatiles was 4.3 MJ/kg of torrefaction volatiles (i.e. 1.9 MJ/kg of dried biomass). The earlier studies [17] reported higher heating value of torrefaction volatiles in the range of 4.43–10.6 MJ/kg. Prins et al. [47] reported a heating value of 3.5 MJ/kg of dry willow biomass. In an another study Arpiainen et al. [11] reported a heating value of 6.3 MJ/kg of torrefaction volatiles. The combustion of these volatiles for heat energy requirement at drying and torrefaction was considered for case 1. However, they can only fulfill partial energy requirement and additional

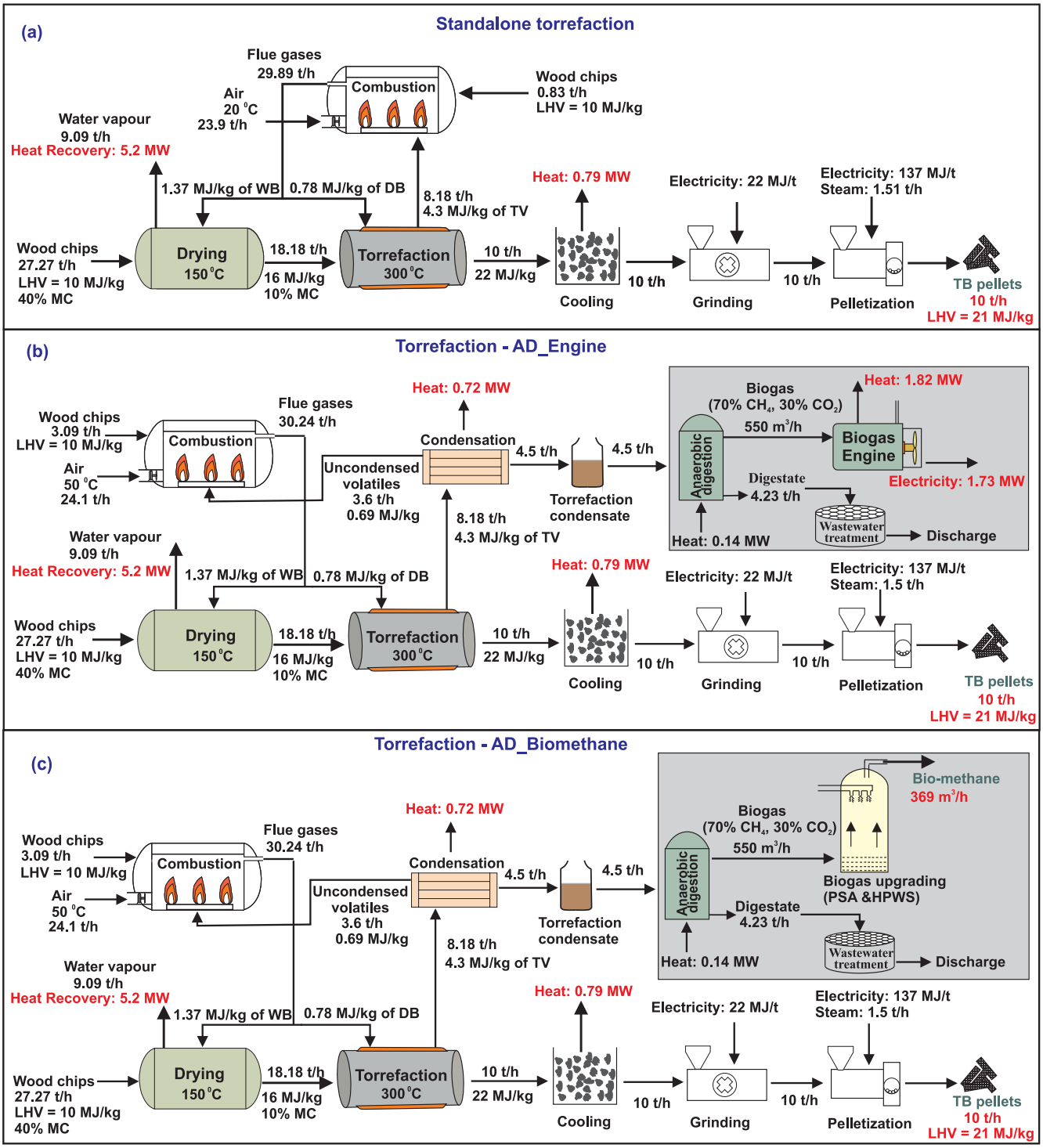

Fig. 2. Mass and energy balance for different cases, (a) Case 1 (standalone torrefaction), (b) Case 2 (Torrefaction –AD_Engine), (c) Case 3 (Torrefaction –AD_Biomethane). WB = Wet biomass, TB = Torrefied biomass, TV = Torrefaction volatiles, MC = Moisture content, HPWS = High-pressure water scrubbing, PSA = Pressure swing adsorption.

utility fuel is required to meet the total energy demand. For this purpose, the combustion of wet wood chips was considered in this study; the extra amount of wet wood required to produce torrefied pellets at 10 t/h was 0.83 t/h for case 1 and 3.1 t/h for case 2 and case 3. The calculated heating value of uncondensed volatiles was around 0.7 MJ/kg of uncondensed volatiles.

The amount of torrefaction condensate produced was 4.54 t/h. The total volume of anaerobic digester required at an organic loading rate of 3 kg VS/m^3·day was 7826 m^3. The total methane production was 9241 m^3/day. The total amount of digestate produced was 101 t/day. The amount of heat energy required to maintain digester temperature was 120 kW. The electricity produced through engine (case 2) was 1.73 MW. However, it was assumed that 5% of energy produced would be consumed for pumps, compressors and other controlling equipment. Thus, the net energy produced was 1.64 MW (i.e. 13,016 MWh/year). In case of biogas upgrading (case 3), the total bio-methane produced

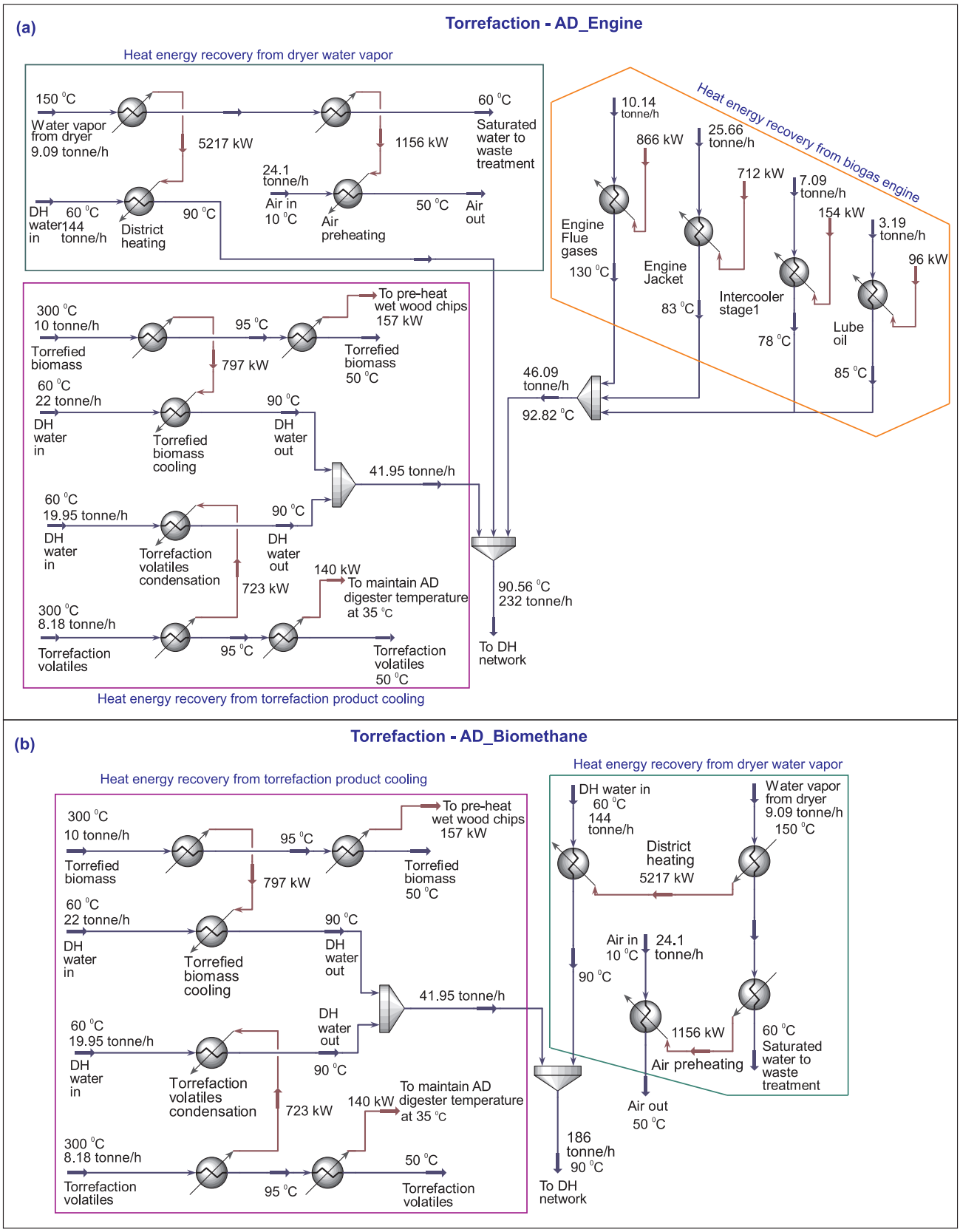

Fig. 3. Energy recovery possibilities for integrated torrefaction process. (a) Case 2 (Torrefaction –AD_Engine), (b) Case 3 (Torrefaction –AD_Biomethane) DH = District heating.

through HPWS and PSA was 8871 m^3/day, respectively. The amount of wastewater produced was around 320 t/day (which includes saturated water vapor from drying and digestate from AD) with a volatile solid content flow of around 12 t/day (volatile solids content 37.5 kg/m^3).

The operating details of two commercial scale biogas plants are provided here to visualize the scale of the AD process considered in this study. The Kristianstad biogas plant in Sweden has a biogas production capacity of around 2.9 million m^3/year with a digester volume of 8500 m^3 and with a capacity of treating 75,000 tons of different kinds of wastes (i.e. organic fraction of municipal solid waste, industrial organic waste and manure). The electrical energy production is 1.8–2 MW [51]. The another plant located at Werlte, Germany, has an installed electrical energy production capacity of 2.6 MW with a digester volume of 6400 m^3 [52]. In the present study, the AD process can handle 35,640 t/year of torrefaction condensate with a digester volume of 7826 m^3 and with a production capacity of 3.04 million m^3/year biomethane and 1.73 MW electrical energy.

3.2. Energy recovery

Fig. 3 presents heat energy recovery from case 2 and 3. The same for case 1 was presented in Fig. S1 (supplementary information). The heat energy recovered from product cooling at selected plant capacity was 797 and 723 kW for torrefied biomass cooling and torrefaction volatiles cooling. The total heat energy recovery from engine was 1829 kW. The total heat energy recovered from dryer exhaust gases for district heating was 5245 kW for case 1 and 5217 for case 2 and 3 respectively. The total heat energy available for DH from case 1, 2 and case 3 was 6042, 8566 and 6737 kW, respectively.

3.3. Economic analysis

3.3.1. Capital investment

Table 3 shows the summarized capital expenditure on various equipment and the total capital investment for different process integration approaches. For all the cases studied, the maximum share of total capital expenditure goes for torrefaction reactor. For standalone torrefaction process, 50% of the total capital investment goes to the torrefaction reactor and the same for case 2 was 38%. Pirraglia et al. [21] reported that torrefaction unit represents 43% of total installed costs for a plant capacity of 100,000 t/year. In this study, the total cost of the torrefaction reactor at considered plant capacity (79,200 t/year) was 14.62 M€, i.e. 1.46 M€/t-h. This is in the range of commercial estimate i.e. 1.2–1.8 M€/t-h reported by Batidzirai et al. [7]. The capital investment (on equipment) for anaerobic digestion at selected plant capacity (i.e. 369 m^3/h of bio-methane production) was 4.1 M€ (which includes investment on biogas engine) for case 2. The same for case 3-HPWS and case 3-PSA was 3.9 and 4.6 M€ respectively. In the literature [53] reported an investment of 1.89 M€ for a plant capacity of 100 m^3/h and in another study [54] reported an invest of 1.3 M€ for a plant capacity of 75 m^3/h. According to [55], the industrial reference for the investment on anaerobic digestion is 4 M€ for a plant capacity of 999 kW of electrical energy production. In this study, the total investment on anaerobic digestion alone was 6.2 M€ (for case 2) at an electrical energy production capacity of 1730 kW.

The total investment for case 1 (standalone torrefaction process) and case 2 (AD-Engine) was 33.63 M€ and 41.54 M€, respectively. For case 3, 41.33 M€ and 42.35 M€ for HPWS and PSA operations, respectively. These TCI values shows that, the integration of torrefaction with AD significantly increases the capital investment. However, this could be compensated through the additional revenue from electrical energy or bio-methane. In the earlier studies, [7] reported a capital investment of 49.46 M€ for 100,000 t/year of torrefied pellets production capacity. Kumar et al. [9] reported 28.2 M€ for 60,000 t/year of torrefied pellets production capacity. Sermyagina et al. [8], reported a total capital investment of 47.7 M€ for torrefaction integrated with CHP-DH at 40,000 t/year of torrefied pellets production capacity.

Table 3
List of major equipment costs and the total capital investment (TCI) for different cases.

Equipment	Operating capacity	Number of units	Cost (€)
Torrefaction			
Front end loader			260,304
Wood chips hopper			214,232
Conveyor			353,599
Blowers			180,359
Dryer	5 t/h	6	1,981,075
Torrefaction unit	18 t/h	1	14,627,703
Hammer mill	8 t/h	3	307,527
Pellet mill	5 t/h	2	1,619,413
Pellet cooler			460,715
Pellets screening			125,545
Pellets storage warehouse			89,839
Boiler	2100 kW	1	562,986
Condensate production			
Volatiles condenser	120 t/d		169,047
Torrefaction Vapor Cyclones and filters	120 t/d		213,615
Volatiles and condensate separation vessel			36,460
Anaerobic digestion (AD)			
AD-digesters	7900 m^3	1	2,708,428
Digestate closed storage tank	11 t/d	1	77,583
Other installations (digester heating, water, control equipment, pump)			783,426
Biogas engine	2 MW		560,000
Biogas upgrading			
High pressure water scrubbing	369 m^3/h		422,725
Pressure Swing Adsorption	369 m^3/h		1,084,729
Heat energy recovery			
Heat exchangers			538,500
Site and building			
Paving, receiving station and load area			58,503
Building and office space			994,554
Total capital investment on equipment, land and buildings (CIE)			
Case 1			22,156,067
Case 2			26,959,025
Case 3-HPWS			26,821,751
Case 3-PSA			27,483,754
Other capital expenses			
Startup expenses			10% on CIE
Engineering and supervision cost			12% on CIE
Contingency			10% on CIE
Working capital			15% on FCI
Total capital investment (TCI)			
Case 1			**33,632,910**
Case 2			**41,543,858**
Case 3-HPWS			**41,332,318**
Case 3-PSA			**42,352,465**

HPWS = High pressure water scrubbing, PSA = pressure swing adsorption, FCI = Fixed capital investment (CIE + startup expenses + Engineering and supervision costs + Contingency).

3.3.2. Production costs

Table 4 shows the summary of various production costs for both standalone and integrated processes. In the total production costs (17.88 M€/year), the feedstock cost (wood chips cost) accounts for 60% in case of standalone torrefaction process. Excluding the feedstock costs, the other operating costs were around 7 M€/year, which includes utilities, manpower and factory overheads. Fig. 4a shows the total production costs for different cases studied. The total production costs were 189, 206, 213 and 221 € per ton of torrefied biomass pellets for case 1, case 2, case 3-HPWS and case 3-PSA, respectively. As expected,

Table 4
List of production costs for different cases.

Cost item	Production costs (€)			
	Case 1	Case 2	Case 3-HPWS	Case 3-PSA
Feedstock	10,818,500	11,688,600	11,688,600	11,688,600
Utilities	1,120,409	1,120,409	1,120,409	1,120,409
Maintenance and repair	877,380	1,083,753	1,078,234	1,473,129
Manpower (operating labor + supervisors)	410,997	410,997	410,997	410,997
Factory overheads	1,130,411	1,336,784	1,331,266	1,357,878
Administration Costs	326,472	388,384	386,728	394,712
Waste treatment	86,391	126,593	126,593	126,593
Biogas upgrading			566,366	740,632
Distribution and selling	148,107	161,555	167,091	173,129
Total	**14,958,870**	**16,317,074**	**16,876,284**	**17,486,080**
Depreciation	2,924,600	3,612,509	3,594,114	3,682,823

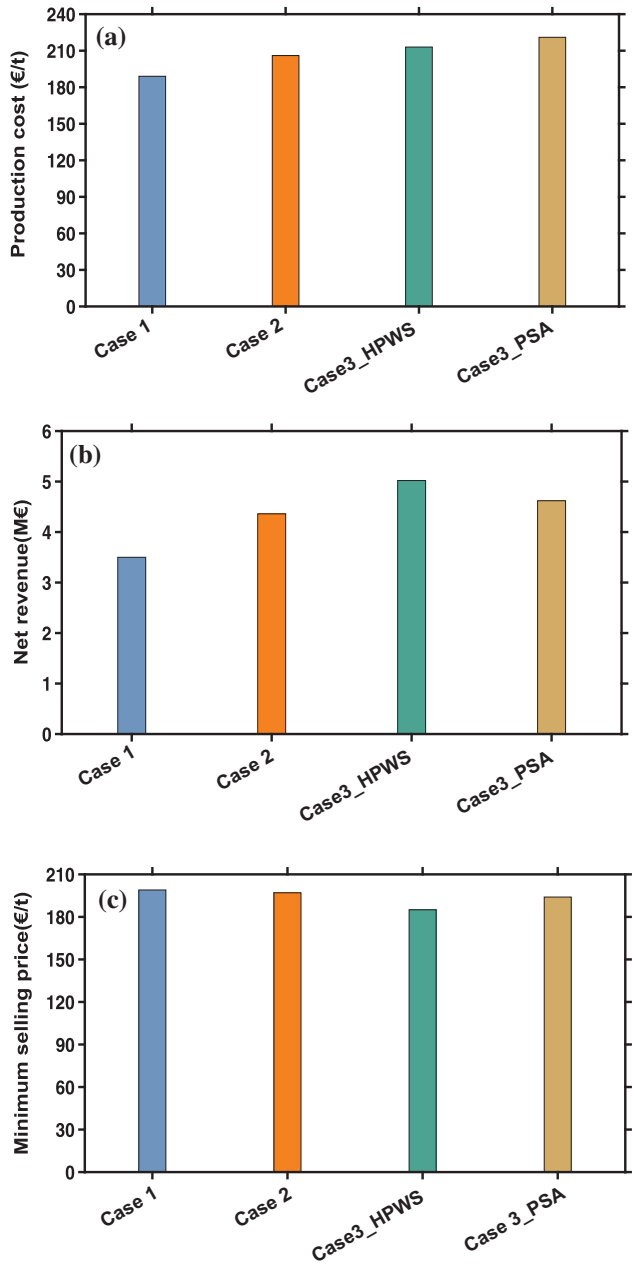

Fig. 4. Production costs and profitability analysis for different cases, (a) production costs, (b) net revenue at torrefied biomass selling price 200 €/t and (c) minimum selling price to reach breakeven point at capital recovery of 10%.

following the capital investments, the operating costs for integrated process increased. In the integrated approaches, PSA has the highest production costs. In the earlier studies [21] reported a production costs of 160 €/t for 100,000 t/year capacity. Pirraglia et al. [56] reported a production cost of 177 €/t for torrefied wood pellets production from southern yellow pine at 80,000 t/year capacity. Arpiainen et al. [11] studied the influence of integrating with different industries and reported the production costs in the range of 175–265 €/t. The variation in the operating cost mainly comes from the feedstock source and moisture content of the feedstock.

3.3.3. Profitability analysis

In the profitability analysis, the selling price of electricity, heat and bio-methane were kept constant at a value presented in Table 2. Fig. 4b shows the net revenue at a price of 200 €/ton of torrefied pellets. The net revenue was higher for integrated approaches (case 2 and case 3) than the standalone torrefaction process (case 1) and in the integrated approaches, case 3-HPWS, has the highest revenue i.e. 5 M€/year.

Fig. 4c shows the minimum selling price of torrefied biomass to reach the breakeven at CRF of 10% (at i = 8%, n = 20 year). From Fig. 4c it can be observed that, integrating the torrefaction with AD has the significant influence on the minimum selling price of torrefied biomass pellets. For example, the minimum selling price for case 1 (standalone torrefaction) and case 3 (AD-HPWS) were 199 and 185 €/ton. The same for case 2 and case 3-PSA was 197 and 194 €/ton respectively. The variation in the minimum selling price is mainly because of the additional revenue from the side products in the integrated approaches.

Fig. 5a shows the, NPV for different cases at varied torrefied biomass pellets selling price. The NPV is a measure of the economic viability of the project, which is a cumulative cash flow in a project over its life period. From, Fig. 5a it can be observed that for standalone torrefaction process the NPV values were negative when the selling price is < 200 €/t. In the literature, Pirraglia et al. [21] also observed negative NPV values for standalone torrefaction process when torrefied pellets selling price is less than 241 €/t. The negative NPV values represents that the process is not economically viable at selected parameters and the higher NPV values represents the high economic viability of the process at selected operating parameters. In this study, case 3_HPWS has the highest NPV values than case 2 at studied torrefied biomass selling prices and this is because of the higher revenue from bio-methane than the electrical energy. For example, at 210 €/t selling price of torrefied biomass, the NPV for case 3-HPWS was 2.1, 2 and 1.6 times higher than case 1, case 2 and case 3-PSA, respectively.

In addition to NPV, IRR is also widely used to understand the economics of the project. IRR (%) represents, the rate of return on the total capital invest. Fig. 5b shows the IRR (%) for different cases at varied torrefied biomass pellets selling price. Following the NPV values, case 3-HPWS has higher rate on investment. At 210 €/ton, the case 1 has

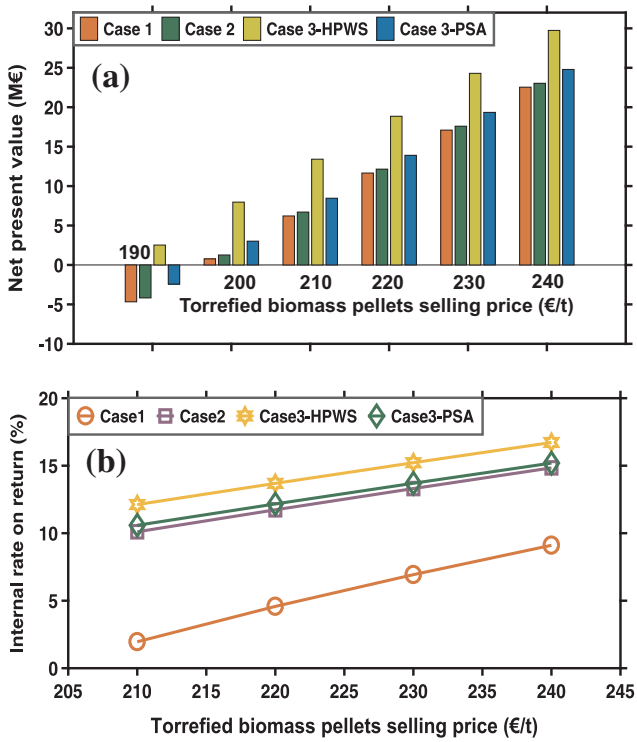

Fig. 5. Net present value (NPV) and internal rate of return for different cases at varied torrefied biomass selling price, (a) NPV (€) and (b) IRR (%).

only 2% return on investment and at the same price of torrefied biomass pellets, case 3-HPWS has 12% of IRR.

The profitability analysis showed that torrefaction process integrated with AD was economically more viable than a standalone torrefaction process. In the integrated approaches, the biogas upgrading and selling as vehicle fuel has a higher economic viability, than electrical energy production using a biogas engine. Again, the comparative analysis between the biogas upgrading technologies, HPWS has the higher economic feasibility than PSA. However, it should be noted that for case 2 the side revenue mainly comes from the heat energy thus the economic feasibility of case 2 depends highly on heat energy demand and the additional subsidies.

3.3.4. Sensitivity analysis

The influence of varied cost parameters on NPV and minimum selling price of the torrefied biomass pellets was presented in Fig. 6 and Fig. 7 respectively. The purchasing price of the wood chips followed by FCI were found to be the most sensitive parameters for all the cases. For example, increasing the wood chips price by 25%, decreased the NPV from 6.2 to −12.5 M€ for case 1 and from 13.4 to −6.8 M€ for case 3-HPWS respectively at 210 €/t of torrefied biomass pellets selling price. At the same time, reducing the wood chips price by 25% increased the NPV to 25 and 33 M€ for case 1 and case 3-HPWS respectively. Earlier studies [21,8] have also reported that the economics of the torrefaction process was more sensitive to the feedstock cost. In this study, FCI was also showing significant influence on the process economics. For example, reducing the FCI by 25% increased the NPV by 47% for Case 3-HPWS.

In case of minimum selling price, increasing the wood chips cost by 25% resulted in increasing the minimum selling price of the torrefied biomass pellets by 14, 16, 17 and 16% for case 1, case 2, case 3-HPWS and case 3-PSA, respectively (Fig. 7). As expected reducing the wood chips price, reduced the minimum selling price of torrefied pellets by, 21, 23, 25 and 23% for case 1, case 2, case 3-HPWS and case 3-PSA respectively. The other parameters such as selling price of electricity, heat energy and bio-methane shows little effect on the process economics in comparison with feedstock cost. As expected, the case 3-HPWS has showed better process economics for variation (± 25%) of all the input parameters.

4. Summary

In this study, for the first time, the techno-economic feasibility of integrating torrefaction with AD was presented. Condensing the torrefaction volatiles to produce torrefaction condensate instead of combusting them to produce heat energy increased the total capital investment by ~8 M€ and raw material cost by 0.87 M€. However, it is compensated through additional revenue from other products such as bio-methane, electricity and heat energy. The major advantage of integrating the torrefaction with AD is that, the selling price of the torrefied biomass pellets could be reduced because of the relatively high net revenue for integrated approaches compared to a standalone torrefaction process. For example, the minimum selling price for standalone torrefaction to reach the breakeven at CRF of 10% was 199 €/t, which was reduced to 185 €/t for case 3-HPWS.

In the total fixed capital, the major portion comes from the torrefaction reactor. Batidzirai et al. [7] predicted the capital expenditure required for torrefaction reactor by 2030 considering the technological learning rate concept. The author reported that at a learning rate of 2%, the capital and operating costs of the torrefaction reactor could be reduced significantly in future. In addition to TCI, the biomass cost is also significantly influenced the process economics. On the other hand, sensitivity analysis shows that reducing the feedstock price by 25%, can reduce the minimum selling price of the torrefied pellets to 148 €/t for case 3-HPWS and 160 €/t for case 2. Thus sourcing the wood from low cost resources such as sawdust, agricultural wastes, forest residues, and wood waste from wood processing industries could be useful to reduce the price of the TB pellets. At this price torrefied pellets can compete with wood pellets, at their current price of 166 €/t (FOEX indexes Ltd) [40]. The carbon credits could be the other source of income for torrefaction industry. According to [21], torrefaction industry can get the carbon credits in the range of € 25 to € 72 per ton of torrefied pellets (based on the US market). The combination of low cost feedstock (around 13 €/kWh), integrating torrefaction with AD, heat energy recovery options and carbon credits (40 €/t) can reduce the minimum selling price of the torrefied pellets to 108 €/t. In addition to carbon credits, the benefits from anaerobic digestion process such as investment subsidy and/or feed-in-tariff can further reduce the selling price of torrefied biomass pellets. The reduction in the capital costs on the torrefaction reactor can further reduce the minimum selling price of the torrefied wood pellets. In addition to bio-methane and/or electricity, utilizing the digestate as a fertilizer may also generates additional income. For that co-digestion of torrefaction condensate with other substrates could be useful, however, further research activities are required to better understand the digestate properties.

The results from this study shows that integrating the torrefaction with AD has better technical and economic feasibility than standalone torrefaction process. However, there is limited research data available on the anaerobic digestion of torrefaction condensate. Thus, further research is required to better understand the advantages and issues that may arise during the process scale up.

5. Conclusion

This study gives measures on improving the techno-economic feasibility of the torrefaction process in order to improve its competitive advantage over coal and wood pellets in energy markets. The operational and economic feasibility of integrating torrefaction with anaerobic digestion including heat energy recovery possibilities was presented. Based on net present value (€) and internal rate on return (%), it can be concluded that torrefaction process integrated with AD was economically more viable than a standalone torrefaction process. When

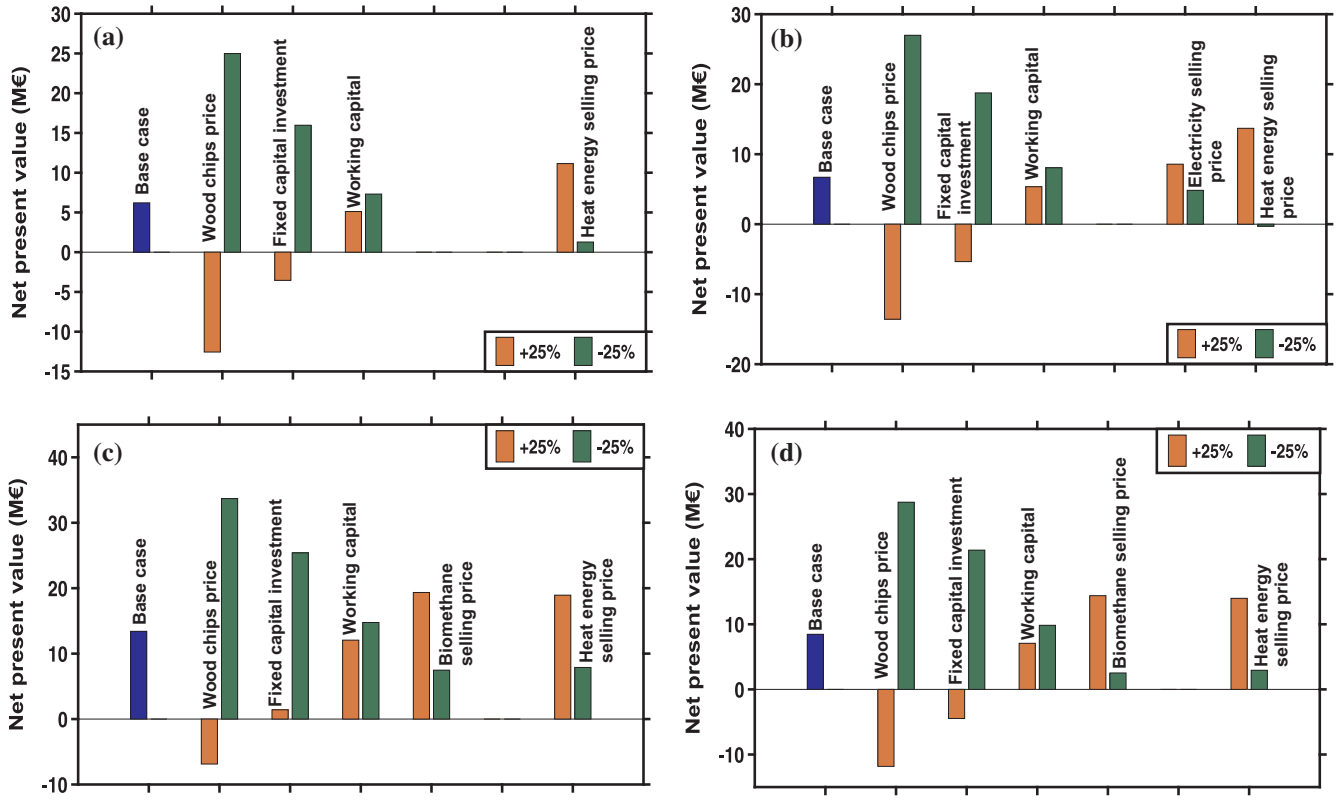

Fig. 6. Sensitivity analysis of net present value (at torrefied biomass selling price of 210 €/t) for different input parameters (a) Case 1, (b) Case 2, (c) Case 3-HPWS and (d) Case 3-PSA.

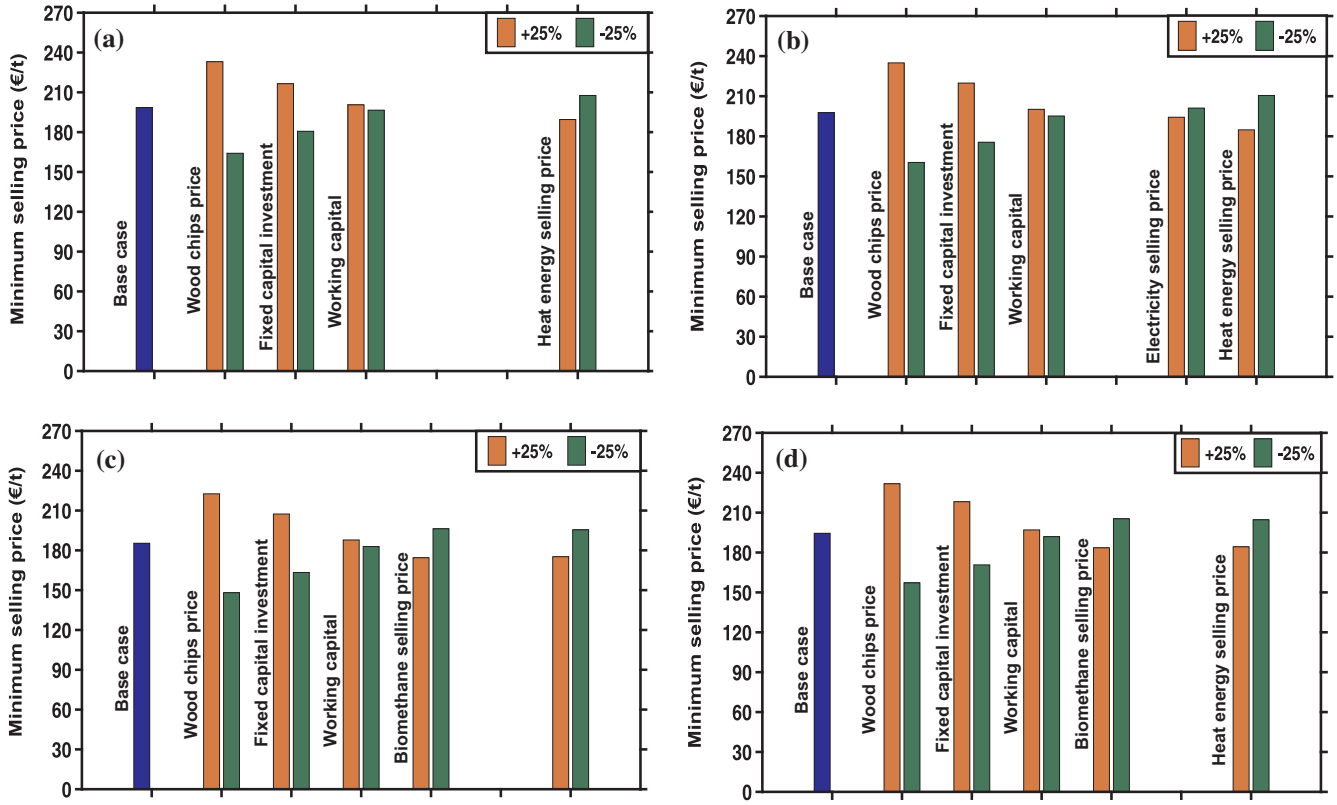

Fig. 7. Sensitivity analysis of minimum selling price for different input parameters (a) Case 1, (b) Case 2, (c) Case 3-HPWS and (d) Case 3-PSA.

it comes to the application of biogas, upgrading and selling it as a vehicle fuel has significantly influenced the minimum selling price of the torrefied biomass pellets in comparison with using it in a biogas engine to produce electrical and heat energy. A sensitivity analysis revealed that wood chips purchasing price could significantly influence the economics of the torrefaction process. Further, the possibilities for reducing the selling price of torrefied biomass was discussed.

Acknowledgement

Ramasamy Praveenkumar acknowledges Tampere University of Technology for the Postdoc. funding provided through University Internal Projects (83289).

Appendix A. Supplementary material

Supplementary data associated with this article can be found, in the online version, at http://dx.doi.org/10.1016/j.apenergy.2018.01.045.

References

[1] Liobikienė G, Butkus M. The European Union possibilities to achieve targets of Europe 2020 and Paris agreement climate policy. Renew Energy 2017;106:298–309. http://dx.doi.org/10.1016/j.renene.2017.01.036.
[2] Thrän D, Witt J, Schaubach K, Kiel J, Carbo M, Maier J, et al. Moving torrefaction towards market introduction – technical improvements and economic-environmental assessment along the overall torrefaction supply chain through the SECTOR project. Biomass Bioenergy 2016;89:184–200. http://dx.doi.org/10.1016/j.biombioe.2016.03.004.
[3] Eurostat. Energy statistics; 2016.
[4] Doddapaneni TRKC, Konttinen J, Hukka TI, Moilanen A. Influence of torrefaction pretreatment on the pyrolysis of Eucalyptus clone: a study on kinetics, reaction mechanism and heat flow. Ind Crops Prod 2016;92:244–54. http://dx.doi.org/10.1016/j.indcrop.2016.08.013.
[5] Koppejan J, Sokhansanj S, Melin S, Madrali S. Status overview of torrefaction technologies (IEA Bioenergy Task 32); 2012.
[6] Hawkins Wright. Global demand for torrefied biomass; 2012. <http://www.forestbusinessnetwork.com/13392/global-demand-for-torrefied-biomass-could-exceed-70-million-tonnes-a-year-by-the-end-of-the-decade/> [accessed July 22, 2017].
[7] Batidzirai B, Mignot APR, Schakel WB, Junginger HM, Faaij APC. Biomass torrefaction technology: techno-economic status and future prospects. Energy 2013;62:196–214. http://dx.doi.org/10.1016/j.energy.2013.09.035.
[8] Sermyagina E, Saari J, Kaikko J, Vakkilainen E. Integration of torrefaction and CHP plant: operational and economic analysis. Appl Energy 2016;183:88–99. http://dx.doi.org/10.1016/j.apenergy.2016.08.151.
[9] Kumar L, Koukoulas AA, Mani S, Satyavolu J. Integrating torrefaction in the wood pellet industry: a critical review. Energy Fuels 2017;31:37–54. http://dx.doi.org/10.1021/acs.energyfuels.6b02803.
[10] Clausen LR. Integrated torrefaction vs. external torrefaction – a thermodynamic analysis for the case of a thermochemical biorefinery. Energy 2014;77:597–607. http://dx.doi.org/10.1016/j.energy.2014.09.042.
[11] Arpiainen V, Wilen C. Production of solid sustainable energy carriers from biomass by means of torrefaction report on requirements of end users on densified and torrefied materials. VTT 2014:1–18.
[12] Fagernas L, Kuoppala E, Arpiainen V. Composition, utilization and economic assessment of torrefaction condensates. Energy Fuels 2015;29:3134–42. http://dx.doi.org/10.1021/acs.energyfuels.5b00004.
[13] Doddapaneni TRKC, Praveenkumar R, Tolvanen H, Palmroth MRT, Konttinen J, Rintala J. Anaerobic batch conversion of pine wood torrefaction condensate. Bioresour Technol 2017;225:299–307. http://dx.doi.org/10.1016/j.biortech.2016.11.073.
[14] Liaw SS, Frear C, Lei W, Zhang S, Garcia-Perez M. Anaerobic digestion of C1–C4 light oxygenated organic compounds derived from the torrefaction of lignocellulosic materials. Fuel Process Technol 2015;131:150–8. http://dx.doi.org/10.1016/j.fuproc.2014.11.012.
[15] Agar D, Gil J, Sanchez D, Echeverria I, Wihersaari M. Torrefied versus conventional pellet production – a comparative study on energy and emission balance based on pilot-plant data and EU sustainability criteria. Appl Energy 2015;138:621–30. http://dx.doi.org/10.1016/j.apenergy.2014.08.017.
[16] Sermyagina E, Saari J, Zakeri B, Kaikko J, Vakkilainen E. Effect of heat integration method and torrefaction temperature on the performance of an integrated CHP-torrefaction plant. Appl Energy 2015;149:24–34. http://dx.doi.org/10.1016/j.apenergy.2015.03.102.
[17] Bates RB, Ghoniem AF. Biomass torrefaction: modeling of reaction thermochemistry. Bioresour Technol 2013;134:331–40. http://dx.doi.org/10.1016/j.biortech.2013.01.158.
[18] National Institute Of Standards and Technology. Chemical formula search n.d. National Institute of Standards and Technology; 2011 [accessed August 14, 2017].
[19] Nocquet T, Dupont C, Commandre JM, Grateau M, Thiery S, Salvador S. Volatile species release during torrefaction of wood and its macromolecular constituents: part 1 – experimental study. Energy 2014;72:180–7. http://dx.doi.org/10.1016/j.energy.2014.02.061.
[20] Peng J, Bi XT, Lim CJ, Peng H, Kim CS, Jia D, et al. Sawdust as an effective binder for making torrefied pellets. Appl Energy 2014;157:491–8. http://dx.doi.org/10.1016/j.apenergy.2015.06.024.
[21] Pirraglia A, Gonzalez R, Saloni D, Denig J. Technical and economic assessment for the production of torrefied ligno-cellulosic biomass pellets in the US. Energy Convers Manage 2013;66:153–64. http://dx.doi.org/10.1016/j.enconman.2012.09.024.
[22] Jansen Jes la Cour. Anaerobic digestion: technology. In: Christensen Thomas, editor. Solid waste technol manag, 2nd ed. West Sussex: Jhon Wiley & Sons Ltd; 2010. p. 1052.
[23] Deublein D, Steinhauser A. Typical design calculation for an agricultural biogas plant. Biogas Waste Renew Resour 2010:357–64. http://dx.doi.org/10.1002/9783527632794.ch35.
[24] Lehto J, Oasmaa A, Solantausta Y, Kytö M, Chiaramonti D. Fuel oil quality and combustion of fast pyrolysis bio-oils. VTT Technol n.d.;87:79.
[25] Akbulut A. Techno-economic analysis of electricity and heat generation from ı case study farm-scale biogas plant: Çiçekdagi case study. Energy 2012;44:381–90.
[26] Drosg B, Braun R, Bochmann G, Al Saedi T. Analysis and characterisation of biogas feedstocks. In: Arthur Wellinger, Murphy J, David Baxter, editors. The biogas handbook: science, production and applications. Elsevier; 2013. p. 52–84.
[27] Petersson A, Holm-nielsen JB, Baxter D. Biogas upgrading technologies – developments and innovations. IEA Bioenergy 2009.
[28] TUV. Biogas to biomethane technology review. Vienna Univ Technol; 2012. p. 1–15.
[29] Drosg B, Linke B, Fuchs W, Madsen M. Nutrient recovery by biogas digestate processing; 2015.
[30] Chen H, Chen X, Qiao Z, Liu H. Release and transformation characteristics of K and Cl during straw torrefaction and mild pyrolysis. Fuel 2016;167:31–9. http://dx.doi.org/10.1016/j.fuel.2015.11.059.
[31] Azuara M, Kersten SRA, Kootstra AMJ. Recycling phosphorus by fast pyrolysis of pig manure: concentration and extraction of phosphorus combined with formation of value-added pyrolysis products. Biomass Bioenergy 2013;49:171–80. http://dx.doi.org/10.1016/j.biombioe.2012.12.010.
[32] Rutz D. Sustainable heat use of biogas plants. A handbook; 2012.
[33] Firdaus N, Prasetyo BT, Sofyan Y, Siregar F. Part II of II: palm oil mill effluent (POME): biogas power plant. Distrib Gener Altern Energy J 2017;32:6–18. http://dx.doi.org/10.1080/21563306.2017.11878943.
[34] Svoboda K, Martinec J, Pohořelý M, Baxter D. Integration of biomass drying with combustion/gasification technologies and minimization of emissions of organic compounds. Chem Pap 2009;63:15–25. http://dx.doi.org/10.2478/s11696-008-0080-5.
[35] Turton R. Analysis, synthesis, and design of chemical processes. Prentice Hall; 2012.
[36] Wright MM, Satrio Ja, Brown RC, Daugaard DE, Hsu DD. Techno-economic analysis of biomass fast pyrolysis to transportation fuels. Natl Renew Energy Lab 2010;89:S2–10. http://dx.doi.org/10.1016/j.fuel.2010.07.029.
[37] Deublein D, Steinhauser A. Attachment II: economy of biogas plants for the year 2007 (calculation on the basis of the example of attachment I). Biogas from Waste Renew Resour 2008;2007:415–7. http://dx.doi.org/10.1002/9783527621705.app2.
[38] de Hullu J, Maassen JIW, van Meel PA, Shazad S, Vaessen JMP, Bini L, et al. Comparing different biogas upgrading techniques; 2008.
[39] Buyukkamaci N, Koken E. Economic evaluation of alternative wastewater treatment plant options for pulp and paper industry. Sci Total Environ 2010;408:6070–8. http://dx.doi.org/10.1016/j.scitotenv.2010.08.045.
[40] FOEX Indexes Ltd. Bioenergy and wood indices; n.d. <http://www.foex.fi/biomass/> [accessed July 15, 2017].
[41] Uusitalo V, Soukka R, Horttanainen M, Niskanen A, Havukainen J. Economics and greenhouse gas balance of biogas use systems in the Finnish transportation sector. Renew Energy 2013;51:132–40. http://dx.doi.org/10.1016/j.renene.2012.09.002.
[42] Biogas price; n.d. <https://www.gasum.com/en/About-gasum/for-the-media/News/2016/Natural-gas-price-reduced-at-Gasum-filling-stations-as-from-July-1-2016/> [accessed August 20, 2017].
[43] Beil M, Beyrich W. Biogas upgrading to biomethane. In: Wellinger Arthur, Murphy J, Baxter David, editors. The biogas handbook: science production and applications. Elsevier; 2013. p. 342–77.
[44] Allen DH. Economic evaluation of projects: a guide. Institution of Chemical Engineers; 1991.
[45] Sen SM, Gürbüz EI, Wettstein SG, Alonso DM, Dumesic JA, Maravelias CT. Production of butene oligomers as transportation fuels using butene for esterification of levulinic acid from lignocellulosic biomass: process synthesis and techno-economic evaluation. Green Chem 2012;7:3289–94. http://dx.doi.org/10.1039/c2gc35881f.
[46] Ghiasi B, Kumar L, Furubayashi T, Lim CJ, Bi X, Kim CS, et al. Densified biocoal from woodchips: is it better to do torrefaction before or after densification? Appl Energy 2014;134:133–42. http://dx.doi.org/10.1016/j.apenergy.2014.07.076.
[47] Prins MJ, Ptasinski KJ, Janssen FJJG. More efficient biomass gasification via torrefaction. Energy 2006;31:3458–70. http://dx.doi.org/10.1016/j.energy.2006.03.008.
[48] Bach QV, Skreiberg Ø, Lee CJ. Process modeling and optimization for torrefaction of forest residues. Energy 2017;138:348–54. http://dx.doi.org/10.1016/j.energy.2017.07.040.
[49] Kohl T, Laukkanen T, Järvinen M, Fogelholm CJ. Energetic and environmental

performance of three biomass upgrading processes integrated with a CHP plant. Appl Energy 2013;107:124–34. http://dx.doi.org/10.1016/j.apenergy.2013.02.021.
[50] Ranta T, Föhr J, Soininen H. Evaluation of a pilot-scale wood torrefcaction plant based on pellet properties and Finnish market economics. Int J Energy Environ 2016;7:159–68.
[51] Mata-Alvarez J. Biomethanization of the organic fraction of municipal solid wastes. IWA Publishing; 2002.
[52] Werlte Biogas Plant; n.d. <https://www.kriegfischer.de/en/biogas-plants/references/europa/germany/werlte/>.
[53] Budzianowski WM, Budzianowska DA. Economic analysis of biomethane and bioelectricity generation from biogas using different support schemes and plant configurations. Energy 2015;88:658–66. http://dx.doi.org/10.1016/j.energy.2015.05.104.
[54] Lantz M. The economic performance of combined heat and power from biogas produced from manure in Sweden – a comparison of different CHP technologies. Appl Energy 2012;98:502–11. http://dx.doi.org/10.1016/j.apenergy.2012.04.015.
[55] Sgroi F, Foderà M, Di Trapani AM, Tudisca S, Testa R. Economic evaluation of biogas plant size utilizing giant reed. Renew Sustain Energy Rev 2015;49:403–9. http://dx.doi.org/10.1016/j.rser.2015.04.142.
[56] Pirraglia A, Gonzalez R, Denig J, Saloni D, Wright J. Assessment of the most adequate pre-treatments and woody biomass sources intended for direct co-firing in the U.S. BioResources 2012;7:4817–42.

Tampereen teknillinen yliopisto
PL 527
33101 Tampere

Tampere University of Technology
P.O.B. 527
FI-33101 Tampere, Finland

ISBN 978-952-15-4119-3
ISSN 1459-2045